



DEVELOPMENT AND APPLICATION OF A NEW MULTISTAGE  
CONFINED DYNAMIC CREEP TEST FOR ASPHALT

A Thesis submitted by

Majid Zargar, M Eng

(Civil Engineering – Highway and Transportation)

For the award of

Doctor of Philosophy

2018

## ABSTRACT

Research on well-designed heavy-traffic flexible pavements in areas with elevated temperatures has shown that their service life is a function of the creep performance of their top asphalt layers. Ranking and predicting the creep performance of asphalt close to the field situation have always been a challenge for pavement designers in both the design and rehabilitation stages of flexible pavement in these critical situations.

To date, several laboratory test methodologies have been applied to model creep performance of asphalt, however, these methods have been unsuccessful compared with data from field assessments. The most important limitations, which make the modelling of the asphalt creep performance in the laboratory difficult, are outlined as: controlling the asphalt mix structure (i.e. air voids); providing in-situ asphalt confinement situations for laboratory samples.

It has been hypothesised that the Australian dynamic creep test can be redesigned to enable multistage evaluation of creep performance of asphalt mixtures to overcome the noted limitations. The research hypothesis is examined through a collaboration of development of two test methods. First, the Ultrasonic Wave Transmission technique (UWT) is used for non-destructive assessment of air voids distribution in the critical position in the centre of laboratory samples. Second, the Confined Dynamic Creep Test (CDCT) is developed to be able to perform multistage stress on the same asphalt sample. Finally, the combination of the two developed tests, MCDC+UWT is used with appropriate numerical and mathematical modelling to introduce a creep life prediction method.

The combination of MCDC+UWT tests together with numerical modelling greatly enhance the ability to rank and predict the creep performance of asphalt in varying operational conditions. This combination is also able to measure the compressive resilient modulus of asphalt at elevated temperatures and stresses.

## Certification of Thesis

This thesis is entirely the work of *Majid Zargar* except where otherwise acknowledged. The work is original and has not previously been submitted for any other award, except where acknowledged.

Professor Frank Bullen

---

Principal Supervisor

Professor Ron Ayers

---

Associate Supervisor

Student and supervisors' signatures of endorsement are held at USQ.

## ACKNOWLEDGEMENTS

First, I would like to thank my supervisors Professor Frank Bullen and Professor Ron Ayers for giving me the opportunity to work under their supervision for their valuable advice, their support, and their continued guidance during this research.

Second, I would like to thank the Brisbane City Council and the Eagle Farm Asphalt Plant staff, especially Dr Gregory John Stephenson and Troy Akers for their assistance throughout my experimental works. I acknowledge Professor John Worden and Dr Barbara Harnes for their professional proofreading advice.

Third, I would like to thank the USQ workshop and laboratory staff: Mr Chris Galligan, Mr Brian Aston from the USQ workshop and Mr Wayne Crowell, Mrs Piumika Ariyadasa, and Mr Daniel Eising from laboratory, for their valuable advice and assistance during this research.

I am also grateful to the following university staff: Dr Kazem Ghabraie, Dr Sourish Banerjee, Dr Soma Sundaraswaran, Dr Habib Alehossein , and Dr Ahmad Sharifian-Barforoush for their unfailing support, advice and assistance during this research.

I would like to thank my friends for accepting nothing less than excellence from me. Last but not least, I would like to thank my family: my parents and to my brothers and sisters for supporting me spiritually throughout the writing of this thesis and throughout my life in general.

# TABLE OF CONTENTS

## Contents

<b>CHAPTER 1</b> .....	1
<b>INTRODUCTION</b> .....	1
1.1 Introduction .....	2
1.2 The research hypothesis .....	6
1.3 The Scope of the Study .....	6
1.4 Research plan .....	8
1.5 Format of the thesis .....	9
1.6 Summary .....	11
<b>CHAPTER 2</b> .....	12
<b>AUSTRALIAN FLEXIBLE PAVEMENTS FOR HEAVY-TRAFFIC ROADS</b>	12
2.1 Introduction .....	13
2.2 Flexible pavements – materials and structures.....	13
2.3 Asphalt mix design for flexible pavements.....	17
2.4 Flexible pavement distress .....	19
2.5 Flexible heavy-traffic pavement structural design .....	21
2.6 Asphalt modulus – measurement and temperature effects.....	23
2.6.1 Measurement of modulus of asphalt .....	25
2.6.2 Temperature and modulus.....	26
2.7 Flexible pavement service life.....	28
2.7.1 Fatigue.....	29
2.7.2 Creep.....	29
2.8 Summary .....	31
<b>CHAPTER 3</b> .....	32
<b>CHALLENGES REGARDING ASPHALT CREEP DEFORMATION MEASUREMENT AND MODELLING</b> .....	32
3.1 Introduction .....	33
3.2 Asphalt creep deformation .....	33
3.2.1 Creep deformation mechanisms.....	33
3.2.2 Factors that influence creep deformation of asphalt .....	36
3.2.3 Creep deformation test methods.....	36
3.3 Challenges with development of creep deformation test methods.....	39

3.3.1	Dynamic load type and magnitude.....	39
3.3.2	Confinement stress for laboratory samples .....	46
3.3.3	Air voids and their distribution .....	47
3.3.4	Environmental conditions .....	50
3.3.5	Summary of challenges for laboratory creep testing.....	54
3.4	Modelling and predicting creep.....	54
3.4.1	Literature review of creep deformation modelling .....	54
3.5	Summary .....	59
<b>CHAPTER 4 .....</b>		<b>60</b>
<b>RESEARCH PLAN AND METHODOLOGY .....</b>		<b>60</b>
4.1	Introduction .....	61
4.2	Material selection .....	63
4.2.1	Aggregate type and gradation .....	63
4.2.2	Binder types .....	65
4.3	Sample fabrication.....	67
4.3.1	Asphalt mix design and sample preparation .....	67
4.3.2	Sample preparation for air voids measurement and UWT test .....	67
4.3.3	PVC ring confinement.....	67
4.3.4	Strain gauges set up.....	68
4.4	Test procedures.....	69
4.4.1	Air voids measurement .....	69
4.4.2	Multistage Confined Dynamic Creep (MCDC) test.....	71
4.5	Finite element modelling of stress distribution .....	74
4.6	Application of the MCDC test for creep resistance ranking of asphalt.....	75
4.7	Creep life prediction method using MCDC test .....	75
4.7.1	Creep slope and conventional intercept measurement.....	76
4.7.2	Creep life estimation .....	76
4.8	Compressive resilient modulus calculation of asphalt using MCDC test ...	78
4.9	Summary .....	79
<b>CHAPTER 5 .....</b>		<b>80</b>
<b>DEVELOPMENT OF AN ULTRASONIC TECHNIQUE TO MEASURE AIR VOIDS .....</b>		<b>80</b>
5.1	Introduction .....	81
5.2	Existing air voids measurement techniques .....	81
5.3	Ultrasonic Wave Transmission (UWT) technique and asphalt mixtures ...	83

5.4	UWT correlation with air voids in the whole sample.....	84
5.5	Air voids distribution in the whole sample .....	86
5.6	Development of UWT Technique to measure air voids under platen .....	88
5.7	Comparison of air void in the centre with air voids of the whole sample... ..	88
5.8	Evaluating UWT techniques.....	89
5.9	Conclusion.....	91
<b>CHAPTER 6 .....</b>		<b>92</b>
<b>THE DEVELOPMENT OF A MULTISTAGE CONFINED DYNAMIC CREEP TEST .....</b>		<b>92</b>
6.1	Introduction .....	93
6.1.1	The confining system .....	95
6.2	The Multistage Confined Dynamic Creep (MCDC) test methodology.....	95
6.2.1	The possibility of conducting the MCDC test in the laboratory .....	96
6.2.2	Stress analysis of MCDC test using Finite Element Modelling (FEM).....	98
6.2.3	Laboratory assessment of confinement stresses.....	105
6.2.4	Summary of laboratory and modelling assessment of confinement stresses	108
6.3	Analysing creep test results from MCDC test.....	108
6.3.1	Analysing creep test data .....	114
6.4	Prediction of creep life using MCDC test .....	117
6.4.1	Creep life prediction based on secant creep slope .....	117
6.4.2	MCDC test analysis and applied mathematical modelling .....	118
6.4.3	Creep life prediction based on creep depth in laboratory samples.....	119
6.4.4	Estimation of creep life .....	119
6.5	Conclusion.....	120
<b>CHAPTER 7 .....</b>		<b>122</b>
<b>MULTISTAGE CONFINED DYNAMIC CREEP TEST AND CREEP RANKING FOR ASPHALT MIXES .....</b>		<b>122</b>
7.1	Introduction .....	123
7.2	Selected samples and tests.....	123
7.3	Creep performance versus air voids .....	124
7.3.1	Air voids effect on permanent strain of conventional asphalt.....	124
7.3.2	Air voids effect on secant creep slope of conventional asphalt .....	126
7.3.3	Air voids effect on permanent strain of multigrade asphalt.....	128
7.3.4	Air voids effect on secant creep slope of multigrade asphalt .....	130
7.3.5	Air voids effect on permanent strain of polymer modified asphalt ...	132

7.3.6	Air voids effect on secant creep slope of polymer modified asphalt .	133
7.4	Conclusion.....	134
<b>CHAPTER 8</b>	.....	<b>136</b>
<b>CREEP LIFE ANALYSIS BASED ON MCDC + UWT TEST</b>	.....	<b>136</b>
8.1	Introduction .....	137
8.2	MCDC +UWT test procedure and creep life calculation .....	137
8.2.1	Air voids estimation under platen using UWT technique.....	137
8.2.2	Creep life calculation using MCDC test .....	138
8.3	Comparison of creep life of three selected asphalts .....	139
8.3.1	Creep life vs air voids .....	141
8.3.2	Creep life vs temperature .....	141
8.3.3	Creep life vs surface stress.....	141
8.3.4	Creep life vs bitumen type .....	141
8.4	Conclusion.....	142
<b>CHAPTER 9</b>	.....	<b>143</b>
<b>ASSESSING THE MODULUS OF ASPHALT USING THE MCDC+UWT TEST</b>	.....	<b>143</b>
9.1	Introduction .....	144
9.2	Compressive resilient modulus calculation of asphalt using the outlined MCDC test.....	145
9.3	The compressive resilient modulus results.....	145
9.3.1	Effect of cycle number .....	145
9.3.2	Effect of air voids on compressive resilient modulus .....	148
9.3.3	Effect of temperature on compressive resilient modulus.....	148
9.3.4	Effect of stress on resilient modulus .....	148
9.4	Conclusion.....	152
<b>CHAPTER 10</b>	.....	<b>153</b>
<b>CONCLUSION AND RECOMENDATIONS</b>	.....	<b>153</b>
10.1	Introduction .....	154
10.2	The literature review.....	154
10.3	Using Ultrasonic Wave Transmission (UWT) technique for air voids measurements .....	155
10.4	The development of MCDC test .....	156
10.5	The effective parameters on creep performance .....	157
10.6	The creep life and the effective parameters.....	157
10.7	The compressive resilient modulus and the effective parameters .....	158

10.8	The MCDC + UWT test .....	159
10.9	Limitations and Recommendations .....	160
	REFERENCES.....	161
	APPENDIX.....	175
	Appendix A. Relevant to the literature review.....	Appendix-1
	Appendix B. Relevant to the air voids measurement in centre and whole sample .....	Appendix-6
	Appendix C. Relevant to FEM modelling outputs for various laboratory and in-situ conditions .....	Appendix-8
	Appendix D. Relevant to the MCDC test results in varying conditions..... .....	Appendix-23
	Appendix E. Relevant to the secant creep slope in varying conditions ....	Appendix-26
	Appendix F. Relevant to the varying asphalt test results .....	Appendix-28

## LIST OF FIGURES

Figure 1.1: Severe creep deformation on flexible pavement .....	2
Figure 1.2: Creep deformation of asphalt and creep distribution.....	4
Figure 1.3: Asphalt structure.....	5
Figure 1.4: Research plan .....	9
Figure 2.1: Distribution of load stress in flexible pavement.....	13
Figure 2.2: Types of flexible pavement based on the materials and thicknesses of the layer	16
Figure 2.3: Dense grade asphalt mix design procedure .....	19
Figure 2.4: Pavement model for Mechanistic Design procedure .....	22
Figure 2.5: Design procedure for flexible pavement .....	23
Figure 2.6: Temperature at depth predicted for hot summer day in Canberra.....	27
Figure 2.7: Modulus at depth for hot summer day, at 10km/h.....	28
Figure 2.8: Different asphalt surface shape related to creep deformation in each asphalt layer: (a) asphalt layer, (b) granular base, (c) Subbase/Subgrade.....	30
Figure 3.1: Schematic diagram of the mechanism of creep (rut) depth .....	34
Figure 3.2: Transverse profile of asphalt creep deformation by increasing loading cycles...	34
Figure 3.3: Creep deformation and creep rate versus loading cycle number.....	35
Figure 3.4: a: Generated stress under moving wheel load .....	39
Figure 3.5: Vertical, longitudinal, and lateral contact stresses generated by wheel loads at the pavement surface .....	41
Figure 3.6: The distribution of shear stress in varying depth.....	42
Figure 3.7: Permanent deformation of specimen under varying conditions .....	44
Figure 3.8: Schematic representation of loading pattern for various axles.....	44
Figure 3.9: A: Specimen with 150mm diameter and 50mm height under 50mm platen size, and exposed to 750 kPa axial load. B: the elastic model of a road pavement under 750kPa load.....	45
Figure 3.10: Stress distribution within asphalt layer under tyre .....	46
Figure 3.11: Varying configuration provided for confining laboratory asphalt samples.....	47
Figure 3.12: Air voids within Asphalt structure .....	48
Figure 3.13: Failure modes and air voids distribution .....	50
Figure 3.14:a: Environmental setup and b: Schematic generated temperature evaluation ....	52
Figure 3.15: Comparison of creep deformation models with repeated load test.....	56
Figure 3.16: The variation of the deviation error in the final creep deformation and R2 of various creep .....	57
Figure 4.1: Overarching outline of the research plan and methodology .....	62
Figure 4.2: BCC Type III aggregate gradation plot .....	64
Figure 4.3: PVC confinement set up.....	68

Figure 4.4: Strain gauge set up .....	69
Figure 4.5: (a): Pundit 7 with two transducers (b): Sample divisions (17 points) for ultrasonic test.....	70
Figure 4.6: a). UTM Normalised BNC Breakout Cable Assembly (IPC part number. 0002-2239) (b). IMACS Chasis of Universal Testing System (UTS) (c). The Universal Amplifier (QuantumX MX1601B).....	72
Figure 4.7: Optimisation of UTS tester using extra data logger .....	72
Figure 4.8: Multistage Confined Dynamic Creep (MCDC) test results.....	74
Figure 4.9: Schematic diagram of creep stages and slope .....	76
Figure 4.10: Transverse profile of rut depth (creep deformation) under the tyre .....	77
Figure 4.11: Shape and duration of applied repeated load .....	78
Figure 4.12: Stress and strain in one load cycle .....	79
Figure 5.1: Models of wave transmission in UWT test (Ultrasonic Pulse Velocity Test- webpage).....	84
Figure 5.2: 17 transducers locations on each sample for UWT test.....	85
Figure 5.3: Ultrasonic velocity versus air voids for mixtures with C320, M1000, and PMB in average 17 points .....	86
Figure 5.4: Ultrasonic velocity for 17 points on the surface of samples with low and high air voids.....	87
Figure 5.5: Vertical and horizontal air voids distribution in specimen with 12.5mm and 19mm maximum aggregate size .....	87
Figure 5.6: Air voids difference (air voids of whole sample minus estimated air voids in centre) .....	89
Figure 5.7: Creep slope vs air voids content of whole sample.....	90
Figure 5.8: Creep slope vs estimated air voids content in centre.....	91
Figure 6.1: Schematic diagram of the laboratory creep sample.....	95
Figure 6.2: MCDC test validation.....	97
Figure 6.3: Schematic diagram of the laboratory creep test sample .....	99
Figure 6.4: Schematic diagram of single asphalt layer used in FEM.....	99
Figure 6.5: Selected points on FEM model of confined laboratory sample for stress analysis .....	100
Figure 6.6: Selected points on FEM model of asphalt layer for stress analysis.....	100
Figure 6.7: Stress and Strain in first cycle of each stage of laboratory test (sample 51M)..	107
Figure 6.8: Representative creep data determination .....	109
Figure 6.9: Slope and intercept .....	109
Figure 6.10: Creep slope vs Cycle .....	110

Figure 6.11: Regression models to predict confined dynamic creep test results .....	112
Figure 6.12: Permanent strain vs air voids under different stress at 50°C .....	115
Figure 6.13: Creep slope vs air voids under different stress based on the secant creep slope between 20,000 and 40,000 cycles.....	116
Figure 6.14: Creep slope vs air voids under different stress based on the secant creep slope between 40,000 and 100,000 cycles.....	116
Figure 6.15: Schematic creep life prediction using different mathematical regression methods .....	118
Figure 6.16: Schematic diagram of MCDC test and the power regression model.....	118
Figure 6.17: Transverse profile of rut depth (creep deformation) under the tyre .....	119
Figure 7.1: Permanent strain vs air voids under different platen stress in 40°C and 50°C.....	125
Figure 7.2: Secant creep slope (20,000-40,000 cycles) versus air voids under various pressures at 40°C and 50°C.....	127
Figure 7.3: Secant creep slope (40,000-100,000 cycles) versus air voids under various pressures at 40°C and 50°C.....	127
Figure 7.4: Permanent strain vs air voids under different stresses in 40°C and 50°C .....	129
Figure 7.5: Creep slope (20,000-40,000 cycles) vs air voids under various pressure at 40°C and 50°C .....	130
Figure 7.6: Creep slope (40,000-100,000 Cycles) vs air voids under various pressures at 40°C and 50°C .....	131
Figure 7.7: Permanent strain vs air voids under various stresses in 40°C and 50°C .....	132
Figure 7.8: Creep slope (20,000-40,000 cycles) vs air voids under various pressure at 40°C and 50°C .....	133
Figure 7.9: Creep slope (40,000-100,000 cycles) vs air voids under various pressure at 40°C and 50°C .....	134
Figure 8.1: Creep life vs air voids in 500kPa.....	139
Figure 8.2: Creep life vs air voids in 750kPa.....	140
Figure 8.3: Creep life vs air voids in 1000kPa.....	140
Figure 9.1: C320: Permanent strain and compressive resilient modulus vs load cycles at 50°C .....	146
Figure 9.2: M1000: Permanent strain and compressive resilient modulus versus load cycles at 50°C .....	147
Figure 9.3: PMB: Permanent strain and compressive resilient modulus vs load cycles at 50°C .....	147

Figure 9.4: C320: Compressive resilient modulus under 500kPa for samples with varying air voids at 40 and 50°C.....	149
Figure 9.5: M1000: Compressive resilient modulus under 500kPa for samples with varying air voids at 40 and 50°C.....	149
Figure 9.6: PMB: Compressive resilient modulus under 500kPa for samples with varying air voids at 40 and 50°C.....	150
Figure 9.7: C320: Compressive resilient modulus for samples with varying air voids at 40 and 50°C under varying stresses.....	150
Figure 9.8: M1000: Compressive resilient modulus for samples with varying at 40 and 50°C under varying stresses.....	151
Figure 9.9: Compressive resilient modulus for samples with varying air voids at 40 and 50°C under varying stresses.....	151
Figure 1.B: Conventional asphalt: Air voids of the whole sample vs. estimated air voids at the centre of samples.....	Appendix-6
Figure 2.B: Multigrade asphalt: Air voids of the whole sample vs. estimated air voids at the centre of samples.....	Appendix-6
Figure 3.B: Polymer modified asphalt: Air voids of the whole sample vs. estimated air voids at the centre of samples.....	Appendix-7
Figure 1.C: 51M, 500kPa, S11, confined laboratory sample.....	Appendix-8
Figure 2.C: 51M, 500kPa, S22, confined laboratory sample.....	Appendix-8
Figure 3.C: 51M, 500kPa, S33, confined laboratory sample.....	Appendix-9
Figure 4.C: 51M, 500kPa, S12, confined laboratory sample.....	Appendix-9
Figure 5.C: 51M, 500kPa, U Magnitude, confined laboratory sample.....	Appendix-10
Figure 6.C: 45M, 750kPa, S11, confined laboratory sample.....	Appendix-10
Figure 7.C: 45M, 750kPa, S22, confined laboratory sample.....	Appendix-11
Figure 8.C: 45M, 750kPa, S33, confined laboratory sample.....	Appendix-11
Figure 9.C: 45M, 750kPa, S12, confined laboratory sample.....	Appendix-12
Figure 10.C: 45M, 750kPa, U Magnitude, confined laboratory sample.....	Appendix-12
Figure 11.C: 56M, 1000kPa, S11, confined laboratory sample.....	Appendix-13
Figure 12.C: 56M, 1000kPa, S22, confined laboratory sample.....	Appendix-13
Figure 13.C: 56M, 1000kPa, S33, confined laboratory sample.....	Appendix-14
Figure 14.C: 56M, 1000kPa, S12, confined laboratory sample.....	Appendix-14
Figure 15.C: 56M, 1000kPa, U Magnitude, confined laboratory sample.....	Appendix-15
Figure 16.C: 51M, 500kPa, S11, asphalt layer.....	Appendix-15
Figure 17.C: 51M, 500kPa, S22, asphalt layer.....	Appendix-16
Figure 18.C: 51M, 500kPa, S33, asphalt layer.....	Appendix-16
Figure 19.C: 51M, 500kPa, S12, asphalt layer.....	Appendix-17

Figure 20.C: 51M, 500kPa, U Magnitude, asphalt layer .....	Appendix-17
Figure 21.C: 45M, 750kPa, S11, asphalt layer .....	Appendix-18
Figure 22.C: 45M, 750kPa, S22, asphalt layer .....	Appendix-18
Figure 23.C: 445M, 750kPa, S33, asphalt layer .....	Appendix-19
Figure 24.C: 45M, 750kPa, S12, asphalt layer .....	Appendix-19
Figure 25.C: 45M, 750kPa, U Magnitude, asphalt layer .....	Appendix-20
Figure 26.C: 56M, 1000kPa, S11, asphalt layer .....	Appendix-20
Figure 27.C: 56M, 1000kPa, S22, asphalt layer .....	Appendix-21
Figure 28.C: 56M, 1000kPa, S33, asphalt layer .....	Appendix-21
Figure 29.C: 56M, 1000kPa, S12, asphalt layer .....	Appendix-22
Figure 30.C: 56M, 1000kPa, U Magnitude, asphalt layer .....	Appendix-22
Figure 1.D: MCDC test results for conventional samples in 40°C .....	Appendix-23
Figure 2.D: MCDC test results for Multigrade samples in 40°C .....	Appendix-23
Figure 3.D: MCDC test results for PMB samples in 40°C .....	Appendix-24
Figure 4.D: MCDC test results for conventional samples in 50°C .....	Appendix-24
Figure 5.D: MCDC test results for Multigrade samples in 50°C .....	Appendix-25
Figure 6.D: MCDC test results for PMB samples in 50°C .....	Appendix-25
Figure 1.E: Secant creep slope of three types asphalt with different air voids under 500kPa .....	Appendix-26
Figure 2.E: Secant creep slope of three types asphalt with different air voids under 750kPa .....	Appendix-26
Figure 3.E: Secant creep slope of three types asphalt with different air voids under 1000kPa .....	Appendix-27

## LIST OF TABLES

Table 2.1: Flexible pavement layers and materials.....	14
Table 2.2: Pavement material categories and characteristics .....	15
Table 2.3: Basic steps of asphalt mix design .....	18
Table 2.4: Flexible pavement distresses and the possible reasons.....	20
Table 2.5: Pavement material input used in structural design .....	23
Table 2.6: Factors effecting modulus of asphalt .....	25
Table 3.1: Factors affecting on creep deformation of asphalt mixtures.....	36
Table 3.2: Loading options in different standards .....	43
Table 3.3: Effective factors on modelling the asphalt creep deformation in the laboratory ..	54
Table 3.4: The deviation error dependency of these two models to cycle number.....	58
Table 4.1: BCC Type III aggregate gradation.....	64
Table 4.2: Aggregate characteristics.....	65
Table 4.3: Filler characteristics.....	65
Table 4.4: Properties of bitumen binder class C320 .....	66
Table 4.5: Properties of Multigrade 1000/320 bitumen binder.....	66
Table 4.6: Properties of Polymer Modified bitumen binder (PMB-A5S).....	66
Table 4.7: Properties of liquid glass epoxy resin .....	68
Table 4.8: Strain gauge specifications .....	69
Table 4.9: Details for MCDC test.....	73
Table 5.1: Air voids measurement laboratory techniques.....	82
Table 6.1: Some of the asphalt creep test advancements from 1970 to date for the universal testing system.....	94
Table 6.2: Three selected samples to compare one stage creep test with MCDC test under different stress levels.....	97
Table 6.3: Material properties and test condition used in the FEM modelling.....	98
Table 6.4: Stress analysis of the FEM models in A row .....	102
Table 6.5: Stress analysis of the FEM models in B row .....	103
Table 6.6: Stress analysis of the FEM models in C row .....	104
Table 6.7: Comparison between confined stresses in the first stage of MCDC test: in the lab and FEM model.....	106
Table 6.8: MCDC test condition for sample 51M in three stage .....	106
Table 6.9: Comparison between confined stresses: in the lab and FEM model for sample 51M in three stage.....	106
Table 6.10: Creep slope vs cycle range.....	110
Table 6.11: Secant creep slope between 20,000 and 40,000 cycles.....	111

Table 6.12: Material properties and test condition of 51M sample .....	111
Table 6.13: Difference between regression model prediction and real data .....	113
Table 6.14: Selected multigrade sample .....	115
Table 6.15: Calculation of creep life for sample 83C .....	120
Table 7.1: Selected samples for MCDC test .....	124
Table 7.2: Linear regression equation between permanent strain and air voids .....	125
Table 7.3: The slope from the linear regression equations between permanent strain after 20,000 cycles and air voids for conventional asphalt .....	126
Table 7.4: Linear regression between secant creep slope (40,000 and 100,000 cycles) and air voids for conventional bitumen.....	128
Table 7.5: Slope calculated from linear regression between secant creep slope (40,000 and 100,000 cycles) and air voids for conventional bitumen .....	128
Table 7.6: Linear regression equation between permanent strain and air voids for multigrade asphalt .....	129
Table 7.7: The slope from the linear regression equations between permanent strain after 20,000 cycles and air voids for multigrade asphalt.....	129
Table 7.8: Linear regression between secant creep slope (40,000 and 100,000 cycles) and air voids for conventional bitumen.....	131
Table 7.9: Slope calculated from linear regression between secant creep slope (40,000 and 100,000 cycles) and air voids for conventional bitumen .....	131
Table 7.10: Linear regression equation between permanent strain and air voids for polymer modified asphalt.....	132
Table 7.11: The slope from the linear regression equations between permanent strain after 20,000 cycles and air voids for polymer modified asphalt .....	133
Table 7.12: Linear regression between secant creep slope (40,000 and 100,000 cycles) and air voids for conventional bitumen .....	134
Table 7.13: S Slope calculated from linear regression between secant creep slope (40,000 and 100,000 cycles) and air voids for conventional bitumen.....	134
Table 7.14: Ranking asphalt mixes based on two methods under varying operational conditions.....	135
Table 9.1: Available international tests to measure resilient modulus.....	144
Table 9.2: Selected samples for assessing load cycle in compressive resilient modulus results .....	146
Table A.1: A comparison of empirical test methods for evaluation permanent deformation of asphalt mixtures .....	Appendix-1
Table A.2: A comparison of fundamental test methods for evaluation permanent deformation of asphalt mixtures.....	Appendix-1

Table A.3: A comparison of Simulative test methods for evaluation permanent deformation of asphalt mixtures ..... Appendix-3

Table A.4: A comparison of Simulative test methods for evaluation permanent deformation of asphalt mixtures ..... Appendix-5

Table F.1: Test results related to the asphalt mix manufactured by C320 ..... Appendix-28

Table F.2: Test results related to the asphalt mix manufactured by M1000 ..... Appendix-29

Table F.3: Test results related to the asphalt mix manufactured by PMB ..... Appendix-30

## ABBREVIATIONS

ALF	Accelerated Loading Facilities
APT	Accelerated Pavement Tester
AV	Air Voids
AS	Australian Standard
BCC	Brisbane City Council
BS	British Standard
C	Conventional Bitumen
CDCT	Confined Dynamic Creep Test
CV	Coefficient of Variation
DEM	Discrete Element Method
DGA	Dense Grade Asphalt
EN	European Standard
FHWA	Federal Highway Administration
FEL	Fatigue Endurance Limit
FEM	Finite Element Modelling
GGA	Gap Grade Asphalt
ICT	Information and Communications Technology
LG	Liquid Glass epoxy resin
LLAP	Long Life Asphalt Pavement
IPC	Industrial Process Controls
M	Multigrade Bitumen
MCDC	Multistage Confined Dynamic Creep
M-E	Mechanistic-Empirical
NCHRP	National Cooperative Highway Research Program
OBC	Optimum Bitumen Content
OGA	Open Grade Asphalt
PAV	Pressure Ageing Vessel
PG	Performance Grade
PMB	Polymer Modified Bitumen
Q	Queensland Department of Transport and Main Roads
RLPD	Repeated Load Permanent Deformation
RLT	Repeated Load Triaxial test
SMA	Stone Mastic Asphalt
TRLPD	Triaxial Repeated Load Permanent Deformation

URL	Uniaxial Repeated Test
UTM	Universal Testing Machine
UTS	Universal Testing Machine
UV	Ultraviolet
UVA	Ultraviolet radiation between 400-320nm wavelength
UWT	Ultrasonic Wave Transmission
VFB	Voids Filled with Bitumen
VIM	Voids In the Mix
VMA	Voids In Mineral Aggregate
WMAPT	Weighted Mean Annual Pavement Temperature

## CHAPTER 1

### INTRODUCTION

#### Contents

1.1	Introduction .....	2
1.2	The research hypothesis .....	6
1.3	The Scope of the Study .....	6
1.4	Research plan .....	8
1.5	Format of the thesis .....	9
1.6	Summary .....	11

## 1.1 Introduction

One of the major distress modes of flexible pavements is creep deformation, also known as rutting or permanent deformation (illustrated in Figure 1.1). Creep deformation of a flexible pavement can be described as the time-dependent accumulation of strain generated by repeated traffic loads, which is normally due to the insufficient stability of pavement related to the prevailing traffic loading and environmental conditions (Steyn 2012). The continuing growth in the magnitude of vehicle axle loads and reduction in vehicle speeds as a result of high traffic levels in cities especially in hot and moderate climate zones exacerbates the issue. Creep deformation is a major factor that must be considered by road authorities designing flexible pavements for a predicted service life (Öztürk 2007).



Figure 1.1: Severe creep deformation on flexible pavement (Pavement interactive 2012)

Historically a variety of tests have been developed and employed to investigate the creep deformation potential of asphalt concrete mixtures by simulating in-situ creep deformation in the laboratory. These tests may be broadly classified as empirical, fundamental and simulative (Ahmadinia et al. 2014). Creep deformation is a complex phenomenon and any laboratory test must be able to accurately simulate the in-situ pavement conditions by considering all design parameters including ambient temperature, dynamic loads (magnitude, pulse shape and duration), lateral confinement stress, material properties, and asphalt mix design (Kandhal & Cooley

2003). The research has shown that only a fully simulative creep deformation test, such as an accelerated pavement testing facility (ALF), is currently able to consider most of the required parameters (Witczak et al. 2013). However, such full scale testing is time consuming, expensive and not widely available worldwide. Researchers and practitioners have been trying to optimise the currently available cost effective, but empirical laboratory tests to simulate and predict the creep deformation of asphalt pavements. The key challenges in developing a laboratory test that better represents field conditions include providing a stress dependent confinement system, evaluation of air voids at critical stress/strain locations and producing sample consistency.

Providing effective lateral confinement stress (Figure 1.2) is one of the key challenges when modelling creep deformation in the laboratory. In simple terms, in-situ asphalt is surrounded by a mass of asphalt, which provides some stress-strain generated lateral confinement under axle loads. In other words, asphalt exhibits some stress dependency. Among the available and proposed tests, some are able to provide a lateral confinement stress (dynamic and static) by varying techniques including water pressure, air vacuum, and air pressure, or using an unconfined annulus of asphalt around the sample (Zargar et al. 2017 a).

Some of the well-known laboratory tests in this area are the Wheel Tracker, Hamburg, triaxial dynamic modulus and the confined dynamic creep test. The confining conditions provided by these tests generally do not vary in response to the load-unload cycle of each load pulse as experienced within actual pavements. A recent test methodology proposed by Ahmadiania (2017), better duplicates the confinement situation seen in the field by allowing a confined asphalt sample to respond to the applied stresses. The test uses a layered confinement methodology, where the asphalt being subjected to load is supported by an asphalt annulus, which in turn is supported by a polymer ring. The asphalt annulus allows the sample to undergo plastic deformation while the polymer ring provides a confining hoop stress that is generated by the load pulse.

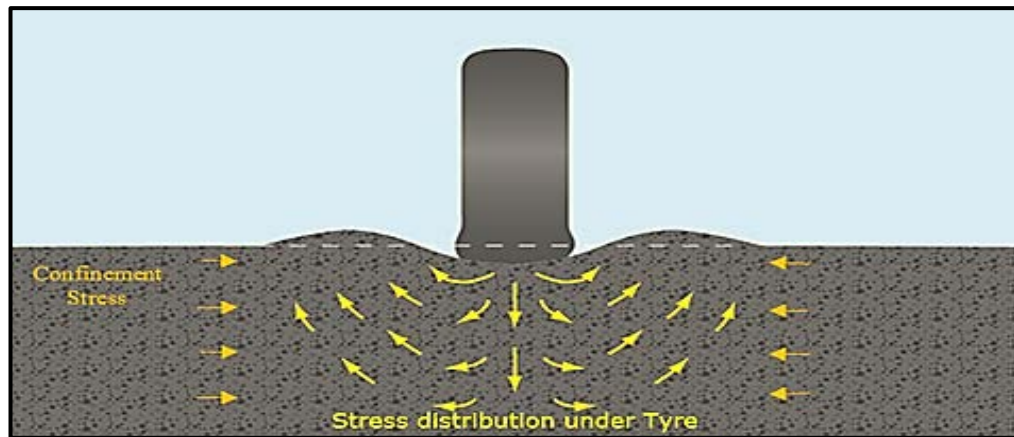


Figure 1.2: Creep deformation of asphalt and creep distribution (Pettersson, 2014)

A second key challenge in designing and assessing creep deformation characteristics in the laboratory is the control and measurement of air voids and their distribution (Figure 1.3) in laboratory asphalt samples (Zargar et al. 2017b). Air voids below a minimum specification limit may lead to excessive creep (rutting) while high air-voids content can also lead to creep deformation in the early life of the pavement due to post placement compaction (Roy et al. 2013). The measurement of air voids and their distribution in laboratory testing samples in critical locations is essential.

However, there is limited past research about creep deformation sensitivity to air voids and their distribution in laboratory samples. The new test methodology proposed by Ahmadinia (2017) provides an ability to assess the creep air voids sensitivity of asphalt during its life because the applied confinement system controls any crack propagation due to sample splitting. However, the work by Ahmadinia used bulk air voids as a test variable rather than air voids under the test platen. The current research has developed an alternative method for air voids that allows a more exact evaluation of air voids at critical locations.

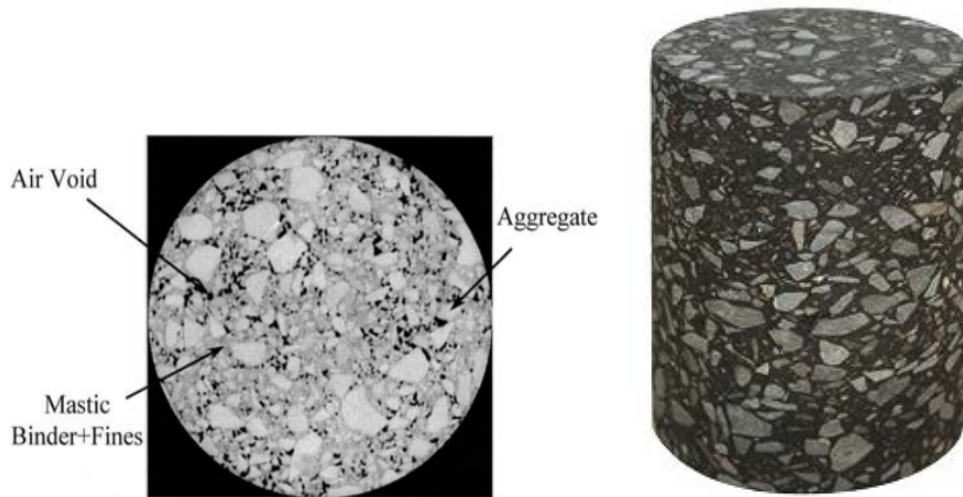


Figure 1.3: Asphalt structure (Tashman et al. 2002)

A third key challenge in designing a suitable test to measure creep deformation is the difficulty of producing asphalt samples with consistent structural composition. Since asphalt is a non-homogenous material made of aggregate, binder, filler, additives and air voids (Figure 1.3), production of consistent test specimens is difficult and can have a significant effect on the results produced in creep deformation tests. Introducing a test protocol using multi-stage testing of a sample means that sample structure does not vary and provides the ability to assess other important parameters. Repeated load triaxial (RLT) testing has been widely used for unbound materials (Arnold and Werkemeister 2010) to successfully generate creep deformation stages under increasing loads. Combining the test methodology proposed by Ahmadinia (2017) and Arnold and Werkemeister (2010) provides an ability to introduce a new test protocol by using the same sample under different load conditions.

However, several questions have been raised about the possibility of considering these three key challenges in one test to investigate the sensitivity of asphalt creep deformation to variations of temperature, air voids, load, and binder types and to predict the creep development in asphalt. It is hypothesised that by introducing a new test methodology the sensitivity of creep deformation to changes of several major parameters can be established, which allows for much better prediction of creep resistance and creep life in the laboratory.

## **1.2 The research hypothesis**

The research hypothesis in this study is:

*“The Australian dynamic creep test can be redesigned to enable multistage evaluation of creep life of asphalt mixtures under varying operational conditions”*

This research has three main aims that underpin the critical examination of the hypothesis. The first aim is to optimise the Australian creep test, by introducing a multistage confined dynamic creep (MCDC) test which reuses the same sample under different stress levels. The MCDC test is also explored for its use in evaluating the compressive resilient modulus of asphalt. The second aim is to evaluate the sensitivity of the creep deformation of asphalt mixture to variations in the major parameters of air voids, ambient temperature, stress levels, and material properties. The third aim is to develop a creep life prediction method using the MCDC test.

## **1.3 The Scope of the Study**

The study developed a new proposed Australian confined dynamic creep test which provides a close replication of field conditions. The sensitivity of creep deformation of asphalt mixtures under various environmental and design conditions such as varying temperature, traffic load, and air voids is evaluated using the new proposed test. The ranges of the variables in this study were as follows:

- Air voids – variation between 0% and 9%
- Temperature – 40 °C and 50 °C
- Tyre pressure – variation between 500kPa and 1000kPa

The research was a multivariable study to introduce a new creep test considering changes in tyre pressure, air voids and temperature on creep performance and development. The results of the research will be of use to road agencies and the asphalt industry to provide a more accurate prediction of the creep deformation of asphalt pavement and also to provide an improved prediction of design life of an asphalt pavement based on the creep test.

In the first stage of the research, an ultrasonic transmission technique was introduced as a new non-destructive method of air voids measurement for laboratory asphalt

samples. The method was applied to better evaluate the effect of air voids in the creep deformation of asphalt.

The second stage of the study focussed on modernising the existing Australian dynamic creep test in order to introduce a more accurate and cost effective version of the test to be able to assess creep deformation at various stress levels. Optimization of this test started previously by Bullen and Preston (1992) and followed by Austroads (Oliver et al. 1995) by using a platen of smaller diameter than the sample in order to provide quasi-confining stress to better replicate field condition. In 1998, a similar approach was used by Nunn et al (1998) to extend the Nottingham asphalt tester using a 96mm diameter platen with 150mm diameter specimen (EN1297-25A). The latest research by Ahmadinia (2017), in Australia, optimised the European standard and solved the reported problem regarding the bursting (i.e. radial splitting) of asphalt samples by using a layered confinement method for test samples. Their research showed promising results to model the in-situ creep deformation condition by introducing dynamic confined creep testing.

The present study focused on optimising the latest research and introduced a multistage confined dynamic creep test capable of investigating the creep deformation of asphalt mixtures under various stress levels using only one sample. The method proved to be cost effective and also increased the accuracy of testing by solving the problem of reproducing the same non-homogenous asphalt material in different samples.

In the third stage, the creep life prediction using a new proposed multistage dynamic creep test is discussed. The Creep life prediction of some Australian asphalt mixes was assessed and a suitable creep resistance mix for different climatic zones in Australia was introduced.

In the fourth stage, the modulus measurement techniques of asphalt were reviewed and the modulus measured using the MCDC test under various operational conditions. The effect of traffic loads, temperature and air voids on modulus of asphalt was also considered.

## 1.4 Research plan

The research consisted of an embedded extensive literature review, extensive laboratory studies and numerical and mathematical modelling. The literature review encompassed:

- The Austroads flexible pavement design for heavy traffic roads and associated challenges,
- The creep deformation mechanisms of asphalt, available tests, limitations and the main challenges for designing a more a realistic creep test,
- Creep life prediction methods.

The extensive laboratory studies were:

- To design a laboratory non-destructive technique able to measure air voids distribution in asphalt samples.
- To develop a laboratory confined dynamic creep test capable of assessing the creep deformation of an asphalt mixture under different stress levels.

The numerical and mathematical modelling involved:

- Validating and assessing the stress distribution in MCDC test asphalt samples,
- Developing a creep life prediction method using the proposed multistage confined dynamic creep test.
- Assessing the sensitivity of creep deformation of some asphalt mixtures under various environmental and design conditions using MCDC test
- Predict the creep life of some asphalt mixtures using the proposed MCDC test.

A schematic of the overarching research plan is shown in Figure 1.4.

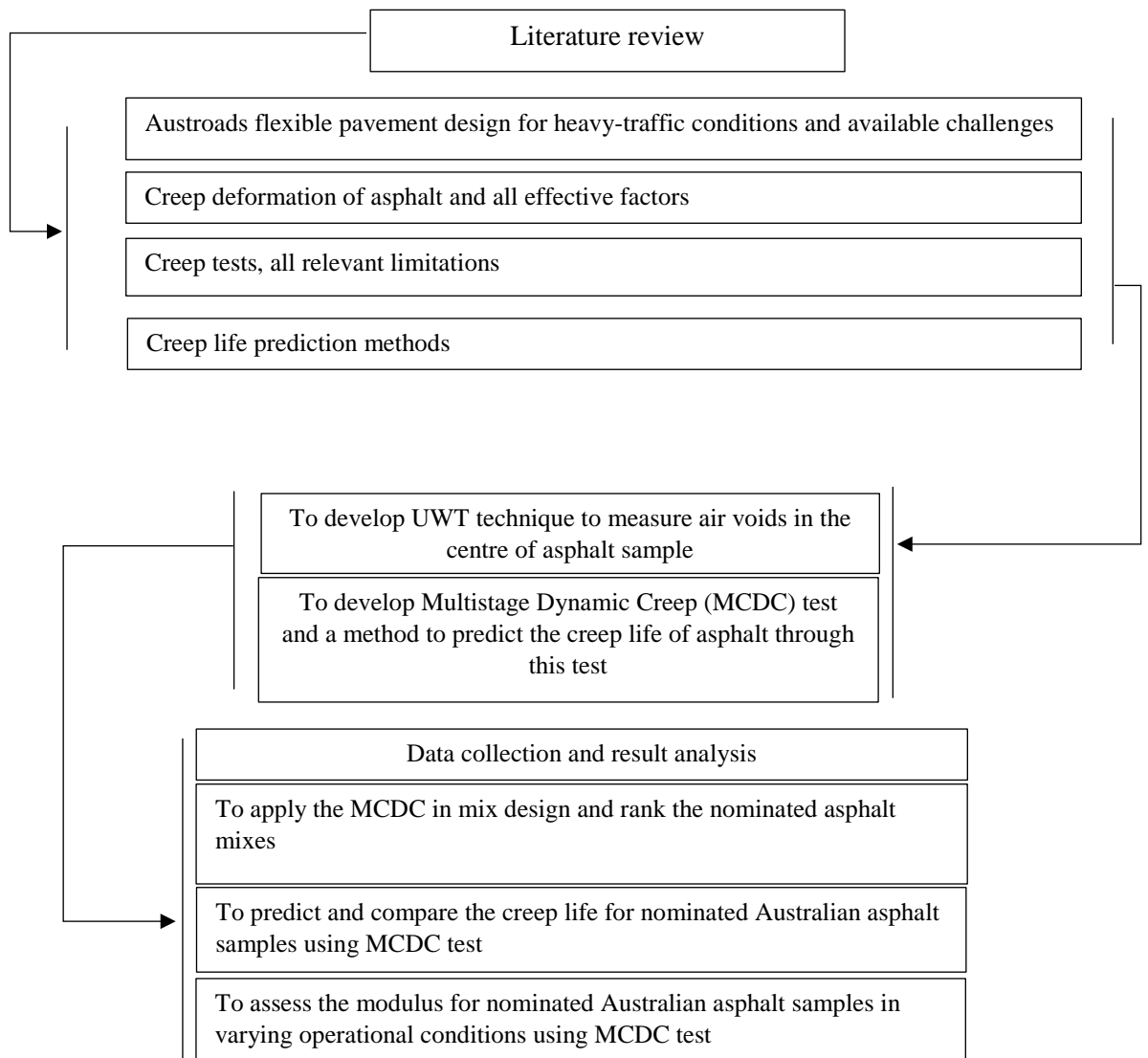


Figure 1.4: Research plan

## 1.5 Format of the thesis

The research is presented in the thesis as follows:

- Chapter one: The topic and scope of the study are introduced in this Chapter, along with the research hypothesis and the underpinning research aims,
- Chapter two: This Chapter is an overview of Austroads heavy-traffic flexible pavement design and the relevant challenges.
- Chapter three: This Chapter reviews literature on the creep deformation of asphalt, relevant effective environmental and design factors and available tests

to measure this type of distress. Here, several mathematical models for explaining creep behaviour of asphalt in the laboratory and in the field are presented. Review of the main challenges including confinement situation, multi-stress application, air voids distribution and temperature is covered in this Chapter.

- Chapter four: This Chapter provides details of the experimental work, numerical and mathematical models undertaken as follows:
  - Material details and asphalt sample fabrications.
  - Research methodology for the development of ultrasonic transmission techniques to assess the air voids content and distribution in the laboratory asphalt samples.
  - Research methodology for the development of the latest Australian confined dynamic creep test (CDCT) to be able to assess creep deformation under various stress levels on one sample and consequently introducing Multistage Confined Dynamic Creep test (MCDC) test.
  - Research methodology for the development of a creep life prediction model using MCDC test.
- Chapter five: This Chapter considers the development of ultrasonic transmission techniques to assess the air voids content and distribution in the laboratory asphalt samples.
- Chapter six: This Chapter considers the validation and development of the latest Australian confined dynamic creep test (CDCT) to be able to assess creep deformation under various stress levels on one sample and consequently introducing MCDC test. A creep life prediction method is also proposed in this Chapter using the developed MCDC test.
- Chapter seven: This Chapter considers the effect of operational parameters including temperature, air voids, bitumen binder types, and stress level on creep deformation.
- Chapter eight: This Chapter compares and evaluates the creep life of applied asphalt mixtures under varying operational conditions.
- Chapter nine: The methods for measuring the modulus of asphalt at elevated temperatures and stresses is discussed in this chapter. This Chapter also

analyses the modulus of nominated Australian asphalt mixes at elevated temperatures using the MCDC test.

- Chapter ten: In this Chapter, the main findings of the study are presented. A summary of study outcomes with some recommendations for further work are also included.

## **1.6 Summary**

Creep deformation is one of the main distress modes seen with flexible pavements with thick asphalt surfacing. Creep can result in an irregular pavement surface that has undesirable effects on serviceability, including road safety. Maintenance of pavements that are subject to creep deformation is expensive and can cost road agencies millions of dollars annually (Sohm et al. 2012). A more accurate methodology for the assessment of the creep potential of an asphalt, under varying operational conditions, within the laboratory, has significant global application. The work described in this thesis has resulted in very significant progress in that research space.

## CHAPTER 2

### AUSTRALIAN FLEXIBLE PAVEMENTS FOR HEAVY-TRAFFIC ROADS

#### Contents

2.1	Introduction .....	13
2.2	Flexible pavements – materials and structures.....	13
2.3	Asphalt mix design for flexible pavements.....	17
2.4	Flexible pavement distress .....	19
2.5	Flexible heavy-traffic pavement structural design .....	21
2.6	Asphalt modulus – measurement and temperature effects.....	23
2.6.1	Measurement of modulus of asphalt .....	25
2.6.2	Temperature and modulus.....	26
2.7	Flexible pavement service life.....	28
2.7.1	Fatigue.....	29
2.7.2	Creep .....	29
2.8	Summary .....	31

## 2.1 Introduction

Flexible pavements, containing an asphalt surface and unbound granular base and/or subbase layers, are widely employed in Australia and throughout the world for the following reasons (Austroads 2012):

- Good riding quality
- Usually much cheaper to construct in comparison to concrete rigid pavements.
- Can be constructed in stages
- Cheaper regarding maintenance and access to underground services

A flexible pavement is normally arranged in the form of consecutive layers of carefully selected materials (Figure 2.1) that are designed to gradually distribute loads from the pavement surface through the pavement layers to the underlying subgrade. Correct design ensures that the load transmitted to each successive lower layer does not exceed that layer's load-bearing capacity (Austroads 2014). The maximum load-bearing capacity of each layer of the flexible pavement is a function of its mechanical properties, such as stiffness and stress dependency, and thickness.

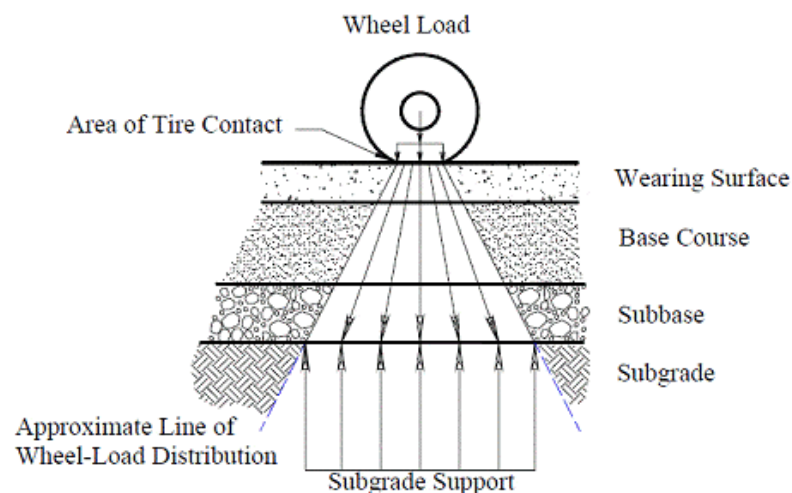


Figure 2.1: Distribution of load stress in flexible pavement (Composition and Structure of Flexible Pavements 2017)

## 2.2 Flexible pavements – materials and structures

Typically, a flexible pavement includes several layers with different material components as shown in Table 2.1. Flexible pavement materials can be classified into essentially four categories according to their fundamental behaviour under the effects

of applied loadings. Thick asphalt surfacing must be capable of good creep resistance to provide adequate functional service.

- asphalt
- unbound granular materials
- modified granular materials
- bound materials-stabilised materials

Material types, behaviour characteristics, and distress modes related to the above categorised materials are shown briefly in Table 2.2.

Table 2.1: Flexible pavement layers and materials (Austroads 2014)

		Application	Materials
1	Surface course	To deliver functional and structural performance depending on the thickness	A mixture of bituminous binder and several, typically, single sized aggregate fractions.
2	Tack coat	To bind two asphalt layers	Binder.
3	Binder course	To deliver structural performance depending on the thickness	A mixture of bituminous binder and several, typically, single sized aggregate fractions.
4	Prime coat	To bind asphalt layer to base course	Binder.
5	Base course	Main load carrying course	Composed of granular material sometimes mechanically stabilised or treated with cement or binder.
6	Sub-base course	Load carrying course to provide support to the base and to reduce the Stress/stains applied to the subgrade	Composed of lower quality granular material. Sometimes mechanically stabilised or treated with cement or binder
7	Sub-grade	To provide sufficient support for the upper layer. It can be either compacted or natural.	In-situ materials. Sometimes mechanically stabilised or treated with cement or lime.

Depending on the design parameters (traffic, environment, and cost), an asphalt surface course can be one of the following asphalt mixtures: Dense Graded Asphalt (DG), Stone Mastic Asphalt (SMA), or Open Graded Asphalt (OGA). The difference in the asphalts relates to the aggregate gradation, shape, size and also binder content and type. The selection of the best surface course is discussed in detail in Austroads (2009).

Table 2.2: Pavement material categories and characteristics (Austroads 2014)

Characteristics	Unbound granular	Modified granular	Bound	
			Stabilised	Asphalt
<ul style="list-style-type: none"> <li>Material types</li> </ul>	<ul style="list-style-type: none"> <li>crushed rock</li> <li>gravel</li> <li>soil aggregate</li> <li>mechanically stabilised materials</li> </ul>	<ul style="list-style-type: none"> <li>chemically modified materials</li> <li>cement, lime, lime/fly ash or slag modified materials</li> </ul>	<ul style="list-style-type: none"> <li>lime stabilised materials</li> <li>cement stabilised materials</li> <li>bitumen binder stabilised materials</li> <li>lime/fly ash stabilised materials</li> <li>slag stabilised materials</li> <li>slag/lime stabilised materials</li> </ul>	<ul style="list-style-type: none"> <li>dense graded asphalt</li> <li>open graded asphalt</li> <li>stone mastic asphalt</li> </ul>
<ul style="list-style-type: none"> <li>Behaviour characteristics</li> </ul>	<ul style="list-style-type: none"> <li>development of shear strength through particle interlock</li> <li>no significant tensile strength</li> </ul>	<ul style="list-style-type: none"> <li>development of shear strength through particle interlock</li> <li>no significant tensile strength</li> </ul>	<ul style="list-style-type: none"> <li>development of shear strength through particle interlock</li> <li>significant tensile strength</li> </ul>	<ul style="list-style-type: none"> <li>development of shear strength through particle interlock and cohesion</li> <li>significant tensile strength</li> <li>properties are temperature sensitive</li> </ul>
<ul style="list-style-type: none"> <li>Distress modes</li> </ul>	<ul style="list-style-type: none"> <li>deformation through shear and densification</li> <li>disintegration through the breakdown</li> </ul>	<ul style="list-style-type: none"> <li>deformation through shear and densification</li> <li>disintegration through the breakdown</li> </ul>	<ul style="list-style-type: none"> <li>cracking developed through shrinkage, fatigue and over-stressing</li> <li>erosion and pumping in the presence of moisture</li> </ul>	<ul style="list-style-type: none"> <li>cracking developed through fatigue, overloading</li> <li>permanent deformation</li> </ul>

Depending on the material types and thicknesses of the layers, flexible pavements can be categorised as follows (Austroads 2014):

1. Unbound granular pavement with thin asphalt surfacing
2. Unbound granular pavement with thick asphalt surfacing
3. Deep strength asphalt
4. Full depth asphalt

An indication of flexible asphalt courses and pavement types is provided in Figure 2.2. Excluding the pavement with thin surfacing, other types can be used for heavy-traffic roads.

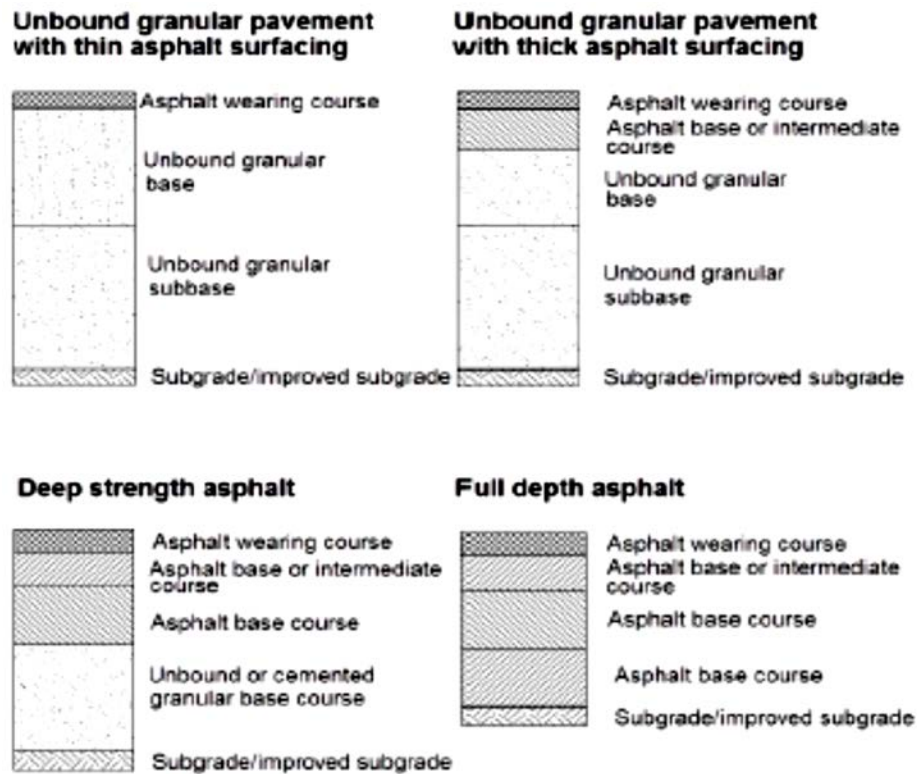


Figure 2.2: Types of flexible pavement based on the materials and thicknesses of the layer (Austroads 2014)

From the first to the fourth types of the illustrated flexible pavements, the thickness and number of asphalt layers increase respectively. The thin asphalt surfacing pavement has a single asphalt layer and the full depth asphalt pavement usually has the greatest number of layers. For some heavily trafficked asphalt pavements, a high binder content asphalt fatigue layer at the bottom of a full depth asphalt pavements must be used (Austroads 2012).

Some advantages of using more asphalt layers in the structure of flexible pavement are summarised as follows:

- Greater speed of construction

- Having a lower risk of water damage in early stages because of having waterproof courses on lower layers
- Reducing the risk of structural deterioration due to moisture infiltration into base and subbase materials
- Low construction and maintenance costs during the pavement service life

This type of pavement can be designed as long-life pavement subject to periodic replacement of the wearing courses.

As discussed above, having more asphalt layers can be beneficial for road authorities in different ways. However, application of more asphalt layers in the pavement structure means having more binder in that pavement. Binder is a viscoelastic material which is load and temperature sensitive. Consequently, more attention should be given to the design and maintenance stages of this type of pavement, particularly where elevated temperatures and traffic loads are likely to occur.

### **2.3 Asphalt mix design for flexible pavements**

While asphalt may be described as a simple mixture of coarse and fine aggregate, filler, and binder, its design can be a complex process that may entail high creep resistance. The asphalt mix design involves the best choice of aggregate type, aggregate grading, binder type, and determination of binder content that will optimise the engineering properties in relation to the desired behaviour in-service (Austroads 2014). After ensuring good properties for each material, asphalt mix design normally follows the basic steps as shown in Table 2.3. The Austroads (2014) mix design for heavy-traffic dense graded asphalts is defined according to Figure 2.3 where creep potential (deformation resistance) is evaluated using wheel tracking.

Even a well-designed asphalt mix may exhibit a broad range of distresses during its service life (Preston 1991). A well designed and compacted asphalt mix in a flexible pavement structure must provide:

- The ability to distribute stresses caused by traffic loads
- Resistance to cracks: fatigue, thermal, and reflective cracks
- Resistance to permanent deformation
- Resistance to moisture and freeze-thaw damage.

To better understand the flexible pavement performance, the exhibited distresses will be discussed in the next section in more detail.

Table 2.3: Basic steps of asphalt mix design

1	Mix type selection	One of the following mix types based on design parameters: <ul style="list-style-type: none"> <li>• DGA</li> <li>• SMA</li> <li>• OGA</li> <li>• GGA</li> </ul>
2	Component materials' selection	Based on mix type selection and material test results
3	Combination of aggregate to reach a suitable design grading	
4	Selection of suitable binder type and content	One of the following bitumen binders based on design parameters: <ul style="list-style-type: none"> <li>• Conventional bitumen</li> <li>• Multigrade bitumen</li> <li>• Polymer modified bitumen</li> </ul>
5	Compaction of the asphalt mix to obtain in service conditions	Using one of the compactors: <ul style="list-style-type: none"> <li>• Shear box compactor</li> <li>• Gyrotory compactor</li> <li>• Marshall compactor</li> </ul>
6	Measurement of the volumetric properties	Optimise the volumetric properties based on: <ul style="list-style-type: none"> <li>• Bulk density</li> <li>• Maximum density</li> <li>• Void in mineral aggregate</li> <li>• Void in the mix</li> <li>• Absorbed binder</li> <li>• Void filled with binder</li> <li>• Void filled with bitumen</li> <li>• Binder film thickness</li> </ul>
7	Mechanical testing of compacted samples	Compare the final mix using these tests: <ul style="list-style-type: none"> <li>• Fundamental tests for stiffness and fatigue</li> <li>• Simulative tests for resistance to deformation and moisture damage</li> <li>• Empirical tests for design of asphalt mix</li> </ul>
8	Mix job selection	Based on conclusion from stages 1 to 7

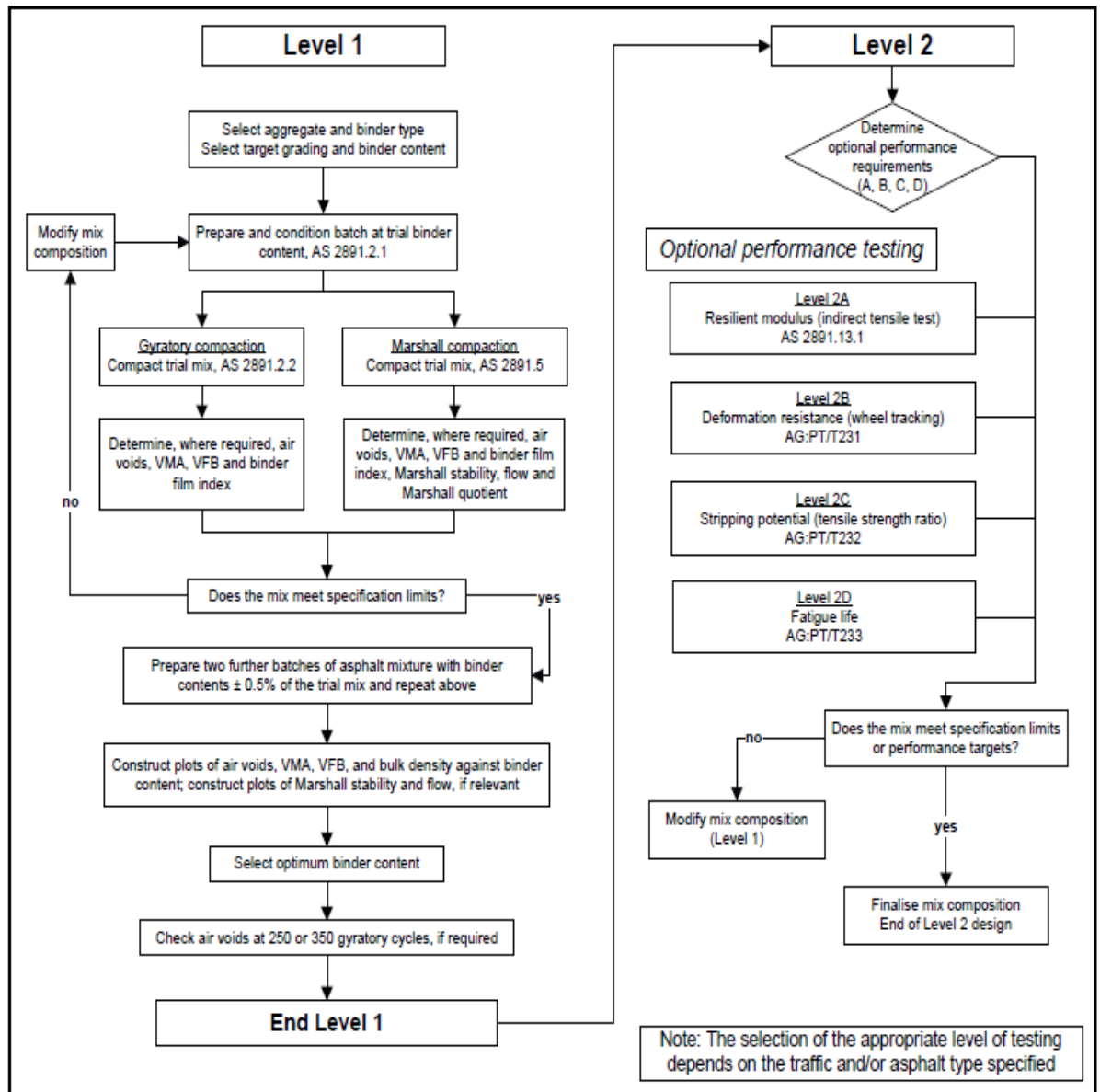


Figure 2.3: Dense grade asphalt mix design procedure (Austroads 2014)

## 2.4 Flexible pavement distress

Flexible pavements can exhibit various types of distress (Table 2.4) during their service life. Flexible pavement deterioration can occur for any of the following reasons:

1. Temperature fluctuations
2. Weather conditions
3. High axle/wheel loads
4. Construction deficiencies
5. Improper material and mix design

Pavement distresses and possible causes are listed in Table 2.4. The well-known modes of structural distress for thick asphalt surfacing are fatigue and creep deformation (rutting).

Current pavement design models appear able to predict and thus control tensile fatigue (perhaps excluding top-down fatigue cracks) (Sullivan 2015; Austroads 2012). However, creep deformation (rutting) largely is addressed through mix design rather than mechanistic modelling. The reasons provided by Austroads (2012) is that no model is available that can reliably predict the development of creep deformation with the passage of traffic/time.

Table 2.4: Flexible pavement distresses and the possible reasons (Ahmadinia 2017)

Type of distress	Possible reasons
Fatigue cracking	Heavy and repeated wheel loads in cold climate
Edge cracking	Insufficient lateral support from the shoulder, inadequate drainage, and growing vegetation around the edge of pavement
Block cracking	Shrinkage due to temperature fluctuations and stiff pavement surface
Longitudinal and transverse cracking	Harsh climates, shrinkage in asphalt mixes, poor constructions and underlying layer cracks
Slippage cracking	Poor bonding between pavement layers and materials
Ravelling	Poor quality of the mixture and excessively stiff bitumen binder
Potholes	Can be a continuation of other deterioration of the pavement such as fatigue cracks and ravelling over a long period of time
Stripping	Loss of adhesion between the bitumen binder and aggregate due to moisture
Bleeding	Excessive binder content in the mixture
Creep deformation (Rutting)	Elevated temperature, air voids, and load

One challenge identified by Austroads (2012) is the difficulty to predict the highest pavement temperature when the asphalt is highly prone to deform. The reason provided by Austroads (2012) is that:

“During the service life of asphalt layer in a road pavement, a very significant proportion of the accumulated permanent deformation in the asphalt layer will have occurred during the very rare times when the asphalt is at a highly elevated temperature. For asphalt layers to reach such

elevated temperatures (throughout the layer) requires a succession of very hot, clear days and accompanying hot nights. Prediction of the occurrences of such weather patterns during the service life of the asphalt can be extremely difficult. Likely problem areas are those associated with heavy vehicles travelling at low speed or accelerating or braking (climbing lanes, intersections, etc.)”.

A second challenge noted by Ahmadinia et al. (2017) is the lack of availability of reliable creep tests able to model the environmental and confinement situation in the laboratory. To be able to model the creep deformation of thick asphalt surfacing both of the above challenges must be considered.

## **2.5 Flexible heavy-traffic pavement structural design**

The following flexible pavements types incorporate thick asphalt surface layers where the temperature and load sensitive viscoelastic asphalt is subjected to axle loads and stresses that induce creep.

1. Unbound granular pavements with thick asphalt surfacing
2. Deep strength asphalt
3. Full depth asphalt

The Austroads (2012) pavement design procedure aim is provided below. The flexible pavement design procedure is shown in detail in Figure 2.3.

“To select the most economical pavement thickness and composition which will provide a satisfactory level of service for the anticipated traffic”.

One of the important stages in mechanistic pavement design is a structural design and stress/strain analysis in order to quantify the critical strains and/or stresses in the pavement. Usually the pavement is represented as a series of layers of different moduli subject to normal traffic loading as shown in Figure 2.4. The critical responses assessed for pavement and subgrade materials in a linear elastic model are as follows:

- Asphalt: horizontal tensile strain at bottom of layer
- Unbound granular: not consider in model
- Cemented: horizontal tensile strain at bottom of layer

- Subgrade: vertical compressive strain at bottom of layer

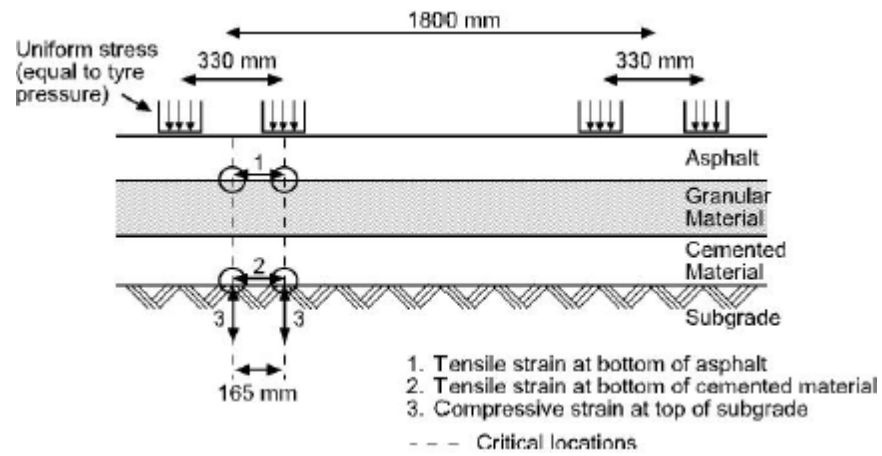


Figure 2.4: Pavement model for Mechanistic Design procedure (Austroads 2012)

Figure 2.5 illustrates the overarching concepts that must be explored during a design process. While creep performance is not explicitly addressed it is implicit in both pavement material and performance criteria.

- Mechanical behaviour of pavement materials under operational variables (loop one in Figure 2.5). For example, parameters such as elastic modulus (unbound or bound materials) are used in analytical models to determine load-induced stresses and strains, that is, pavement response to load.
- Pavement performance criteria under operational conditions (loop 2 in Figure 2.5). Pavement performance criteria are used only to predict when distress (rutting, cracking, etc.) will occur.

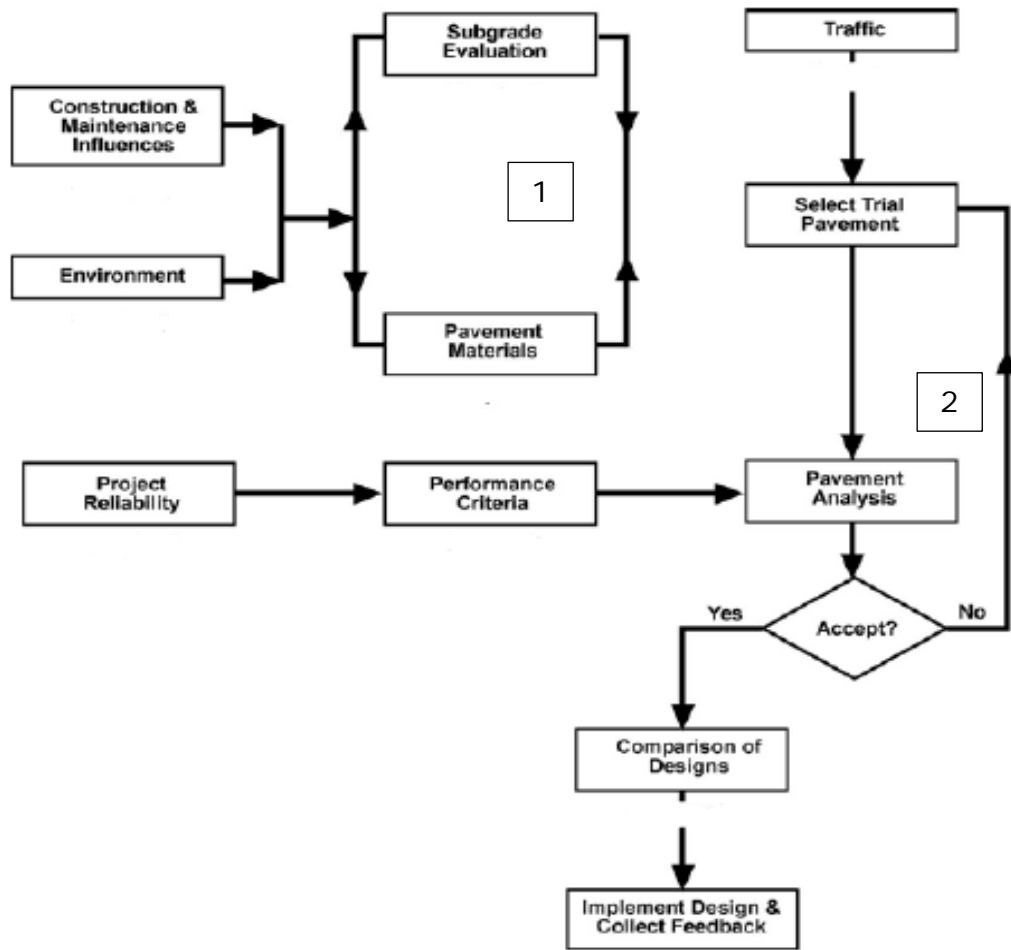


Figure 2.5: Design procedure for flexible pavement (Austroad 2012)

## 2.6 Asphalt modulus – measurement and temperature effects

The performance of any pavement material, including asphalt, is related to its modulus. Table 2.5 indicates that the current relevant performance criteria for asphalt is fatigue. There is no reference to creep.

Table 2.5: Pavement material input used in structural design (Austroads 2014)

Characteristics	Unbound granular	Modified granular	Bound	
			Stabilised	Asphalt
Input parameters for design	Modulus Poisson's ratio Degree of anisotropy	Modulus Poisson's ratio Degree of anisotropy	Modulus Poisson's ratio	Modulus Poisson's ratio
Performance criteria	Current material specifications	Current material specifications	Fatigue relationships	Fatigue relationships

The modulus of asphalt is one of the input parameters in analytical models for structural analysis of flexible pavements. The optimisation of modulus related to fatigue performance can impact significantly on creep performance. One aspect of the research undertaken here is to measure both creep and compressive resilient modulus simultaneously using a redesigned laboratory creep methodology. The following provides some contextual background related to asphalt modulus and its measurement.

The modulus of asphalt is a function of:

- Friction between the aggregate particles;
- The viscosity of the bitumen binder in varying operational conditions; and
- The cohesion within the composite material resulting from adhesion in the bitumen mastic and also between aggregate and bitumen binder.

The modulus of asphalt depends on the factors that are summarised in Table 2.6. The information provided is for asphalt mixtures manufactured using conventional bitumen. In addition to the mix design, and effective factors listed above according to Austroads (2012), there are some other important test related factors that influence the measurement of modulus in the laboratory. These effective factors are as follows: (and it is important to note that the last factor related to confinement is applicable for any modulus that might be measured during a creep test).

1. Load related factors: direction and platen.
  - The modulus of asphalt when the asphalt sample is subject to tensile loading is different to that for compressive loading.
  - The friction between loading platen and the surface of the specimen can affect the test results. It is also important to understand how the load distribution under the platen relates to the real situation.
2. Specimen size: specimen size has a direct effect on the asphalt modulus (Witczak & Kaloush 2000).
3. Confining stress: in-situ asphalt is surrounded by a mass of asphalt, which provides stress-strain generated lateral confinement under axle loads. This lateral confinement stress needs to be provided in laboratory tests. (Majid et al. 2017).

Table 2.6: Factors affecting on modulus of asphalt (Austroads 2012)

Factor	Effect of increasing factor
Proportion of coarse angular particles	Increase
Density	Increase
Stress level	No change
Age	Increase
Extent of cracking	Decrease
Efficiency of mixing	Increase
Bitumen binder content	Increase then decrease
Bitumen binder class	Increase
Bitumen binder viscosity	Increase
Percent air voids	Decrease
Temperature	Decrease
Rate of loading	Increase

### 2.6.1 Measurement of modulus of asphalt

The current method of measuring flexural modulus is with the four point bending test AGPT/T274-2016, (Austroads 2016), which is used as a replacement for the resilient modulus. The use of the indirect tensile test (AS 2891.2.2 -1995) for measuring resilient modulus however remains an effective quality control tool for material evaluation under varying loading regimes. Both tests however have standard conditions with test temperature ( $25 \pm 0.5^{\circ}\text{C}$  for indirect tensile test and  $30 \pm 0.5^{\circ}\text{C}$  for four-bending test), stress levels (maximum of 200 kPa) and air voids ( $5 \pm 0.1\%$  for indirect tensile test and  $5 \pm 0.5\%$  for four-bending test). Both tests suffer from limitations of high stress levels and at high temperatures. The tests cannot be performed continuously in the noted situations and because of lack of confinement the sample will collapse.

Tests are not undertaken typically under any confining stresses and it has been reported by some researchers (Mamlouk & Sarofim 1998; Masada et al. 2004) that across the axial, diametrical and triaxial methods for resilient modulus measurement of asphalt, the triaxial test would be the best. This is because this type of test better represents the actual in-situ behaviour of asphalt. It is also due to the fact that at higher temperatures,

the modulus of asphalt largely relies on the aggregate structure and the level of confinement and samples are prone to collapse if unconfined.

In addition to the tests above, the dynamic modulus test (AASHTO TP62-07) is also used in Australian research (Sullivan 2015) to measure the modulus of asphalt and can meet the majority of the above challenges. The main issue regarding the dynamic modulus test is the type of applied confinement stress and the load waveform. The confining conditions provided do not vary in response to the load-unload stage of each load pulse as seen within real pavements (Ahmadinia 2017). The load wave form also is continuous in the dynamic modulus test while in real in-situ situations there is a loading and rest period (Zhou et al. 2010).

The development of the Confined Dynamic Creep Test (CDCT) approach by Ahmadinia (2017) provides a foundation to allow the development of a new methodology for evaluating compressive resilient modulus across a broad range of load-temperature environments, possibly within a staged confined creep test methodology.

### **2.6.2 Temperature and modulus**

For the asphalt layer in a flexible pavement, the temperature is a critical factor in the design procedure due to the viscoelastic behaviour of binder in the structure of asphalt mixtures. Mechanical properties of the asphalt layer are consequently a function of the binder temperature sensitivity.

The effect of temperature on asphalt mechanical properties can be summarised as follows:

- Asphalt becomes stiff and relatively brittle at low temperature. At this stage, asphalt is susceptible to fatigue cracking distress.
- In hot temperatures, asphalt becomes soft and viscoelastic and becomes susceptible to creep deformation distress.
- Temperature has a significant effect on the ageing of asphalt in the long term. It can lead to ravelling which affects pavement surface service life.
- Asphalt modulus increases with time because of ageing of the bitumen but asphalt modulus in it's early life is highly dependent on temperature and the asphalt is susceptible to creep deformation.

Historically for pavement design, the Weighted Mean Annual Pavement Temperature (WMAPT) was used by Austroads (2012) as the temperature to estimate the asphalt moduli at-service temperature. WMAPT considers the daily and monthly variation in pavement temperature but does not provide information on the extremes in temperature conditions (hourly temperature) to which an asphalt layer is subjected. It is also not able to provide information about the temperature distribution within the depth of the pavement (Austroads 2013).

A new model being developed by Austroads (2013) can better predict the pavement temperature from air temperature data. This model is able to predict temperature in any depth of asphalt pavement layer at anytime during a day. As an example, Figure 2.6 shows the diurnal temperature profile at different depths, predicted using weather station data from Canberra on a hot summer day using the Austroads model.

The WMAPT temperature of 23°C is the temperature to calculate the design moduli for a pavement in this area in accordance with Austroads (2012). As Figure 2.6 shows, there is a significant difference between this temperature and real measured hourly temperature data in each layer.

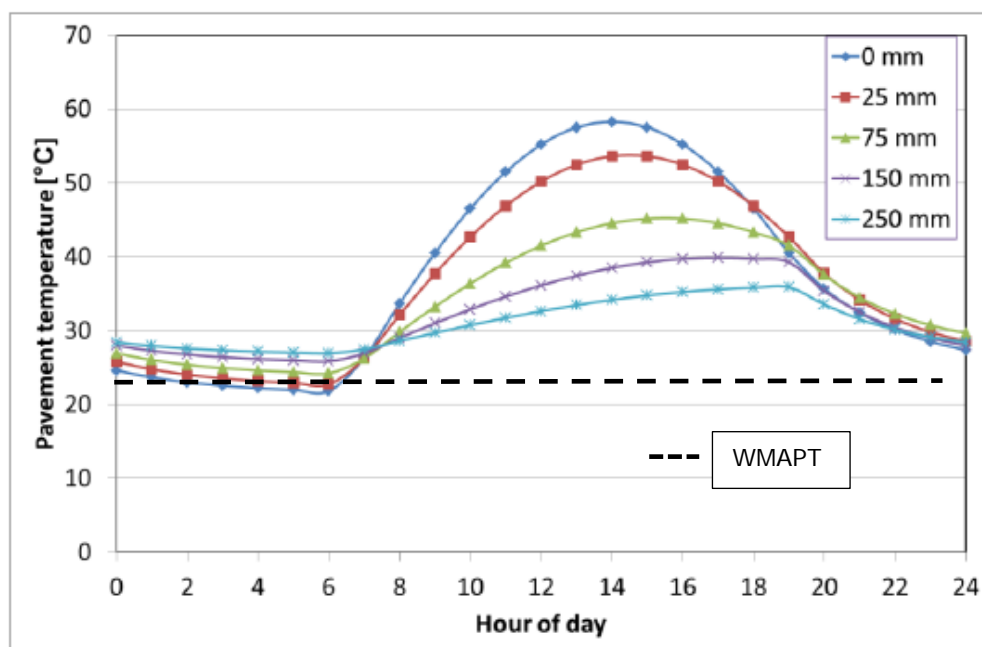


Figure 2.6: Temperature at depth predicted for hot summer day in Canberra (Austroads 2013)

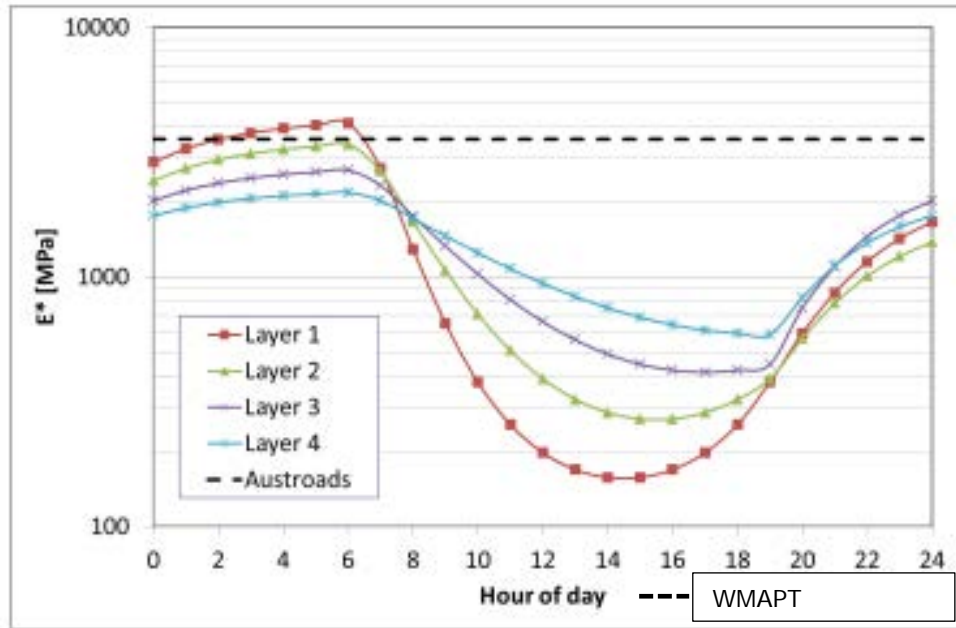


Figure 2.7: Modulus at depth for hot summer day, at 10km/h (Austroads 2013)

As explained earlier, the modulus of an asphalt layer is a direct function of temperature because of the viscoelastic nature of the binder in its structure. The corresponding moduli of different asphalt layers during a hot day in Canberra was estimated for vehicles with a velocity of 10 km/h using temperature profiles and the master curve related to the applied pavement (Austroads 2013). The estimated hourly moduli are shown in Figure 2.7. The results indicate that during hot summer days, the moduli of the asphalt pavement layers are consistently lower than the annual average value applied in the Austroads (2012) procedure.

This example illustrates the importance of the design temperature in the estimation and evaluation of moduli in the pavement design procedure. This is the situation in which the possibility of creep deformation will be increased and highlights the need for better information on the variation of resilient moduli with temperature under confined conditions.

## 2.7 Flexible pavement service life

The service life of a pavement may be defined as the time from construction to the first major structural rehabilitation or to when the pavement degrades to unacceptable serviceability condition (Von Quintus et al. 2005). The service life of a flexible

pavement is determined by the most common pavement defects such as fatigue cracks, creep deformation (rutting), and roughness (Austroads 2009).

### **2.7.1 Fatigue**

While fatigue life is not core to this research a brief description follows for completeness and context. Fatigue is considered in the structural design steps by designing the thickness of the layer based on the critical horizontal tensile strain at the bottom of the asphalt layer (Austroads 2012; Gupta & Adhikari 2016). If the critical horizontal strain is a strain level below fatigue endurance limit (FEL), damage to an asphalt mix does not appear to occur (Monismith & Mclean 1997). The pavement designed by this concept is a long-life asphalt pavement (LLAP). Well-designed long life asphalt pavement would not be expected to require major structural rehabilitation or reconstruction for at least 50 years (Newcomb et al. 2010). This type of pavement only needs periodic surface renewal in response to distress confined to the top of the pavement. Research conducted by Sullivan (2015) in Australia on the development of a long-life design procedure defines the fatigue endurance limit (FEL) for Australian pavements.

For heavy-traffic thick asphalt pavements, some researchers (Al-Qadi et al. 2008; Merrill, Van Dommelen & Gáspár 2006) have reported that cracking in this type of flexible pavement is normally confined to the pavement surface. It is due to the reduction in intensity of strains at the bottom of asphalt layer as a result of increasing the asphalt thickness.

### **2.7.2 Creep**

Creep deformation (rutting), which is a common distress type in flexible pavements, may be defined as “the surface depression in the wheel path which is accumulated total plastic deformation that develops in each of the pavement layers”. The shape of the asphalt surface is suggested by some researchers as an indicator to which pavements layers are contributed to creep deformation. Three different asphalt surface shape and possible layer contribution scenarios are shown in Figure 2.8.

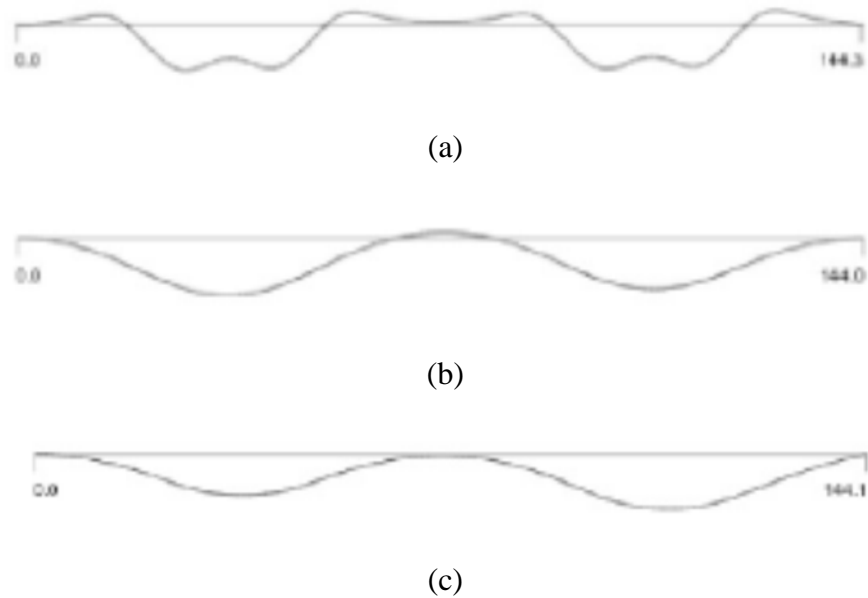


Figure 2.8: Different asphalt surface shape related to creep deformation in each asphalt layer: (a) asphalt layer, (b) granular base, (c) Subbase/Subgrade (White et al. 2002).

In unbound layers, insufficient stability in aggregate combinations under prevailing traffic and environmental loading may allow plastic deformation. In Austroads (2012) VESYS model (Austroads 2007) the potential of permanent deformation is evaluated using the Repeated Load Triaxial Test (RLTT) with a static confining pressure being used. A creep model development has been developed by Werkmeister et al., (2008) using the RLTT. The wheel-tracking test (Austroads 2015) is the latest test suggested as a complementary test for RLTT.

Asphalt layers deform (creep) under high axle stress and/or operating temperatures and structural creep deformation rarely occurs in lower layers in well-designed heavy-traffic thick asphalt structures (Nunn 2001; Newcomb et al. 2010). In heavy-traffic asphalt pavements, structural creep deformation can be limited by using the creep endurance limit which is the controlled compressive strain at the top of subgrade level (Harvey et al. 2004; Walubita et al. 2008). Creep deformation in this type of flexible pavement is normally confined to the surface asphalt layers (Rolt 2001; Brown et al. 2002).

Creep is not directly considered in the Austroads (2012) structural design procedure. Creep is only considered via a material deformation ranking as illustrated previously in Figure 2.3 (level 2). There is no reliable model or test available to predict the

development of creep deformation with traffic/time (Austroads 2012; Ahmadinia 2017).

## **2.8 Summary**

In this chapter, the design concepts related to heavy-traffic flexible pavements according to Austroads have been reviewed and some key limitations in the design procedure outlined. The review indicated that asphalt modulus and creep deformation modelling in the laboratory at elevated temperatures under stress responsive confinement are missing and unsolved elements for the relevant aspects of the Austroads pavement design procedures. The measurement and prediction of these pavement elements are important for design, maintenance and rehabilitation strategies of heavy-traffic flexible pavement.

It is noted that the work reported by Ahmadinia (2017) can be further developed to evaluate asphalt creep deformation resistance and compressive modulus at elevated temperatures through a staged confined dynamic creep test methodology. It is also considered that laboratory long life creep potential can be estimated through extrapolation of earlier life performance. It is believed that such outcomes will enhance current Australian pavement design procedures and that tenet is explored in detail within subsequent Chapters.

## CHAPTER 3

### CHALLENGES REGARDING ASPHALT CREEP DEFORMATION MEASUREMENT AND MODELLING

#### Contents

3.1	Introduction .....	33
3.2	Asphalt creep deformation .....	33
3.2.1	Creep deformation mechanisms.....	33
3.2.2	Factors that influence creep deformation of asphalt .....	36
3.2.3	Creep deformation test methods.....	36
3.3	Challenges with development of creep deformation test methods.....	39
3.3.1	Dynamic load type and magnitude.....	39
3.3.2	Confinement stress for laboratory samples .....	46
3.3.3	Air voids and their distribution .....	47
3.3.4	Environmental conditions .....	50
3.3.5	Summary of challenges for laboratory creep testing.....	54
3.4	Modelling and predicting creep.....	54
3.4.1	Literature review of creep deformation modelling .....	54
3.5	Summary .....	59

### **3.1 Introduction**

This chapter builds on the broader pavement design principles outlined in Chapter 2 and reviews the specific research related to asphalt creep deformation. The mechanisms of creep deformation in asphalt and its contributing parameters are explored. The broad spectrum of laboratory tests employed worldwide to measure creep deformation are examined along and their limitations. Finally, methods of early detection of creep deformation for preventive maintenance purposes is reviewed.

### **3.2 Asphalt creep deformation**

#### **3.2.1 Creep deformation mechanisms**

Creep deformation in asphalt as a composite material may be described as the tendency of the material to deform permanently under the influence of repeated traffic and environmental stresses. Creep normally appears as longitudinal depressions in the wheel paths (De Carvalho 2012) and can occur in any of the pavement layers (asphalt surfaces, granular base, and subbase) and the subgrade. For well-designed and constructed flexible pavements surfaced with thick asphalt, the distress typically occurs in the top 100 to 150 mm of the asphalt (Epps et al. 2002; Mulvaney & Worel 2002).

The mechanism of creep deformation in asphalt layers can be explained by Figure 3.1 where the distributed surface stresses represent a tyre. Vertical deformation (densification) occurs under the tyre in the active zone and due to Poisson's effect lateral deformation increases at the same time. Horizontal stresses are then generated in the passive zones that resist the lateral deformation in the active zone. In the situation where the horizontal stress generated as a result of lateral deformation in the active zone is equal to the hoop stress that the passive zone can provide, the vertical stress in the passive zone starts to increase. The incremental vertical and lateral stresses in the passive zone can lead to an accumulated increase in the shear flow which appears as heave in the asphalt surface around the wheel path.

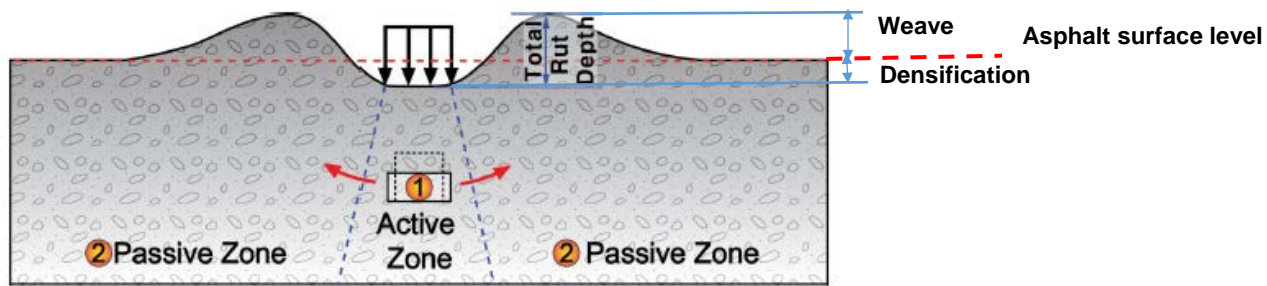


Figure 3.1: Schematic diagram of the mechanism of creep (rut) depth (a part of a figure from Choi et al. (2013))

Two main mechanisms that cause creep deformation development in an asphalt layer in a well-designed flexible pavement are described by De Carvalho (2012) as follows:

- **Deformation as a result of compaction:** as a primary mechanism, compaction occurs at the initial stage of loading. In this stage material volume, under the wheel path, decreases with no significant upheaval along the sides.
- **Deformation as a result of shear:** as a secondary mechanism, shear deformation occurs in the second stage. In this stage, along with further material volume reduction under the wheel path, the distortion caused by shear force starts to occur and forms upheaval along the side of the wheel path. A transverse profile of asphalt creep deformation caused by increasing traffic load cycle numbers is illustrated in Figure 3.2.

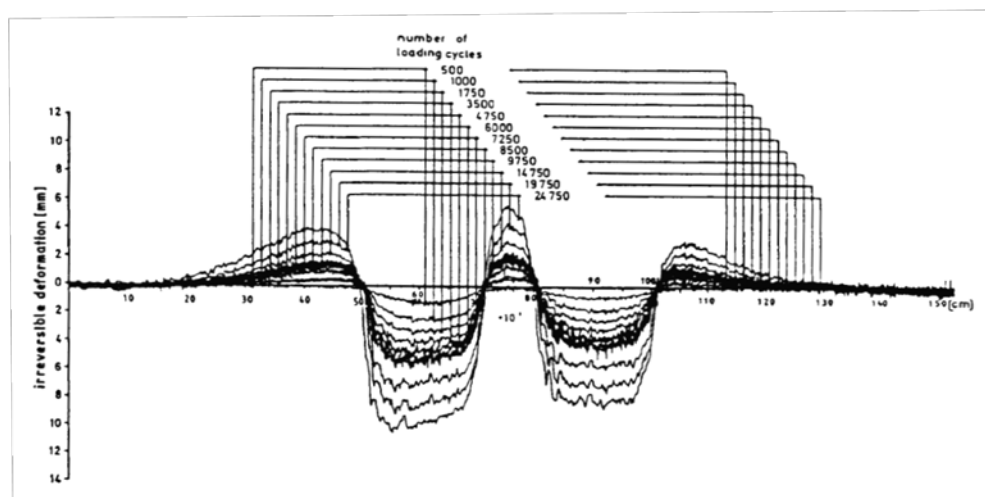


Figure 3.2: Transverse profile of asphalt creep deformation by increasing loading cycles (Eisenmann & Hilmer 1987)

According to these two mechanisms, a typical creep (permanent) deformation curve, which is divided into three stages, is drawn as shown in Figure 3.3. Creep deformation stages in this figure are as follows (Bonaquist et al. 2003; Zhang et al. 2012; Coleri et al. 2012):

- **Stage 1 (primary):** in this stage creep deformation is caused mainly by material densification. It is a decelerating phase of creep in which strain rate decreases by increasing loading cycles. It normally occurs early in the pavement service life (De Carvalho 2012).
- **Stage 2 (secondary or steady-state):** in this stage, shear deformation is predominant. It is a stationary phase of creep deformation in which the strain rate remains constant. This stage is normally used to design the maintenance strategies.
- **Stage 3 (tertiary):** in this stage strain rate quickly increases and is an accelerating flow stage of asphalt creep deformation.

Creep deformation in the laboratory using available tests may (nominally) exhibit all three stages however Stage 3 may often be related to sample cracking and/or collapse rather than accelerated creep. Creep deformation of heavy-traffic pavements in the field is normally restricted to the secondary phase (steady-state) because of the confinement stress provided by both asphalt mass around the wheel pass and common preventative maintenance. This is one reason why laboratory testing should preferably employ an effective confining system.

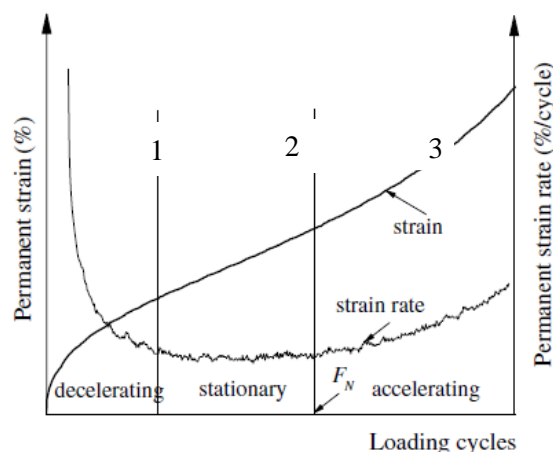


Figure 3.3: Creep deformation and creep rate versus loading cycle number (Zhang et al. 2012)

### 3.2.2 Factors that influence creep deformation of asphalt

Asphalt is a composite with a complex heterogeneous microstructure. The aggregate that forms the stone skeleton, the binder matrix (binder, filler and additives) and air voids all influence creep performance under variable traffic and environments. The impact of various factors on the permanent deformation of asphalt pavement in the field were reviewed and categorised by Sousa et al. (1991) as shown in Table 3.1.

Table 3.1: Factors effect on creep deformation of asphalt mixtures (Sousa et al. 1991)

	Factor	Change in factor	Effect of change in factor on creep resistance
Aggregate	Surface texture	Smooth to rough	Increase
	Gradation	Gap to continuous	Increase
	Shape	Rounded to angular	Increase
	Size	Increase in maximum size	Increase
Binder	Stiffness at highest pavement temperature	Increase	Increase
Mixture	Binder content	Increase	Decrease
	Air voids (min 3%)	Increase	Decrease
	VMA (min 10%)	Increase	Decrease
	Method of compaction	Depends on the compaction method	
Field conditions	Temperature	Increase	Decrease
	Moisture	Dry to wet	Decrease if mix is water sensitive
	State of stress/strain	Increase in tyre contact pressure	Decrease
	Load repetitions	Increase	Decrease

### 3.2.3 Creep deformation test methods

To evaluate the potential creep deformation of asphalt, all the effective parameters must be considered. The types of test that have been historically utilised to measure creep deformation in the laboratory and evaluate the impact of the various test parameters are grouped under the following three categories.

1. **Empirical tests:** tests which are useful when the practical experience is available. They cannot provide sufficient measure of the mix quality.
2. **Fundamental tests:** tests which are performance-related and normally able to provide the mechanical properties of asphalt for mechanistic design procedure.
3. **Simulative tests:** tests which are performance-based where the actual traffic loads and environment are modelled.

The three types of the tests, their relevant advantages and limitations have been summarised and listed in Tables 1 to 3 in Appendix A. A summary of the limitations from table 1 to 3 in Appendix A is provided below.

- Equipment is not widely available
- Equipment is too complex and expensive
- Equipment needs specific sample sizes and compaction
- Equipment has restricted test temperatures and load levels
- Equipment is not able to apply a dynamic load similar to in-situ traffic load
- Equipment requires a triaxial chamber to provide the confinement stress
- Sample size (height) is specific and cannot be cored from the in-situ pavement
- Sample cannot withstand high level loads for high cycles and will collapse
- Load is diametric and results are found to overestimate creep deformation
- Load is not dynamic and/or cannot simulate the real load situation
- Test is difficult to perform and needs special training
- Stress distribution between tyre and asphalt is difficult to model
- Confinement stress provided by test facilities is not realistic

### **Wheel Tracker**

The wheel tracker is categorised as a semi-confined simulative test as outlined in Table 3 in Appendix A. Numerous types of wheel trackers have existed internationally, including the Georgia Loaded Wheel Tester (GLWT), the French Wheel Tracker, the Hamburg Wheel Tracker and the Asphalt Pavement Analyzer (APA) (Kandhal & Cooley 2003). While wheel trackers have been widely adopted as a useful tool to evaluate rutting potential in asphalt mix design, the test does not yield a fundamental material property. As summarised by the NCHRP (Kandhal, PS & Cooley 2003):

*“a key issue with the APA (or with any other method intended for this purpose, including other types of loaded wheel testers and simple strength tests) is the degree to which the relationship between the APA’s test results and actual field performance depends on specific project-associated factors such as aggregate properties, mix design type, traffic level, and traffic speed.*

Internationally the wheel tracker test’s ranking ability has been accepted, however its capacity to predict asphalt creep (rutting) rates remains under research (Beecroft and Petho 2015 & Tsai et al. 2016). It is noted that some progress has been made as

outlined in AP-T228-13 “Feasibility Study of Using Wheel-tracking Tests and Finite Element Modelling for Pavement Deformation Prediction”, (Austroads 2013).

The publication of EN 12697-22, “Bituminous mixtures - Test methods for hot mix asphalt - Part 22: Wheel tracking” (EN 2003) and most recently AASHTO T 324-17, “Standard Method of Test for Hamburg Wheel-Track Testing of Compacted Hot Mix Asphalt (HMA)”, (AASHTO 2017) have helped ensure the wheel trackers’ worldwide use as a simulation test for estimating rutting potential of asphalt mixes (Tsai et al. 2016). This has been echoed within Australia (Beecroft and Petho 2015) as seen by the publication of AGPT-T231-06 Deformation Resistance of Asphalt Mixtures by the Wheel Tracking Test (Austroads 2006).

This study attempts to redesign the existing Australian dynamic creep test (AS 2891.12) to overcome some of the available challenges regarding the cited rutting tests in Table 3 in Appendix A. This redesign and enhancement of the Australian dynamic creep test does not attempt to replace the Austroads wheel tracker test (Austroads 2006) but rather provides an additional tool for pavement designers and researchers to apply in the evaluation and prediction of rutting in asphalt surface layers.

### **ALF**

Most of the limitations regarding the test facilities can be solved (in Australia) by the use of Accelerated Load Facilities (ALF) and the Accelerated Pavement Tester (APT). Koniditsiotis (1996) described the ALF as “a mobile, relocatable accelerated pavement testing device which applies a unidirectional rolling wheel load to a 12m pavement test strip in order to simulate many years of heavy vehicle loading into a few months”.

The ability of ALF to rank the performance of different asphalt pavements and also to predict the creep deformation of asphalt pavements has been verified, accepted and applied through several studies (Hugo et al. 2012; Ritter et al. 2012; Moffatt et al. 2012). However, the difficulty of using ALF in modelling the mechanical properties of asphalt to incorporate mechanistic design has also been highlighted (Koniditsiotis 1996). This test requires substantial testing costs and effort and few institutions possess this testing facility. ALF testing is normally used to verify existing creep models rather than developing new models (Choi 2013).

A fundamental test is needed to link the ALF creep deformation trials with mechanical properties of asphalt, in order to apply laboratory testing outcomes in mechanistic design procedures (Koniditsiotis 1996). Several studies have been attempted using the repeated simple shear test, dynamic modulus test and triaxial creep test for this purpose (Witzcak et al. 2002; Ali et al. 2017). However, these test procedures all have some of the limitations noted in Appendix A. A need remains for the development of an economic and easily accessible test to model asphalt creep in the laboratory under conditions that better replicate those in the field.

### **3.3 Challenges with development of creep deformation test methods**

The main challenges regarding the development of a realistic test to better predict asphalt creep deformation are listed below.

1. Test facilities should provide a realistic dynamic load type and magnitude
2. Realistic confinement should be provided for laboratory asphalt samples
3. Air voids and their distribution are measured accurately
4. Realistic environmental conditions (temperature, moisture, and ageing) are provided during testing

All of the creep deformation test methods provided in Table 1 to 3 in Appendix A remain under continual review as researchers attempt to develop more realistic, economic and easily accessible tests to model asphalt pavement permanent deformation while considering the four points above. Those points are discussed in more detail.

#### **3.3.1 Dynamic load type and magnitude**

Since asphalt mixture is a visco-elasto-plastic material its creep is both temperature and load rate dependent. To introduce a realistic creep deformation test, the accurate modelling of an in-situ moving load and stresses is needed in the laboratory. These include stresses under a moving wheel, their magnitude and frequency and interface conditions.

##### **Stresses under a moving wheel**

The stresses generated by wheel loads can be complex (Figure 3.4a and b). The principal stresses rotate under a moving wheel load (Figure 3.4b). Lekarp et al. (2000) stated that among the fundamental tests only the confined Hollow Cylinder Test is capable of modelling the real

rotation of in-situ principal stresses. This principal stress rotation cannot be modelled with conventional triaxial tests.

Regarding the stress distribution between tyre and asphalt surface, the research conducted by De Beer et al. (1997) and Shuiyou (2003), illustrated that contact stresses (longitudinal, vertical, and lateral) are non-uniform, discontinuous, and non-circular. They are a function of load magnitude, shape of tyres, tread patterns of tyres, and inflation pressure (Hjort et al. 2008). Typical patterns of the contact stresses are shown in Figure 3.5. Among the creep deformation tests, only simulative wheel type tests are able to model the exact surface contact stress distribution. The fundamental tests are not capable of modelling the situation under a load platen. Austroads (2012) reported that this stress variation has little impact on the performance of thick asphalt pavement but that it can have a pronounced effect on thin surfacing.

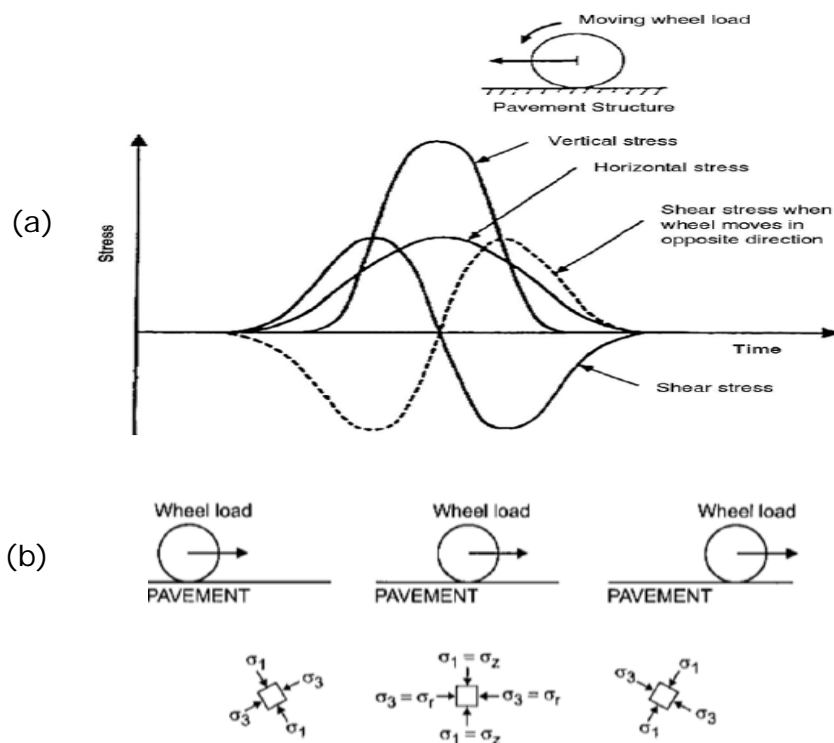
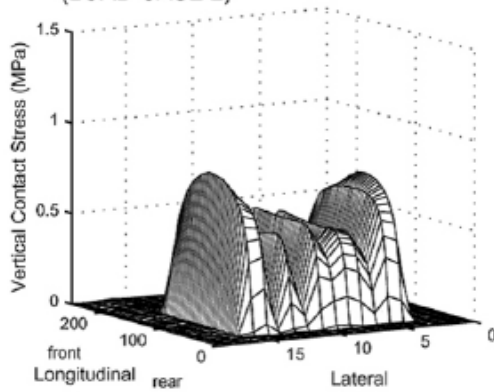
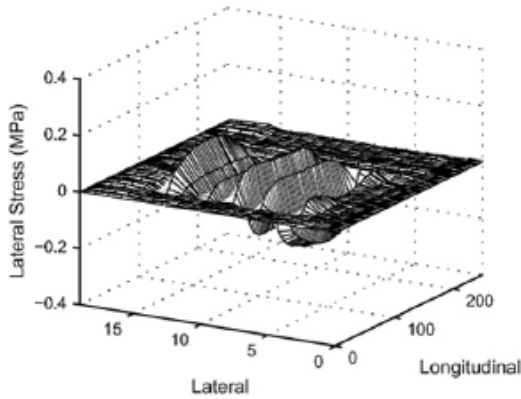


Figure 3.4: a: Generated stress under moving wheel load (Brown 1978).  
b: Rotation of principal stress (Lekarp et al., 2000)

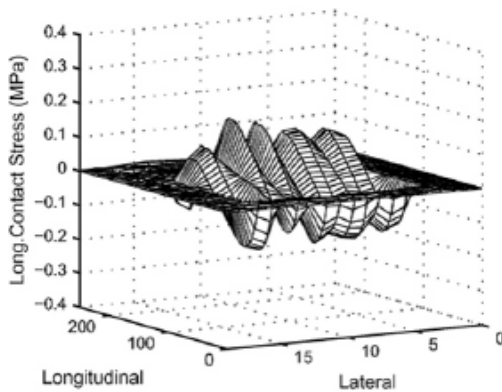
UCB GOODYEAR G159A, 11R22.5 (radial) Tyre  
 Inflation Pressure=420 kPa ; Load=26 kN  
 (LOAD CASE 2)



Vertical Contact Stress

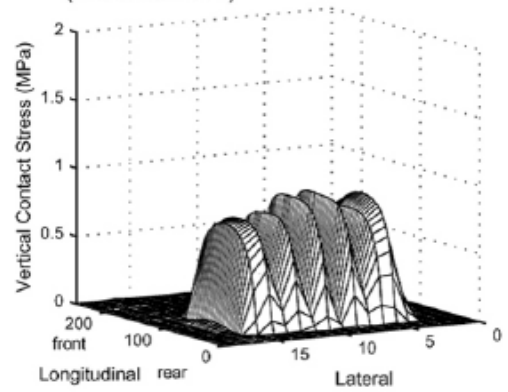


Lateral Contact Stress

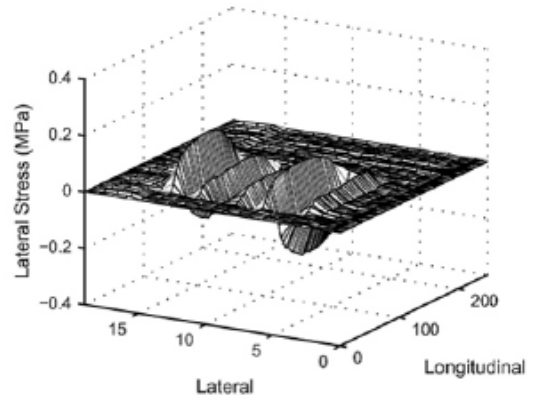


Longitudinal Contact Stress

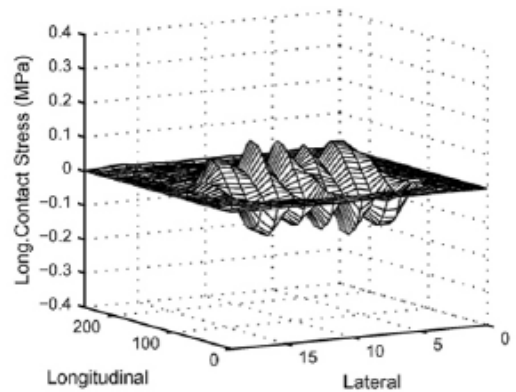
UCB GOODYEAR G159A, 11R22.5 (radial) Tyre  
 Inflation Pressure = 690 kPa ; Load = 26 kN  
 (LOAD CASE 3)



Vertical Contact Stress



Lateral Contact Stress



Longitudinal Contact Stress

Figure 3.5: Vertical, longitudinal, and lateral contact stresses generated by wheel loads at the pavement surface (De Beer et al. 1997)

In addition to the above stress condition, the stress distribution as a function of asphalt depth should also be considered when constructing a realistic laboratory creep test. A study conducted by Su et al. (2008) regarding the shear stresses generated within asphalt under the tyre (Figure 3.6) showed that the shear stresses below the tyre edge vary with depth. When modelling creep within a deep asphalt layer such stress variation should be taken into account.

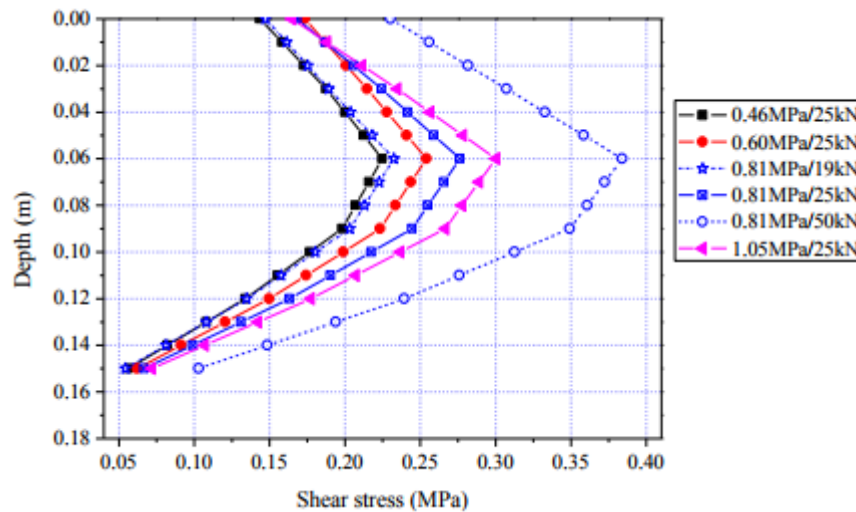


Figure 3.6: The distribution of shear stress in varying depth (Su et al. 2008)

### Load magnitude and frequency (waveform)

As outlined previously creep rates will vary both as a function of load magnitude and frequency (Garba 2002; Zhang et al. 2016). In Australia 750kPa is the assumed default tyre pressure in pavement design (Austroads 2012). It has been reported that actual tyre pressure vary between 500 and 1000 kPa depending on the tyre shape, number, and inflation pressure and/or road slope and position (Potter & Youdale 1998; Gribble & Patrick 2008; Hjort et al. 2008; Austroads 2012). A range of stresses (such as 500 to 1000 kPa) could be applied during laboratory tests to better gauge creep sensitivity.

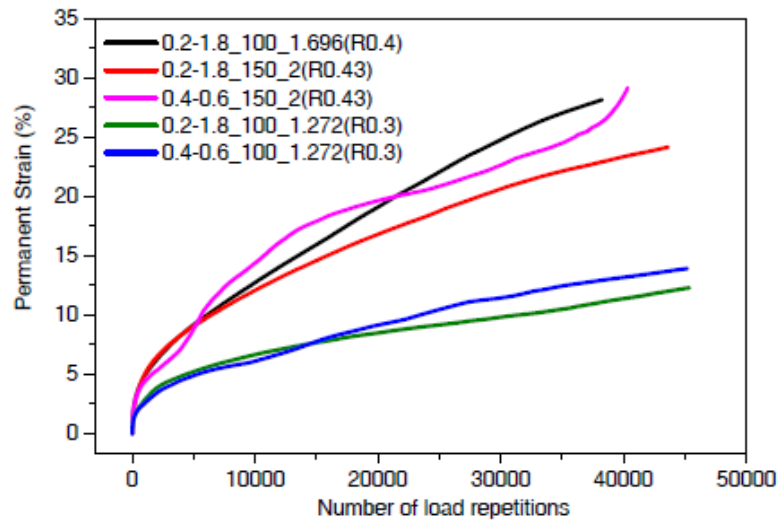
The load waveform that is a function of loading time and rest period also affects the creep deformation of asphalt (Qi & Witczak 1998; Mansourkhaki & Sarkar 2015). Depending on the type of test facilities and specifications most waveforms applied in laboratory testing are square pulse or haversine (Table 3.2).

Table 3.2: Loading options in different standards (Mansourkhaki & Sarkar 2015; Wang 2015)

Standard	Reference	Loading options			
		Wave form	Pulse wide: ms	Rest period: ms	Deviator stress: kPa
Australian: AS 2891.12.1	SA (1995)	Square pulse	500	1500	200
British: DD 226	BSI (1996)	Square pulse	1000	1000	100
European: pr EN 12697	CEN (2001)	Square pulse	1000	1000	100
NCHRP 9-19	NCHRP (2000)	Haversine pulse	100	900	69
VESYS manual	Zhou and Scullion (2002)	Haversine pulse	100	900	138
European: pr EN 12697	NEN-EN 2005	Haversine (continuous) Block	1 Hz to 5 Hz 1000 (200)	1000 (800)	100 to 300kPa 100 to 700kPa
C.R.O.W RAW standard 2010	Wang (2015)	Haversine pulse	400	600	600

It is generally believed that a too short rest period would affect the permanent deformation test results due to insufficient time for elastic recovery. In the study conducted by Wang (2015) the effect of loading time and loading ratio on creep deformation were assessed during 50,000 load cycles using the Triaxial Repeated Load Permanent Deformation (TRLPD) test. Varying loading and resting time were used under different confinement levels and stress ratios as illustrated in figure 3.7. In the legend, for instance 0.2-1.8-100-1.272 (R0.3), the first and second number indicate the loading and rest time in seconds, the third number indicates the confining pressure in kPa, the fourth is the applied vertical force in kN and the last one, between brackets, is the stress ratio of deviator stress to the deviator failure strength (Figure 3.7). The research was shown that the selected ratio of loading time to rest period has little effect on creep (permanent) deformation during 50,000 load cycles. The creep deformation was seen to be more sensitive to the stress ratio. It is worth mentioning that the research

was conducted at low stress levels and low cycle numbers (50,000). The assessment also was based on the creep deformation and creep slope was not assessed.



\*The first and second number indicates loading and rest time in second. The third and fourth indicates confining pressure (kPa) and a vertical force (KN) and the last is the stress ratio (deviator stress to deviator failure strength).

Figure 3.7: Permanent deformation of specimen under varying conditions (Mansourkhaki & Sarkar 2015)

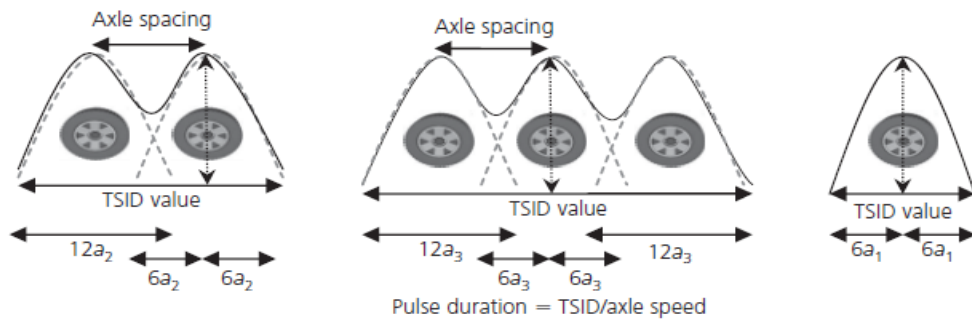


Figure 3.8: Schematic representation of loading pattern for various axles (Mansourkhaki & Sarkar 2015)

Mansourkhaki and Sarkar (2015) reported that the studies about creep deformation potential have been based on a single load pulse and loading duration corresponding to a constant speed. In reality, pavements are under the passage of single, double, and triple axles (multiple load pulses) at different speeds. The loading frequency depends on axle configuration and vehicle speed as shown in Figure 3.8, subsequently, in-situ frequency is different from the one used in current standards. The effect of wave form

and loading time on creep deformation is still an issue and is under development (Hafeez 2017).

### Interface conditions - platen and asphalt sample surface

Within the laboratory scale, the contact conditions between the specimen and platen has a significant influence on the characterization of asphalt materials (Erkens 2002; Wang 2015). It was recommended by Erkens (2002) that a combination of foil (50 $\mu$ m thick, Luflexen from Basf), and with a layer of soap minimised friction effects. The Austroads (2008b) standard, recommends 1g of “temperature stable silicon based lubricating medium” as a solution to friction. Interestingly neither approach relates to the actual interfacial condition between a moving tyre and an asphalt road surface where high friction is relied upon to provide traction.

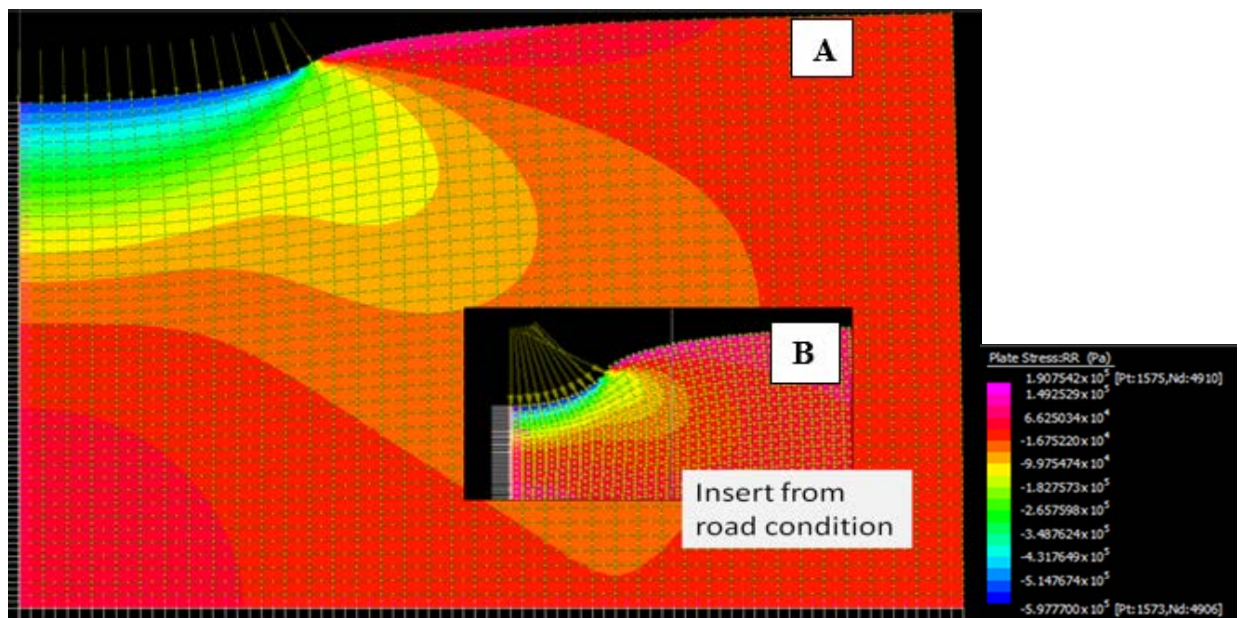


Figure 3.9: A: Specimen with 150mm diameter and 50mm height under 50mm platen size, and exposed to 750 kPa axial load. B: The elastic model of a road pavement under 750kPa load (Ahmadinia et al. 2014)

Using a small diameter platen on a larger diameter asphalt sample is another loading related recommendation for modelling creep deformation in the laboratory scale. This idea was first proposed by Bullen and Preston (1992) and Oliver et al. (1995). Later Nunn et al. (1998) applied it in the extension of the Nottingham Asphalt Tester (NAT) using a similar approach. The work was presented in European standard EN12697-25A (EN 2005) and further optimised by Ahmadinia (2017). The benefits of using a small platen are shown in Figures 3.9. It can be seen that when the test procedure uses

smaller platens on samples, the test provides a restraining annulus of asphalt. In this situation, the stress distribution in the laboratory sample then becomes a closer approximation of actual field conditions (Ahmadinia et al. 2014).

### 3.3.2 Confinement stress for laboratory samples

Perhaps one of the most important issues to reproduce for in-situ asphalt pavement conditions in the laboratory is replicating the lateral confinement stress. In-situ asphalt is surrounded by a mass of asphalt (the passive zone in Figure 3.1), which provides a strain generated lateral confinement under axle loads (Figure 3.10). This in-situ confinement stress changes as a function of traffic load, asphalt mix structure, level of permanent strain, and temperature (Sun, 2005, Choi et al. 2013). Since creep deformation is a longitudinal depression of material under stress the deformation can be affected by the lateral confinement stress (Tan et al. 1994; Murray 2007; Dołżycki & Judycki, 2008; Rahmani et al. 2013; Javilla et al. 2017). This type of lateral confinement stress should be provided in laboratory tests for better evaluation and prediction of creep.

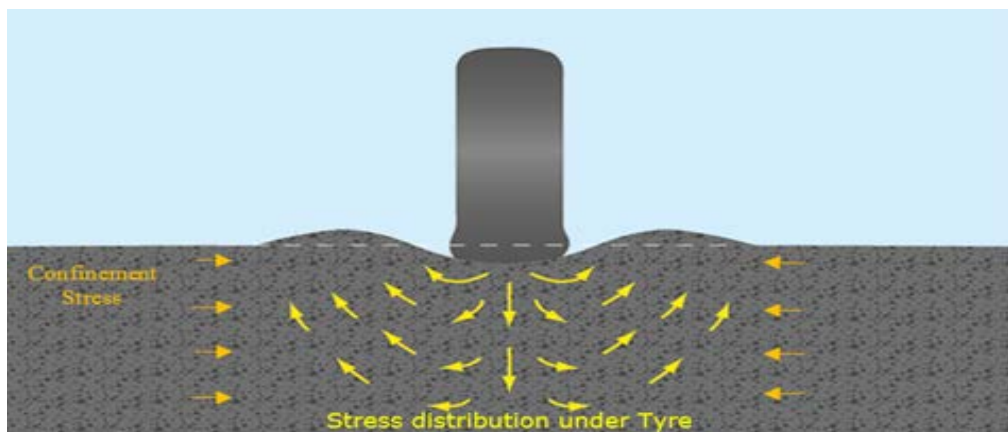


Figure 3.10: Stress distribution within asphalt layer under tyre (a part of figure is from Petersson 2014)

Existing permanent deformation tests (Tables 1 to 3 in Appendix A) use a range of means of generating confinement. The fully confined tests in Tables 1 to 3 in Appendix A, (with the exception of the Accelerated Loading Facility) typically provide their lateral confinement stress (Partl et al. 2012) via different techniques including water pressure, air vacuum, air pressure or using an unconfined annulus of asphalt around the sample.

The confining conditions provided by these tests do not vary in response to the load-unload stage of each load pulse as seen within real pavements (Sun 2005). The improved test methodology proposed by Ahmadinia et al. (2016) better replicates the confinement situation seen in the field by allowing the asphalt sample to respond to the applied stresses. The test uses a layered confinement methodology, where the asphalt being subjected to tyre pressure is supported by an asphalt annulus, which in turn is supported by a polymer (PVC) ring with an infill thermoplastic between the asphalt and PVC. The asphalt annulus allows the sample to undergo plastic deformation while the polymer ring provides a confining hoop stress that is generated in response to the load pulse. A sample under creep testing is shown in Figure 3.11e with a mounted strain gauge that was used to measure the confining hoop stress pulses generated within the polymer ring (Ahmadinia 2017). Figure 3.11a to e shows the varying confinement configuration methods that have been developed for laboratory testing. The benefits and limitations of each configuration will be discussed in more detail in Chapter 6.

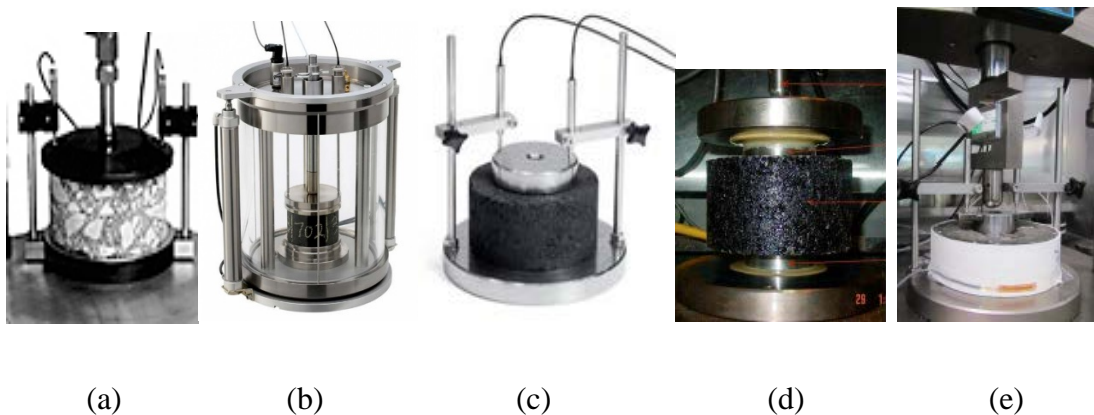


Figure 3.11: Varying configurations provided for confining laboratory asphalt samples

- a Without confinement
- b Confined chamber set up which provides confinement with any of water pressure, air vacuum, air pressure
- c Annulus of asphalt (smaller platen on one side of sample) with or without confinement system shown in b
- d Annulus of asphalt (smaller platens on both side of sample) with or without confinement system shown in b
- e Annulus of asphalt (smaller platen on one side of sample) with PVC ring

### 3.3.3 Air voids and their distribution

One largely unmet challenge in assessing asphalt creep is the measurement of air voids and their distribution. Total air voids (Figure 3.12) and distribution is a function of

aggregate shape, gradation, binder content, and compaction. The mechanical properties and behaviour of asphalt under stress can be a function of air voids and their distribution (Garba 2002; Tashman et al. 2010).

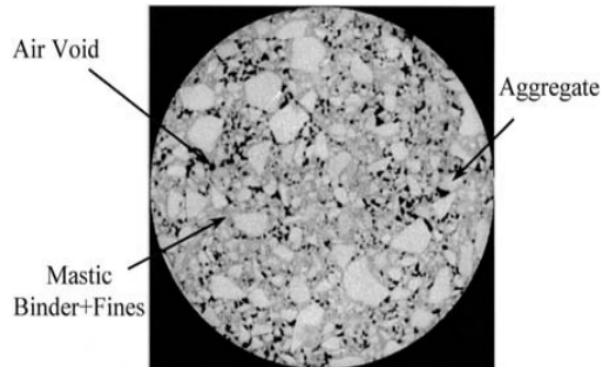


Figure 3.12: Air voids within Asphalt structure (Tashman et al. 2010)

Much research has been conducted about the effect of air voids on the mechanical behaviour of asphalt mixtures. In general, the research indicates that air voids below a minimum specification limit may lead to excessive creep deformation (Roy et al. 2013), flushing, bleeding and/or mix instability. Air voids above a maximum specification limit may lead to accelerated hardening of the binder through oxidation, ravelling and stripping of the asphalt layer (MRTS30, 2016). High air-voids content can also lead to creep deformation in the early life of the pavement due to post placement compaction (Garba 2002; Roy et al. 2013). Fatigue damage, reduced strength and durability of asphalt may also result due to excessive air voids (Ren & Sun 2017). At elevated temperatures an asphalt mix tends to behave more like a granular material due to the low viscosity of the binder. In this situation air voids as a part of granular structure play a key role in mechanical behaviour such as creep deformation of asphalt mixtures (Wang 2015).

#### **Low air voids and creep deformation:**

A study conducted by Brown and Cross (1989) about in-place creep deformation involved a comparison of pavements, which had experienced creep deformation with pavements that had no creep deformation record, after ten years of service life. Coring, trenching and laboratory tests were used to assess the source of the ruts. The research showed that low air voids in asphalt in the field or in the laboratory re-compacted specimens were related to creep deformation. The results were in line with the findings

of a previous study conducted by Huber and Herman (1987). Another study conducted by Brown and Cross (1992) on 42 pavements from 14 different American states concluded that pavements with air voids below 3% have more potential for creep deformation and that creep was mostly confined to the top 75 to 100 mm (3 to 4 in.) of the pavement.

Research was conducted by Willis et al. (2009) and Levenberg et al. (2012) regarding the risk of low air voids and its correlation with pavement distresses such as creep deformation. Both studies recommended the critical air voids of 2.75% as the lower permitted air voids for dense graded asphalt manufactured with conventional bitumen binder. This criterion was regardless of having air voids as result of either a high binder content or poor aggregate gradation. It should be noted that asphalt made with polymer modified binders indicates a different relationship regarding the air voids and permanent deformation, with greater tolerance for lower air voids (Willis et al. 2009).

#### **Air void distribution:**

A study conducted by Wang (2015) assessed the effect of air voids and their distribution on the permanent deformation of asphalt at 50°C after about 100,000 load cycles in a confined situation. The Triaxial Repeated Load Permanent Deformation (TRLPD) test, X-Ray computer Tomography and ICT image processing were used in this research to evaluate the effect of air voids and their distribution after testing. The research showed that deformation modes were dependent on the air voids and their distribution, which may develop a weak zone in the asphalt sample. The air voids range for the research samples was 2.7% to 4.1%. It was interesting that the small difference between samples air voids (1.4%) had significant effect on the failure mode. The deformation modes based on their research are divided into three categories as shown in Figure 3.13.

- **Deformation A:** Tensile failure with uniform deformation as a result of the uniform distribution of air voids in the asphalt sample (Figure 3.13a).
- **Deformation B:** Shear failure as a result of the non-uniform distribution of air voids in the asphalt sample. Most of the air voids in this failure form are located in the centre of the sample and small air voids can be found in other areas (Figure 3.13b).

- **Deformation C:** shear failure (barrelling) as a result of the non-uniform distribution of air voids in the asphalt sample. The concentration of air voids can be found in the middle of the sample and few air voids are distributed at both ends (Figure 3.13c).

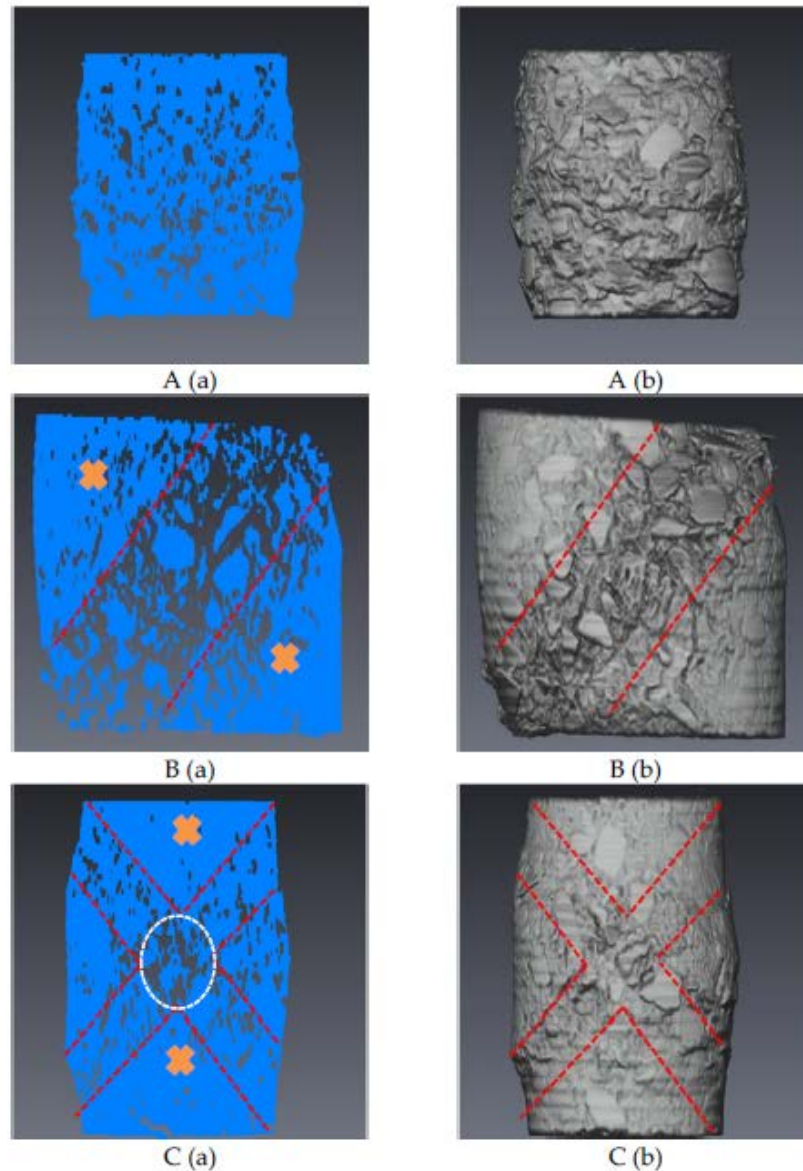


Figure 3.13: Failure modes and air voids distribution (Wang 2015)

### 3.3.4 Environmental conditions

The operational environmental has a significant effect on asphalt creep deformation, and subsequently the service life of flexible pavements (Ongel & Harvey 2004). Three

main environmental factors for asphalt surface layers which can influence their creep deformation are (Yang et al. 2014; Yang et al. 2015; Hasan et al. 2016):

- Ambient temperature
- Solar radiation which influences the ageing rate of asphalt
- Moisture

Moisture is normally considered as having more relevance in lower granular layers in the flexible pavement. The prediction of in-situ creep deformation for asphalt layers in the laboratory depends on how well in-situ temperature and solar radiation is modelled in the laboratory tests.

### **Temperature effects**

The correlation between the increase of temperature and an increase of creep deformation is explained by the thermo-susceptibility of the binder in the asphalt mixtures, which leads to more movement of granular materials under traffic loads (Partl et al. 2012).

In most of the laboratory tests, the temperature conditions are under control using an environmental chamber. The temperature is normally constant during creep deformation tests and is an important parameter for ranking creep sensitivity of asphalt mixes. However, in the field, the temperature is not constant and can fluctuate hourly during the day. A temperature fluctuation is also seen in the depth of asphalt as outlined earlier in Chapter 2.

Temperature fluctuation affects the mechanical behaviour of asphalt mixtures in surface layers, and thus their service life. Asphalt mixtures expand in elevated temperatures and contract in low temperatures leading to the generation of temperature-induced stresses (Islam & Tarefder 2014). Such repeated temperature fluctuations can produce many defects in asphalt pavement and should to be included in the design process for such flexible pavements (Merbouh 2012).

Ideally to best predict creep deformation as a function of temperature, hourly temperature fluctuations should be replicated in laboratory tests. As explained earlier in Chapter 2, the estimation of temperature gradients is based on numerical and presumptive techniques (Merbouh 2012). Research reported by Islam and Tarefder (2014), also attempted to model the gradual increase of temperature in field asphalt

layers in the laboratory. Mohd Hasan et al. (2016) designed an environmental chamber able to reproduce the hourly increase of temperature during a day (Figures 3.14a and 3.14b).

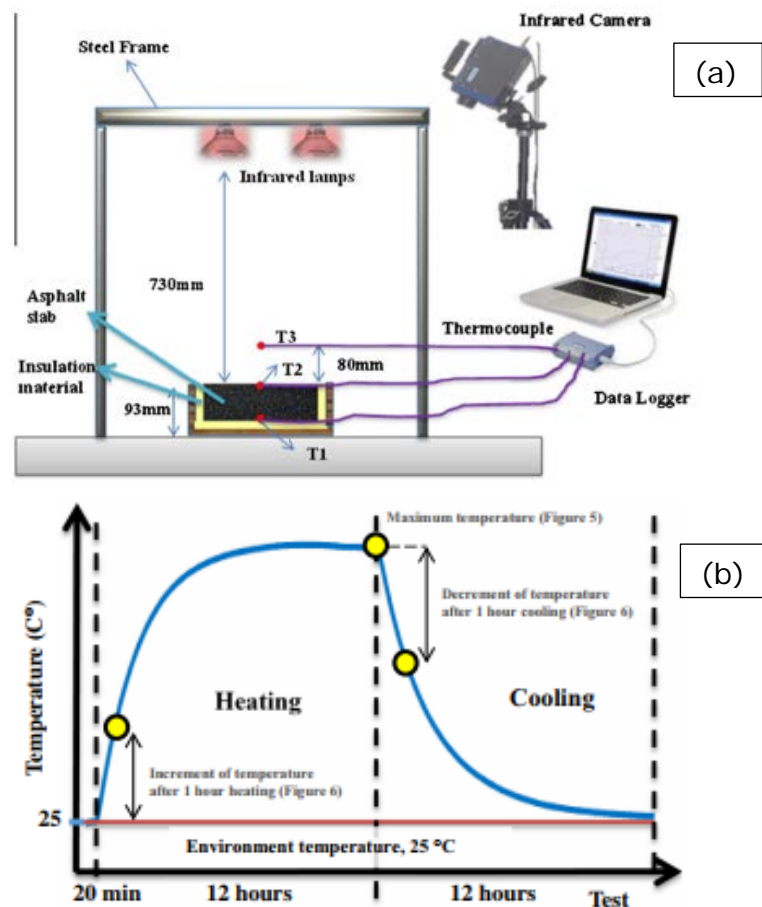


Figure 3.14: a: Environmental setup and b: Schematic generated temperature evaluation (Mohd Hasan et al. 2016)

### Solar radiation

Asphalt ageing is a function of binder ageing and is generally classified as either short or long-term. The former ageing refers to the oxidation and volatilization of the binder in the production process, as well as laying and compaction (it also includes storage time for laboratory samples). The latter is a result of oxidation of binder due to the simultaneous effect of chemical composition, temperature, moisture, and UV radiation throughout its service life (Fernández-Gómez et al. 2016). Most of the latter ageing is caused by ultraviolet ageing (Wu & Airey 2009) that is the result of ultraviolet radiation and oxygen. It can significantly affect the performance of asphalt and its durability (Jiani et al. 2013). Most studies involve the use of specialist environmental

chambers and it is recognised that the use of such chambers, would be helpful to better evaluate creep in the laboratory.

The effect of ultraviolet radiation on creep deformation and dynamic modulus of dense grade asphalt was assessed by Reyes Ortiz and Camacho Tauta (2008). The results showed that the permanent deformation of asphalt decreased by 57% and the dynamic modulus of the asphalt mixture increased between 90% and 132%. Another study that assessed the effect of ultraviolet radiation on permanent deformation of asphalt was conducted by Fernández-Gómez et al. (2016). In this study two methods of ageing were applied for making aged asphalt samples in the laboratory artificially: The PAV (ASTM D-6521, for periods of 5, 20, and 50 hours) and specific UV ageing chamber. To validate the ageing methods, cored samples from the asphalt pavement with varying ages (1.5, 3 and 5 years old) and unaged samples were also prepared. Creep deformation tests were undertaken based on the French standard NLT 173 - 84, at 60 °C under  $900 \pm 25$  kN/m<sup>2</sup> pressure.

The research showed a lower level of creep deformation for the samples that were aged in the UV chamber (for 1.5, 3 and 5 years), compared to unaged samples (10.7, 30.8 and 47.9% creep deformation reduction, respectively). Similarly, the field mixture experienced an increase in creep deformation resistance with higher environmental exposure. The UV chamber used by this project, “enabled the recreation of the effects of ageing faced by asphalt mixtures in the field especially throughout the early stages of ageing—and allowed parallels to be drawn between UV chamber exposure time and field exposure time” (Fernández-Gómez et al. 2016).

The UV chamber used for the project was capable of simulating UV radiation and temperature at a relative humidity of 99%. The chamber used eight lamps that emitted radiation in a wavelength of 340nm in the UVA range equivalent to 0.77 W/m<sup>2</sup>/nm. The chamber employed cycles that consisted of a radiation period followed by a condensation period. The former consisted of a two hour period when the UV lamps were turned on and the temperature was increased to 60°C. The last was a two hour period when the lamps were turned off and the temperature decreased to 50°C (Fernández-Gómez et al. 2016).

### 3.3.5 Summary of challenges for laboratory creep testing

To better predict the creep performance in the laboratory, researchers endeavour to reproduce the various operational parameters that influence creep life. These are categorised in Table 3.3. The variables investigated in this research are air voids and their distribution, lateral confinement stresses, loading stress, and temperature.

Table 3.3. Effective factors on modelling the asphalt creep deformation in the laboratory

1. Environment	Temperature (hourly, daily, and seasonal) Solar radiation (in long term) Moisture
2. Material (Aggregate, Filler, Bitumen, Additives)	Material mechanical properties Material durability and ageing sensitivity Material chemical properties Material size, shape, gradation Material temperature sensitivity
3. Structure of Asphalt mix and layer	Structural confinement situation Sample air voids and their distribution Sample aggregate structure and thickness Sample compaction method
4. Load	Type of load pulse (Square, haversine, triangular or sinusoidal) Loading and resting time (as a function of speed, axle number, and axle distance) Load type (static, cyclic, constant deformation rate) Load rate Load magnitude Loading platen (size, contact situation)
5. Tyre	Tyre shape, inflation pressure, and size Number of tyres Distance between tyres Tyre contact situation

### 3.4 Modelling and predicting creep

Existing laboratory creep evaluation methodologies are largely employed to rank asphalt mixes. For example, a mix may be ranked as being suitable for light, moderate or heavy traffic in high speed, medium or slow traffic environments. Extrapolating relative short-term creep testing in a laboratory that is meaningful and involves only (say) 40,000 cycles out to (say)  $10^6$  cycles would be a significant advancement in asphalt creep research.

#### 3.4.1 Literature review of creep deformation modelling

Creep deformation of asphalt under traffic load is usually modelled through three methods as introduced earlier in this Chapter. Empirical models are based on

observation and recorded distress data such as regression equations fitted to observed data in field and laboratory tests. These models are normally the simplest material form and have limitations regarding in-situ parameters and properties of materials. Mechanistic-empirical (M-E) models “are normally developed based on a combination of simple mechanistic responses predictions (i.e., often using elastic theory) with empirical equations calibrated using laboratory testing in which stress conditions representing field conditions are replicated” (De Carvalho 2012). Fully mechanistic models are able to predict the creep deformation directly based on complex constitutive models. These models have an ability to analyse imposed stresses and subsequent strains, by external loads without needing empirical transfer functions (De Carvalho 2012).

Among the models, fully mechanistic models are known as most accurate models to predict creep deformation. However, Mechanistic-empirical (M-E) models are preferable and commonly used by pavement designers for design, management, and maintenance purposes.

In general, an empirical model must have the following parameters to be accepted as a common creep performance model able to be used in Mechanistic-empirical (M-E) design:

1. Must be simply formulated (have a low number of coefficients to consider)
2. Must be able to accurately model both the primary and secondary stages of creep.
3. Should be implemented in a finite element model.
4. Must be able to be calibrated through a simple test with the following conditions:
  - Simple and easy to understand for asphalt engineers, such as agency practitioners
  - Requires low testing time and costs
  - Models the in-situ asphalt conditions as much as possible by providing realistic confinement, stress, and environmental condition.

Some of the Empirical and Mechanistic-empirical models are summarised in Table 4 in Appendix A. These models were fitted on the experimental or field data, and by

extrapolation they could be used to predict creep deformation development. So based on the test type or experiments the accuracy of the available models will vary. Based on the best test conditions which were noted earlier, several research studies (De Carvalho 2012; Choi 2013; Rushing et al. 2014; Javilla et al. 2017) were recently conducted to assess the accuracy of these models to predict the creep performance of asphalt mixtures.

Rushing et al. (2014) reported that some of the simple creep deformation models, including the models introduced by Monismith et al. (1985) which use a power base, could be successfully used to simulate the creep deformation development behaviour of asphalt mixtures for laboratory tests in the secondary region of the creep curve (for a maximum of 8000 cycles). Choi (2013) also reported that most of the classic power law models are able to predict the creep deformation accurately only in the second region of creep curve (during 10,000 cycles). The incremental model (Table 4 in Appendix A) was reported by Choi (2013) as the best fit for a creep deformation prediction of a repeated load creep deformation test (maximum 50,000 cycles). The rut depth can be calculated through this model if the creep depth correction factor is used.

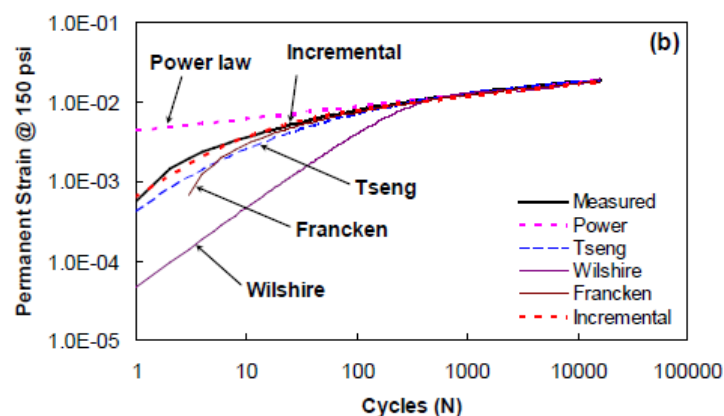


Figure 3.15: Comparison of creep deformation models with repeated load test (Choi 2013)

Javilla et al. (2017) compared some of the models noted in Table 4 in Appendix E which can be seen in Figure 3.15. The model parameters were optimised using two repeated load laboratory tests: Uniaxial Repeated Load (URL) test and Wheel Tracking Test (WTT) in 1000 cycles. The calibrated models in the first stage (10, 100, and 1000 cycles) were used to predict the creep deformation in 10,000 cycles. Average deviation error (%) and  $R^2$  for the creep tests were calculated and compared for all

models. As the results in Figure 3.16 show, by increasing the  $R^2$  value, the deviation error decreased. However, it has been proven that the accuracy of the model to predict the creep deformation in the long term is not related to the  $R^2$  alone.

It was shown that the model accuracy, in addition to the model's  $R^2$ , depended on the number of cycles which were used to calibrate the model parameters. The best prediction results belonged to the Tseng-Lyton model ( $N \geq 2000$  cycles) and Monismith et al. (1975) model ( $N \geq 3000$  cycles). The deviation error dependency of these two models to the cycle number in the study is shown in Table 3.4.

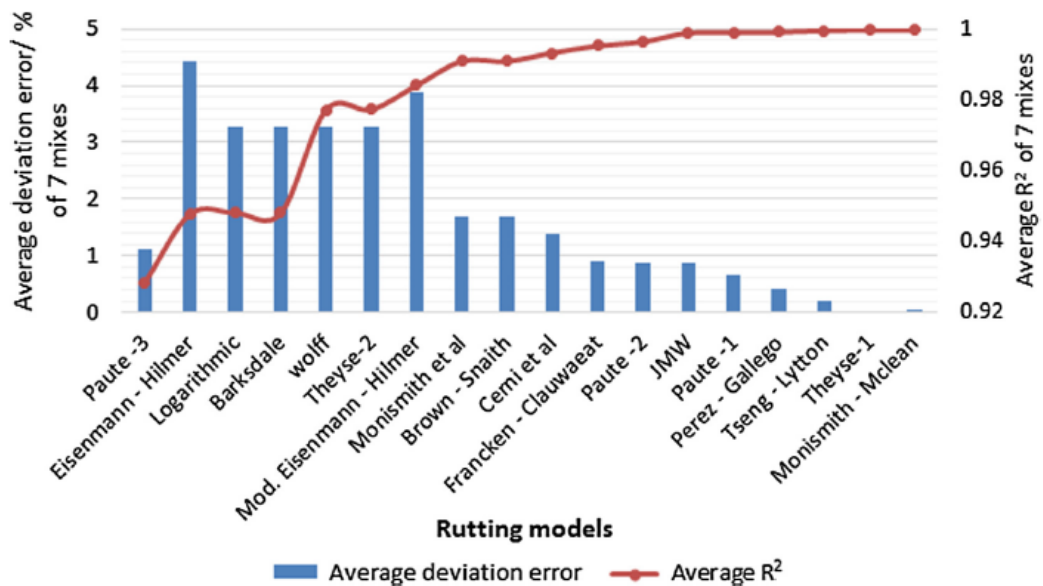


Figure 3.16: The variation of the deviation error in the final creep deformation and  $R^2$  of various creep models (Javilla et al. 2017).

Table 3.4: The deviation error dependency of these two models to cycle number (Javilla et al. 2017)

Base cycles	Monismith - 1 model		Tseng - Lytton model	
	Minimum $D_e$	Maximum $D_e$	Minimum $D_e$	Maximum $D_e$
10	211.9	1713.9	1.6	80.4
100	33.7	240.7	0.0	33.3
500	0.9	73.3	0.7	35.1
1000	1.9	42.9	1.4	28.5
2000	2.8	23.6	0.3	18.5
5000	0.2	10.9	0.4	7.2
7000	1.0	6.0	0.1	3.4
10,000	0.4	2.6	0.0	1.3

Most of the models in Table 4 in Appendix E are the outcomes of different mathematical fittings on test data. The accuracy and capability of the models to predict the creep deformation and creep depth directly depends on the ability of applied tests to simulate the real in-situ situation.

Among the existing asphalt creep deformation tests (Table 1 to 3 in Appendix A), most of the literature (Khandehal & Cooley 2003; Huang & Zhang 2011; Partl et al. 2013) recommended the triaxial compression repeated load tests or loaded wheel testers to simulate the development of creep deformation and also to optimise the model parameters. For the Mechanistic – empirical design, the triaxial compression repeated load tests are more common because of accessibility, low price, the known stress distribution, and the capability to easily calculate the modulus of asphalt (Di Benedetto et al. 2001; Huang & Zhang 2011).

However, as discussed earlier in section 3.3, the TRLPD tests of the ability to predict the creep deformation development in the field is not reasonable at the moment and is under development to overcome the following listed issues for the laboratory condition:

- Simulating the in-situ confinement in laboratory
- Simulating the real in-situ stress distribution under tyres
- Controlling the air voids distribution in the laboratory
- Simulating the in-situ environmental situation such as daily temperature and UV fluctuations.

### 3.5 Summary

The Chapter provided details of an extensive literature review that encompassed the following aspects:

1. The creep deformation mechanisms in flexible asphalt pavement
2. The critical parameters that influence the creep deformation of asphalt in the field
3. The range of globally available tests employed to evaluate creep deformation in the laboratory and their limitations
4. The key challenges to optimise creep deformation testing and the current attempts to address those challenges
5. The available Mechanistic-empirical creep deformation models and the major limitations regarding these models for accurate prediction of creep.

The review has indicated that there appears to be much research remaining to be undertaken for improving laboratory testing methodologies that will generate superior models that can be used to better predict in-situ behaviour. The literature review indicated that laboratory creep testing should be undertaken while applying stress responsive confinement that reflects in-situ behaviour. Air voids and their distributions in the laboratory samples is another factor which should be considered to better rank the creep resistance through laboratory creep tests. It was also noted that stress levels should represent tyre pressures of 500 to 1000 kPa as seen in most heavy vehicles. The focus of this research will be on creep prediction through optimising the current Australian (Ahmadinia 2017) approaches to creep testing by considering the noted challenges.

## CHAPTER 4

### RESEARCH PLAN AND METHODOLOGY

#### Contents

4.1	Introduction .....	61
4.2	Material selection .....	63
4.2.1	Aggregate type and gradation .....	63
4.2.2	Binder types .....	65
4.3	Sample fabrication.....	67
4.3.1	Asphalt mix design and sample preparation .....	67
4.3.2	Sample preparation for air voids measurement and UWT test .....	67
4.3.3	PVC ring confinement.....	67
4.3.4	Strain gauges set up.....	68
4.4	Test procedures.....	69
4.4.1	Air voids measurement .....	69
4.4.2	Multistage Confined Dynamic Creep (MCDC) test.....	71
4.5	Finite element modelling of stress distribution .....	74
4.6	Application of the MCDC test for creep resistance ranking of asphalt.....	75
4.7	Creep life prediction method using MCDC test.....	75
4.7.1	Creep slope and conventional intercept measurement.....	76
4.7.2	Creep life estimation .....	76
4.8	Compressive resilient modulus calculation of asphalt using MCDC test ...	78
4.9	Summary .....	79

## 4.1 Introduction

Asphalt creep is dependent on the mix design, environmental and traffic factors. Any laboratory creep tests need to consider numerous factors to best predict the resistance of an asphalt pavement to creep deformation under repetitive trafficking.

The current research focuses on development of a Multistage Confined Dynamic Creep (MCDC) test and an Ultrasonic Wave Transmission (UWT) technique to better rank asphalt creep deformation resistance and subsequently to estimate the asphalt creep life for flexible pavements.

The chapter encompasses the following aspects and provide an overarching outline of the research plan and methodology (Figure 4.1).

- Asphalt mix materials and their properties;
- Asphalt sample fabrication and preparation for testing;
- Universal Testing System (UTS) optimisation;
- Numerical modelling; and
- Application of the UWT technique and the MCDC test.

Subsequent chapters provide details.

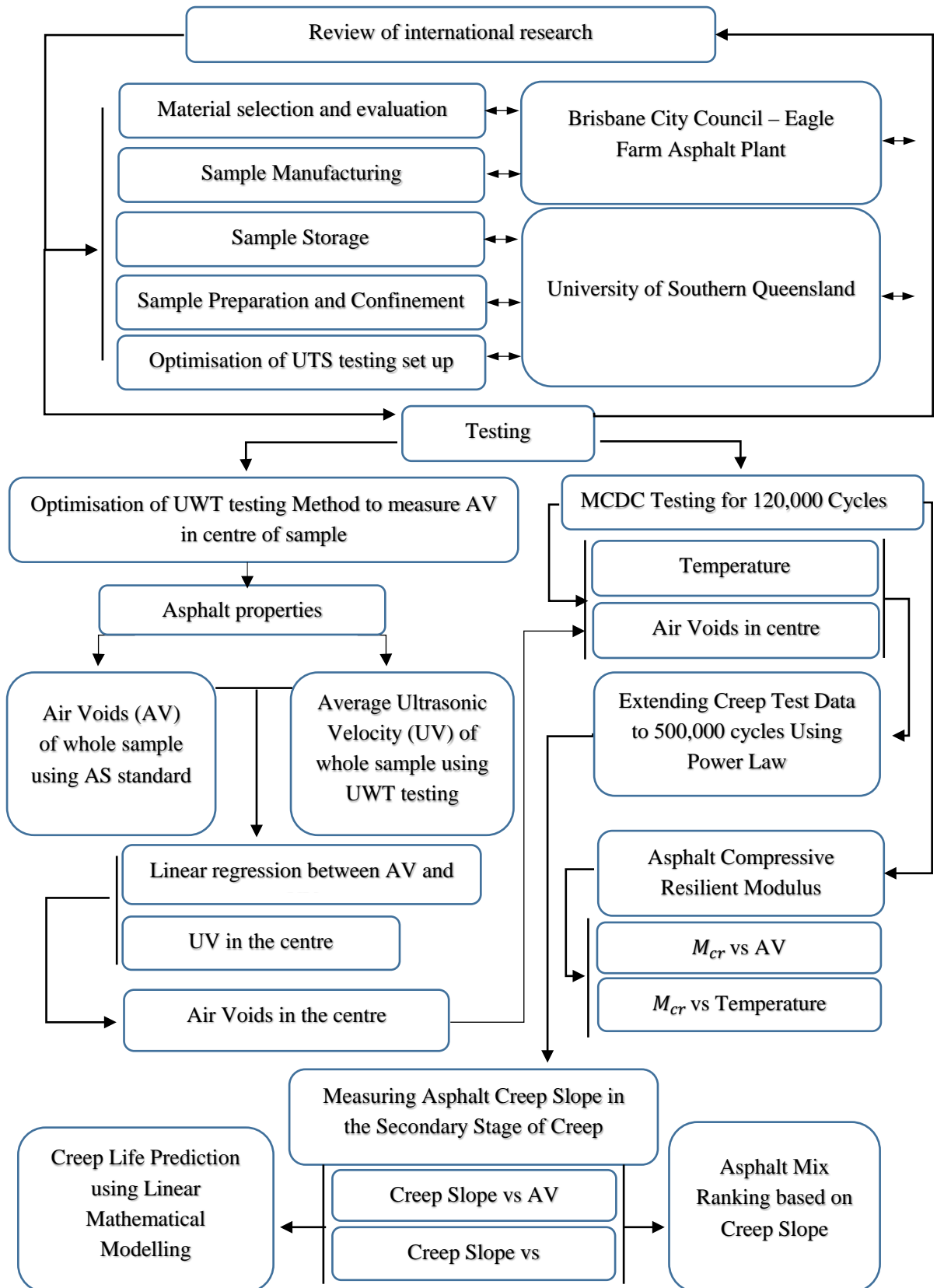


Figure 4.1: Overarching outline of the research plan and methodology

## **4.2 Material selection**

The performance characteristics of an asphalt mixture depend on the asphalt mix design which is influenced by the following key factors:

- Maximum aggregate size and gradation
- Aggregate type and properties
- Binder type and properties
- Air voids
- Additive types and properties

The laboratory work for this study used a type III BCC (Brisbane City Council) Mix with a 20mm nominal aggregate size made with three types of binder: Conventional Bitumen (C320), Multigrade Bitumen (M1000) and Polymer Modified Bitumen (PMB-A5S) binder. All asphalt samples used in this study were fabricated with the same aggregate type and gradation using the same binder content (5%). The target air voids (1% to 10%) were achieved by changing the level of compaction using a shear box compactor. All asphalt mixes used were plant produced at the BCC mixing plant located at Eagle Farm in Brisbane. In order to ensure the quality of the selected materials, each of the materials was subjected to standard compliance testing prior to mix production.

### **4.2.1 Aggregate type and gradation**

The properties of coarse and fine aggregates used for fabricating all asphalt specimens are described in Table 4.1 and Figure 4.2.

Relevant tests to Australian Standards (AS) and Queensland Department of Transport and Main Roads (Q) specifications were undertaken for the selected coarse and fine aggregates and filler. The test results are summarised in Tables 4.2 and 4.3.

Table 4.1: BCC Type III aggregate gradation

Sieve (mm)	Design Grading (% passing)	Upper Limit (% passing)	Lower Limit (% passing)
53.0	100	100	100
37.5	100	100	100
26.5	100	100	100
19.0	100	100	100
13.2	98	100	91
9.5	78	85	71
6.7	62	69	55
4.8	46	53	39
2.4	34	39	29
1.2	25	30	20
0.6	19	23	15
0.3	12	16	8
0.2	6.8	9.3	4.3
0.1	5.8	7.3	4.3

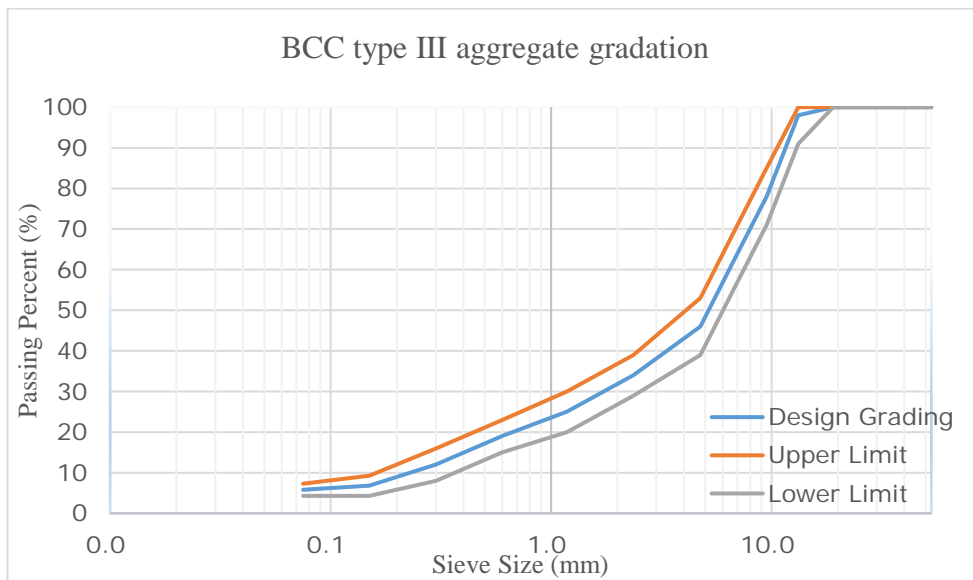


Figure 4.2: BCC Type III aggregate gradation plot

Table 4.2: Aggregate characteristics

Test Method	Description	Limits	7 mm agg result	9 mm agg result	14 mm agg result
AS 1141.11	Grading	-	Conforming	Conforming	Conforming
AS 1141.15	Flakiness	<30%	11.6	12.4	7.8
Q 214 B	Water Absorption	Max 2%	0.68	0.39	0.5
Q 214 B	Particle density (Dry)	t/m <sup>3</sup>	2.666	2.668	2.672
Q 215	Crushed Particles	Min 80%	100	100	100
Q 217	Weak Particles	Max 1%	0.7	0	0
Q 205 B	10% Fines	Min 150 KN	296	272	239
	Product Conforms	(Yes/ No)	Yes	Yes	Yes

Note: Q refers to a Queensland Department of Transport and Main Roads test method

Table 4.3: Filler characteristics

Test Method	Description	Limits	Baghouse test result	Rockflour test result	Combined BH/RF test result
AS 1141.11	600 µm Grading (AS 2357 Limits)	100	100	100	100
AS 1141.11	300 µm Grading (AS 2357 Limits)	95-100	100	100	100
AS 1141.11	75 µm Grading (AS 2357 Limits)	75-100	92.8	97.1	97.1
AS 1141.17	Voids in Compacted Filler	Min 38%	48	49	46
AS 1141.7	Apparent Particle Density	TBR	2.706	2.756	2.729
	Products Conforms	(Yes/ No)	Yes	Yes	Yes

#### 4.2.2 Binder types

In asphalt wearing courses, where asphalt has greater exposure to the environment, the selected binder type and content play the key role in the pavement performance (Austroads 2008a). The sub-tropical/temperate climates of most Australian states

make the selection of appropriate binder critical in order to deal with such common pavement temperature sensitive distresses, such as the creep deformation of asphalt.

In this research, to assess the influence of the binder type on the creep deformation of asphalt pavements in short and long term under different temperature, three types of bitumen binder are selected; Conventional, Multigrade and PMB. These three binder types have different rheology properties. One unmodified bitumen binder (C320) and two bitumen binders known to enhance rut resistance, i.e. Multigrade (1000/320) and SBS Polymer Modified Bitumen (PMB-A5S), were used to fabricate the asphalt specimens. The rheological properties of the three selected bitumen binder were determined using standard Australian test procedures and details are provided in Tables 4.4, 4.5, and 4.6.

Table 4.4: Properties of bitumen binder class C320

Property	Test Method	Limits	Test result
Viscosity at 60°C (Pa.s)	AS 2341.2	260-380	328
Penetration at 25°C, 100g, 5s	AS 2341.12	Min 40	49
Softening point (°C)	AS 2341.18	Report	51.2
Viscosity at 135°C (Pa.s)	AS 2341.2	0.4-0.65	0.53

Table 4.5: Properties of Multigrade 1000/320 bitumen binder

Property	Test Method	Limits	Test results
Viscosity at 60°C (Pa.s)	AS 2341.2	Report value	910
Viscosity at 135°C (Pa.s)	AS 2341.4	1.5 max	0.78
Viscosity at 60°C after RTFOT (Pa.s)	AS 2341.2	3500 - 6500	5550
Softening Point (°C)	AS 2341.18	Report	58.5
Flash Point, °C	AS 2341.14	250 min	348
Density at 15°C (t/m <sup>3</sup> )	AS 2341.7	Report	1.031

Table 4.6: Properties of Polymer Modified bitumen binder (PMB-A5S)

Property	Test Method	Limits	Test result
Consistency at 60°C (Pa)	AG: PT/T121	5000 min	11254
Stiffness at 25°C (kPa)	AG:PT/T121	30 max	19
Viscosity at 165°C (Pa.s)	AG:PT/T111	0.9 max	0.64
Softening Point (°C)	AG:PT/T131	82-105	103.0
Flash Point, °C	AS 2341.14	250 min	334
Loss on heating (%)	AG:PT/T103	0.6 max	0.1

### **4.3 Sample fabrication**

#### **4.3.1 Asphalt mix design and sample preparation**

The material properties of three selected asphalt mixes were provided in the previous section. The same binder content was used for all three types of mixes (5%) to be able to evaluate the effect of the binder type in the performance of the selected mixes. Air voids were controlled from 1 to 10% during mix compaction in the laboratory. All three selected mixtures are well known within the industry as having different creep-resistance ability based on the binder used (Austroads 2010, Austroads 2014).

All asphalt mixes were produced from the same production runs to ensure that the quality and the production processes of mixes were the same. Bulk uncompacted mixes were stored in a covered container before compaction. Compacted slabs were produced using a shear box compactor. The 150mm diameter samples were cored from the slabs and cut into 50mm thicknesses, and trimmed using a belt sander. Finally, all samples were stored in containers and transferred to the USQ laboratory for measurement and testing.

#### **4.3.2 Sample preparation for air voids measurement and UWT test**

Specimens received from the Eagle Farm plant were washed, dried and preconditioned at a temperature of 25°C for 48h before being subjected to air voids measurement as per Australian Standard (AS/NZS 2891).

After finalising the air voids measurement, all samples were kept in a temperature controlled sealed dry environment. Both lower and upper surface of the cylindrical samples were coated with silicone mastic to fill all surface voids for smooth surfaces. Finally, samples were conditioned in the oven at 25°C for 48 hours to be ready for the ultrasonic transmission test (UWT). The UWT technique, using a Pundit7 apparatus, was applied according to BS EN 12504-4 standard to generate the ultrasonic wave and to determine the ultrasonic pulse velocity of the asphalt sample. Further details of ultrasonic testing are provided in Chapter 5.

#### **4.3.3 PVC ring confinement**

The confining system that was used in this research involved encasing the asphalt sample in a PVC ring and a Liquid Glass (LG) epoxy resin. Previous research conducted by Ahmadinia et al. (2017) showed that the PVC wall and resin thickness

have a direct effect on the magnitude of confinement. A PVC ring of 150 mm nominal internal diameter with a 2.5mm thickness was selected based on this previous research. To fill the 2.5mm gap between asphalt sample and PVC ring, a flowable LG epoxy resin was used. The LG epoxy resin properties are outlined in Table 4.7.

The asphalt sample was located in the centre of the PVC ring and the gap between the two was filled with LG epoxy resin as shown in Figure 4.3. Samples were then preconditioned in an environment of 25°C for two weeks to let the resin cure completely. The confinement procedure was the same for all samples, in order to assess the effect of other variables.

Table 4.7: Properties of liquid glass epoxy resin

Property	Description
Appearance	Water-Clear when mixed
Mix ratio	Volume: 2 base to 1 hardener
Drying time	7-10 days for 100%
Proprietary name	Norglass epoxy resin



Figure 4.3: PVC confinement set up

#### 4.3.4 Strain gauges set up

The validation of the new confinement system was assessed based on the generated load related stress around the PVC ring. For this purpose, and also in order to evaluate the effect of other variables such as load, air voids, and the temperature on the confinement stress, two 30mm strain gauges were glued on the sides of the PVC ring for all samples (Figure 4.4). The measured strain in the laboratory was then compared

with the results of numerical models in order to better investigate the impact of the confining system variables. Table 4.8 provides details of the applied strain gauges.

Table 4.8: Strain gauge specifications

Property	Description
Gauge type	PFL-30-11
Gauge factor	$2.13 \pm 1\%$
Gauge resistance	$119.6 \pm 0.5\Omega$
Transverse Sensitivity	- 0.1 %
Gauge length	30 mm
Element	Single element



Figure 4.4: Strain gauge set up

#### 4.4 Test procedures

##### 4.4.1 Air voids measurement

##### 4.4.1.1 The Australian Standard (AS/NZS 2891)

A key challenge in assessing the deformation characteristics of asphalt is the control and measurement of air voids. For all preconditioned samples (25°C for 48h) the air voids content of the whole sample was determined using the Australian Standard method (AS/NZS 2891) as follows:

$$AV = \frac{\rho_{\max} - \rho_{\text{bulk}}}{\rho_{\max}} \times 100 \quad (4.1)$$

AV = air voids content (%)

$\rho_{\max}$  = Maximum Density ( $\text{t}/\text{m}^3$ )

$\rho_{\text{bulk}}$  = Bulk Density ( $\text{t}/\text{m}^3$ )

#### 4.4.1.2 Ultrasonic Wave Transmission (UWT) technique

The Australian Standard method is only able to determine the air voids value for the whole sample and cannot reveal the complex distribution of internal air voids based on the aggregate structure in an asphalt sample. In this research, the vertical stress is applied by using the 50mm platen size on 150mm diameter sample. Knowledge of the air voids under the platen enables a better analysis of creep deformation data.

In this research, the UWT technique used a Pundit 7 apparatus (Figure 4.5a), applied according to BS EN 12504-4 standard to generate the ultrasonic wave and to determine the ultrasonic pulse velocity of the asphalt sample. Two 54-kHz piezoelectric crystal transducers (transmitter and receiver) were placed in parallel at each side of the specimen to measure ultrasonic wave transit time (for P-wave) at 17 different locations of the sample at 25°C as shown in Figure 4.5.b. The transit time for the compression wave (P-wave) to pass the length of the asphalt sample was recorded to calculate the ultrasonic pulse velocity using the 5.1 formula in chapter 5.

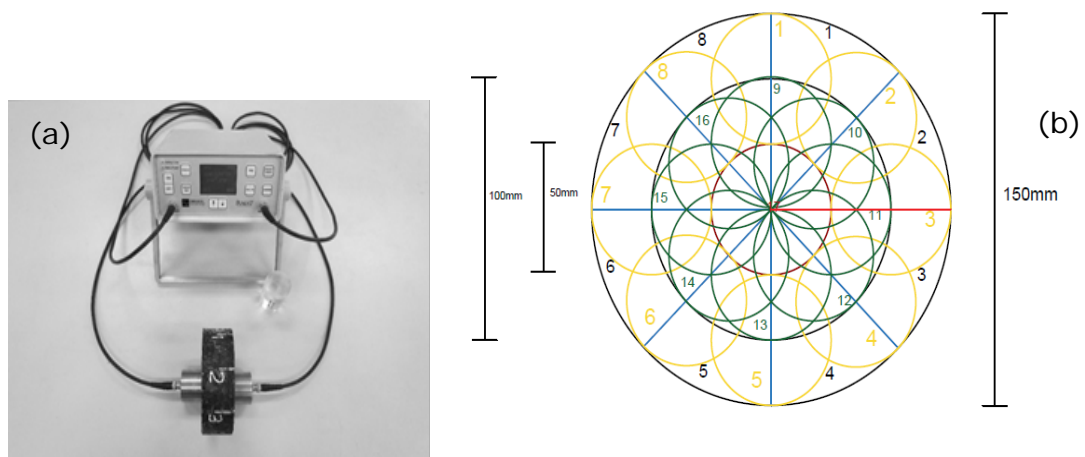


Figure 4.5: (a): Pundit 7 with two transducers (b): Sample divisions (17 points) for ultrasonic test

#### 4.4.1.3 Measuring Air voids in the centre of sample

The air voids in the centre of sample were determined according to the following steps:

1. Measure Ultrasonic Velocity (UV) for 17 locations;
2. Measure Air Voids (AV) of the whole sample using Australian Standard;

3. Generate the regression equation between the data generated in steps 1 and 2 for all samples; and
4. Calculate the AV in centre of the sample using UV in the centre (step1) and the calculated regression equation (step 3).

In Chapter 5 the UWT development procedure is explained in more details and all related calculations discussed.

#### **4.4.2 Multistage Confined Dynamic Creep (MCDC) test**

##### **4.4.2.1 Universal testing system (UTS) optimisation**

The Industrial Process Controls (IPC Global) company introduced its UTS 14 software for the Universal Testing System (UTS) machine to calculate and measure the permanent strain in each load cycle. Limitations of the software are (i) it is unable to record and present the details for a single complete load cycle data, and (ii) it is not possible to continue the test while changing the magnitude of the load.

An extra data logger was attached to the UTS machine using three “UTM Normalised BNC Breakout Cable Assemblies” (Figure 4.6a) to extract and record more data from the UTS machine. The cables provided the required connection between UTS IMACS Chassis (Figure 4.6b) and Universal amplifier (Figure 4.6 c). The set up was able to record the data from the LVTs and strain gauges at the same time. This enabled continuous recording of data for different load pulses and also for analysing data over a single load pulse. The UTM set up details are illustrated in Figure 4.7.

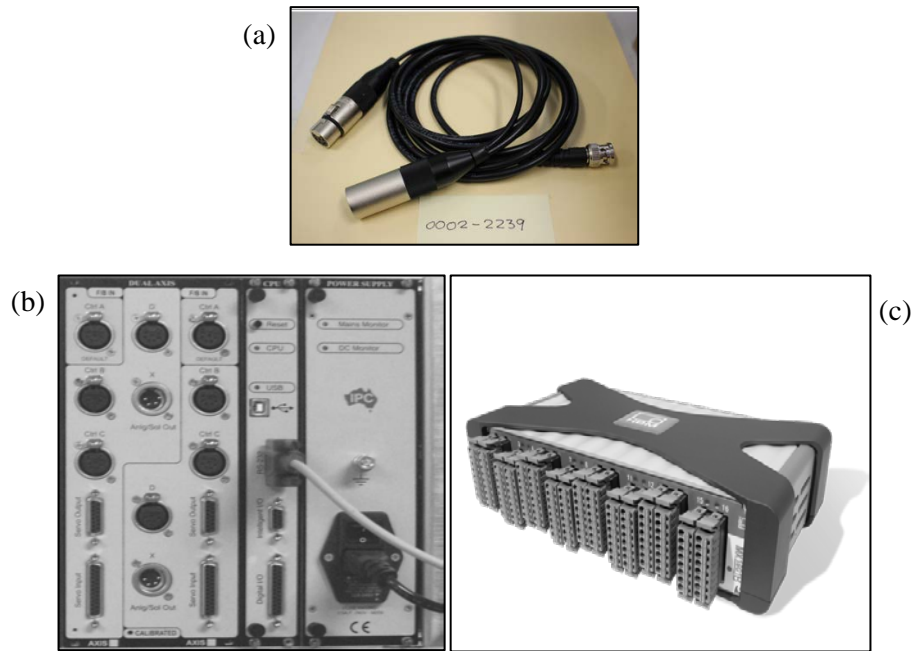


Figure 4.6:  
 (a). UTM Normalised BNC Breakout Cable Assembly (IPC part number. 0002-2239)  
 (b). IMACS Chasis of Universal Testing System (UTS)  
 (c). The Universal Amplifier (QuantumX MX1601B)



Figure 4.7: Optimisation of UTS tester using an extra data logger

#### 4.4.2.2 Multistage Confined Dynamic test procedure

The Multistage confined dynamic creep test was undertaken using the IPC Universal Testing System (UTS) machine. The test steps were as follows:

- Confinement and strain gauge setup (as outlined in sections 4.3.3 and 4.3.4);
- Smoothing sample surface using 80 grit emery paper to remove any surface defects to ensure a flat testing surface;
- Reduction of the end friction using silicone lubricant on both ends of the sample;
- Placing the confined sample centrally aligned under the actuator;
- Attaching strain gauges to the data logger;
- Conditioning the sample in the control chamber at the desired test temperature for a minimum of two hours;
- Setting up the UTS 014 software using the parameters in Table 4.9 and applying the selected dynamic load; and
- Running the other data logger and UTS014 software simultaneously to record data for 12 hours.
- Record the data for analysis the creep slope and creep deformation. An example outcome of multistage confined creep testing is provided in Figure 4.8.

Table 4.9: Details for MCDC test

Parameter	Description	
Compressive stress (stage 1, 2, and	500,750, and 1000 kPa	
Seating stress	20 kPa	
Loading period 1	500 milliseconds (ms)*	*Represent the vehicle speed of 3.2 km/h
Pulse repetition period 1	2000 milliseconds (ms)*	
Loading period 2	100 milliseconds (ms)*	*Represent the vehicle speed of 16.1 km/h
Pulse repetition period 2	1000 milliseconds (ms)*	
Test temperature (one of)	40°C or 50°C	
Minimum termination pulse count	40,000 cycles for each stage	

\* Vehicle speed is a function of loading period and calculated based on the frequency concept of NCHRP 9-19 which is presented in Kumlai et al at 2014.

The development process of MCDC test will be explained in detail in Chapter 6.

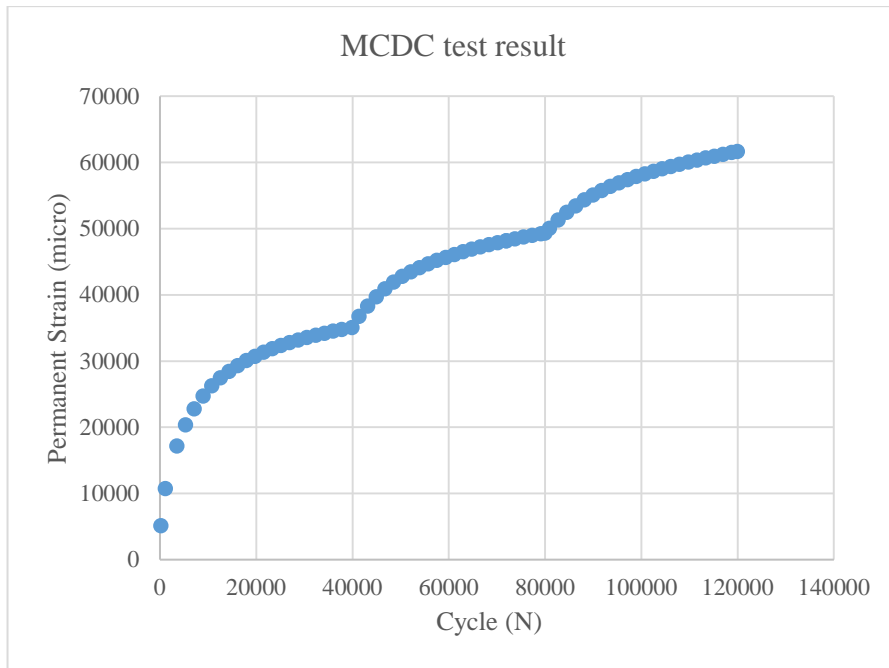


Figure 4.8: Multistage Confined Dynamic Creep (MCDC) test results

#### 4.5 Finite element modelling of stress distribution

Elastic modelling of the dynamic test with the new confinement system was undertaken for the following purposes:

- To validate the new confinement system by assessing the stress distribution in the laboratory dynamic creep test; and
- To compare the stress/strain distribution in the sample to that in an asphalt layer.

Abaqus, one of the most popular finite-element programs, was used for two dimensional modelling of asphalt pavement layer and laboratory confined samples as follows:

- Elastic model of single layer asphalt pavements under different tyre pressure (500, 750 and 1000 kPa stress); and
- Elastic model of laboratory specimens (with 150mm diameter and 50mm height confined by multilayer system including 2.5mm LG resin and 2.5mm PVC ring, using 50mm platen sizes) and the above pressures.

Some characteristics of the elastic models are as follows:

- a) Model subdivision: 40 × 40 nodes.
- b) Model elements: 8 node quadrilateral elements.

- c) Axisymmetric model: ( $R_x=R_y=R_z=0$  and Z translation= 0).
- d) Edge Restraints: (Y axial symmetric:  $D_y$  free,  $D_x$ =fixed, and, X axle:  $D_x$  free,  $D_y$ = fixed, where in all the other places:  $D_x= D_y=$  free).
- e) Material properties input; a) Material; Isotropic  
b) Type; axisymmetric.

Further details of the FEM models are provided in Chapter 6.

#### **4.6 Application of the MCDC test for creep resistance ranking of asphalt**

The MCDC test procedure involved obtaining permanent deformation for 120,000 cycles for some samples in order to ascertain the use of early stage creep to predict later stage performance. The long term 120,000 cycles indicated that the following would provide the valuable information. Full details are provided in Chapter 6.

1. Permanent deformation in 20,000 cycles in each stage.
2. Secant creep slope between 20,000 and 40,000 cycles.
3. Secant creep slope between 40,000 cycles and estimated one in 100,000 cycles for each stage.

This methodology was used for asphalt samples ranking under varying operational conditions using the MCDC test. The test, supported by the UWT void evaluation technique, was adopted as a measure to better predict extended laboratory creep performance.

#### **4.7 Creep life prediction method using MCDC test**

Predicting the service life of asphalt pavements as a function of permanent deformation at high loads and temperatures remains an ongoing challenge for Australian road agencies as they model future maintenance strategies.

The application of MCDC data for estimating creep life was investigated through:

1. Creep slope and conventional intercept calculation
2. Creep life estimation using calculated parameters

The development process of creep life estimation using MCDC test methodology is discussed in detail in Chapter 6.

### 4.7.1 Creep slope and conventional intercept measurement

To predict a creep life, the accurate measurement of creep slope in the steady state of creep (Figure 4.9) is required as an input variable. The creep data from the MCDC test in each test stage was analysed to calculate a secant creep slope as follows:

1. A power regression model was used to predict the creep deformation up to 500,000 cycles, based on laboratory testing data between 20,000 cycles and 40,000 cycles.
2. Permanent strain at 100,000 cycles and 500,000 cycles obtained from the power regression model was used to calculate a secant creep slope and “conventional intercept” (Figure 4.9 Schematic).

The secant creep slope calculation will be discussed in detail in Chapter 8.

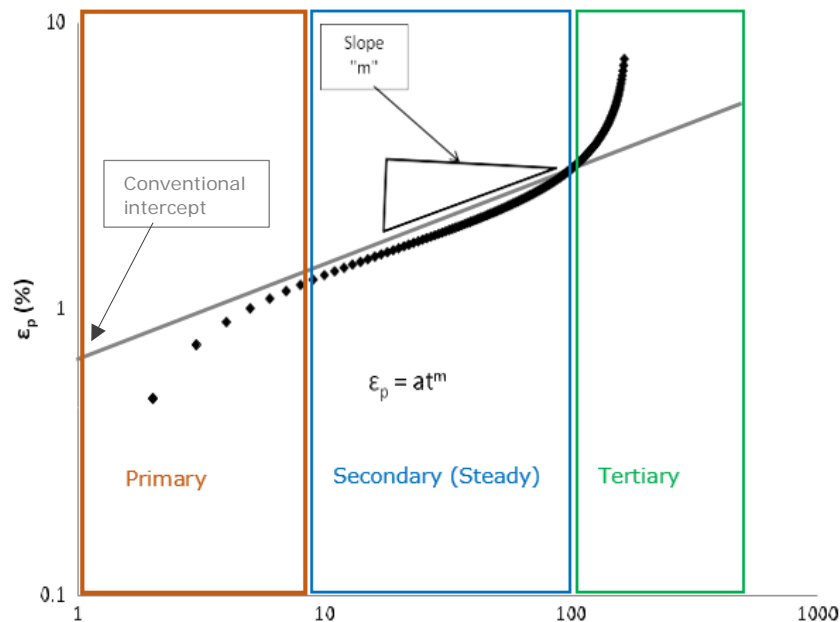


Figure 4.9: Schematic diagram of creep stages and slope

### 4.7.2 Creep life estimation

A schematic transverse profile of creep deformation within an asphalt surface is shown in Figure 4.10. For the following analysis, a pavement’s serviceability is considered to be affected by creep deformation when it exhibits a total creep depth of 25mm. This 25mm level includes both densification and shear deformations. Since it was possible to measure heave in the laboratory samples the analysis used a 20mm creep deformation depth to calculate the creep life of asphalt. To allow modelling, the 20mm was assumed to occur within a 200mm asphalt layer to obtain an estimation to the end

of serviceability. As the laboratory samples were 50mm in depth a 4:1 ratio of 5mm was used as the end of creep life for laboratory samples.

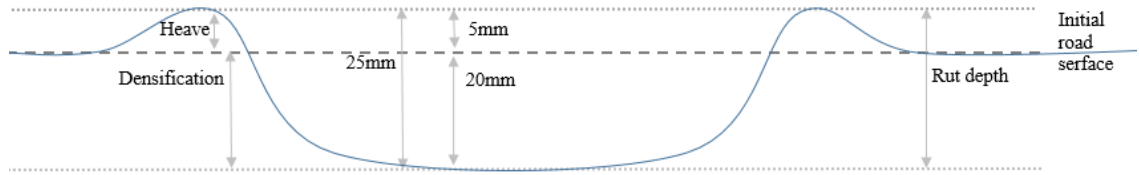


Figure 4.10: Transverse profile of rut depth (creep deformation) under the tyre

The creep life of the asphalt mixes, based on the laboratory data was determined as follows:

1. The permanent strain was estimated at 500,000 cycles in each stage by fitting a power regression model ( $y = ax^b$ ) to the data between 20,000 and 40,000 load cycles and extrapolating the data to 500,000 cycles.
2. Both secant creep slope (m) and conventional intercept (c) (Figure 4.9) were calculated using the secant between permanent strain at 100,000 and 500,000 load cycles.
3. The permanent strain life ( $\epsilon_{max}$ ) was calculated in using the height of sample (h) and a 5mm target creep depth (creep depth limit in the laboratory) as follow:

$$\epsilon_{max} = \frac{5 \cdot 10^6}{h} \quad (4.2)$$

4. Creep life finally in cycles can be calculated using the following formula:

$$\text{Creep life} = \frac{(\epsilon_{max} - c)}{m} \quad (4.3)$$

Creep life estimation using MCDC test will be discussed in detail with an example of the procedure in chapter 6.

#### 4.8 Compressive resilient modulus calculation of asphalt using MCDC test

The applied load pulse in MCDC test includes 0.1s loading and 0.9s resting time illustrated in Figure 4.11. The resilient modulus determined from the MCDC test (Figure 4.12) can be defined as the ratio of the repeated axial deviator stress to the recoverable or resilient axial strain:

$$M_{cr} = \frac{\sigma_d}{\epsilon_r} \quad (4.4)$$

$M_{cr}$  : Compressive resilient modulus

$\sigma_d$  : Deviator stress (cyclic stress in excess of confining pressure)

$\epsilon_r$  : Resilient strain in the vertical direction

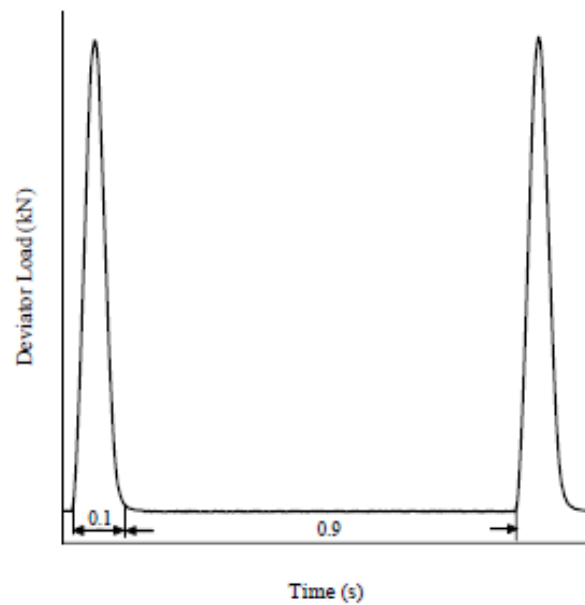


Figure 4.11: Shape and duration of applied repeated load (Titi 2006)

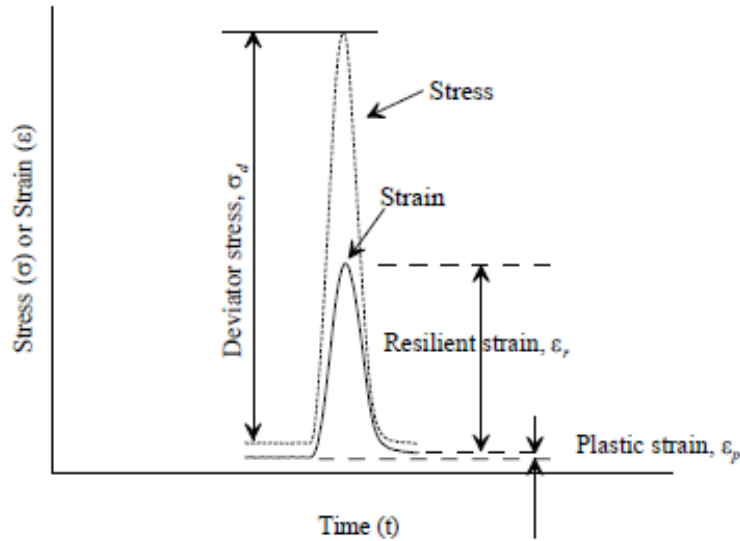


Figure 4.12: Stress and strain in one load cycle (Titi 2006)

The applied deviator stresses were 500, 750, and 1000 kPa. The shape and duration of applied repeated load were the same (0.1s loading and 0.9 rest) for all tests.

#### 4.9 Summary

The chapter outlines the overarching research plan and methodology and provides introductory explanation of the various research components commencing with material selection, mix design, sample preparation. Testing configuration and confinement setup using the stress repulsive confinement approach developed by Ahmadiania (2018) was described along with further development in instrumentation and data acquisition.

In this chapter, in two steps the applied test methods were discussed. First, two applied air voids measurement techniques: Australian Standard and UWT technique and the method of using UWT to measure the air voids under the load platen. Second, the MCDC test arrangement including IPC-UTM development and data acquisition. Then, the applied finite element methodology to validate the MCDC test was explained. The creep life measurement procedure using both MCDC test data and applied mathematical modelling also discussed. The final test, which is the measurement of compressive resilient modulus of asphalt using MCDC test, is also explained.

All key research components are discussed in detail in subsequent Chapters.

## CHAPTER 5

### DEVELOPMENT OF AN ULTRASONIC TECHNIQUE TO MEASURE AIR VOIDS

#### Contents

5.1	Introduction .....	81
5.2	Existing air voids measurement techniques .....	81
5.3	Ultrasonic Wave Transmission (UWT) technique and asphalt mixtures ....	83
5.4	UWT correlation with air voids in the whole sample.....	84
5.5	Air voids distribution in the whole sample .....	86
5.6	Development of UWT Technique to measure air voids under platen .....	88
5.7	Comparison of air void in the centre with air voids of the whole sample...	88
5.8	Evaluating UWT techniques.....	89
5.9	Conclusion.....	91

## **5.1 Introduction**

It is widely accepted that air voids play an important role in asphalt creep deformation. To better enable correlation between laboratory evaluations and field behaviour it is important to know air voids and their distribution. Most available air voids tests are only able to measure the air voids in whole samples and only a few of them are able to measure air voids distribution without sample destruction. Non-destructive techniques such as a combination of X-ray Computed Tomography (CT) and image analysis methods (Castillo & Caro 2014; Masad et al. 1999; Masad et al. 2002; Partl et al. 2012) are time consuming, expensive and complex. A simple test for measuring the air voids distribution for laboratory samples would greatly enhance data analysis and correlation.

In this part of the research, a simple non-destructive test methodology is outlined. The test is expected to:

- Determine the air voids distribution
- Detect sample defects
- Determine the air voids in the centre of sample

The Ultrasonic Wave Transmission Technique (UWT) is able to measure the true air voids under the small platen (50mm) which is used in the multistage confined creep test. Measuring the air voids under the platen enables better creep data to be generated.

## **5.2 Existing air voids measurement techniques**

The accurate assessment of air voids within asphalt is a vital and critical component of quality assurance and control (QA/QC) procedures (MRTS30 2016; Dubois et al. 2010). There is a range of different methods (Table 5.1) employed to measure the air voids content dependent on the mix type (Dense Graded, Open Graded or Stone Mastic Asphalt), maximum aggregate size, compaction method and water absorption. The main difference across the various standards relates to the measurement method used for bulk specific gravity and maximum specific gravity as illustrated in Table 5.1.

All the laboratory techniques mentioned in Table 5.1 are useful when the total air voids of the sample is required. However, none provide any information regarding air voids distribution within the laboratory sample. Investigating the impact of the air voids characteristics and distributions is thus difficult when using the methods provided in

Table 5.1 (Ren & Sun 2017). A non-destructive technique, which could quickly evaluate the distribution and microstructure of air voids of compacted asphalt in the laboratory would be well received by industry (Ma et al. 2016).

Over the last few years, research has focused on developing non-destructive laboratory techniques to evaluate the complexity of internal air voids structures within asphalt samples. In 2010, Vincent et al. successfully used a gamma-densitometer to assess the influence of the compaction process on the air voids homogeneity of asphalt samples (Dubois et al. 2010). Other non-destructive techniques such as X-ray Computed Tomography (CT) and image analysis methods (Castillo & Caro 2014; Masad et al. 1999; Masad et al. 2002; Partl et al. 2012) have been applied by other researchers and the research outcomes have shown that air voids within compacted asphalt are not uniformly distributed (Castillo & Caro 2014; Masad et al. 2002). In addition to the methods noted above, researchers have used Discrete Element Methods (DEM) for modelling air voids in asphalt to assess the impact of air voids distribution and microstructure on mechanical properties and pavement distresses (Castillo & Caro; 2014, Partl et al. 2013).

Table 5.1: Air voids measurement laboratory techniques (a part of data extract from Praticò & Moro 2012)

Outcome	Method	Application	Indicator	Standards
Calculating air voids content (%) in the laboratory compacted specimens	AASHTO	Depends on the mix type, aggregate size and water absorption one of the methods can be chosen for air voids calculation	Dimensional	AASHTO T 269-97(2007) EN 12697-6:2003
			Parafilm	ASTM D 1188-07 (abs > 2%)
	Or		Vacuum Sealing Device	ASTM D 6752-09/AASHTO T 331-08(2008) WA-733.2-2008
	ASTM		Paraffin	AASHTO T 275-07(2007) A (abs > 2%) EN 12697- 6:2003
	Or		Saturated surface dry	AASHTO T 166-07(2007) ASTM D 2726-09 (abs < 2%) UNI EN 12697-6:2003 AS/NZS 2891
	EN		Bucket vacuum assembly	ASTM D 2041-11 AASHTOT-209–10-UL (rice method)
	Or		Water displacement method	ASTM D 6857-09 AS/NZS 2891 TMR-Q306A
	AS/NZS		Silicone sealed	TMR-Q306C

Abs: water absorption; EN: European standard; AS/NZS: Australian standard; ASTM: American Society for Testing and Materials; AASHTO: American Association of State Highway and Transportation Officials; TMR: Transport & Main Roads (Australia); WA: Main Roads Western Australia.

The research techniques outlined above have typically required advanced equipment and/or modelling knowledge. The research reported here describes a simple technique using ultrasonic assessment for laboratory use to predict the air voids content and distribution in asphalt samples. This technique will be useful for better evaluating some tests such as fatigue and creep where the applied load and stresses (dynamic or static) are localised at a specific part of the asphalt sample.

### **5.3 Ultrasonic Wave Transmission (UWT) technique and asphalt mixtures**

Non-destructive tests (NDT) have been successfully applied widely in civil engineering to obtain information on materials and structures. NDT techniques give information about material and structure properties without deteriorating their structure and serviceability. NDT methods applicable to use in engineering fields can be categorised as follows:

- Rebound hammer methods
- Acoustic methods (Ultrasound, acoustic emission, impact-echo, and etc.)
- Radiation methods (gamma ray, Neutron emission, etc.)
- Electromagnetic method
- Infrared thermography methods

The Ultrasonic Wave Transmission (UWT) method is one acoustic method that has been widely used in civil engineering fields for the quality control with the following purpose (Garbacz & Garboczi 2003):

- Evaluating of material strength and homogeneity
- Evaluating of structural integrity (detection of various types of defect)
- Monitoring strain gain
- As a complement to other tests

The UWT method (also called pulse velocity) employs the determination of travel time of a longitudinal ultrasonic wave over a known path length after its transmission through the tested medium. Transducers for emitting and receiving are usually positioned on the different sides of the tested sample (figure 5.1). Based on the transducer positions, the technique is categorised as; direct method, semi-direct method or indirect method. Between the noted methods, the direct method is the simplest and most widely used arrangement of transducers, and results in accurate outcomes.

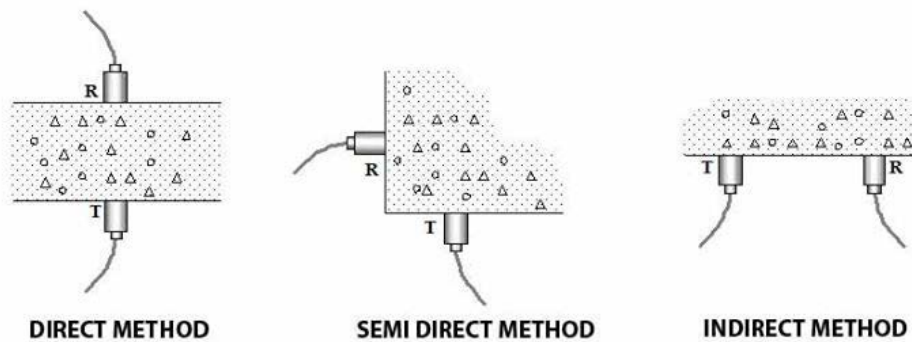


Figure 5.1: Models of wave transmission in UWT test (Ultrasonic Pulse Velocity Test- webpage)

The common procedure for evaluation of material properties using the UWT method consists of regression analysis of the experimental relationship between the pulse velocity and selected technical properties such as modulus. The regression analysis (linear or/and nonlinear) is applied to the development of a calibration (correlation) curve. For composite or nonhomogeneous materials, the reference curve is sensitive to material parameters. One of the well-known examples of this calibration curve is concrete compressive strength versus Pulse velocity.

The UWT method has been used for determining the mechanical properties of asphalt such as modulus (Partl et al. 2012; Stephenson & Manke 1972). The technique also has been used to evaluate and predict asphalt pavement fatigue (Houel & Arnaud 2009; Tigdemir et al. 2004). There have been other attempts to generate UWT correlation curves for other asphalt material deteriorations ( Mounier et al. 2012; Norambuena-Contreras et al. 2010). However, none employ the UWT technique to generate the correlation curve related to air voids volume and distribution in asphalt laboratory samples. Due to the non-destructive nature of this test, there is a high potential of using it as an air voids indicator for asphalt laboratory samples. The test can be used as complementary for the multistage confined dynamic creep test in this research in order to better analyse data.

#### 5.4 UWT correlation with air voids in the whole sample

To better understand the UWT correlation with air voids in an asphalt sample a specific test was designed. The plant produced mixes (Conventional (C320), Multigrade (M1000) and a SBS Polymer Modified (PMB-A5S) with 5% bitumen binder) discussed in Chapter 5 were used. As outlined previously an asphalt shear box

compactor using different compaction efforts was used to produce asphalt slabs with a range of target air voids from 1% to 10%. Samples with a 150mm diameter and 50 mm height were cored and cut from the compacted asphalt slabs. The specimens were washed, dried and preconditioned at the test temperature of 25°C for 48 hours before being subjected to the air voids measurement test and UWT test as follow:

- For all preconditioned samples the air voids content of the whole sample was calculated using the specimen's bulk specific gravity (Saturated Method) and the asphalt's theoretical maximum specific gravity (Rice Method) according to Australian standard (AS/NZS 2891).
- The UWT technique used a Pundit 7 apparatus applied according to BS EN 12504-4 standard to generate the ultrasonic wave and to determine the ultrasonic pulse velocity of the asphalt sample. As introduced in Chapter 4 two 54-kHz piezoelectric crystal transducers (transmitter and receiver) were placed in parallel at each side of the specimen (direct method) to measure ultrasonic wave transit time at 17 different locations at 25°C as shown in Figure 5.2. The transit time for the compression wave (P-wave) to pass the length of the asphalt sample was calculated using following formula:

$$UV = L/T \quad (5.1)$$

Where,

- UV = Ultrasonic pulse velocity (km/s)
- L = Length of specimen (mm)
- T = Transit time (ms)



Figure 5.2: 17 transducers locations on each sample for UWT test

After the measurement of air voids of the whole sample and ultrasonic velocity at 17 points on the same sample, the UWT correlation with air voids in the whole sample was generated. The results for ultrasonic velocity and air voids content (0% to 10%) for all asphalt mixes (C320, M1000 and PMB-A5S), calculated at the reference temperature of 25°C, are summarised in Figure 5.3 for the overall average of the 17 locations.

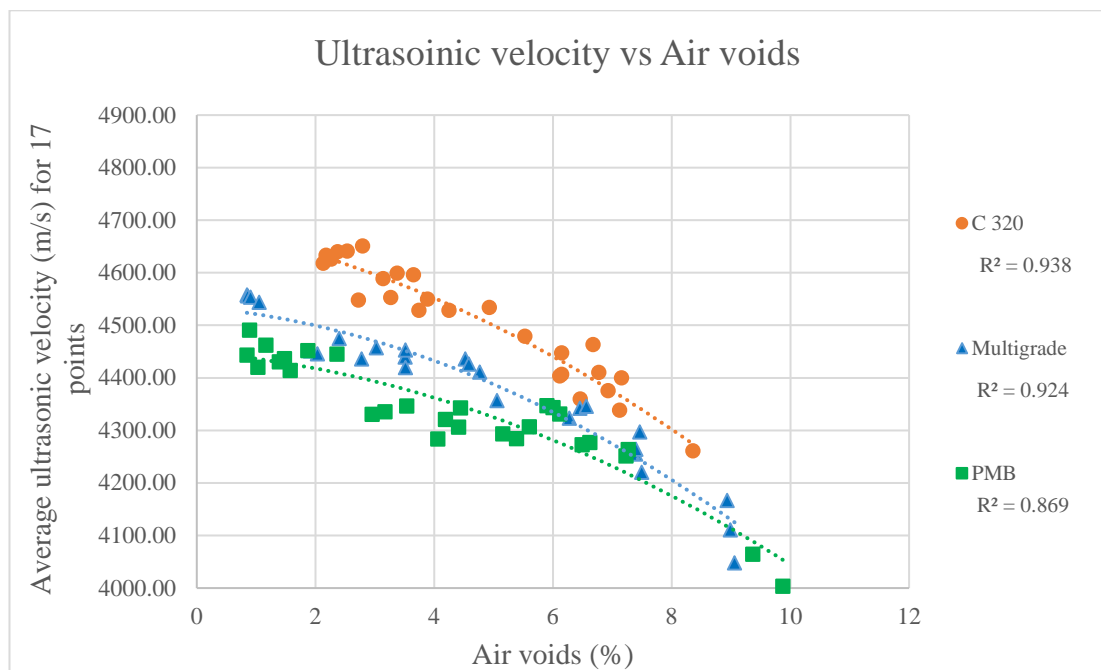


Figure 5.3: Ultrasonic velocity versus Air voids for mixtures with C320, M1000, and PMB in average 17 points

It can be clearly noted that the trend lines indicate that an increase of air voids content from 0% to 10% results in a decrease in ultrasonic velocity for all three mix types when considering the average of all 17 locations on the sample. From this good correlation between the ultrasonic velocities magnitude with measured air voids in the whole sample, it can be concluded that the measured ultrasonic velocity using UWT technique can be used as an air voids indicator in a sample.

### 5.5 Air voids distribution in the whole sample

Figure 5.4 displays the ultrasonic velocity across the 17 locations for C320, M1000 and PMB-A5S at their highest and lowest air voids contents. The ultrasonic velocity at each point is an indicator of a specific air voids content at that point as discussed in

the previous section. The data clearly indicates that air voids vary considerably within the sample.

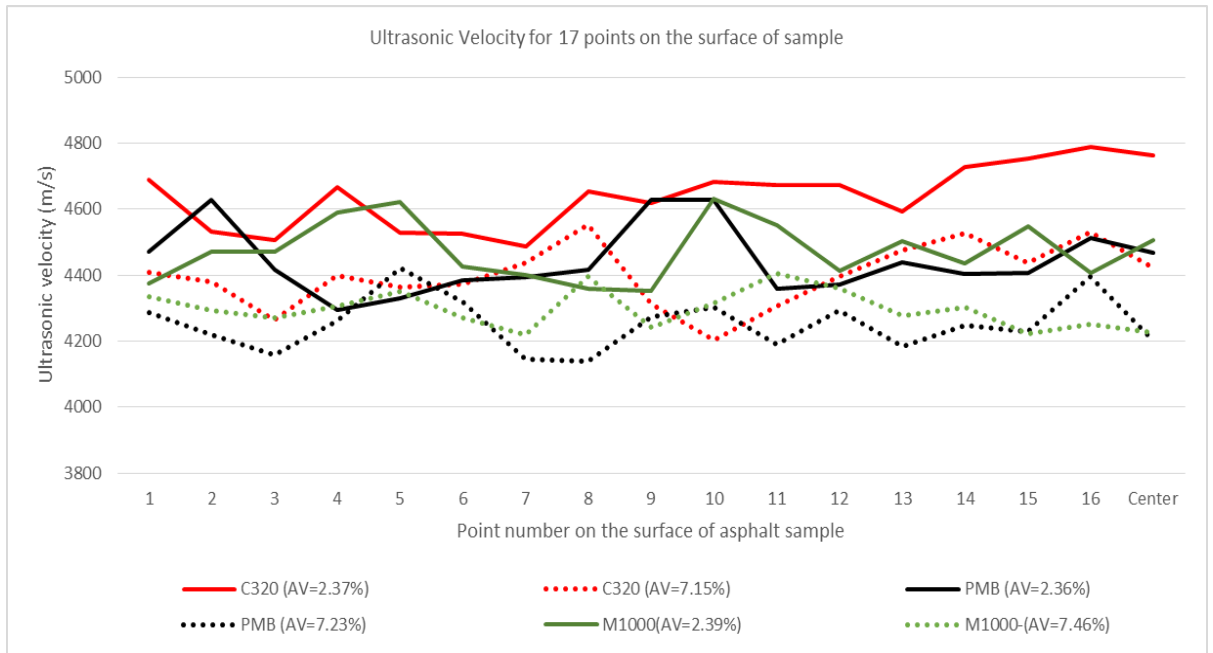


Figure 5.4: Ultrasonic velocity for 17 points on the surface of samples with low and high air voids

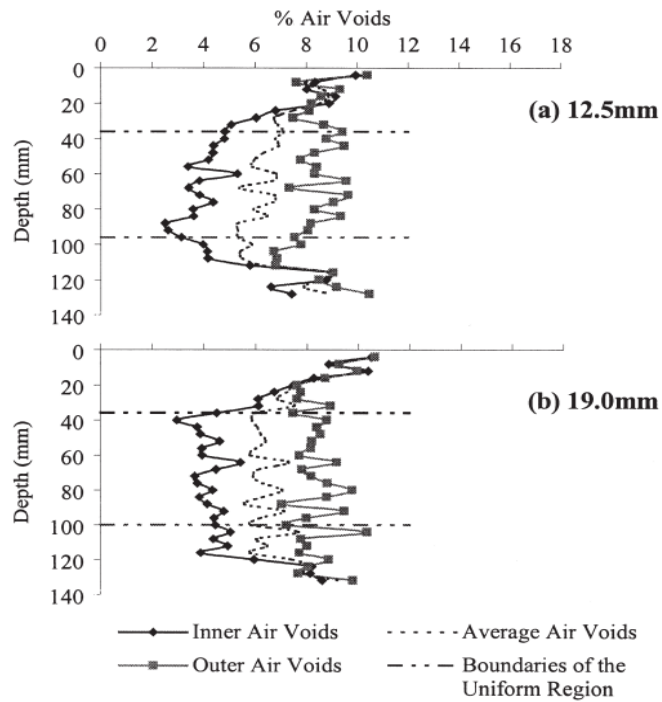


Figure 5.5: Vertical and horizontal air voids distribution in specimens with 12.5mm and 19mm maximum aggregate size ( a part of Figure from Tashman et al. 2002)

This outcome is similar to that obtained by other researchers using X-Ray techniques (Masad et al. 2002; Tashman et al. 2002) as shown in Figure 5.5 where the air voids distribution in asphalt samples vertically and horizontally is seen.

## 5.6 Development of UWT Technique to measure air voids under platen

The UWT technique used to measure the air voids in the centre of the sample is briefly described below:

1. A Pundit 7 apparatus was applied according to BS EN 12504-4 standard to generate an ultrasonic wave and to determine the ultrasonic pulse velocity of the asphalt sample. Two 54-kHz piezoelectric crystal transducers (transmitter and receiver) were placed in parallel at each side of the specimen to measure Ultrasonic wave transit time at 17 different locations at 25°C as shown in Figure 5.2. The transit time for the compression wave (P-wave) to pass the length of the asphalt sample was recorded to calculate the ultrasonic pulse velocity using equation 5.1.
2. The air voids content of whole samples was measured using the specimen's bulk specific gravity (Saturated Method) and the asphalt's theoretical maximum specific gravity (Rice Method) according to Australian Standard (AS/NZS 2891).
3. The correlation between average ultrasonic velocities at 17 points and air voids of the whole sample was generated (Figure 5.3) to obtain the linear regression equation for each asphalt.

$$\text{C320} \quad \quad \quad AV = -0.0168UV + 80.441 \quad \quad \quad (5.2)$$

$$\text{M1000/320} \quad \quad \quad AV = -0.019UV + 87.79 \quad \quad \quad (5.3)$$

$$\text{PMB-A5S} \quad \quad \quad AV = -0.0214UV + 96.983 \quad \quad \quad (5.4)$$

In the above linear regression formula, UV is an ultrasonic velocity at the centre of sample and AV is air voids in the centre of the sample.

4. Air voids at the centre of samples were calculated using 'ultrasonic velocity in the centre'. It is a value that has been used in the current research.

## 5.7 Comparison of air void in the centre with air voids of the whole sample

The results for average ultrasonic velocity and air voids content of the whole sample (0% to 10%) for all asphalt mixes (C320, M1000 and PMB-A5S), calculated at the reference temperature of 25°C, were summarised in Figure 5.3. From Figure 5.3, the

ultrasonic velocity at the centre of all three types of laboratory compacted asphalts was estimated using linear regression relationship.

The difference between air voids of the whole sample measured by Australian standard (AS/NZS 2891) with estimated air voids at the centre of samples using UWT technique is seen in Figure 5.6 and Appendix B. The data indicates that the air voids at the centre of the sample is different from that of the whole sample.

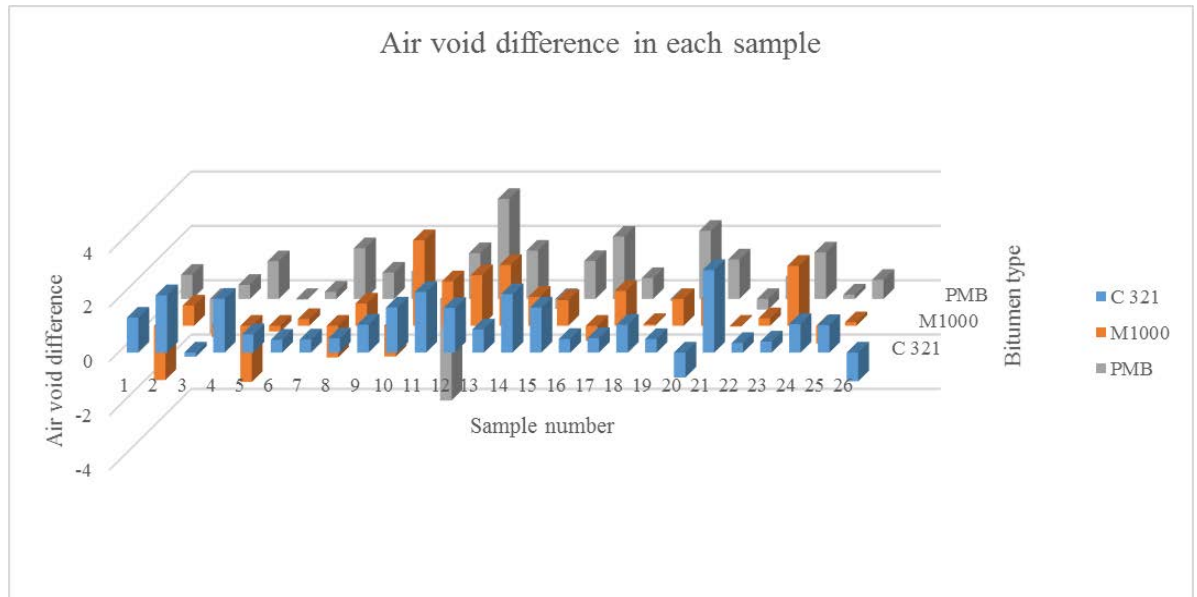


Figure 5.6: Air voids difference (air voids of whole sample minus estimated air voids in centre)

### 5.8 Evaluating UWT techniques

To review the benefits of the UWT technique compared with the bulk air voids measurement technique, a trial creep test was designed. In the designed test the following parameters were considered:

- Three types of asphalt; C320, M1000 and PMB-A5S
- Air voids between 1% and 10%
- Load magnitude: 500kPa
- Dynamic Load (rectangular): 0.1s load period - 0.9s rest period
- Cycle number: 40,000
- Test temperature: 50°C

The secant creep slope between 20,000 cycle and 40,000 cycles was measured for the samples in the trial. The air voids content of the entire sample (AS/NZS 2891) was measured and the air voids in the centre determined using the UWT technique.

In Figure 5.7, the secant creep slope is plotted versus air voids content of the entire sample for the three types of binders. The data shows a good correlation between increasing air voids contents and creep slope for each mix type. The data could be interpreted as ranking the PMB mix as the most creep resistant, followed by C320 and then closely by Multigrade M1000.

The creep slope versus estimated air voids at the centre of the sample under the load platen for the three types of asphalt is plotted in Figure 5.8. A good correlation is observed again between increasing ultrasonic velocity and increasing creep slope for each type of mixture. The data could be interpreted as ranking the mix types, and PMB is again ranked as the most creep resistant. However, the data now suggests that the Multigrade M1000 is the next best performer with C320 being ranked last. Such a change in mix ranking is of significance and a cause for further investigation. The creep sensitivity to the effective parameter in this research will be assessed later in Chapter 8 using both air voids measurement techniques.

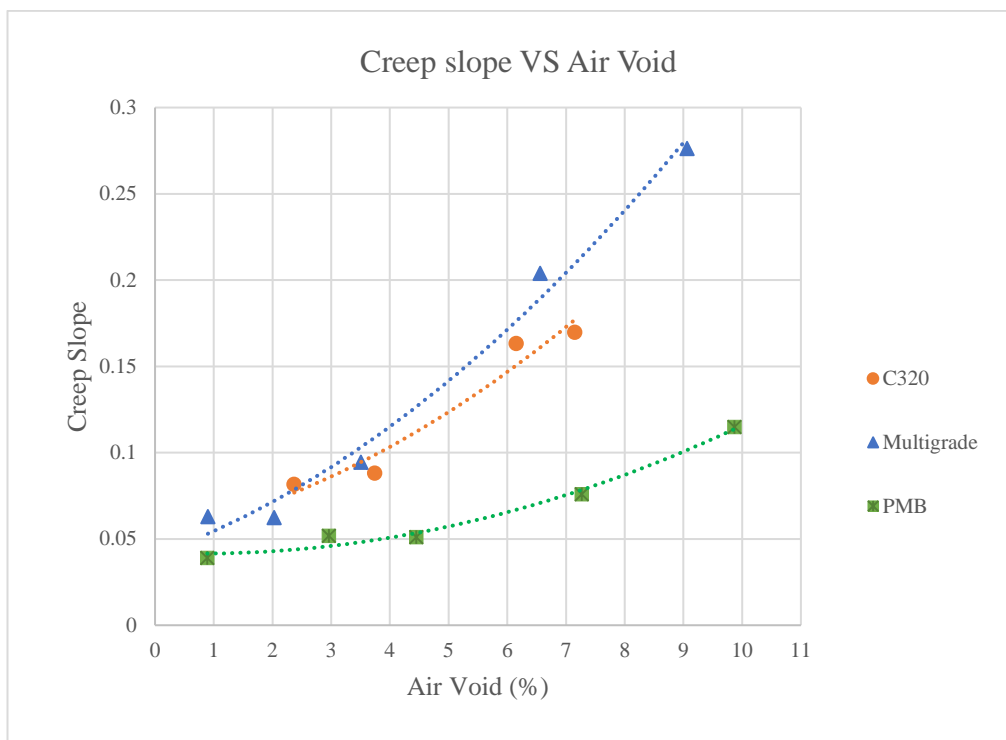


Figure 5.7: Creep slope vs air voids content of whole sample

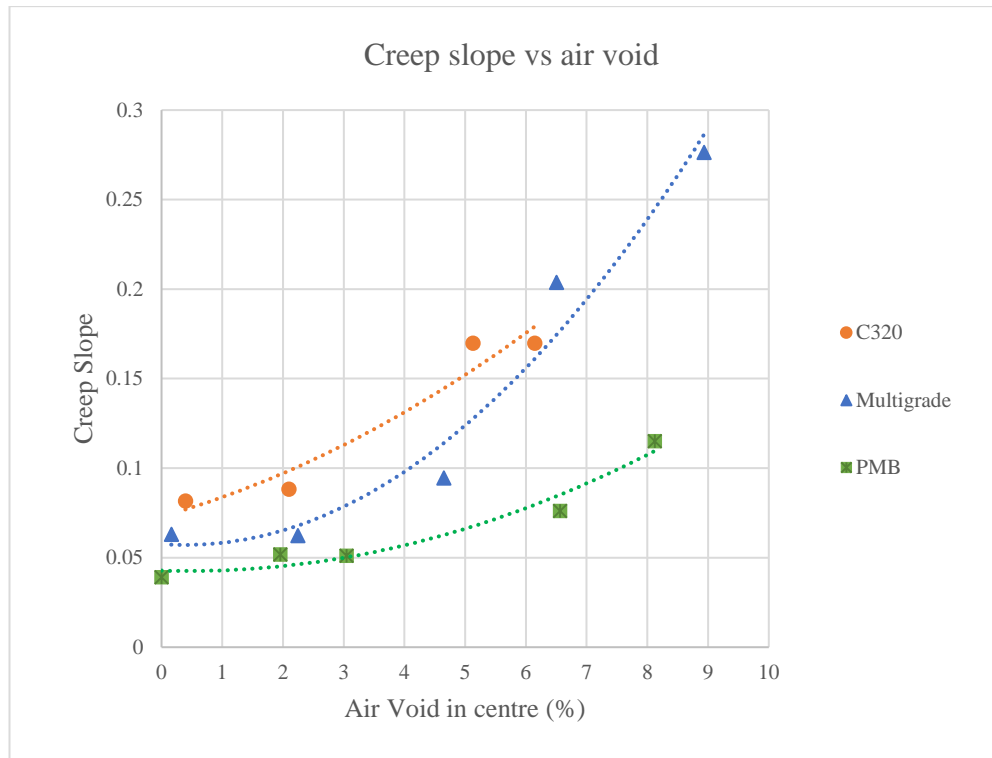


Figure 5.8: Creep slope vs estimated air voids content in centre of sample under load platen

## 5.9 Conclusion

The research outlined in this chapter has shown that the UWT technique can be applied as a fast and effective non-destructive tool to estimate the air voids content and distribution in asphalt mixes. It was found that the air voids are non-uniformly distributed in laboratory compacted asphalt samples. The UWT technique can be applied to assist researchers in the analysis and application of asphalt test data involving air voids as an experimental variable.

The usefulness of the UWT technique to measure air voids and their distribution has been verified using a designed dynamic confined creep test. A change in the ranking of mix types occurred when asphalt sample creep was based on UWT estimated air voids. It is believed that the use of UWT techniques allows for more accurate ranking of mixes by enabling the use of local air voids content at the point of stress application as a test variable.

The technique was applied throughout the research reported on in the thesis, to better improve analysis of creep data with respect to air voids content and temperature.

## CHAPTER 6

### THE DEVELOPMENT OF A MULTISTAGE CONFINED DYNAMIC CREEP TEST

#### Contents

6.1	Introduction .....	93
6.1.1	The confining system .....	95
6.2	The Multistage Confined Dynamic Creep (MCDC) test methodology.....	95
6.2.1	The possibility of conducting the MCDC test in the laboratory .....	96
6.2.2	Stress analysis of MCDC test using Finite Element Modelling.....	98
6.2.3	Laboratory assessment of confinement stresses.....	105
6.2.4	Summary of laboratory and modelling assessment of confinement stresses .....	108
6.3	Analysing creep test results from MCDC test.....	108
6.3.1	Analysing creep test data .....	114
6.4	Prediction of creep life using MCDC test .....	117
6.4.1	Creep life prediction based on secant creep slope .....	117
6.4.2	MCDC test analysis and applied mathematical modelling .....	118
6.4.3	Creep life prediction based on creep depth in laboratory samples.....	119
6.4.4	Estimation of creep life .....	119
6.5	Conclusion.....	120

## 6.1 Introduction

This chapter describes the underpinning methodology for the development of the Multistage Confined Dynamic Creep (MCDC) test. The research enhances the efficiency and accuracy of earlier work by Ahmadinia (2017) and also reduces the required time, cost and number of samples to evaluate creep potential. As discussed in the literature chapter, the most important challenges to designing such a creep test to predict asphalt creep performance and life are:

- The test procedure must provide realistic dynamic stresses in the test sample that model real tyre pressure in field;
- The test procedure must provide realistic confinement during testing that reproduces the stresses generated within the asphalt;
- Accurate measurement of air voids must be undertaken for the asphalt specimens at critical stress locations;

The information provided in Table 6.1 summarises the progress of creep test methodologies from 1970 to the present time. It is evident that the tests have become increasingly sophisticated in their attempts to model in-situ pavement conditions. The table also highlights how the new approach addresses many of the issues inherent in creep evaluation. The latest improvements of the creep test were undertaken recently by Ahmadinia (2017) to provide a more realistic confinement stress using a multilayer confinement system. The table also indicates how the MCDC approach, combined with UWT should be able to address many of the earlier test limitations. It is noted that the generation of the transient pulse via a sample loaded via a steel plated and a low friction interface remains an approximation of field conditions.

Table 6.1: Some of the asphalt creep test advancements from 1970 to date for the universal testing system.

References	Test development and outcome	Limitations	Issues addressed by MCDC + UWT test
Brown (1970) in (Brown & Cooper 1984), Hills (1973) in (Sousa et al. 1991)	Development of UTS facility to perform static creep test under different temperatures. The outcome is plastic deformation under static load.	<ul style="list-style-type: none"> <li>• Unable to perform dynamic loading</li> <li>• Unable to provide confinement stresses</li> <li>• Unable to perform at high temperature for long period of time</li> <li>• Single stage</li> <li>• Unable to assess the Air voids effect</li> </ul>	<ul style="list-style-type: none"> <li>• Able to perform dynamic loading</li> <li>• Able to provide stress dependent confinement</li> <li>• Able to control crack propagation due to the PVC confinement</li> <li>• Able to operate at high temperatures for long periods of time</li> <li>• Able to perform multistage stress evaluation</li> <li>• Able to assess local air voids effect</li> <li>• Requires shorter testing times and lower sample numbers</li> </ul>
Bowering (1989) in (Sharp 1992), Brown (1989)	Development of UTS facility to apply dynamic loading. The outcome is creep modulus which can be used in mix design optimisation.	<ul style="list-style-type: none"> <li>• Unable to present realistic creep deformation under high magnitude of temperature and load</li> <li>• Unable to provide confinement stresses</li> <li>• Crack propagation during test is not observed in field situation</li> <li>• Single stress</li> <li>• Unable to assess the air voids effect</li> </ul>	
Bullen & Preston (1992)	Development of a creep test by providing confinement using small diameter platen on a larger diameter sample to be able to assess both confinement and air voids	<ul style="list-style-type: none"> <li>• Unable to measure creep deformation under high temperatures and loads</li> <li>• Confinement stress provided by the asphalt thickness around the platen</li> <li>• Unable to reveal the rut depth</li> <li>• Single stress</li> </ul>	
ARRB (APRG 1996) in (Stephenson & Bullen 2000)	Using a triaxial cell to provide static and pulsed confining using air pressure. Using small 75mm platen on 150mm diameter specimen.	<ul style="list-style-type: none"> <li>• Static confinement is not stress dependent when compared</li> <li>• Pulse confinement was difficult to control</li> <li>• Single stress</li> <li>• Unable to assess the air voids effect</li> </ul>	
Brown et al (1998)	Provided confinement through the application of an internal vacuum (negative pressure relative to atmospheric pressure)	<ul style="list-style-type: none"> <li>• Easier to perform but confinement stress is not stress dependent</li> <li>• Rut depth unable to be observed during the test</li> <li>• Single stress</li> <li>• Unable to assess the air void effect</li> </ul>	
(Huang & Zhang 2010)	Using top and bottom smaller platen size under the confinement stress through the application of an internal vacuum to assess the air voids effect	<ul style="list-style-type: none"> <li>• Confinement stress provided by the asphalt thickness around the platen and static vacuum pressure and is not stress dependent</li> <li>• Rut depth cannot be observed</li> <li>• Crack propagation is not realistic</li> <li>• Single stress</li> </ul>	
Ahmadinia et al (2017)	Applying 3D confinement through using PVC ring+ resin + asphalt and small size platen to assess the combination of both confinement and air voids	<ul style="list-style-type: none"> <li>• lengthy testing time</li> <li>• The introduced confinement system hasn't been validated yet by field performance</li> <li>• Single stress</li> </ul>	

### 6.1.1 The confining system

The research adopts the creep test method reported by Ahmadinia (2017). That research investigated a multilayer confinement system and the application of load through small platens (50, 75, and 100mm diameter) for different diameter asphalt samples (100 and 150mm diameter). Based on the research by Ahmadinia (2017) sample size, platen size and confinement system (Figure 6.1) chosen for this research were:

- 50 mm diameter loading platen,
- 150 mm diameter asphalt sample with 50mm thickness,
- 2.5 mm liquid glass resin infill,
- 2.5mm PVC ring.

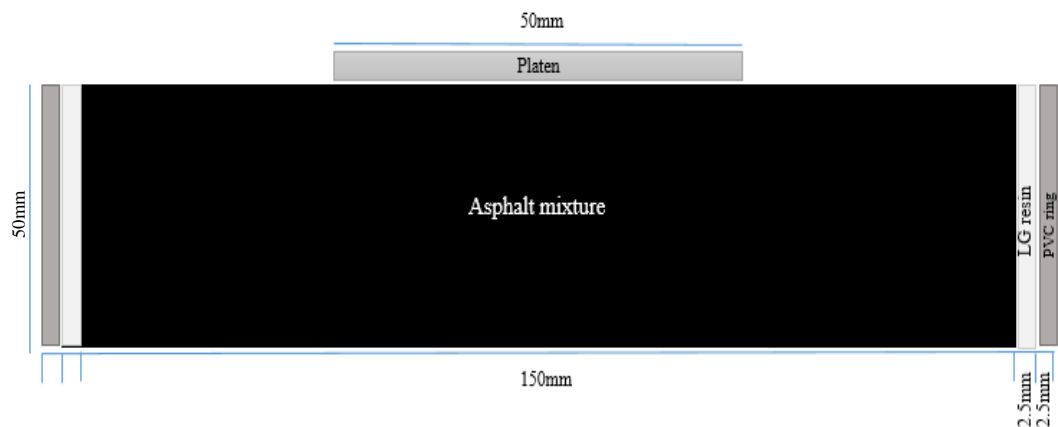


Figure 6.1: Schematic diagram of the laboratory creep sample

These characteristics were chosen to optimise asphalt confinement (50mm) around the platen for 150mm diameter samples. The sensitivity and ability of the selected confinement system were examined using FEM modelling, and experimental testing.

### 6.2 The Multistage Confined Dynamic Creep (MCDC) test methodology

As discussed previously the confined dynamic creep test reported by Ahmadinia (2017) appeared to be the best available to simulate creep deformation of asphalt. The test methodology was further developed as follows:

- Evaluation of air voids distribution and at critical stress locations under the loading platen;

- Minimising the required number of samples and reducing the test time by using a multistage stress test approach.

The ultrasonic technique was discussed in Chapter 5 and in this Chapter the possibility of using a multistage loading system will be assessed and discussed. The application of the MCDC test to predict the creep life also will be explained in detail.

### **6.2.1 The possibility of conducting the MCDC test in the laboratory**

A Multistage methodology for the confined dynamic creep test is proposed based on three reasons:

1. The hoop stress in a multi-layer confinement system eliminates crack propagation and models a real pavement situation. This means that the test sample will not collapse under cyclic loads and the creep test can be continued to ensure a more realistic second stage of asphalt material creep deformation.
2. Producing asphalt samples with the same structural composition is difficult. Asphalt is a non-homogeneous material consisting of aggregate, binder, filler, additives and air voids. Uniformity of samples is hard to achieve and variations have a significant effect on the creep deformation in the laboratory. Introducing the test protocol to reuse the same sample at different stress levels gives the opportunity of having the same composite structure and the ability to assess changes in other effective parameters such as load tolerance and material type.
3. Creep testing is normally time-consuming and introducing the multistage methodology provides a time saving solution by reducing the required sample numbers and testing time.

The possibility of conducting the MCDC test under different stress levels was initially investigated by using three confined samples. All samples had the same design properties as described in Table 6.2.

Three stage creep testing was undertaken for sample 51M using 500, 750 and 1000kPa platen stress applying 21500 cycles in each stage (Figure 6.2). The other two samples; 45M and 56M were tested continuously to 100,000 cycles using two platen stress of 750kPa and 1000kPa respectively. All nominated samples have similar air voids (close to 3%) and assess the effect of the number of load cycles by limiting the effect of varying air voids.

The results (Figure 6.2) show that the permanent strain of continuous test under 750kPa in 43000 cycles is close to the results obtained from sample 51M in the same cycle number conducted using MCDC test (point 1). The same trend was observed for sample 56M for 64500 cycles which is close to the results of the 51M sample in the third stage (point 2).

Table 6.2: Three selected samples to compare one stage creep test with MCDC test under different stress levels

Test parameters			
Sample name	51M (three stage )	45M (continuous)	56M (continuous)
Bitumen type	Multigrade	Multigrade	Multigrade
Pressure (kPa)	500-750-1000	750	1000
Air Void (%)	3.52	3.52	3.02
Thickness (mm)	50.19	51.07	50
Ultrasonic velocity (m/s)	4521.6	4601.3	4504.5
Test temperature (C°)	50	50	50
Cycles number (N)	21500-21500-21500	100000	100000

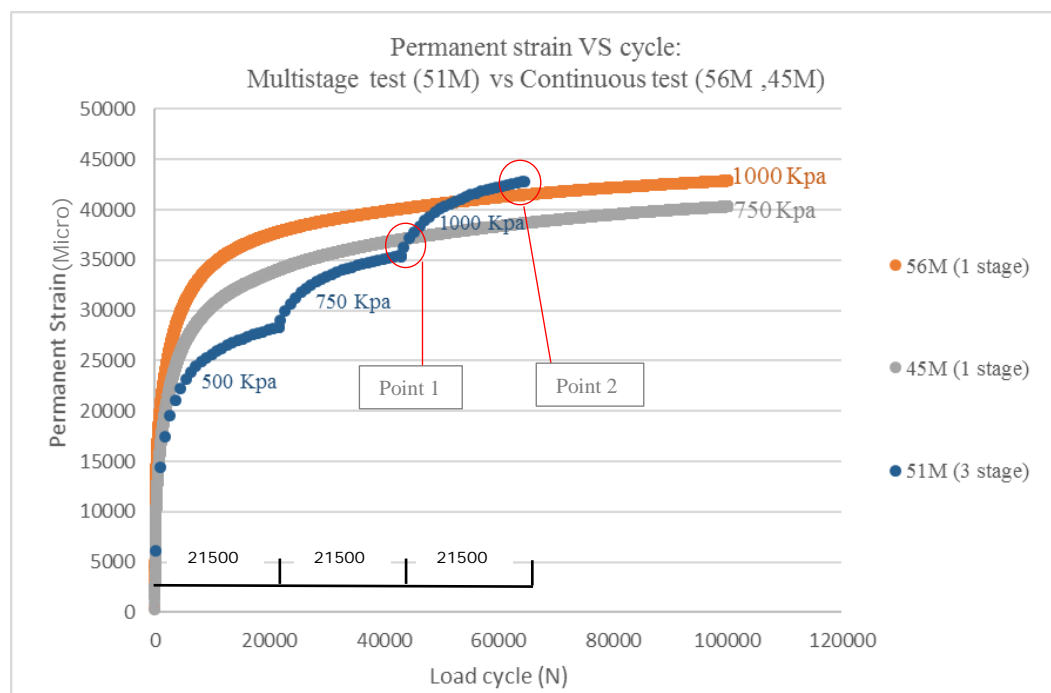


Figure 6.2: MCDC test validation

It is also observed, from the comparison of the data in Figure 6.2 that the permanent strain of an asphalt sample accumulated over all stages of 21500 cycles under a specific platen stress approximated permanent strain induced under the highest stress.

It is expected from the trend of the creep results in the trial test that by increasing the number of load cycles in each stage, a better indication of secondary creep will be obtained. Evaluating the creep results of the previous research conducted by Ahmadiania et al (2017) demonstrated that most of the samples reached the second stage creep between 20,000 and 40,000 cycles. It was decided to adopt 40,000 cycles as a reference level for each stage of the MCDC test.

In the next section, the lateral stress in the MCDC test will be assessed and compared with stresses within an asphalt layer, in order to validate the applied confinement system and the new test methodology.

### 6.2.2 Stress analysis of MCDC test using Finite Element Modelling (FEM)

To review the stresses within the confinement system FEM models of a confined laboratory sample and an asphalt layer (length of 1000mm and thickness of 200mm) were evaluated using constant asphalt properties. The tyre pressure /platen stresses used were 500, 750, 1000 kPa. The properties of samples 51M, 45M, and 56M (Table 6.3) were used in the models created for confined samples.

A 4:1 model scale was adopted for asphalt thickness (200/50) and loaded area diameter (200/50). The asphalt model was 1000mm to ensure that edge effects were minimised. The schematic diagram of generated models is illustrated in Figure 6.3 and 6.4.

Table 6.3: Material properties and test condition used in the FEM modelling

Sample number	51M	45M	56M
Test temperature (C°)	50	50	50
Platen stress (kPa)	500	750	1000
Asphalt resilient modulus (MPa)	982	997	1103
Asphalt Poisson's Ratio	0.44	0.44	0.44
LG epoxy resin resilient modulus (MPa)	160	160	160
LG epoxy resin Poisson's Ratio	0.35	0.35	0.35
PVC resilient modulus (MPa)	1500	1500	1500
PVC Poisson's Ratio	0.4	0.4	0.4

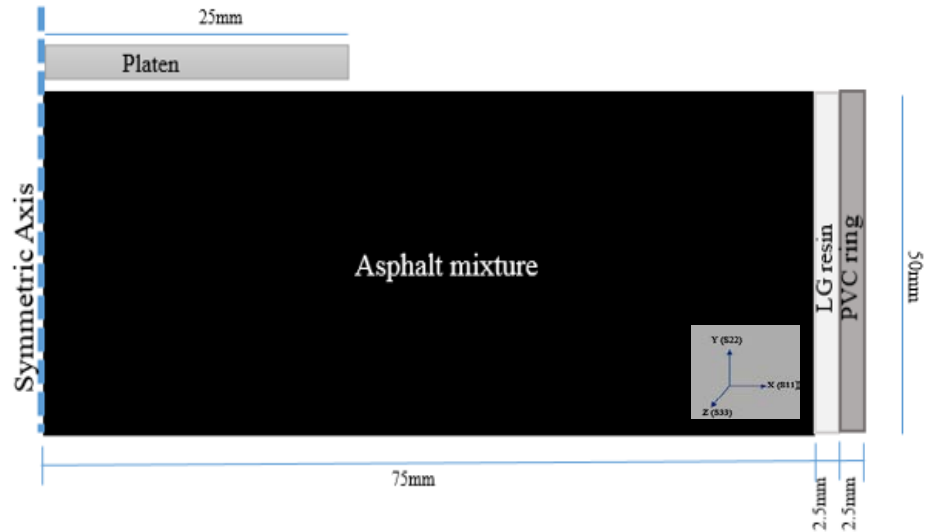


Figure 6.3: Schematic diagram of the laboratory creep test sample used in FEM



Figure 6.4: Schematic diagram of single asphalt layer used in FEM

The stresses in both generated models were extracted (Figures 6.5 and 6.6) at different grid points as follows:

- In vertical direction (Y):
  - Surface (A),
  - Midpoint (B),
  - Bottom (C)
- In horizontal direction (X):
  - The centre of laboratory asphalt sample or cross point (4:1 scale) in the asphalt layer (1),
  - Middle of laboratory sample and cross point (4:1 scale) in the asphalt layer (2),

- The Edge of laboratory sample and cross point (4:1 scale) in the asphalt layer (3),
- The middle of resin in the laboratory sample (4),
- The PVC outer surface in the laboratory sample (5).

The grid points of the selected axle in both models are illustrated schematically in Figure 6.5 and 6.6. All FEM models are shown in Figure 1 to Figure 25 in Appendix C.

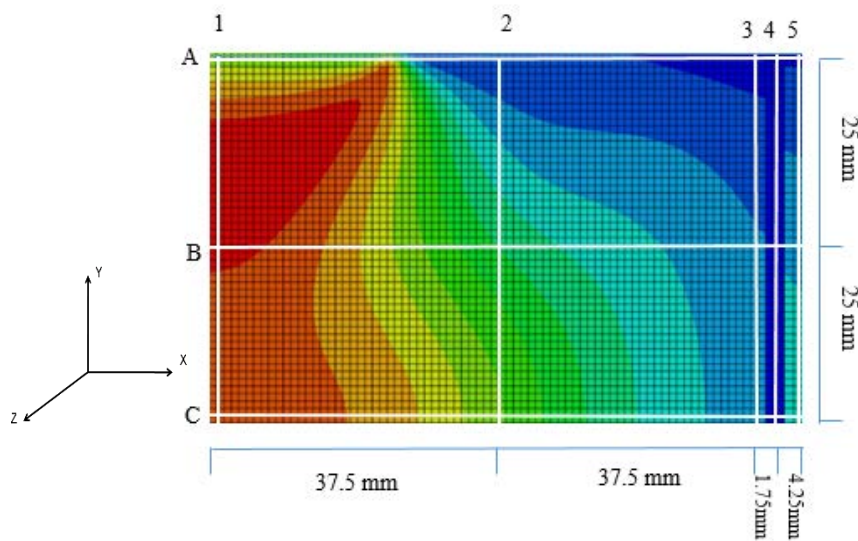


Figure 6.5: Selected points on FEM model of confined laboratory sample (laboratory model) for stress analysis

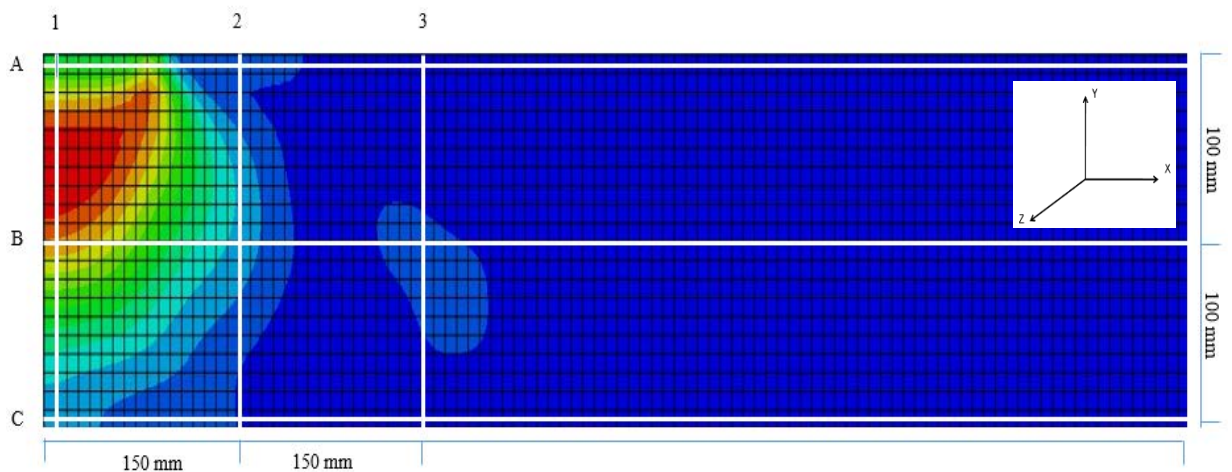


Figure 6.6: Selected points on FEM model of asphalt layer for stress analysis

The calculated stress at each grid point in the models is the average of the values generated for the 4 surrounding pixels. The stresses were calculated in three directions for both models as follows:

1. S11: X direction
2. S22: Y direction
3. S33: Z direction

The magnitude of calculated stresses can be either + or –, meaning compressive or tensile stress respectively. The stresses for each grid point (as illustrated in Figure 6.5 and 6.6) were calculated for both models (confined laboratory sample and asphalt layer) and the results are presented in Table 6.4 to 6.6.

The analysis outcome indicates that the calculated stresses in the confined asphalt laboratory samples, at all points, are similar to those within the asphalt layer model at the same grid points (for three selected samples under similar surface stress conditions). The overall similar stress ranges for the two model indicates that the confinement system including asphalt, resin and PVC is able to approximate the stresses in the field asphalt layer model. In the next section, the confined laboratory model will be used to assess stresses on the PVC ring for the 50/150 mm test configuration.

Table 6.4: Stress analysis of the FEM models in A row

			Stres (kPa)				
			A				
			1	2	3	4	5
Stress comparison in sample 51M 500kPa	In the Model of asphalt layer (200mm)	S11	-338 to -215	-61 to +54	+5 to +31	-	-
	in the Model of confine labortory Sample	S11	-423 to -339	+36 to +77	-5 to +36	-5 to +36	-5 to +36
	In the Model of asphalt layer (200mm)	S22	-496 to -453	-19 to +26	-19 to +26	-	-
	in the Model of confine labortory Sample	S22	-514 to -424	-19 to +24	-19 to +24	-19 to +26	-19 to +26
	In the Model of asphalt layer (200mm)	S33	-346 to -274	-4 to +26	-4 to +26	-	-
	in the Model of confine labortory Sample	S33	-423 to -343	+14 to +53	+14 to +53	-25 to +14	+14 to +53
			Stres (kPa)				
			A				
			1	2	3	4	5
Stress comparison in sample 45M 750kPa	In the Model of asphalt layer (200mm)	S11	-521 to -386	-63 to +89	-63 to +38	-	-
	in the Model of confine labortory Sample	S11	-500 to -352	-8 to +89	-8 to +40	-8 to +40	-8 to +40
	In the Model of asphalt layer (200mm)	S22	-757 to -691	-28 to +37	-28 to +37	-	-
	in the Model of confine labortory Sample	S22	-750 to -687	-62 to -2	-62 to -2	-62 to -2	-62 to -2
	In the Model of asphalt layer (200mm)	S33	-519 to -368	+33 to +84	-16 to +33	-	-
	in the Model of confine labortory Sample	S33	-478 to -373	+46 to +98	-6 to +46	-6 to +46	-6 to +98
			Stres (kPa)				
			A				
			1	2	3	4	5
Stress comparison in sample 56M 1000kPa	In the Model of asphalt layer (200mm)	S11	-663 to -479	-49 to +73	-50 to +11	-	-
	in the Model of confine labortory Sample	S11	-866 to -661	+24 to +195	-61 to +24	-61 to +24	-61 to +24
	In the Model of asphalt layer (200mm)	S22	-991 to -904	-42 to +43	-42 to +43	-	-
	in the Model of confine labortory Sample	S22	-1064 to -971	-43 to +49	-43 to +49	-43 to +49	-43 to +49
	In the Model of asphalt layer (200mm)	S33	-663 to -412	+27 to +90	+27 to +90	-	-
	in the Model of confine labortory Sample	S33	-834 to -576	+25 to +197	+25 to +111	-60 to +25	+25 to +111

Table 6.5: Stress analysis of the FEM models in B row

			Stres (kPa)				
			B				
			1	2	3	4	5
Stress comparison in sample 51M 500kPa	In the Model of asphalt layer (200mm)	S11	-61to -30	-61to -30	-30 to +5	-	-
	in the Model of confine laborotory Sample	S11	-89 to -5	-89 to -47	-47 to +36	-5 to +36	-5 to +36
	In the Model of asphalt layer (200mm)	S22	-280 to -193	-106 to -19	-19 to +26	-	-
	in the Model of confine laborotory Sample	S22	-379 to - 334	-109 to +24	-19 to +24	-19 to +26	-19 to +26
	In the Model of asphalt layer (200mm)	S33	-64 to -4	-4 to +26	-4 to +26	-	-
	in the Model of confine laborotory Sample	S33	-65 to +14	+14 to +53	+14 to +53	-25 to +14	+14 to +53
			Stres (kPa)				
			B				
			1	2	3	4	5
Stress comparison in sample 45M 750kPa	In the Model of asphalt layer (200mm)	S11	-63 to -12	-142 to -63	-12 to +38	-	-
	in the Model of confine laborotory Sample	S11	-8 to +40	-8 to +40	-8 to +40	-8 to +40	-8 to +40
	In the Model of asphalt layer (200mm)	S22	-492 to -296	-94 to +37	-94 to -28	-	-
	in the Model of confine laborotory Sample	S22	-562 to -312	-187 to -125	-125 to -2	-62 to -2	-62 to -2
	In the Model of asphalt layer (200mm)	S33	-66 to -16	-16 to +33	-16 to +33	-	-
	in the Model of confine laborotory Sample	S33	-6 to +46	+46 to +98	-6 to +46	-6 to +46	+98 to +151
			Stres (kPa)				
			B				
			1	2	3	4	5
Stress comparison in sample 56M 1000kPa	In the Model of asphalt layer (200mm)	S11	-172 to -49	-111to -49	-50 to +73	-	-
	in the Model of confine laborotory Sample	S11	+24 to +110	-147 to +24	-61 to +24	-61 to +24	-61 to +24
	In the Model of asphalt layer (200mm)	S22	-560 to -387	-128 to -42	-42 to +43	-	-
	in the Model of confine laborotory Sample	S22	-971 to -878	-321 to -136	-43 to +49	-43 to +49	-43 to +49
	In the Model of asphalt layer (200mm)	S33	-161 to -35	-35 to +90	-35 to +90	-	-
	in the Model of confine laborotory Sample	S33	+25 to +197	+25 to +111	+25 to +197	-60 to +25	+111 to +197

Table 6.6: Stress analysis of the FEM models in C row

			Stres (kPa)				
			C				
			1	2	3	4	5
Stress comparison in sample 51M 500kPa	In the Model of asphalt leyer (200mm)	S11	-30 to +5	-30 to +5	-30 to +5	-	-
	in the Model of confine labortory Sample	S11	-5 +36	-47 to -5	-47 to +36	-5 to +36	-5 to +36
	In the Model of asphalt leyer (200mm)	S22	-323 to -236	-106 to -19	-19 to +26	-	-
	in the Model of confine labortory Sample	S22	-334 to -199	-109 to -64	-19 to +24	-19 to +26	-19 to +26
	In the Model of asphalt leyer (200mm)	S33	-4 to +26	-4 to +26	-4 to +26	-	-
	in the Model of confine labortory Sample	S33	-25 to +14	-25 to +53	-25 to +14	-25 to +14	-25 to +53
			Stres (kPa)				
			C				
			1	2	3	4	5
Stress comparison in sample 45M 750kPa	In the Model of asphalt leyer (200mm)	S11	-63 to -12	-63 to -12	-12 to +38	-	-
	in the Model of confine labortory Sample	S11	+40 to +80	+40 to +89	-8 to +40	-8 to +40	-8 to +40
	In the Model of asphalt leyer (200mm)	S22	-293 to -94	-94 to -28	-28 to +37	-	-
	in the Model of confine labortory Sample	S22	-427 to -312	-250 to -127	-125 to -2	-62 to -2	-62 to -2
	In the Model of asphalt leyer (200mm)	S33	-66 to -16	-16 to +33	-16 to +33	-	-
	in the Model of confine labortory Sample	S33	+46 to +98	+98 to +151	+98 to +152	-6 to +46	+98 to +151
			Stres (kPa)				
			C				
			1	2	3	4	5
Stress comparison in sample 56M 1000kPa	In the Model of asphalt leyer (200mm)	S11	-50 to +11	-111 to -49	+11 to +73	-	-
	in the Model of confine labortory Sample	S11	+110 to +196	+24 to +110	-61 to +24	-61 to +24	-61 to +24
	In the Model of asphalt leyer (200mm)	S22	-646 to -473	-128 to -43	-42 to +43	-	-
	in the Model of confine labortory Sample	S22	-878 to -785	-414 to -229	-43 to +49	-43 to +49	-43 to +49
	In the Model of asphalt leyer (200mm)	S33	-35 to +27	-35 to +27	-35 to +27	-	-
	in the Model of confine labortory Sample	S33	+111 to +197	+111 to +197	+111 to +197	+25 to +111	+111 to +197

### 6.2.3 Laboratory assessment of confinement stresses

To further validate the selected confinement system in the laboratory, three asphalt samples were chosen (Table 6.2 and 6.3) with similar air void content (3 - 4%) with 5% binder. The dynamic creep test was undertaken using the UTS testing machine for fabricated confined samples with the following test conditions:

- Compressive stress: 500 (51M), 750 (45M), and 1000kPa (56M)
- Seating stress: 20 kPa
- Loading period: 500 milliseconds (ms)
- Pulse repetition period: 2000 milliseconds (ms)
- Test temperature: 50°C
- Termination pulse count: 21,500 cycles
- Platen size: 50mm diameter
- Sample size: 150mm
- Confinement situation: Confined

The stress and strain within the PVC ring for the three selected multigrade samples under three different platen stresses was measured in the laboratory using strain gauges (as described in Chapter 5) and compared with the calculated stresses from the FEM model of laboratory confined asphalt with the PVC ring. The results are shown in Table 6.7.

The measured stress from the strain gauge is compared to the stress range in PVC in C5 position calculated from the elastic dynamic FEM. There is overall agreement between the stresses measured at the PVC ring and those obtained from the FEM model. As the platen stress increases the confining stress generated by the confinement system also increases. The data indicates that the redesigned confined dynamic creep test has good potential for simulating in-situ stress conditions.

Table 6.7: Comparison between confined stresses in the first stage of MCDC test: in the lab and FEM model

Sample number	51M	45M	56M
Platen stress (kPa)	500	750	1000
Strain in one cycle ( $\mu\text{m}/\text{m}$ ) measured by strain gauge on PVC	40	79.7	115
Hoop stress measured from strain gauge in C5 position in one cycle (kPa) in PVC	60	119.55	172.5
S33 stress from optimised laboratory confined asphalt model in C5 position in one cycle (kPa)	-25 to +53	+98 to +151	+111 to +197

Sample number 51M was selected to conduct a three stage test to assess the hoop stress within the PVC ring in the multilayer confinement system. The test conditions are described in Table 6.8 at platen stresses of 500, 750, and 1000kPa with 21500 cycles for each stage. The hoop stress within the PVC ring at the C5 position was measured using a strain gauge. The S33 stress (i.e. stress in the z direction) from the laboratory confined asphalt model at the C5 position is compared with the generated hoop stress in strain gauge, as shown in Table 6.9.

Table 6.8: MCDC test condition for sample 51M in three stages

Test parameters			
Sample name	51M (Stage1 )	51M (Stage2)	51M(Stage3)
Bitumen type	Multigrade	Multigrade	Multigrade
Pressure (kPa)	500	750	1000
Air Void (%)	3.52	3.52	3.52
Thickness (mm)	50.19	50.19	50.19
Ultrasonic velocity (m/s)	4521.6	4521.6	4521.6
Test temperature (C°)	50	50	50
Cycles number (N)	21500	21500	21500

Table 6.9: Comparison between confined stresses in the laboratory and FEM model for sample 51M in three stages

Sample number	51M		
Stage number	1	2	3
Platen stress (kPa)	500	750	1000
Strain in one cycle ( $\mu\text{m}/\text{m}$ ) which measured by strain gauge in PVC	40	70	101
Hoop stress measured from strain gauge in C5 position in one cycle (kPa) in PVC	60	105	151
S33 stress from optimised laboratory confined asphalt model in C5 position in one cycle (kPa)	-25 to +53	+38 to +98	+66 to +153

The stress and strain analysis and comparison in C5 position on PVC ring are summarised as follows:

- For each stage, the measured stress from strain gauge results is similar to the stress ranges in PVC in C5 position calculated from MDCD FEM elastic dynamic model.
- The stress in C5 position on PVC in each stage of the multistage test (Table 6.9) is similar to the stress in a single stage test in the same position under the same platen stress (Table 6.7).
- The strain in C5 position in each stage of the multistage test (measured by the strain gauge and presented in Table 6.9) is similar to the strain in a single stage test in the same position under the same platen stress (Table 6.7).

In the laboratory, the strains within the PVC ring for each load cycle applied to the asphalt sample corresponded to the variation in the applied stress. As seen in Figure 6.7, the confining system provided stress and strain responses proportional to the applied loads on the sample.

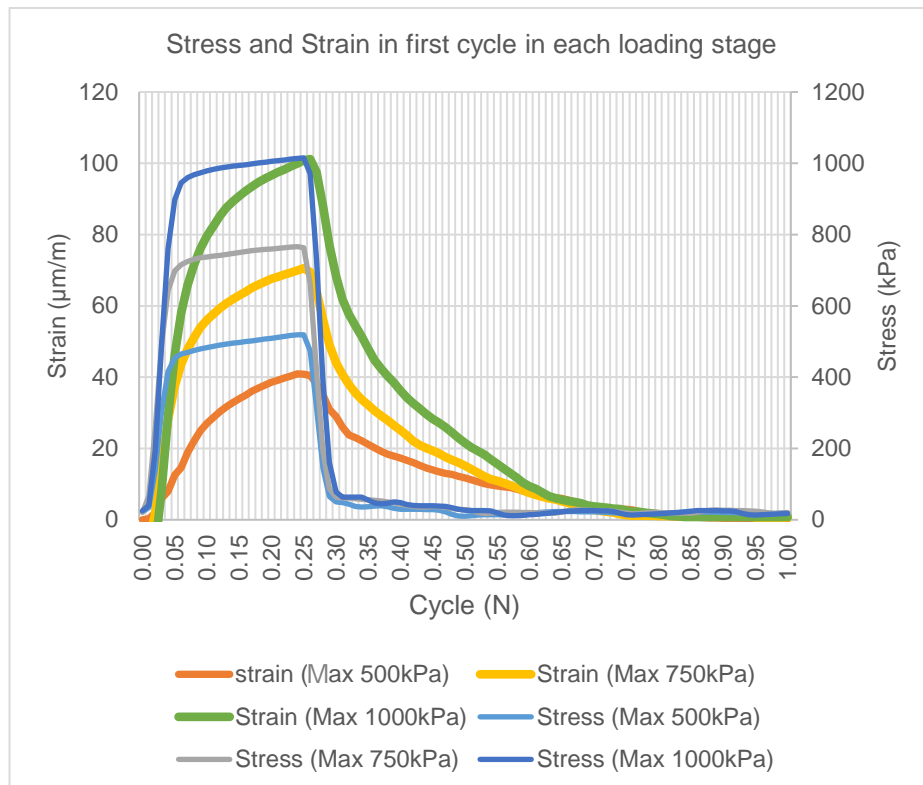


Figure 6.7: Stress and Strain in first cycle of each stage of laboratory test (sample 51M)

#### **6.2.4 Summary of laboratory and modelling assessment of confinement stresses**

The laboratory and FEM model outcomes related to the trial MCDC tests are summarised as follows:

1. Experimental work shows that the magnitude of the permanent strain at the end of each stress stage in the MCDC test, is close to the permanent strain at the same number of cycles in the MCDC test at that stress level.
2. FEM modelling of both asphalt layer and laboratory sample shows that the stress within the asphalt layer under dynamic load is similar to the stress in the laboratory confinement sample under the same load.
3. Strain gauge reading from laboratory work verify that the lateral confinement stress at the beginning of each stage of MCDC test (generated by confinement system including asphalt, resin and PVC) is close to the generated stress in continuous tests (i.e. CDC tests).
4. The lateral confinement stress at each stage of the MCDC test is load dependent. This means that the confinement system can automatically generate higher confinement stress for higher applied platen stress. In existing triaxial testing for soil and unbound materials (Arnold et al., 2010), the confinement stress must be artificially provided at each stage and depends on the load magnitude. However, this load dependent lateral stress is provided in the MCDC test.

### **6.3 Analysing creep test results from MCDC test**

Test results from creep tests are normally presented using a range of methods:

- Plastic deformation or the total accumulated deformation (average of LVDTs reading in millimetre)
- Permanent strain at some selected cycle number
- Creep slope ( $m$ ) which is the rate of permanent deformation ( $\mu\text{s}/\text{cycle}$ ) in the secondary phase of creep curve and is cycle dependent (Figure 6.8 and 6.9)
- Conventional intercept ( $a$ ) as indicated in Figure 6.9.
- Flow number ( $F_n$ ): the number of load cycles corresponding to the minimal rate of change of permanent axial strain during the repeated load test
- Resilient modulus at flow

- Ratio of permanent to elastic strain ( $\epsilon_p/\epsilon_r$ )

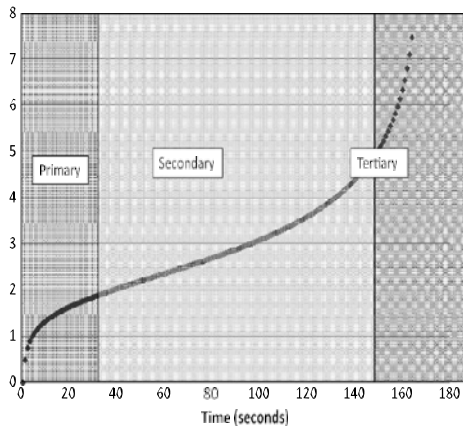


Figure 6.8: Representative creep data determination (Rushing et al. 2014)

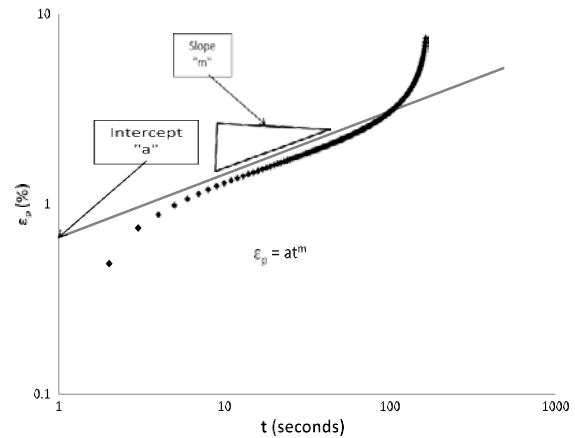


Figure 6.9: Slope and intercept (Rushing et al. 2014)

As explained previously in Chapter 3, creep deformation of heavy-traffic pavements in the field is normally restricted to the secondary phase (steady-state) because of the confinement stress provided by asphalt mass around the wheel pass and preventative maintenance (Zhang et al. 2012). Using the “asphalt + resin + P VC ring” confinement system in the MCDC creep test eliminates sample collapse and the test will not reach the third stage of creep. The following analytical approach that relies only on the second stage of creep test results has been used to analyse creep results:

- Permanent strain at selected cycle number
- Creep slope (m):
- Conventional intercept

Accurate calculation of the above creep measurement parameters relies on the correct calculation of these parameters in the steady stage. All the parameters are cycle dependent so it is necessary to decide the optimum cycles at which to measure the parameters.

Evaluation of the secant creep slope results of two samples; 56M and 45M (sample details in Table 6.8) is shown in Table 6.10 and Figure 6.10. It is seen from the results that creep slope is totally cycle dependant. It appears that after around 40,000 cycles

the rate of change of the creep slope significantly decreases and approaches linearity. The slope between 20,000 and 40,000 is also calculated for both samples (56M and 45M) and presented in Table 6.11. It was decided to adopt the secant creep slope between 20,000 and 40,000 for further exploration as an indicator of creep performance.

Table 6.10: Creep slope vs cycle range

	Creep Slope (%)	
	45M	56M
	750 kPa	1000 kPa
0.0000 - 10000 cycle	1.698	1.712
10000 - 20000 cycle	0.3122	0.2898
20000 - 30000 cycle	0.1838	0.1399
30000 - 40000 cycle	0.1225	0.0912
40000 - 50000 cycle	0.0871	0.0763
50000 - 60000 cycle	0.0728	0.0633
60000 - 70000 cycle	0.0633	0.0516
70000 - 80000 cycle	0.0528	0.0432
80000 - 90000 cycle	0.0432	0.0363
90000 - 100000 cycle	0.0354	0.032

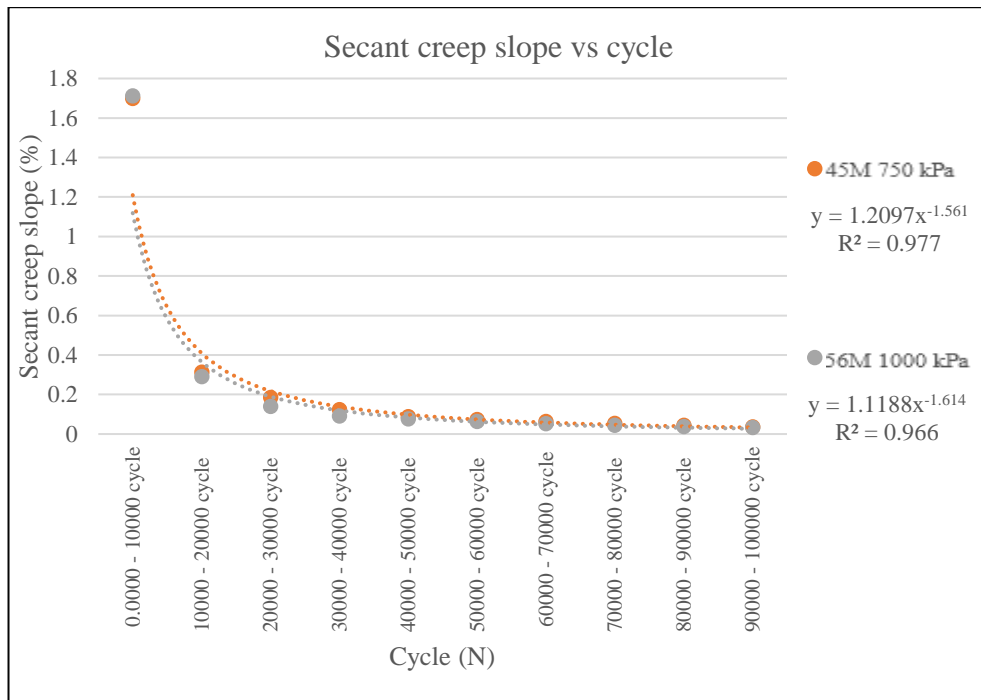


Figure 6.10: Creep slope vs Cycle

Table 6.11: Secant creep slope between 20,000 and 40,000 cycles

		Secant creep slope (%) between 20,000 and 40,000 cycles
Sample	45M	0.1533
	56M	0.116

The results also show that the rate of change of creep slope continues to decrease as the cycle number increases. To have a more realistic and accurate creep slope to evaluate the creep life, it is essential to continue the test to a higher cycle number. However, continuing the creep test to cycles representative of the field situation is time consuming and costly. The use of mathematical regression predictions has been adopted for further study.

A test was designed to check the possibility of using the mathematical method to predict the creep at higher cycle numbers and consequently to predict more realistic creep slopes. For this purpose, a multigrade asphalt sample number 59M, with the information noted in Table 6.12 was tested for 360,000 cycles. The creep deformation versus cycles for this sample is illustrated in Figure 6.11.

Table 6.12: Material properties and test condition of 51M sample

Sample name	59M
Bitumen type	Multigrade
Pressure (kPa)	1000
Air Void (%)	6.27
Ultrasonic velocity (m/s)	4260
Cycles number (N)	360,000

The outcome of the trial test showed that fitted regression mathematical models on data between 20,000 cycles and 40,000 cycles correlated well with real test data for higher cycles. Different regression models were fitted on results between 20,000 and 40,000 cycles using:

- Linear regression
- Logarithmic regression
- Power regression

The predicted results from these regression models at 360,000 cycles, was compared with real test results in 360,000 cycles were compared and illustrated in Figure 6.11 and Table 6.13. The power regression model fitted on data between 20,000 and 40,000

provided the best fit to the actual test data. The power mathematical model form,  $Y = ax^b + c$  was chosen and fitted to data between 20,000 and 40,000 cycles to extend the permanent deformation data to 500,000 cycles for each stage of the MCDC tests.

The ability to extend the creep deformation of asphalt samples to 500,000 cycles by using MCDC test results up to 40,000 cycles will provide a better use of laboratory creep data for potential long-term performance of asphalt pavement.

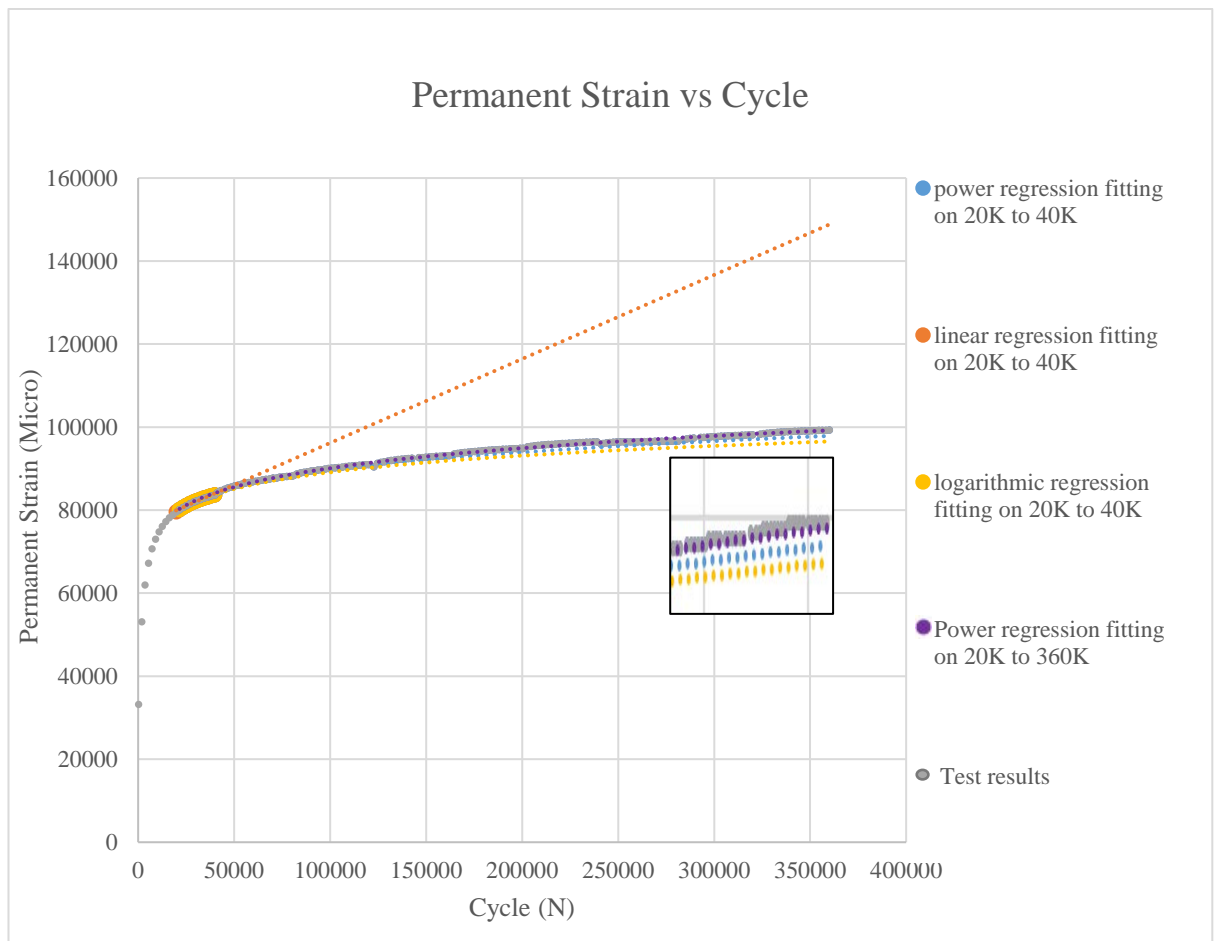


Figure 6.11: Regression models to predict confined dynamic creep test results

Table 6.13: Difference between regression model prediction and real data

Regression Model	Cycle Number	Permanent Deformation (Predicted)	Permanent Deformation (test data)	Difference
		Micro	Micro	(%)
Linear	20,000	79992	79805	0.23
	40,000	84040	84075	-0.04
	100,000	96184	90073	6.35
	360,000	148808	99181	33.35
Logarithmic	20,000	79815	79805	0.01
	40,000	83822	84075	-0.30
	100,000	89119	90073	-1.07
	360,000	96523	99181	-2.75
Power	20,000	79834	79805	0.04
	40,000	83832	84075	-0.29
	100,000	89426	90073	-0.72
	360,000	97878	99181	-1.33

The following three outcomes regarding creep slope were concluded from this section:

- The creep slope is totally cycle dependent.
- The data between 20,000 cycle and 40,000 cycles can be used to predict the creep performance at higher cycle numbers.
- The best mathematical regression model to predict creep slope to 500,000 cycles is a power regression model.

Based on these outcomes, it was decided to break the permanent deformation data in this research into the following four areas to analyse the creep data and apply it to predict the creep life of asphalt:

1. Early behaviour: 0-20,000 load application. To assess the plastic deformation and related air void densification.
2. Mid-term behaviour: 20,000-40,000 load application. To provide an indication of second stage creep and to provide an indication of performance to 500,000 cycles.
3. Mid-term behaviour: 40,000-100,000 load application (extended). To assess the creep sensitivity to the operational parameters.

4. Late behaviour: 100,000-500,000 load application (extended). To predict the creep life based on the secant creep slope on this range of data to represent the long term behaviour and estimate creep life.

### **6.3.1 Analysing creep test data**

To investigate the best way to use the outcomes of the MCDC test, multigrade asphalt creep results at 50<sup>0</sup>C for air voids between 0 to 10% under three different platen stress (500, 750, and 1000 kPa) were examined as follows:

- Permanent strain after 20,000 cycles.
- Secant creep slope from 20,000 to 40,000 cycles.
- Secant creep slope from 40,000 to 100,000 cycles using a power model to predict behaviour.

Information regarding the tested Multigrade samples is summarised in Table 6.14. The permanent strain in 20,000 cycles and the secant creep slope are summarised in Figures 6.12, 6.13, and 6.14. The permanent strain in each stage in Figure 6.12 shows the effect of air void and stress on the creep deformation. The creep slope results based on data between 20,000 and 40,000 (Figure 6.13) show that the rate of creep is air void sensitive. The air void sensitivity of creep slope also is observed in Figure 6.14 which is related to creep slope in higher cycles.

The load sensitivity of creep slope, however, is not observed clearly in the early cycles (Figure 6.13) as well as for higher cycles (Figure 6.14). Creep slope between 40,000 and 100,000 cycles seems to be more suitable to show the creep sensitivity to varying stresses.

Based on the above discussion, it was decided to use two parameters to assess and discuss the creep sensitivity to air voids and bitumen type:

1. Permanent strain at 20,000 cycles for each stage
2. Secant creep slope data between 40,000 and 100,000 cycles

Table 6.14: Selected multigrade sample

All multigrade samples where tested under MDCD test in 50°C	
Sample number	Air voids in centre
44M	0.16
39M	2.24
46M	4.64
41M	6.50
53M	8.93

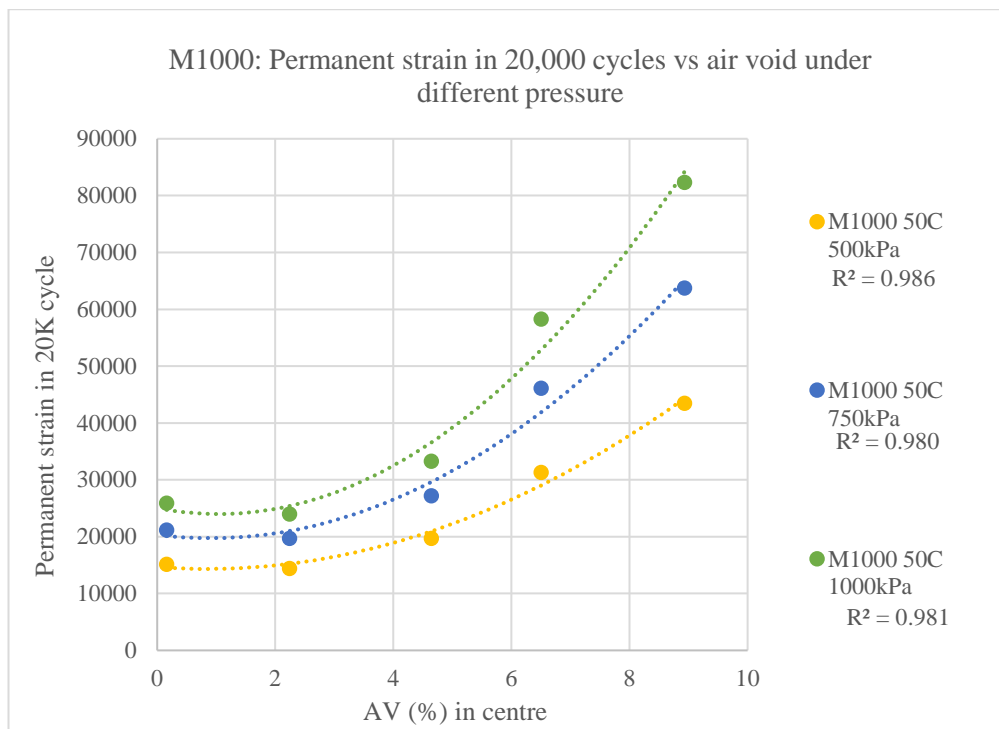


Figure 6.12: Permanent strain vs air voids under different stress at 50°C

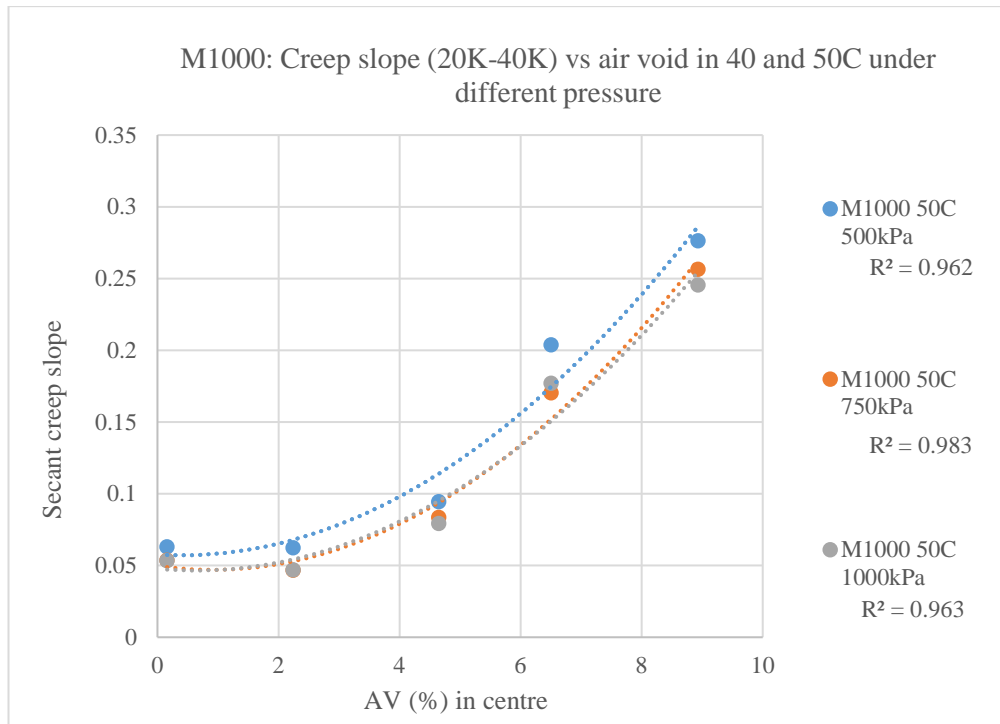


Figure 6.13: Creep slope vs air voids under different stress based on the secant creep slope between 20,000 and 40,000 cycles.

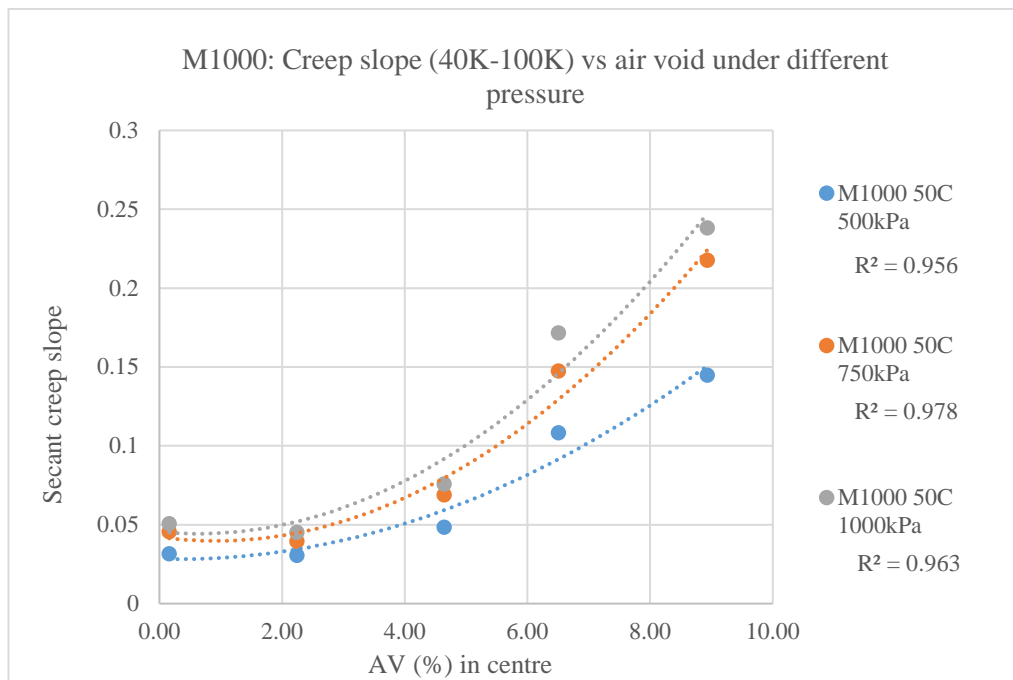


Figure 6.14: Creep slope vs air voids under different stress based on the secant creep slope between 40,000 and 100,000 cycles.

## **6.4 Prediction of creep life using MCDC test**

In asphalt surface layers at high in-service temperatures under heavy slow-moving traffic, creep deformation can be manifested in a relatively short period and affect the service life of asphalt pavements. To develop better pavement design in models, the prediction and assessment of creep life based on creep deformation is necessary.

### **6.4.1 Creep life prediction based on secant creep slope**

As discussed in Chapter 5 and Section 6.3 of this chapter, it was outlined how the secant modulus in the early stage of a creep test is useful for ranking performance but not for predicting creep life. The secant creep slope and estimated creep life are significantly cycle dependent. Figure 6.15 illustrated the effect of selected cycles on the estimated permanent strain for the following cycles:

- Secant creep slope calculated using data at 20,000 and 40,000 cycles
- Secant creep slope calculated using data at 40,000 and 100,000 cycles
- Secant creep slope calculated using data at 100,000 and 500,000 cycles
- Secant creep slope calculated based on power regression on all permanent strain data between 20,000 and 40,000 cycles

To have a realistic estimation of secant creep slope and consequently creep life, secant creep slope must be measured in the steady state portion of the creep curve. The laboratory assessment of creep deformation of the confined sample by Ahmadinia (2017) and also in section 6.3 of this research showed that up to 40,000 cycles the rate of creep deformation continued to decrease and that around 40,000 cycles the creep rate approached linear behaviour.

The level of 500,000 cycles (late behaviour) was chosen based on the assumption that around this cycle the rate of creep deformation becomes constant.

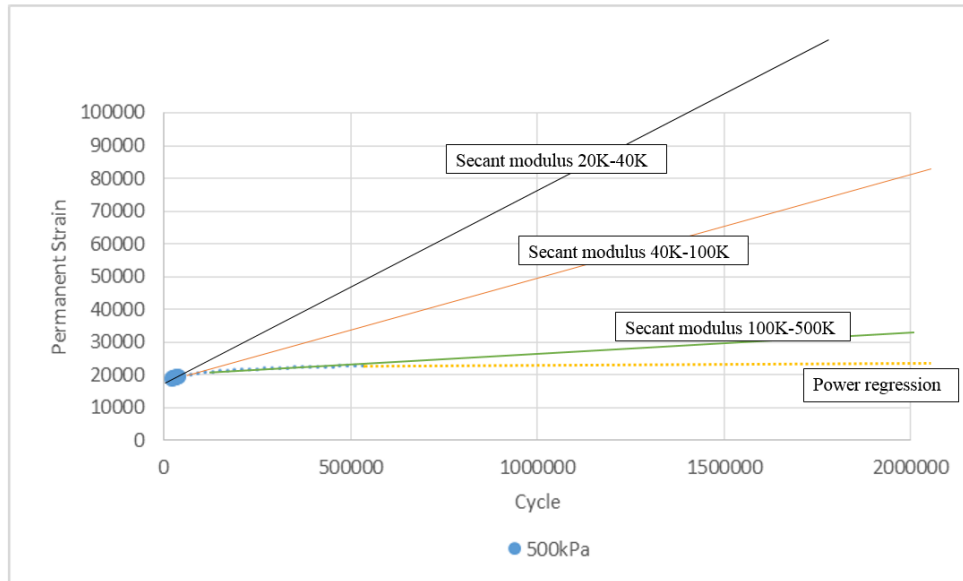


Figure 6.15: Schematic creep life prediction using different mathematical regression methods

#### 6.4.2 MCDC test analysis and applied mathematical modelling

In the MCDC test, the asphalt samples were prevented from splitting and collapse by the multilayer confinement system. Similar to in-situ asphalt, the creep deformation in the laboratory samples reached a steady state of creep. The underpinning methodology adopted was to estimate pavement deformation to 500,000 cycles using a power regression model based on test data to 40,000 cycles and extrapolation of that data to 500,000 cycles. The schematic diagram of the MCDC test and the power regression model is represented in Figure 6.16.

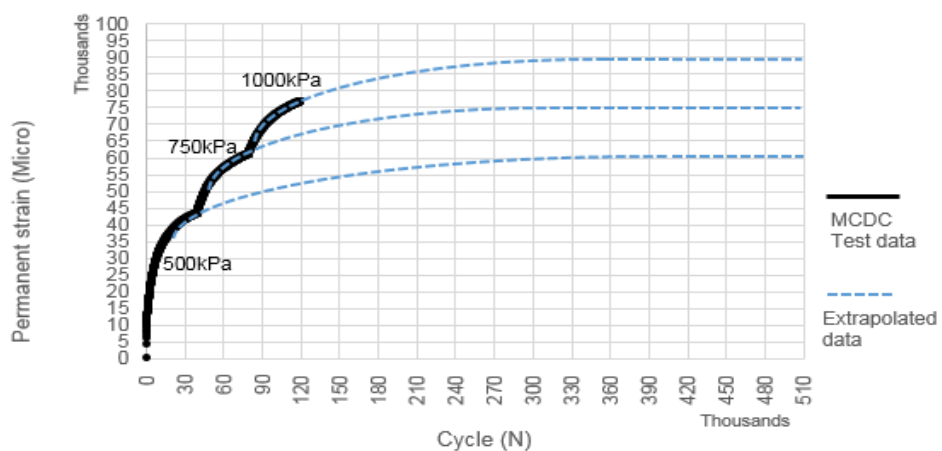


Figure 6.16: Schematic diagram of MCDC test and the power regression model

### 6.4.3 Creep life prediction based on creep depth in laboratory samples

It is assumed for modelling in this study that the creep deformation has occurred within a HMA surface layer. Creep depth (rut depth) in the asphalt surface may be divided into densification and shear deformation. Densification is a result of aggregate movement under the cyclic traffic load. Shear deformation is a result of the viscous behaviour of the material at high temperatures (De Carvalho 2012). A schematic transverse profile of creep deformation within an asphalt surface is shown in Figure 6.17.

For the following analysis, a pavement's serviceability is considered to be affected by creep deformation when it exhibits a total creep depth of 25mm. This 25mm level includes both the densification and shear deformations. Since it was possible to measure heave in the laboratory the analysis used a 20mm creep deformation depth to calculate a creep life of asphalt. To allow modelling, the 20mm was assumed to occur within a 200mm asphalt layer to obtain the estimation to the end of serviceability. As the laboratory samples were 50mm in depth a 4:1 ratio of 5mm was used as the end of creep life.

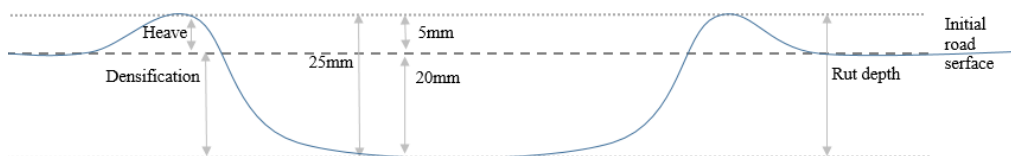


Figure 6.17: Transverse profile of rut depth (creep deformation) under the tyre

### 6.4.4 Estimation of creep life

The creep life of the asphalt mixes, based on the laboratory data was determined as follows:

1. The permanent strain was estimated at 500,000 cycles in each stage by fitting a power regression model ( $y = ax^b$ ) to the data between 20,000 and 40,000 load cycles and extrapolating the data to 500,000 cycles. The permanent strain

estimation based on a power regression model is shown schematically in Figure 6.16.

2. Both secant creep slope ( $m$ ) and conventional intercept ( $c$ ) (Figure 6.9) were calculated using the secant between permanent strain at 100,000 and 500,000 load cycles.
3. The permanent strain life ( $\epsilon_{max}$ ) was calculated by using the height of sample ( $h$ ) and a 5mm target creep depth (creep depth limit in the laboratory) as follow:

$$\epsilon_{max} = \frac{5 \cdot 10^6}{h} \quad (6.1)$$

4. Creep life finally in cycles can be calculated using the following formula:

$$\text{Creep life} = \frac{(\epsilon_{max} - c)}{m} \quad (6.2)$$

The calculation of creep life for sample 83 fabricated with conventional bitumen (details of mix type, and voids is provided in Table 6.15) as an example of the process.

Table 6.15: Calculation of creep life for sample 83C

	Stress in each stage (kPa)	Height (mm)	Permanent strain endurance limit (Micro)	Secant creep slope	Conventional Intercept (Micro)	Creep life (Cycle)
		$(h)$	$(\epsilon_{max})$	$(m)$	$(c)$	$= (\epsilon_{max} - c)/m$
Creep life prediction for sample 83 in 50C	Stage 1 500kPa	50.21	99582	0.0252	42720	2,256,419
	Stage 2 750kPa	50.21	99582	0.0565	52934	825,624
	Stage 3 1000kPa	50.21	99582	0.0821	58322	502,555

## 6.5 Conclusion

Historically, many methods have been undertaken by researchers for predicting field creep deformation within the laboratory. However, most developed methods are not sufficiently realistic and have their own specific drawbacks. Commonly identified drawbacks are related to the modelling of real in-situ confinement stress, duplicating the nonhomogeneous composite structure of asphalt and the required time and cost of

the proposed methods. These drawbacks in the laboratory limit the ability of existing creep tests to reflect the real creep performance of existing or new asphalts under variables such as air voids, temperature and stress levels.

This Chapter reviews the historical approaches to evaluating creep within the laboratory and identifies their common deficiencies. It was identified how the proposed MCDC methodology largely addressed these concerns.

The Chapter evaluates the applied confinement system for the MCDC test. The outcomes proved the effectiveness of the applied confinement system and are as follows:

1. The stress within the asphalt layer under dynamic load is similar to the stress in the laboratory confinement sample under the same load.
2. Lateral confinement stress at the beginning of each stage of the MCDC test, generated by confinement system including asphalt, resin and PVC, is close to the generated stress in continuous tests.
3. Lateral confinement stress at each stage of the MCDC test is load dependent. It means that the confinement system can automatically generate higher confinement stress for higher applied platen stress.

Extrapolation of short term data for prediction of long term creep potential was assessed in this Chapter. The creep data between 20,000 and 40,000 cycles was used to extend the creep data to 500,000 cycles.

The Chapter explores the best way to rank the asphalt samples using the MCDC test for Permanent strain after 20,000 cycles and secant creep slope from 40,000 to 100,000 cycles (Extended data). Creep life prediction using the MCDC test was explored in this Chapter as well.

In the next chapters, the possibility of using UWT technique and MCDC test to better rank the creep deformation of three selected asphalt types and the effective parameters will be assessed and explained.

## CHAPTER 7

### MULTISTAGE CONFINED DYNAMIC CREEP TEST AND CREEP RANKING FOR ASPHALT MIXES

#### Contents

7.1	Introduction .....	123
7.2	Selected samples and tests.....	123
7.3	Creep performance versus air voids .....	124
7.3.1	Air voids effect on permanent strain of conventional asphalt.....	124
7.3.2	Air voids effect on secant creep slope of conventional asphalt .....	126
7.3.3	Air voids effect on permanent strain of multigrade asphalt .....	128
7.3.4	Air voids effect on secant creep slope of multigrade asphalt .....	130
7.3.5	Air voids effect on permanent strain of polymer modified asphalt ...	132
7.3.6	Air voids effect on secant creep slope of polymer modified asphalt .	133
7.4	Conclusion.....	134

## **7.1 Introduction**

Current laboratory creep test methods employed by road agencies and construction contractors are not able to reliably or quickly predict the development of creep under varying operational conditions. This Chapter outlines the use of the MCDC and UWT to better predict creep deformation.

The effects of some of the major parameters such as air voids and bitumen binder types on creep deformation under varying temperature and stresses was assessed using both the MCDC and UWT tests. The laboratory test data was then extrapolated to predict the longer term creep performance.

## **7.2 Selected samples and tests**

To evaluate the effects of air voids and bitumen binder type, the MCDC and UWT tests were undertaken for 30 samples. The details of the samples are represented in Table 7.1. Air voids were calculated in the centre of samples using the UWT technique as discussed in Chapter 5. The MCDC test was undertaken for the samples under three different stresses (500, 750, and 1000kPa) in three stages and at two temperatures of 40°C and 50°C. The MCDC test conditions are outlined below:

- Compressive stress: 500, 750, and 1000kPa
- Seating stress: 20 kPa
- Loading period: 100 milliseconds (ms)
- Pulse repetition period: 1000 milliseconds (ms)
- Test temperature: 40°C and 50°C
- Termination pulse count: 40,000 cycles
- Platen size: 50mm diameter
- Sample size: 150mm diameter
- Confinement situation: Confined with PVC ring + Resin infill

Full details of the MCDC test outcomes are summarised in Figures 1 to 6 in Appendix D for the asphalt mix manufactured with three types of binders; conventional, multigrade and polymer modified.

Table 7.1: Selected samples for MCDC test

Selected samples with different air voids for MCDC test in 40°C and 50°C											
C320				M1000				PMB			
40°C		50°C		40°C		50°C		40°C		50°C	
Sample number	AV in centre (%)	Sample number	AV in centre (%)	Sample number	AV in centre (%)	Sample number	AV in centre (%)	Sample number	AV in centre (%)	Sample number	AV in centre (%)
82C	0.07	81C	0.39	42M	1.46	44M	0.16	93P	0.10	91P	0.10
68C	2.24	67C	2.10	36M	2.15	39M	2.24	88P	1.39	100P	1.96
71C	3.27	83C	5.13	48M	2.35	46M	4.64	98P	2.41	96P	3.05
66C	5.59	84C	6.14	58M	6.40	41M	6.50	102P	4.55	107P	6.56
79C	6.07	85-2C	9.42	55M	9.64	53M	8.93	108P	7.07	110-1P	8.12

The MCDC test outcomes were analysed to obtain the following:

1. Early behaviour: 0-20,000 load cycles application. To calculate the permanent strain at 20,000 load cycles.
2. Mid-term behaviour: 20,000-40,000 load cycles application. To calculate secant creep slope between those cycles.
3. Mid-term behaviour: 40,000-100,000 load cycles application. To calculate secant creep slope between those cycles.
4. Late behaviour: 100,000-500,000 load cycles application. Data extrapolated to predict the creep life of asphalt mix.

### 7.3 Creep performance versus air voids

Creep deformation develops more rapidly in asphalt layers at elevated temperatures where bitumen binders show more viscous behaviour and the contribution of the aggregate structure and the confining stresses becomes more crucial. The aggregate structure includes aggregate gradation, size, and the interlocked particles. The confining stress is the stress generated by the mass of asphalt around the stressed asphalt under the tyre. To better understand creep mechanisms, variation in air voids at different temperatures and stresses in a confined condition were investigated.

#### 7.3.1 Air voids effect on permanent strain of conventional asphalt

The permanent strain of samples manufactured by conventional bitumen is presented in Figure 7.1 at 40°C and 50°C respectively for varying stresses. The data indicates that there is a fair correlation coefficient between air voids and permanent strain at 40°C for each applied stress. An improved correlation ( $R^2 \geq 0.9$ ) is observed at the higher temperature of 50°C.

The linear regression equations between permanent strain (at 20,000 cycles) and air voids content are presented in Table 7.2. The slope calculated from the linear regression equation in Table 7.2 is presented in Table 7.3. The comparison of the slopes of the equations in Table 7.3 shows that the effect of air voids content increases when the stress increases. It also shows that the effect of the increase of stress is higher at higher temperatures. The permanent strain changes in asphalt are related to the bitumen binder viscoelastic behaviour under varying stresses and temperatures.

The data in Figure 7.1, Table 7.2 and 7.3 indicate that permanent strain increases as a function of air voids in all cases. The data also indicates that the rate of increase becomes greater with both increase in temperature and stress.

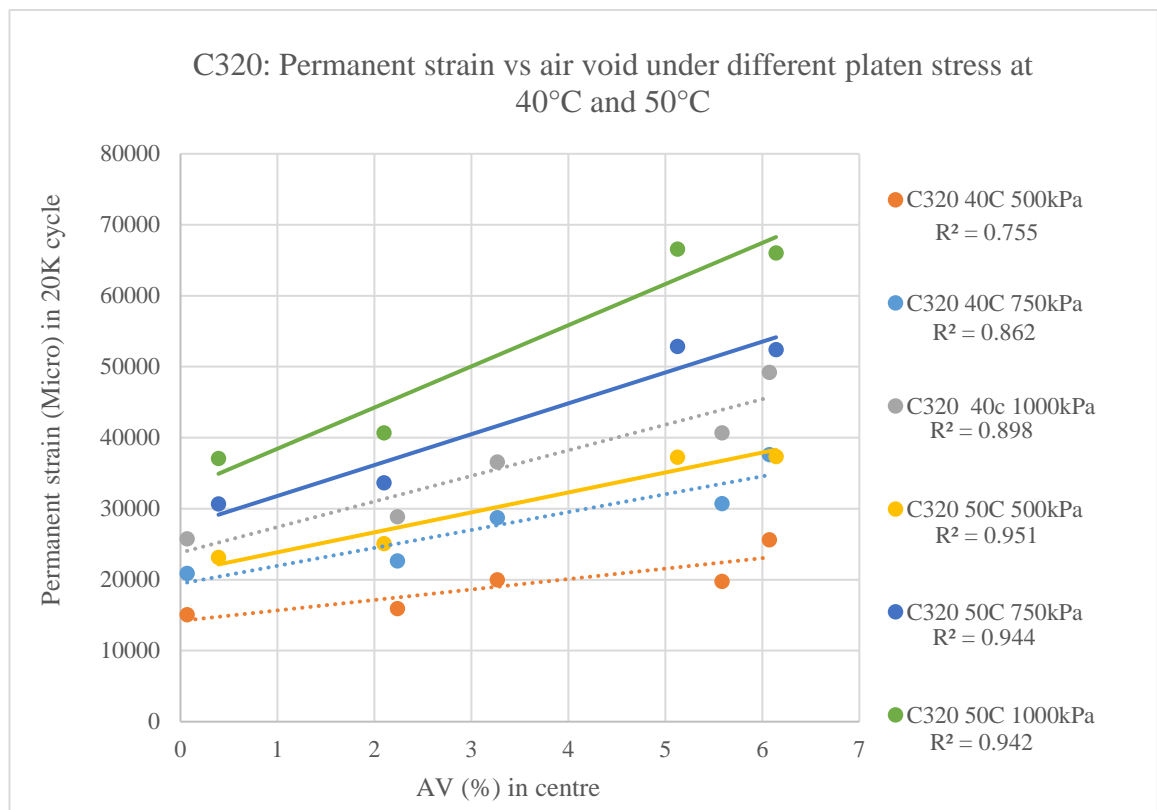


Figure 7.1: Permanent strain vs air voids under different platen stress in 40°C and 50°C

Table 7.2: Linear regression equation between permanent strain and air voids

	Platen stress	Temperature	
		40°C	50°C
Linear regression equation	500kPa	$y = 1472x + 14202$	$y = 2810x + 21049$
	750kPa	$y = 2521x + 19437$	$y = 4347x + 27454$
	1000kPa	$y = 3603 + 23815$	$y = 5799x + 32654$

Table 7.3: The slope from the linear regression equations between permanent strain after 20,000 cycles and air voids for conventional asphalt

	Platen stress	Temperature	
		40°C	50°C
Slope (%)	500kPa	1472	2810
	750kPa	2521	4347
	1000kPa	3603	5799

### 7.3.2 Air voids effect on secant creep slope of conventional asphalt

The Secant creep slope was calculated in mid-term; between 20,000 and 40,000 cycles and between 40,000 and 100,000 cycles. The results are presented in Figures 7.2 and 7.3 respectively. Good correlation between secant creep slope and air voids for varying temperature and stress can be observed from Figure 7.2. The same correlations and trends were also observed for secant creep slope calculated between 40,000 cycles and 100,000 cycles in Figure 7.3. The data presented in Figure 7.2 and 7.3 also shows that the magnitude of secant creep slope is higher at a higher temperature.

Mid-term behaviour (based on 20,000 and 40,000 cycles) of secant creep slope which is presented in Figure 7.2 is clustered with limited trends related to stress. The mid-term behaviour of secant creep slope in higher cycle numbers (40,000 and 100,000 cycles) which is presented in Figure 7.3 better shows the effect of higher stresses. Increasing stress from 500kPa to 1000kPa leads to an increase in the secant creep slope for each air voids content. It was concluded from this comparison that secant creep slope from 40,000 to 100,000 cycles may be a better indicator of the effect of stress.

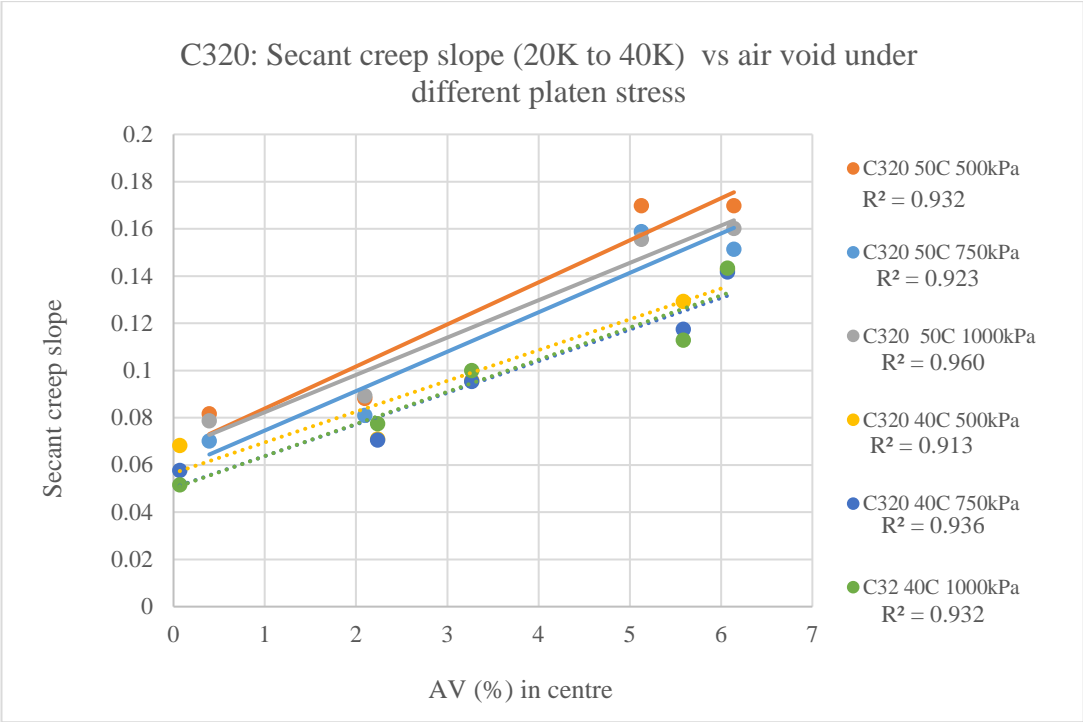


Figure 7.2: Secant creep slope (20,000-40,000 cycles) versus air voids under various pressures at 40°C and 50°C

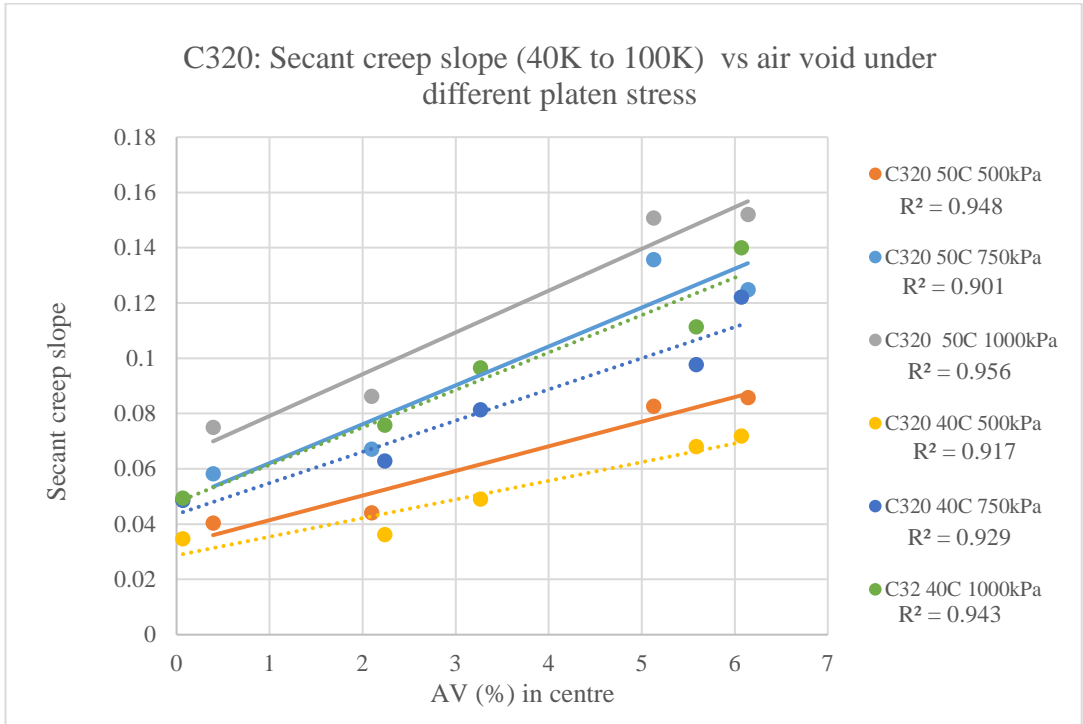


Figure 7.3: Secant creep slope (40,000-100,000 cycles) versus air voids under various pressures at 40°C and 50°C

The slope calculated from Table 7.4, which are the linear regression equation between secant creep slope (40,000 and 100,000 cycles) and air voids in varying test conditions are presented in Table 7.5. The calculated slope in Table 7.5 shows that secant creep slope of conventional asphalt is stress and temperature sensitive. The higher slope can be observed at the higher stress and temperature. The slope trends in Table 7.5 are similar to the slope trends that were calculated based on linear regression on the permanent strain in 20,000 cycles shown in Table 7.3.

Table 7.4: Linear regression between secant creep slope (40,000 and 100,000 cycles) and air voids for conventional bitumen

	Platen stress	Temperature	
		40°C	50°C
Slope	500kPa	$y = 0.0067x + 0.0287$	$y = 0.0089x + 0.0325$
	750kPa	$y = 0.0113x + 0.0436$	$y = 0.0141x + 0.048$
	1000kPa	$y = 0.0135x + 0.0479$	$y = 0.0151x + 0.064$

Table 7.5: Slope calculated from linear regression between secant creep slope (40,000 and 100,000 cycles) and air voids for conventional bitumen

	Platen stress	Temperature	
		40°C	50°C
Slope (%)	500kPa	0.0067	0.0089
	750kPa	0.0113	0.0141
	1000kPa	0.0135	0.0151

### 7.3.3 Air voids effect on permanent strain of multigrade asphalt

Permanent strains of samples manufactured with multigrade bitumen are presented in Figure 7.4 at 40°C and 50°C respectively for varying stress at 20,000 cycles. Good correlation ( $R^2 \geq 0.85$ ) was seen between permanent strain and air voids for both temperatures. The data indicates that permanent strain is higher at greater temperatures for any specific stress.

The linear regression equations between permanent strain in 20,000 cycles and air voids content are presented in Table 7.6. The slopes calculated from the linear regression equations in Table 7.6 are provided in Table 7.7. The slope results show that the effect of air voids content increases when the stress increases. It is also shown that the effect of the increase of stress is higher at higher temperatures.

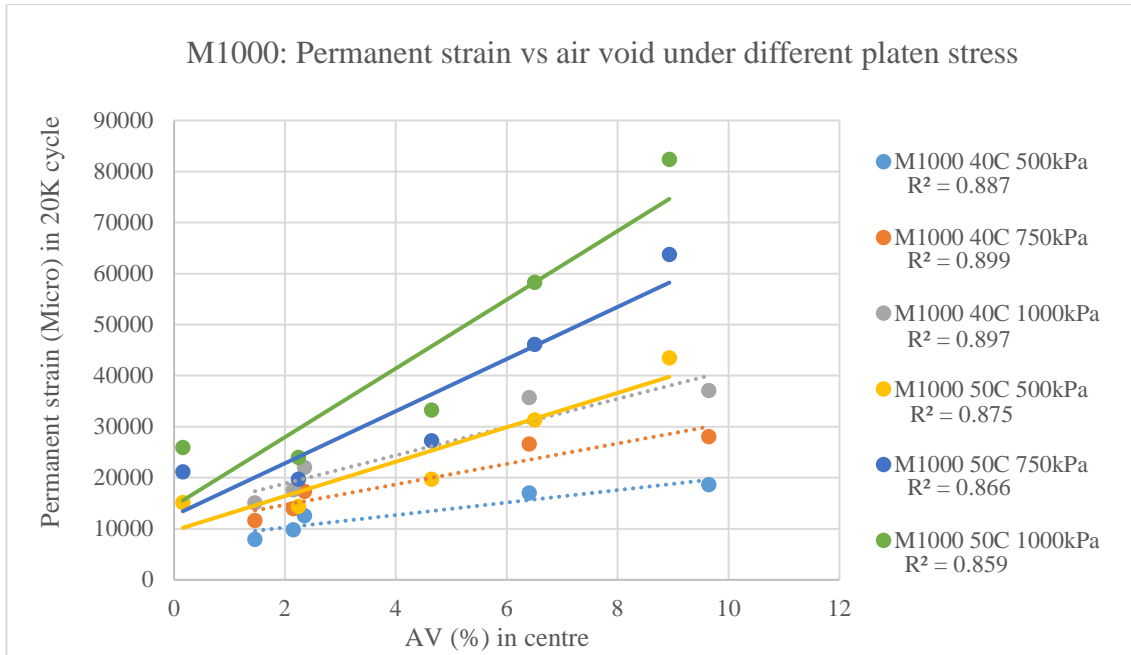


Figure 7.4: Permanent strain vs air voids under different stresses in 40°C and 50°C

Table 7.6: Linear regression equation between permanent strain and air voids for multigrade asphalt

	Platen stress	Temperature	
		40°C	50°C
Linear regression equation	500kPa	$y = 1222x + 7806$	$y = 3371x + 9657$
	750kPa	$y = 2004x + 10680$	$y = 5105x + 12629$
	1000kPa	$y = 2766x + 13328$	$y = 6732x + 14494$

Table 7.7: The slope from the linear regression equations between permanent strain after 20,000 cycles and air voids for multigrade asphalt

	Platen stress	Temperature	
		40°C	50°C
Slope (%)	500kPa	1222	3371
	750kPa	2004	5105
	1000kPa	2766	6732

### 7.3.4 Air voids effect on secant creep slope of multigrade asphalt

Secant creep slope was calculated in mid-term, between 20,000 and 40,000 cycles and between 40,000 and 100,000 cycles, and presented in Figure 7.5 and 8.6 respectively.

Good correlation ( $R^2 \geq 0.85$ ) between creep slope and air voids for varying temperatures and stress existed, where creep slope increased with air voids. The secant creep slope sensitivity to air voids was greater at higher air voids content and higher temperatures. As with samples fabricated with C320, the data generated from the secant creep slope between 40,000 and 100,000 cycles was more significant.

Slopes calculated from linear regression equation in Table 7.8 between secant creep slope (40,000 and 100,000 cycles) and air voids in varying test conditions are provided in Table 7.9. The slope results show that secant creep slope of multigrade asphalt is stress and temperature sensitive. The higher slope can be observed at the higher stress and temperature conditions. The slope trends in Table 7.9 are similar to the slope trend that is calculated based on linear regression on permanent strain data at 20,000 cycles in Table 7.7.

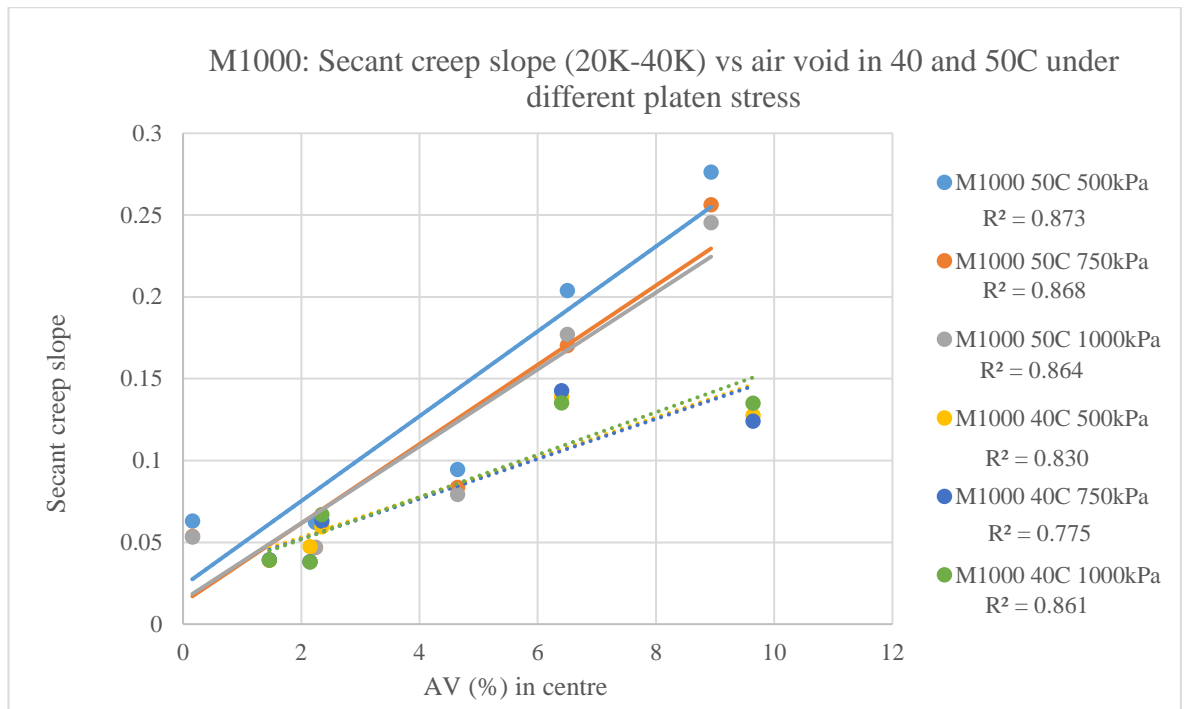


Figure 7.5: Creep slope (20,000-40,000 cycles) vs air voids under various pressures at 40°C and 50°C

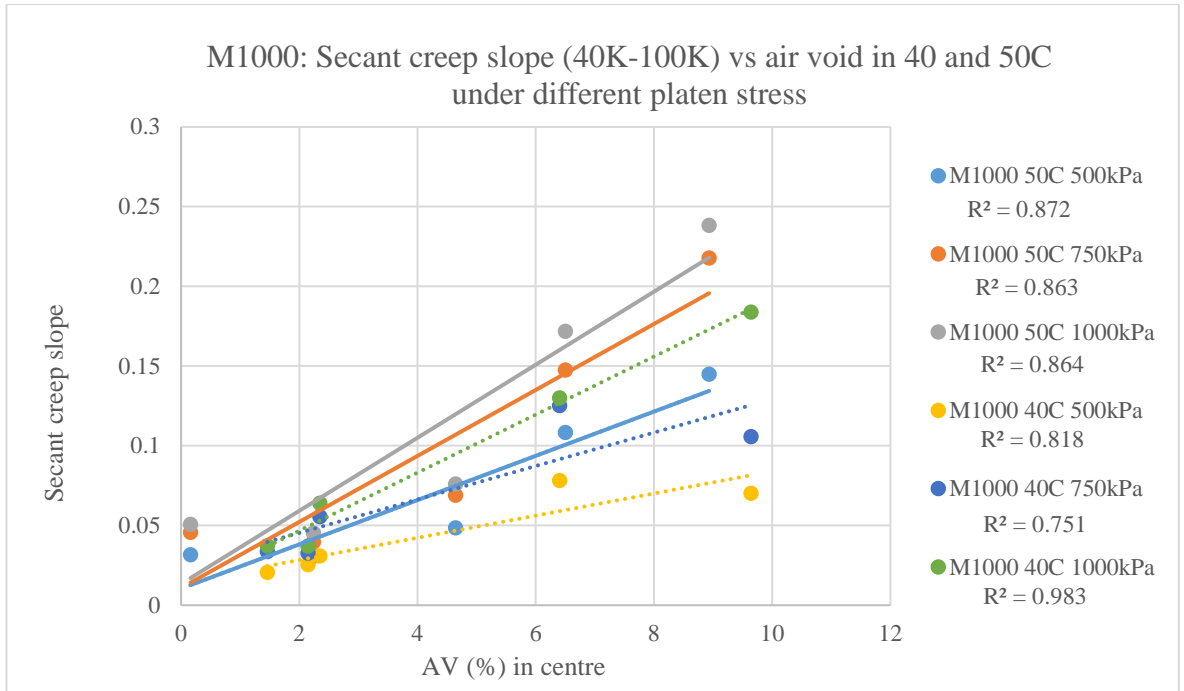


Figure 7.6: Creep slope (40,000-100,000 Cycles) vs air voids under various pressures at 40°C and 50°C

Table 7.8: Linear regression between secant creep slope (40,000 and 100,000 cycles) and air voids for conventional bitumen

	Platen stress	Temperature	
		40°C	50°C
Slope	500kPa	$y = 0.007x + 0.0144$	$y = 0.0139x + 0.0104$
	750kPa	$y = 0.0105x + 0.0244$	$y = 0.0207x + 0.0109$
	1000kPa	$y = 0.0182x + 0.0103$	$y = 0.0229x + 0.0134$

Table 7.9: Slope calculated from linear regression between secant creep slope (40,000 and 100,000 cycles) and air voids for conventional bitumen

	Platen stress	Temperature	
		40°C	50°C
Slope (%)	500kPa	0.007	0.0139
	750kPa	0.0105	0.0207
	1000kPa	0.0182	0.0229

### 7.3.5 Air voids effect on permanent strain of polymer modified asphalt

The permanent strain of samples manufactured by polymer modified bitumen is presented in Figure 7.7 in 40°C and 50°C for varying stresses at 20,000 cycles.

Similar to the behaviour exhibited by samples manufactured by conventional and multigrade bitumen, polymer modified samples also show air voids sensitive behaviour. The effect of stress and temperature was assessed based on the slope data in Table 7.10, which was calculated from linear regression equation between permanent strain and air voids. Results presented in Table 7.11 show that creep of polymer modified asphalts is a function of stress, temperature, and air voids.

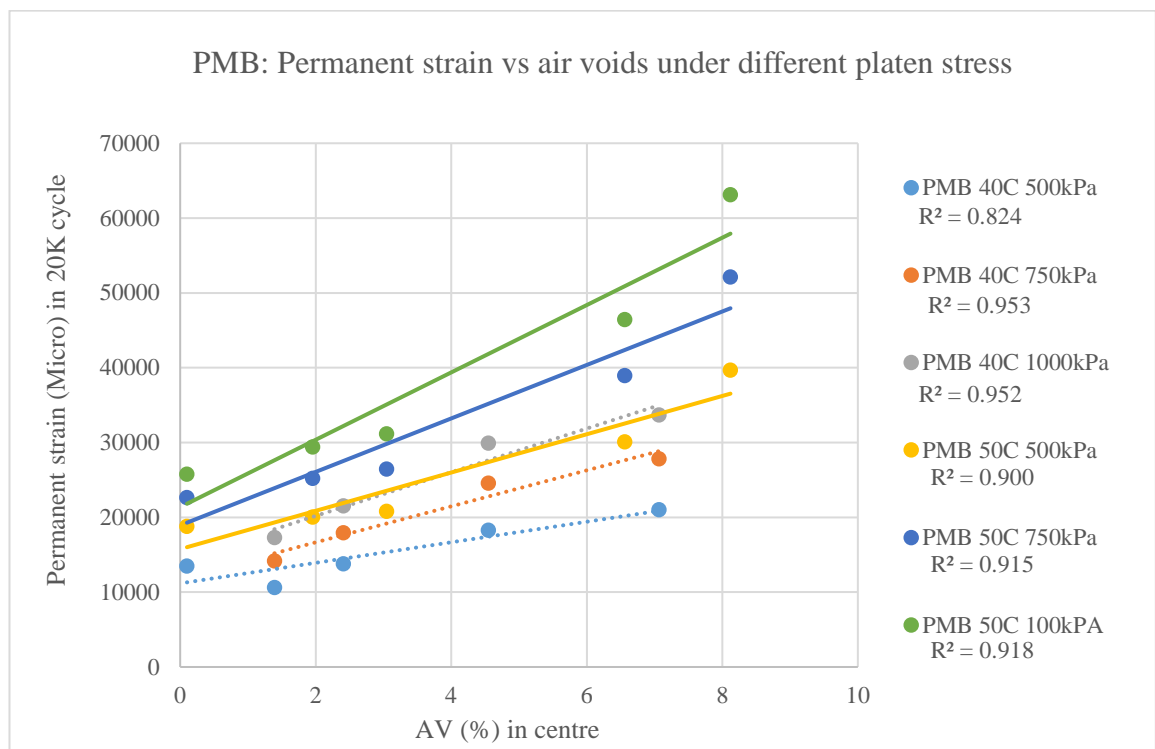


Figure 7.7: Permanent strain vs air voids under various stresses in 40°C and 50°C

Table 7.10: Linear regression equation between permanent strain and air voids for polymer modified asphalt

	Platen stress	Temperature	
		40°C	50°C
Linear regression equation	500kPa	$y = 1373x + 11175$	$y = 2558x + 15756$
	750kPa	$y = 2406x + 11847$	$y = 3573x + 18929$
	1000kPa	$y = 2919x + 14353$	$y = 4501x + 21368$

Table 7.11: The slope from the linear regression equations between permanent strain after 20,000 cycles and air voids for polymer modified asphalt

	Platen stress	Temperature	
		40°C	50°C
Slope (%)	500kPa	1373	2558
	750kPa	2406	3573
	1000kPa	2919	4501

### 7.3.6 Air voids effect on secant creep slope of polymer modified asphalt

The creep sensitivity of samples manufactured with polymer modified bitumen at 40°C and 50°C is shown in Figure 7.8, and 7.9 for varying stresses and cycle number. Both Figures exhibit a good correlation with the data for secant modulus for 20,000-40,000 cycles being more tightly clustered.

The slope calculated from linear regression equation in Table 7.12 for the secant creep between 40,000 and 100,000 cycles and air voids at varying test conditions is presented in Table 7.13. The data shows a similar trend to the other types of asphalt mix manufactured with conventional and multigrade bitumen binders.

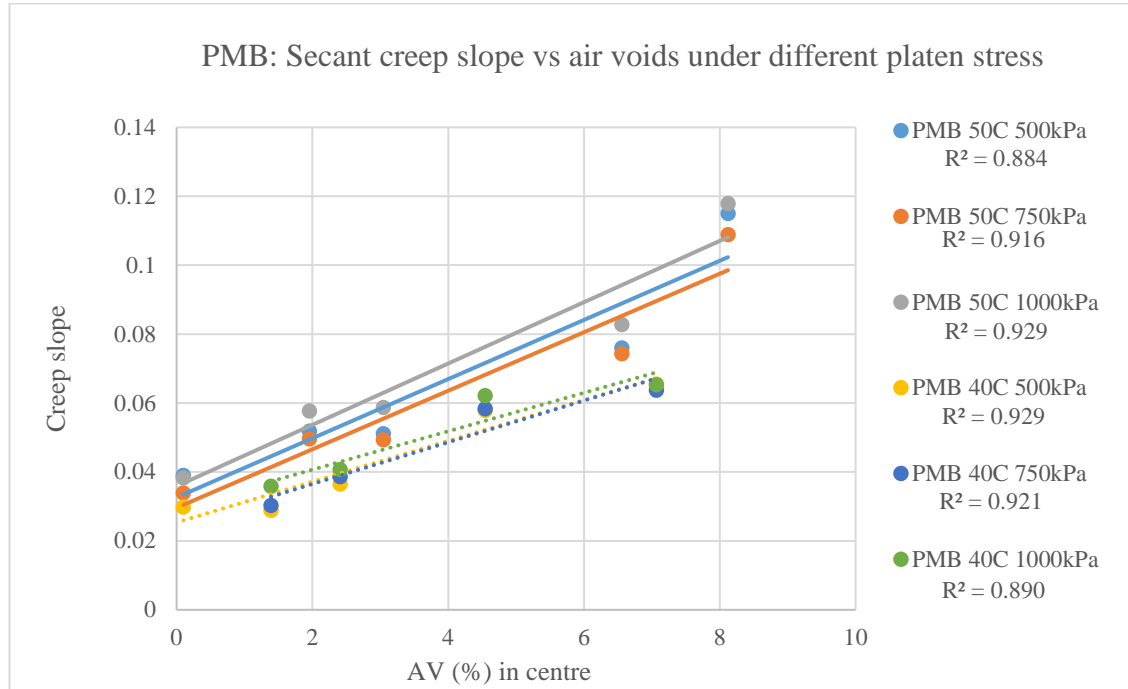


Figure 7.8: Creep slope (20,000-40,000 cycles) vs air voids under various pressures at 40°C and 50°C

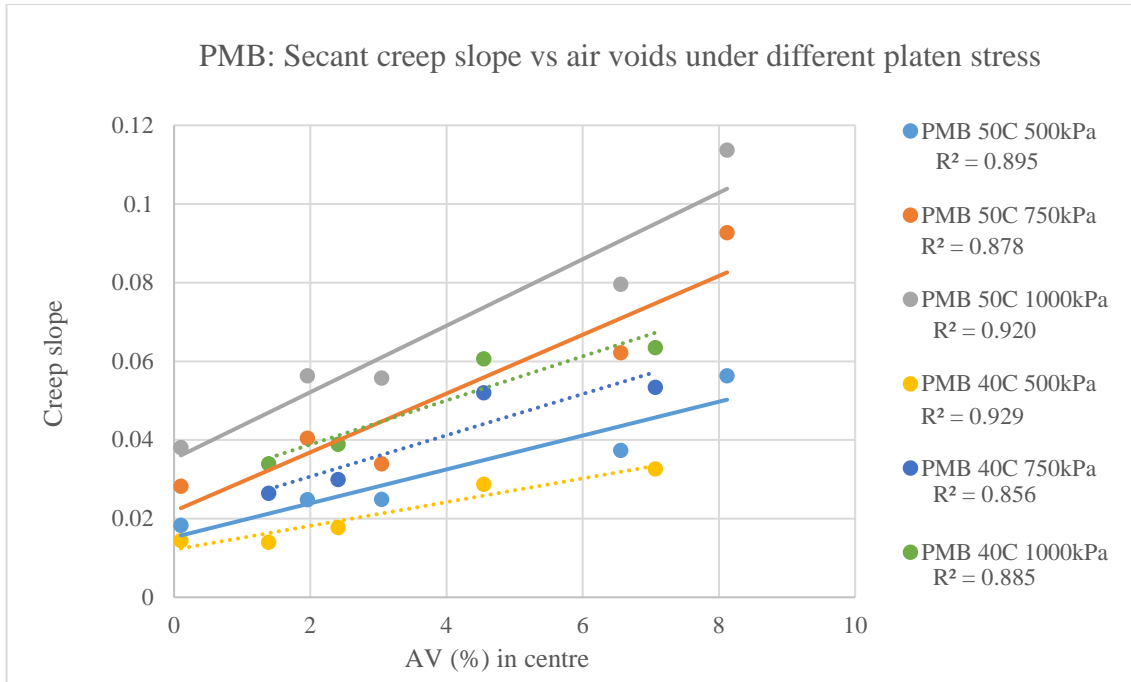


Figure 7.9: Creep slope (40,000-100,000 cycles) vs air voids under various pressures at 40°C and 50°C

Table 7.12: Linear regression between secant creep slope (40,000 and 100,000 cycles) and air voids for conventional bitumen

	Platen stress	Temperature	
		40°C	50°C
Slope	500kPa	$y = 0.003x + 0.0121$	$y = 0.0043x + 0.0153$
	750kPa	$y = 0.0052x + 0.0202$	$y = 0.0075x + 0.0219$
	1000kPa	$y = 0.0056x + 0.0276$	$y = 0.0085x + 0.0352$

Table 7.13: Slope calculated from linear regression between secant creep slope (40,000 and 100,000 cycles) and air voids for conventional bitumen

	Platen stress	Temperature	
		40°C	50°C
Slope (%)	500kPa	0.003	0.0043
	750kPa	0.0052	0.0075
	1000kPa	0.0056	0.0085

## 7.4 Conclusion

The MCDC test was undertaken for asphalts manufactured using conventional, multigrade and polymer modified binders for a range of air voids, temperatures, and stresses. A summary of the testing outcomes is outlined below and provided in table 7.14:

- Permanent strain at 20,000 cycles is sensitive to stress, temperature, and air voids and able to discriminate between bitumen binder types.
- Secant creep slope between 40,000 and 100,000 cycles is temperature and stress dependent and able to discriminate between bitumen binder types.

The ranking of the three asphalts is summarised in Table 7.14 for all test data. The consistent ranking was that PMB demonstrates the best performance followed by multigrade and C320.

Table 7.14: Ranking asphalt mixes based on two methods under varying operational conditions

				Methods applied to rank the three mixtures	
				Permanent strain (Micro) at 20,000 cycle	Secant creep slope calculated from data at 20,000 and 40,000 cycles
Ranking asphalt mixtures based on the creep performance	40°C	500kPa	C320	3	3
			M1000	2	2
			PMB	1	1
		750kPa	C320	3	3
			M1000	2	2
			PMB	1	1
		1000kPa	C320	3	3
			M1000	2	2
			PMB	1	1
	50°C	500kPa	C320	3	3
			M1000	2	2
			PMB	1	1
		750kPa	C320	3	3
			M1000	2	2
			PMB	1	1
1000kPa		C320	3	3	
		M1000	2	2	
		PMB	1	1	

## CHAPTER 8

### CREEP LIFE ANALYSIS BASED ON MCDC + UWT TEST

#### Contents

8.1	Introduction .....	137
8.2	MCDC +UWT test procedure and creep life calculation .....	137
8.2.1	Air voids estimation under platen using UWT technique.....	137
8.2.2	Creep life calculation using MCDC test .....	138
8.3	Comparison of creep life of three selected asphalts .....	139
8.3.1	Creep life vs air voids .....	141
8.3.2	Creep life vs temperature .....	141
8.3.3	Creep life vs surface stress.....	141
8.3.4	Creep life vs bitumen type .....	141
8.4	Conclusion.....	142

## **8.1 Introduction**

The service life of a pavement may be defined as the time from construction to the first major structural rehabilitation or to when the pavement degrades to an unacceptable serviceability condition (Von Quintus et al., 2005). The service life of a flexible pavement, especially as it relates to the pavement surface, is determined by defects such as cracks, creep deformation (rutting), bleeding, and ravelling (Austroads 2009). At high in-service temperatures under heavy slow-moving traffic, creep deformation can be manifested in a relatively short period and becomes a key factor in defining the service life of the pavement (Santagata et al., 2017).

Predicting the service life of asphalt pavements as a function of permanent deformation at high stress and temperatures has been an ongoing challenge for Australian road agencies to best model future maintenance strategies for flexible pavements. Creep deformation (rutting), is a critical distress mode which is not adequately considered in the current flexible pavement design procedures. One reason is that the existing Australian laboratory creep test method is not able to reliably predict the development of creep over a realistic range of air voids, temperatures and tyre pressures.

This Chapter reports the application of the MCDC + UWT test method to analyse the creep life of asphalt samples with different air voids at high temperatures under different traffic loading regimes.

## **8.2 MCDC +UWT test procedure and creep life calculation**

### **8.2.1 Air voids estimation under platen using UWT technique**

The UWT technique used to measure the air voids in the centre of the sample is briefly described below and the reader is referred to the Chapter 4 and 5 for more details.

1. A Pundit 7 apparatus was applied according to the BS EN 12504-4 standard to generate an ultrasonic wave and to determine the ultrasonic pulse velocity of the asphalt sample. Two 54-kHz piezoelectric crystal transducers (transmitter and receiver) were placed in parallel at each side of the specimen to measure Ultrasonic wave transit time at 17 different locations at 25°C. The transit time for the compression wave (P-wave) to pass the length of the asphalt sample was recorded to calculate the ultrasonic pulse velocity using the below formula:

$$UV=L/T \quad (8.1)$$

Where, UV = ultrasonic pulse velocity (km/s)  
L = length of specimen (mm)  
T = transit time (ms)

2. The air voids content of whole samples was measured using the specimen's bulk specific gravity (Saturated Method) and the asphalt's theoretical maximum specific gravity (Rice Method) according to Australian Standard (AS/NZS 2891).
3. The linear correlation between average ultrasonic velocities at 17 points was used to obtain the air voids for the whole sample.
4. Air voids at the centre of samples were calculated using 'ultrasonic velocity in the centre'. It is this value that has been used in the current Chapter.

### 8.2.2 Creep life calculation using MCDC test

The calculation of creep life under varying operational conditions based on MCDC test data was developed previously and can be found in detail in Chapter 4 and 6. The calculation steps are briefly as follows:

5. The permanent strain was estimated at 500,000 cycles in each stage by fitting a power regression model ( $y = ax^b$ ) to the data between 20,000 and 40,000 load cycles and extrapolating the data to 500,000 cycles.
6. Both secant creep slope (m) and conventional intercept (c) were calculated using the secant between permanent strain at 100,000 and 500,000 load cycles.
7. The permanent strain life ( $\epsilon_{max}$ ) was calculated using the height of the sample (h) and a 5mm target creep depth (creep depth limit in the laboratory as follow:

$$\epsilon_{max} = \frac{5 \cdot 10^6}{h} \quad (8.2)$$

8. Creep life in cycles can then be calculated using the following formula:

$$\text{Creep life} = \frac{(\epsilon_{max}-c)}{m} \quad (8.3)$$

Creep life of all asphalt samples noted in Table 7.1 in Chapter 7 will be assessed and compared in this Chapter. The effect of the noted parameters on the creep life also will be discussed.

### 8.3 Comparison of creep life of three selected asphalts

Cumulative creep deformation of asphalt layers leads to a decreased performance of asphalt pavements. Effective pavement maintenance and management could significantly reduce the damage incident of this type of pavement. The key step of this task is defining the exact time of required maintenance which depends on calculating accurate creep life and its related effective parameters.

Creep life for the three selected asphalt mixes in this research was calculated by considering parameters such as air voids, temperature, and platen stress. The creep life results for the three types of asphalt are presented in Figure 8.1 to 8.3 for 500, 750 and 1000 kPa respectively. It can be found from the comparison of the results that, in a similar way to a secant creep slope, creep life is also dependent on the temperature, platen stress and air voids.

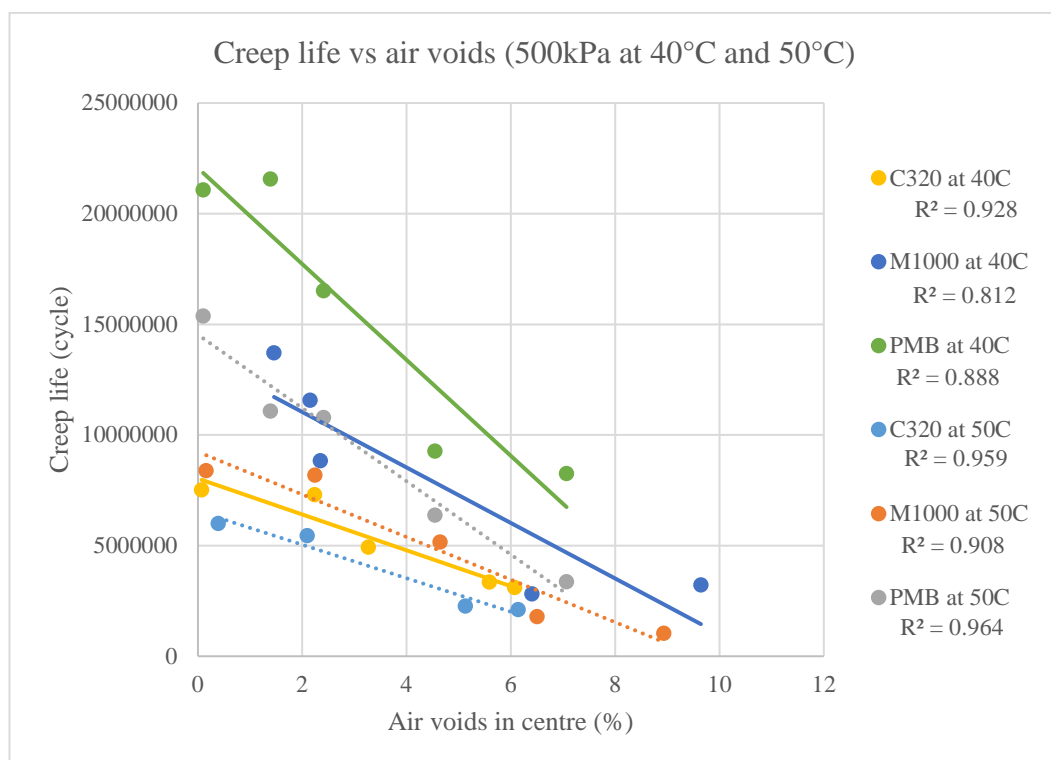


Figure 8.1: Creep life vs air voids in 500kPa

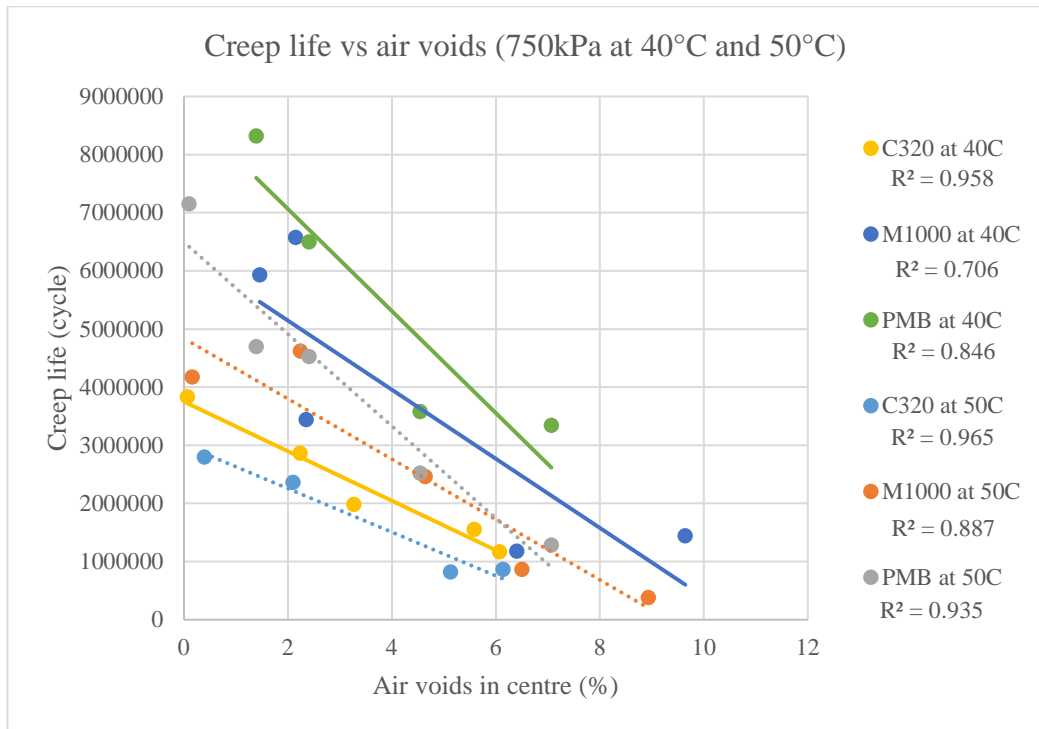


Figure 8.2: Creep life vs air voids in 750kPa

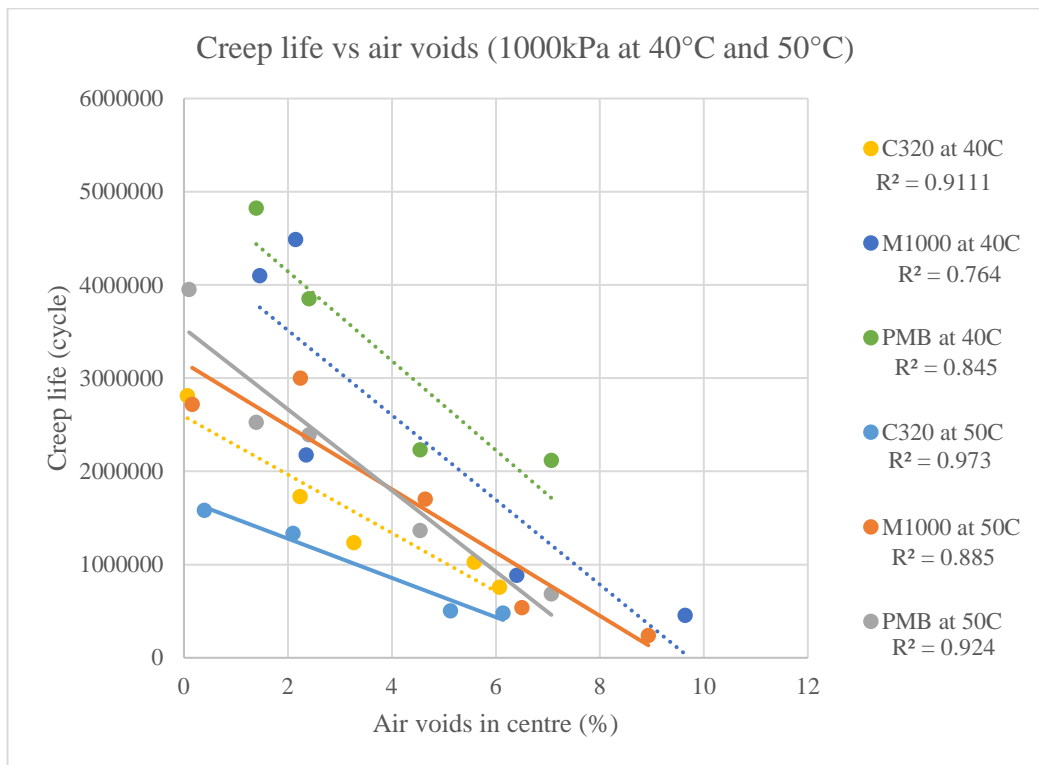


Figure 8.3: Creep life vs air voids in 1000kPa

### **8.3.1 Creep life vs air voids**

It can be seen from the regression analysis results provided in Figures 8.1 to 8.3, that there is a reasonable correlation between air voids content under the loading platen and creep life for all three types of asphalt mixes under varying stresses and temperatures. In all cases, there is a reduction in creep life with an increase in air voids, which highlights the importance of tight specification controls around compacted air voids.

### **8.3.2 Creep life vs temperature**

Creep life of selected asphalts with varying air voids content at 40°C and 50°C under varying stresses is provided in Figures 8.1 to 8.3. As expected, it can be concluded from the results that creep life is affected directly by the temperature. The data shows that for each mix an increase in temperature results in a reduced creep life.

### **8.3.3 Creep life vs surface stress**

It is well known that the stress under a tyre varies significantly from the nominal tyre pressure. De Beer et al (1997) showed that the actual pressure between the tyre and the asphalt surface can range from 500kPa to 1000kPa depending on varying circumstances. The current Australian pavement design model uses 750kPa as the default tyre pressure. In this research creep life associated with surface stresses equating to 500, 750 and 1000 kPa was assessed and the data is presented in Figures 8.1 to 8.3. The results indicate that the surface stress has a significant effect on the creep life with an increased surface stress resulting in a reduced creep life.

### **8.3.4 Creep life vs bitumen type**

As expected a review of the data provided in Figures 8.1 to 8.3 indicates that the best creep performance as evaluated by creep life is displayed by the polymer modified asphalt in most cases. The superior creep performance of polymer modified bitumen and mixes has been well reported in other research (Santagata et al., 2017). For mixes with air void of 4%, the polymer modified bitumen mix performed better than Multigrade bitumen mix at 40°C, However at 50°C the performance of the two mixes was the same.

## **8.4 Conclusion**

The following outcomes can be summarized from the comparison of the presented data in this Chapter:

1. The highest creep life occurs with polymer modified asphalts and the lowest belongs to the multigrade and conventional asphalt respectively.
2. The lower the air voids, the higher the creep life can be.
3. The higher the stress, the lower the creep life can be.
4. The higher the temperature, the lower the creep life can be.

In practice, the temperature cannot be controlled but by controlling the bitumen type, air voids and vertical stresses, higher creep life can be expected for the flexible asphalt pavements.

The developed test methodology has significant potential for further development as part of the quality assurance/control processes applied within asphalt production. The research outcomes also illustrate the critical nature of end specifications regarding the control of compacted air voids in asphalt surfacing.

## CHAPTER 9

### ASSESSING THE MODULUS OF ASPHALT USING THE MCDC+UWT TEST

#### Contents

9.1	Introduction .....	144
9.2	Compressive resilient modulus calculation of asphalt using the outlined MCDC test.....	145
9.3	The compressive resilient modulus results.....	145
9.3.1	Effect of cycle number .....	145
9.3.2	Effect of air voids on compressive resilient modulus .....	148
9.3.3	Effect of temperature on compressive resilient modulus .....	148
9.3.4	Effect of stress on resilient modulus .....	148
9.4	Conclusion.....	152

## 9.1 Introduction

As discussed earlier in Chapter 2, the modulus (stiffness) of asphalt is one input parameter in mechanistic pavement design and analysis. The modulus measurement of asphalt at elevated temperature (more than 40°C) and under high stress levels through the available Australian modulus tests (the indirect tensile test and four-bending test) is not possible. The measurement of the modulus at high temperature includes the following challenges:

1. Limitations regarding the maximum possible stress level
2. The unrealistic confinement situation compared to the in-situ condition

The international modulus measurement techniques are summarised in Table 9.1. Among all modulus tests, only “AASHTO TP62-03 2003” is possible at elevated temperature. However, the confining conditions provided by this test do not vary in response to the load-unload stage of each load pulse as seen within real pavements (Ahmadinia 2017). Also Load wave form is continuous while in real in-situ situations there is a loading and rest period (Zhou et al. 2010).

Table 9.1: Available international tests to measure resilient modulus (Zhou et al., 2010)

Test	Test title	Temperature and loading situation
ASTM D4123-82	Standard test method for indirect tension test for resilient modulus of bituminous mixtures	Max T 40°C Pulse load
AASHTO TP31-94	Standard test method for determination of the resilient modulus of bituminous mixtures by indirect tension	Max T 40°C Pulse load
NCHRP 1-28 (1996)	Proposed test protocol for determination of the resilient modulus of bituminous mixtures by indirect tension	Max T 40°C Pulse load
NCHRP 1-28A (2003)	Recommended standard test method for determination of the resilient modulus of bituminous mixtures by indirect tension	Max T 40°C Pulse load
AASHTO TP62-03 2003	Standard Method of Test for Determining Dynamic Modulus of Hot-Mix Asphalt Concrete Mixtures	Max T 55°C Continuous haversine

The stress responsive confinement within the MCDC test, provides an opportunity to address this challenge. In this Chapter, the MCDC+UWT test is used to investigate the modulus of asphalt at elevated temperature and stress.

## 9.2 Compressive resilient modulus calculation of asphalt using the outlined MCDC test

The measurement of compressive resilient modulus was explained in detail in Chapter 4. The applied load in the MCDC test consists of 0.1s loading and 0.9s resting time. The compressive resilient modulus determined from the MCDC test (Figure 4.10 and 4.11 in Chapter 4) is defined as the ratio of the repeated axial deviator stress to the recoverable or resilient axial strain:

$$M_r = \frac{\sigma_d}{\varepsilon_r} \quad (9.1)$$

$M_r$  : Compressive resilient modulus

$\sigma_d$  : Deviator stress (cyclic stress in excess of confining pressure)

$\varepsilon_r$  : Resilient strain in the vertical direction

The applied deviator stresses applied were 500, 750, and 1000 kPa.

## 9.3 The compressive resilient modulus results

The MCDC test data of 30 selected samples (Table 7.1 in Chapter 7) were analysed to evaluate the effects of cycle number, air voids, stress and temperature on the compressive resilient modulus at 40°C and 50°C. The resulting data are presented and discussed in this section.

### 9.3.1 Effect of cycle number

The compressive resilient modulus at different numbers of cycles is calculated for all three stages of the MCDC test. To assess the effect of load cycles on the compressive resilient modulus three samples were selected (Table 9.2) from each binder types with similar air voids. The compressive resilient modulus ( $M_r$ ) and permanent strain versus load cycles at 50°C for the selected samples are shown in Figure 9.1 to 9.3.

As the results indicate, the compressive resilient modulus is load cycle dependent for each stage. For example in stage one the reduction in modulus from 180 to 20,000 cycles is 50.4, 41.6, and 13.5% for C320, M1000 and PMB samples respectively. The results in Figure 9.1 to 9.3 show that between 20,000 and 40,000 load cycles, which is a part of the steady state for permanent strain results (as discussed before in Chapter 6), the variation in compressive resilient modulus is not significant. Therefore, the  $M_r$  in 20,000 cycles is calculated as a reference compressive resilient modulus for all

samples as presented in Table 1 to 3 in Appendix F. This reference  $M_r$  will be used to assess the effective parameters on compressive resilient modulus of asphalt.

Table 9.2: Selected samples for assessing load cycle in compressive resilient modulus results

Sample number	Bitumen binder types	Air voids (%) in centre	$M_r$ at 180 cycles	$M_r$ at 20,000 cycles	Reduction in modulus from 180 to 20K cycles (%)
67C	C320	2.10	1960	972	50.4
39M	M1000	2.15	2674	1561	41.6
100P	PMB	1.96	729	630	13.5

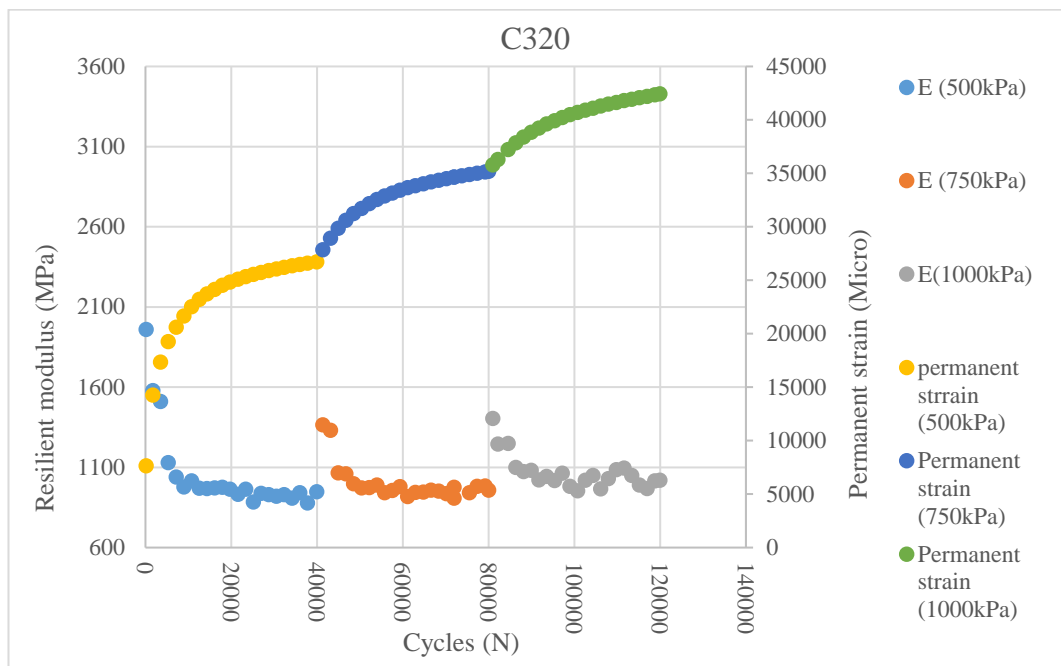


Figure 9.1: C320: Permanent strain and compressive resilient modulus vs load cycles at 50°C

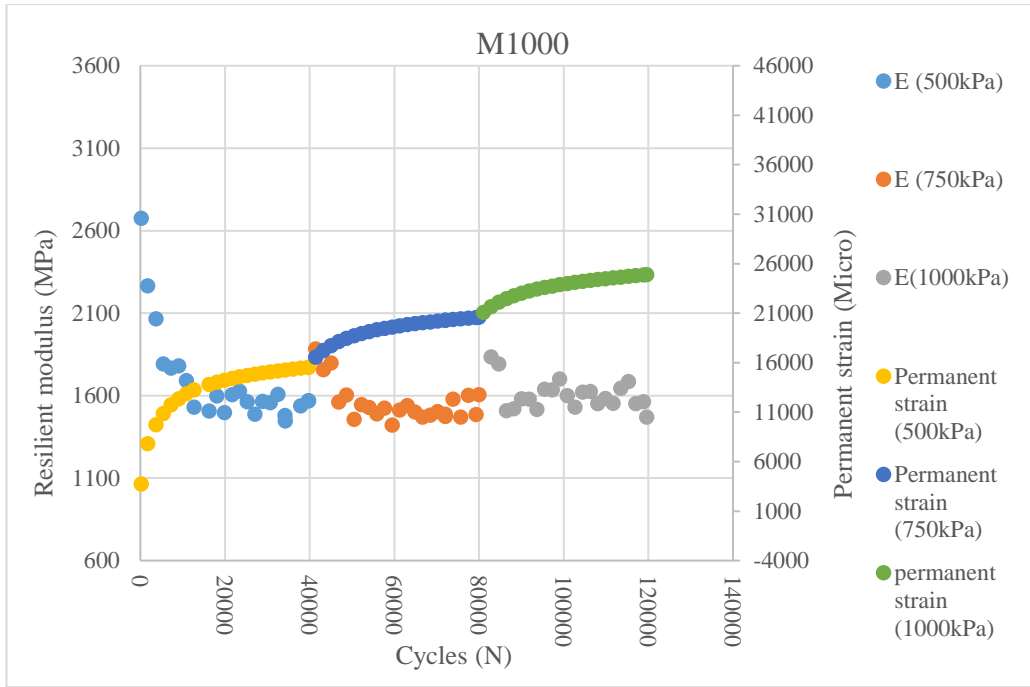


Figure 9.2: M1000: Permanent strain and compressive resilient modulus versus load cycles at 50°C

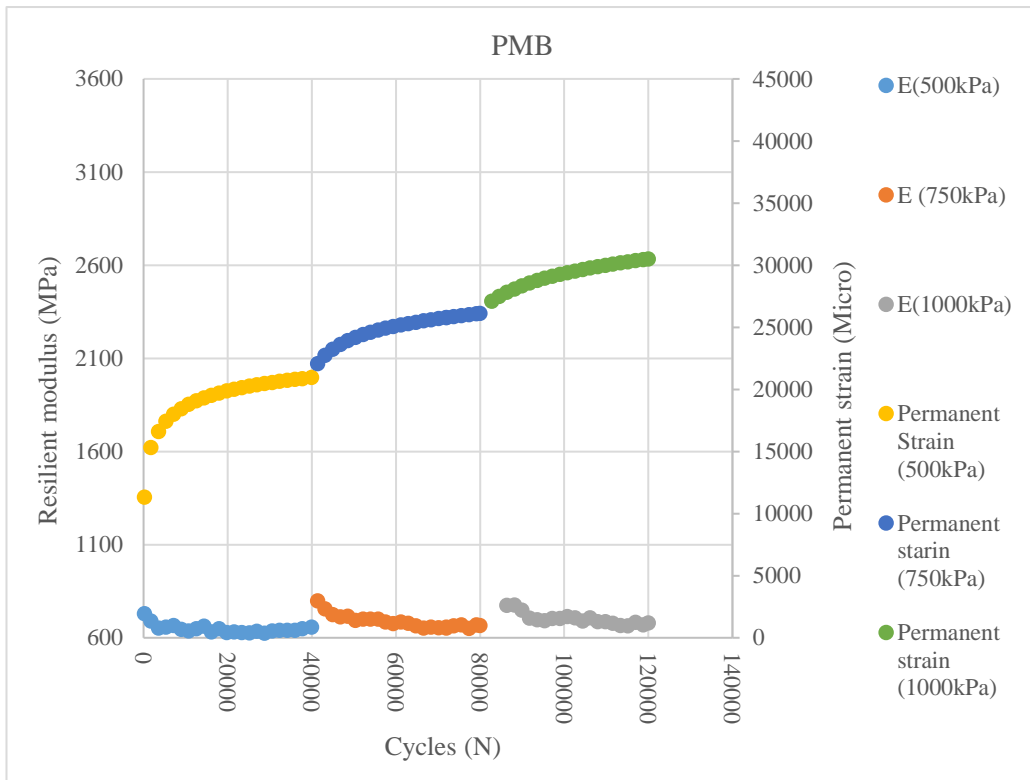


Figure 9.3: PMB: Permanent strain and compressive resilient modulus vs load cycles at 50°C

### **9.3.2 Effect of air voids on compressive resilient modulus**

The air voids and their effects are important in mix and pavement design. As discussed earlier in Chapter two, with the increase of the air voids in asphalt samples, a reduction in compressive resilient modulus is expected at normal temperatures and stresses. However, at elevated temperature and stress, the effect of air voids has not been evaluated previously.

During the MCDC test, the compressive resilient moduli of samples manufactured with three types of bitumen binders were calculated. Figures 9.4 to 9.6 show the compressive resilient modulus for samples with varying air voids at 180 and 20,000 cycles at 40°C and 50°C. Figures 9.7 and 9.9 also show the compressive resilient modulus in 20,000 cycles for samples under varying stresses at 40°C and 50°C. The following outcome can be concluded by comparing the  $R^2$  in Figure 9.4 to 9.9:

1. Better correlation could be observed between air voids and compressive resilient modulus in early cycles (180) than the late ones (20,000).
2. The effect of air voids in compressive resilient modulus at a higher temperature (50°C) is more significant compared to the lower temperature of 40°C.

### **9.3.3 Effect of temperature on compressive resilient modulus**

Assessing of the data presented in Figure 9.4 to 9.9 shows that temperature has a direct effect on the compressive resilient modulus of asphalt. The results show that the higher the temperature the lower the compressive resilient modulus.

### **9.3.4 Effect of stress on resilient modulus**

The Modulus data provided in Figure 9.4 to 9.9 shows that the effect of stresses between 500kPa to 1000kPa is not significant in compressive resilient modulus at 20,000 cycles for asphalt mix manufactured by all three types of bitumen binders.

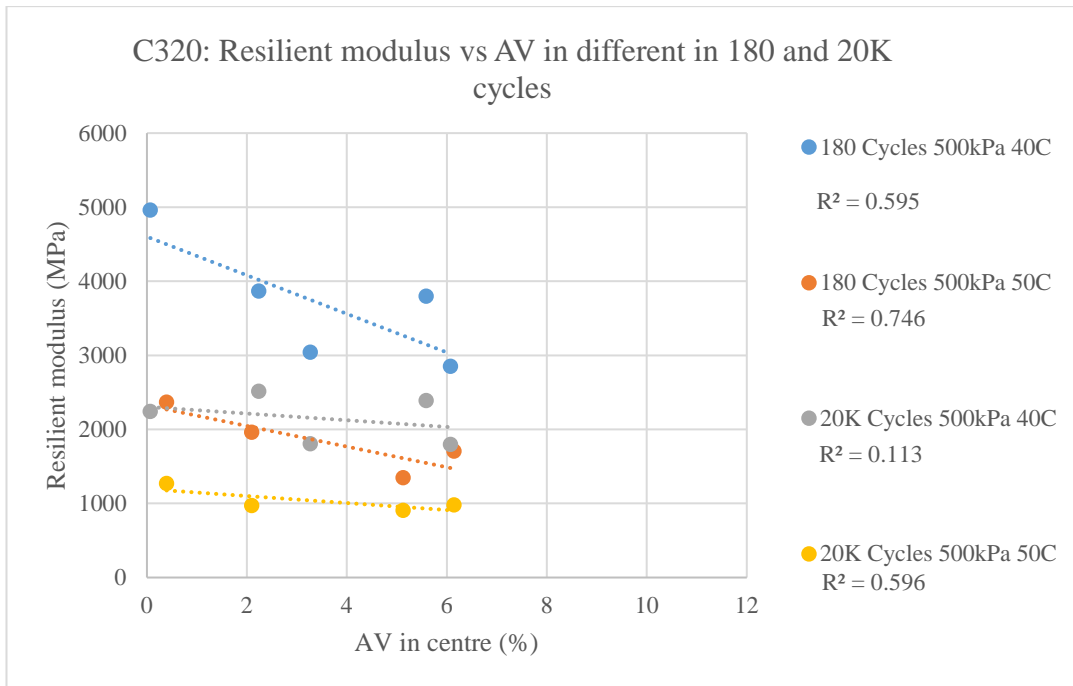


Figure 9.4: C320: Compressive resilient modulus under 500kPa for samples with varying air voids at 40 and 50°C

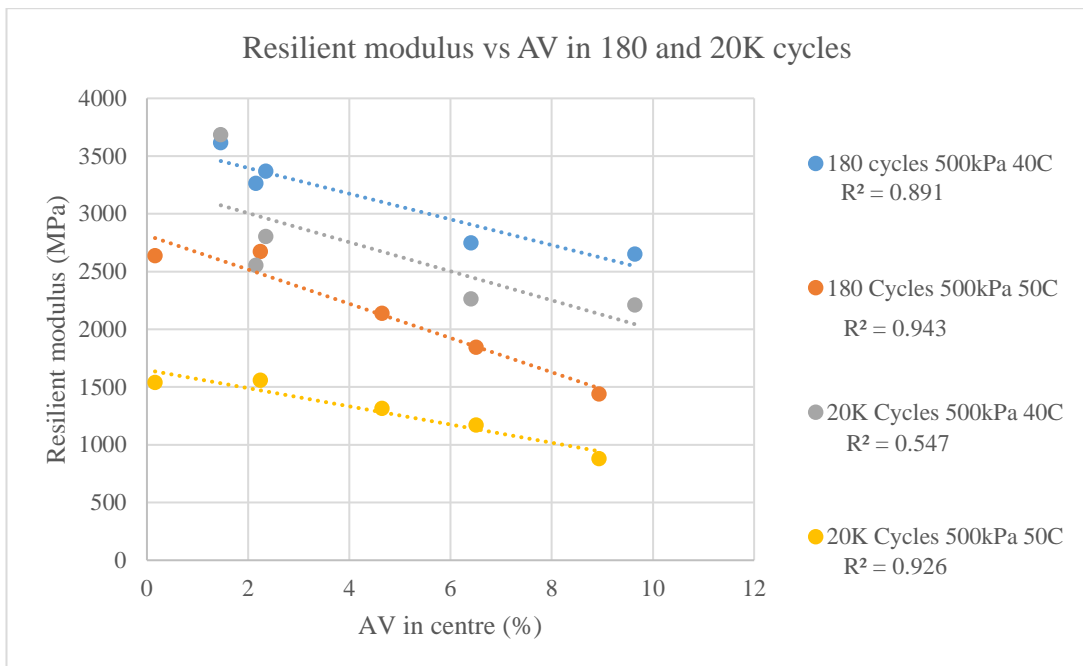


Figure 9.5: M1000: Compressive resilient modulus under 500kPa for samples with varying air voids at 40 and 50°C

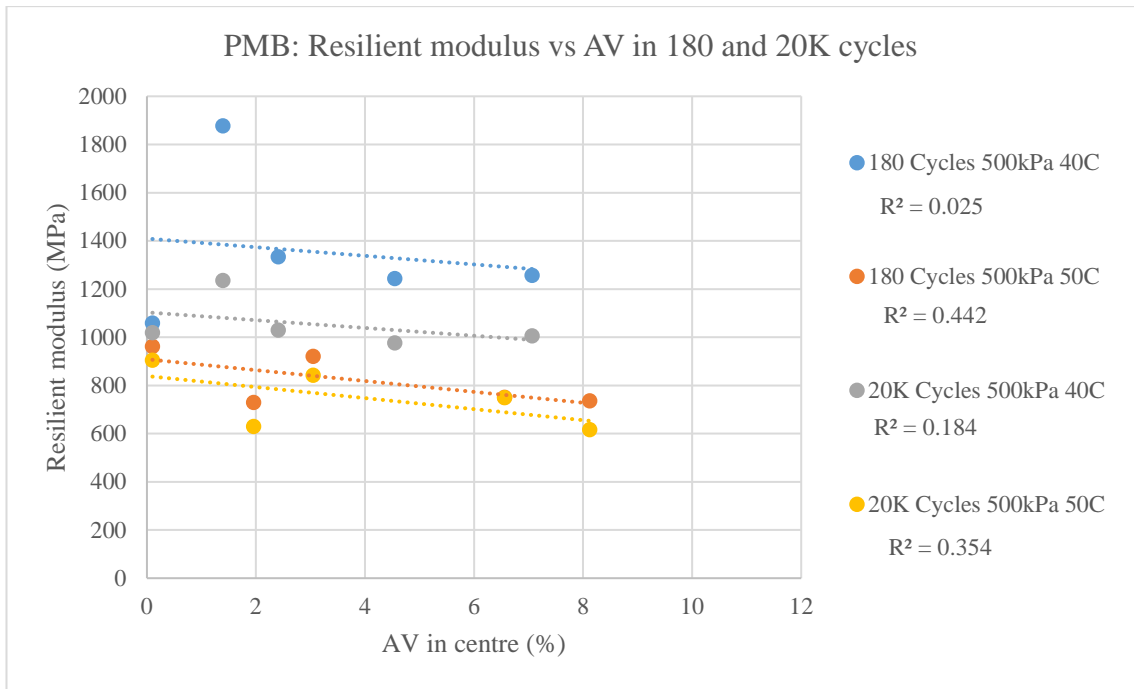


Figure 9.6: PMB: Compressive resilient modulus under 500kPa for samples with varying air voids at 40 and 50°C

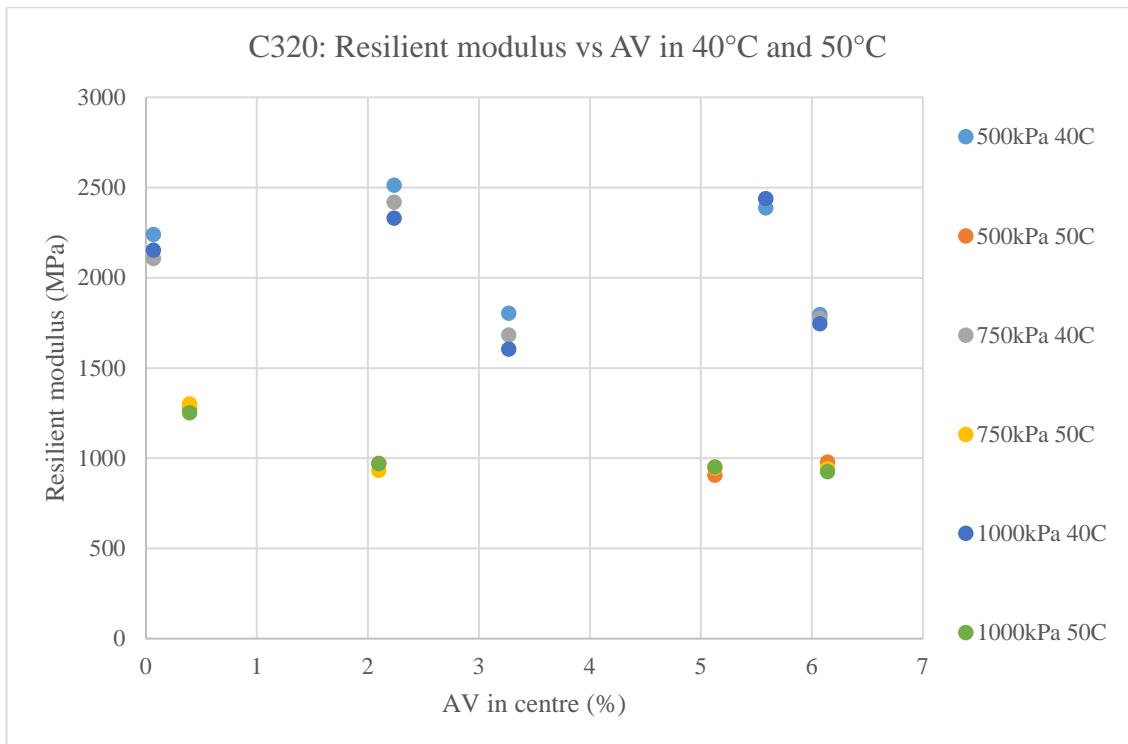


Figure 9.7: C320: Compressive resilient modulus for samples with varying air voids at 40 and 50°C under varying stresses.

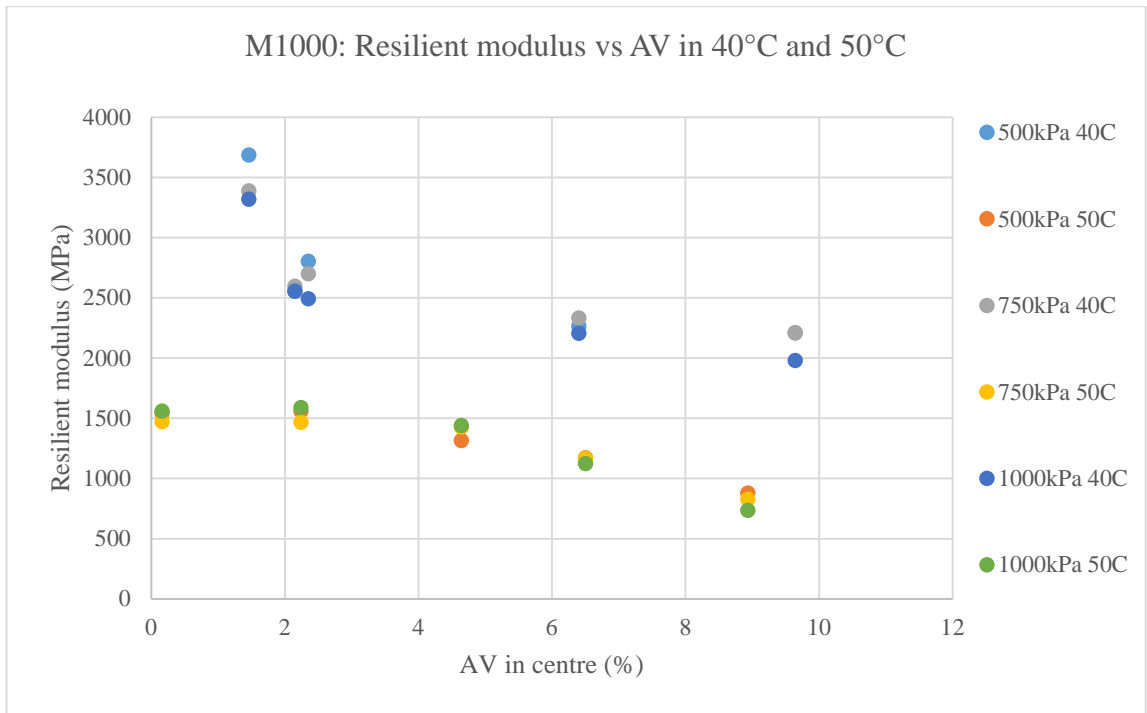


Figure 9.8: M1000: Compressive resilient modulus for samples with varying at 40 and 50°C under varying stresses.

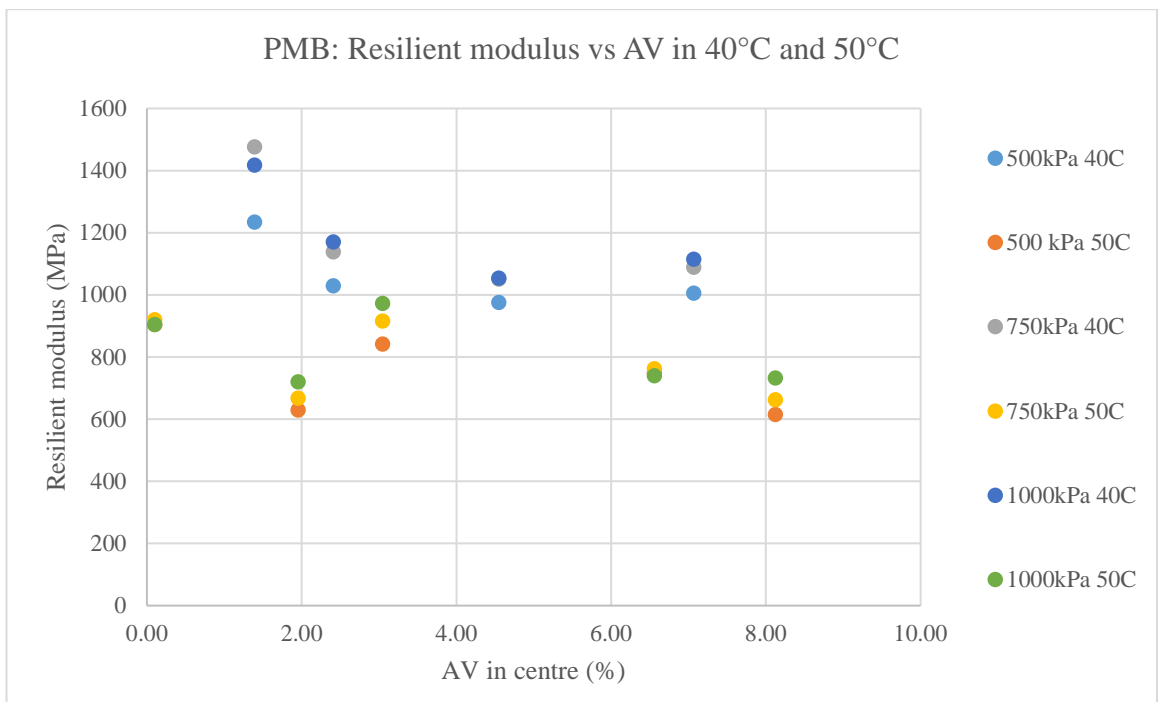


Figure 9.9: Compressive resilient modulus for samples with varying air voids at 40 and 50°C under varying stresses.

## 9.4 Conclusion

After assessing the Compressive resilient modulus using the MCDC+UWT test at elevated temperatures and stresses the following outcomes were concluded:

1. Load cycles could be considered during the measurement of compressive resilient modulus at elevated temperatures. 20,000 load cycles in each stage of MCDC test were introduced as a reference cycle to measure the compressive resilient modulus.
2. Air voids have more effect on compressive resilient modulus of asphalt mixes at higher temperatures.

By considering the above outcomes, MCDC test can be applied to measure the compressive resilient modulus in elevated temperatures and stresses. These outcomes maybe useful in the future development of mechanistic pavement design models and their underpinning material performance specifications.

## CHAPTER 10

### CONCLUSIONS AND RECOMMENDATIONS

#### Contents

10.1	Introduction .....	154
10.2	The literature review.....	154
10.3	Using Ultrasonic Wave Transmission (UWT) technique for air voids measurements .....	155
10.4	The development of MCDC test .....	156
10.5	The effective parameters on creep performance .....	157
10.6	The creep life and the effective parameters.....	157
10.7	The compressive resilient modulus and the effective parameters .....	158
10.8	The MCDC + UWT test .....	159
10.9	Recommendations .....	160
	REFERENCES.....	161

## 10.1 Introduction

The overarching goal of the research was to examine the hypothesis of “*The Australian dynamic creep test can be redesigned to enable multistage evaluation of creep life of asphalt mixtures under varying operational conditions*”. The research has successfully confirmed that the hypothesis was correct. The development of a multistage confined creep test, supported by the use of Ultrasonic evaluation of air voids, can significantly improve the evaluation of creep potential of asphalt.

The Hypothesis studied through the following elements:

- A review of the Austroads heavy-traffic flexible pavement design for elevated temperature and its relevant challenges.
- A review of international literature around the creep deformation mechanism of asphalt, the effective factors, available measurement techniques and their relevant challenges.
- Development of a new technique to measure the air voids and their distribution within an asphalt sample through a review on the relevant literature.
- Development of the MCDC creep test in order to optimise laboratory methodology and minimise the required sample and testing time.
- Creep life prediction using MCDC + UWT test.
- Assess and compare the Performance parameters of permanent strain and creep slope of asphalt.
- Assess and compare the creep life of asphalt manufactured by three types of Australian binders.
- Investigate the use of the MCDC+UWT test to determine the modulus of asphalt at elevated temperatures.

This chapter considers the above elements and provides some recommendations for future research in that context.

## 10.2 The literature review

1. The review outcomes of Austroads heavy-traffic flexible pavement showed that:
  - There are two main unsolved issues in the structural design of the heavy-traffic flexible pavement. They are as follows:

- Lack of availability of appropriate creep performance assessment technique for flexible pavements and an accurate and efficient creep measurement test method for ranking asphalt mixtures.
  - Lack of availability of appropriate method to measure the mechanical behaviour of asphalt at elevated temperatures and stresses.
2. The international review of creep deformation mechanism, its effective factors, available measurement techniques and relevant challenges indicate the following:
- Creep deformation in the laboratory is considered to consist of primary, secondary and tertiary. However, creep deformation in the field is normally restricted to the secondary phase (steady-state). This is due to the confinement stress provided by asphalt mass.
  - The main limitations regarding the available creep tests are known as providing more realistic in-situ confinement situation and stress conditions. To overcome these limitations, the CDCT creep test introduced by Ahmadinia (2017) was selected and developed to assess the creep mechanism of asphalt. Existing test methods did not allow for laboratory evaluation under multiple stress conditions. The MCDC test was developed to address this limitation.
  - To better assess creep deformation and its development using MCDC test, the air voids distribution in the centre of sample under the platen should be measured.

### **10.3 Using Ultrasonic Wave Transmission (UWT) technique for air voids measurements**

1. International air voids measurement techniques were reviewed (Table 6.1) and the related limitations were discussed. The outcomes are as follows:
- The available Australian test methodologies are not able to define the air voids distributions in asphalt samples
  - The only available international method to measure air voids distribution is the combination of X-ray Computed Tomography (CT) and image analysis methods which are very complex and expensive.

2. The available non-destructive test using for asphalt samples assessment were reviewed and the Ultrasonic Wave Transmission (UWT) adopted for development.
3. The trial creep tests proved that the creep deformation is better correlates to air voids in the centre than air voids of whole sample.

#### **10.4 The development of MCDC test**

1. To further develop the CDCT creep test to be more efficient and accurate, the MCDC test and UWT methodology were introduced. In the MCDC test three different stresses were applied on the same sample for specific number of load cycles (40,000). The aim of application of this method was to reduce the testing time and the number of samples. The UWT technique was used as a supplementary test to better analyse the MCDC test results regarding the air voids.
2. The possibility of application of MCDC test was assessed and test was validated using laboratory tests and finite element modelling (FEM) and the outcomes are as follows:
  - The permanent strain measured by MCDC test in multistage was close to the permanent strain measured by continuous test.
  - The stress distribution in MCDC confined samples in each stage was close to the stress value estimated in a finite element asphalt layer model.
  - The stress in the optimised confined asphalt model was close to the stress generated in the PVC in multilayer confinement system in the laboratory MCDC test. The stress dependency of a confinement system for multistage stress condition was also illustrated through this study.
3. The possibility of extending the MCDC laboratory test results from 40,000 cycles to 500,000 cycles using mathematical modelling was assessed. The results showed that power regression on data between 20,000 cycles and 40,000 cycles was the best model be used for extrapolating the creep strain to 500,000 cycles.
4. The best ways of presenting MCDC results was investigated and the outcomes were:

- For ranking of asphalt pavements: permanent strain at 20,000 cycles and the secant creep slope for permanent strain data between 40,000 and 100,000 cycles were selected.
  - For creep depth prediction, the secant creep slope for permanent strain data from 100,000 and 500,000 cycles was selected.
5. The creep life prediction using MCDC test was developed as follows:
- The mathematical models to predict the laboratory and field permanent deformation were reviewed. The review showed that the power regression models best estimates the laboratory results in the second stage of laboratory creep test.
  - The permanent strain was estimated at 500,000 cycles in each stage by fitting a power regression model to the data between 20,000 and 40,000 load cycles and extrapolating the data to 500,000 cycles.
  - Both secant creep slope ( $m$ ) and conventional intercept ( $c$ ) were calculated using the permanent strain at 100,000 and 500,000 load cycles.
  - The creep life ( $\epsilon_{max}$ ) was calculated using geometrically similarities between the field condition.

### **10.5 The effective parameters on creep performance**

1. Permanent strain at 20,000 cycle is sensitive to load, temperature, and air voids.
2. Secant creep slope, which presents the increased rate of permanent strain, is less sensitive to load, temperature, and air voids at lower cycles (20,000 and 40,000 cycles). The sensitivity of the secant creep slope increases at higher cycle numbers (40,000 and 100,000 cycles). The secant creep slope at higher cycle number is a more reliable to evaluate the effectiveness of parameters in creep deformation.
3. The asphalts were ranked from 1 to 3 based on the two above methods for all operational conditions. The consistent ranking for creep resistance was that PMB demonstrates the best performance followed by multigrade and C320.

### **10.6 The creep life and the effective parameters**

1. The effective parameter of the creep life

- In all asphalt mixtures (C320, M1000 and PMB) there is a reduction in creep life with an increase in air voids. This highlights the importance of tight specification controls around compacted air voids.
- The creep life is affected directly by temperature. Analysing of data showed that for either mixtures, an increase in temperature resulted a reduced creep life.
- The results indicated that the surface stress magnitude, which is a function of tyre inflation, surface slope and road position, has a significant effect on the creep life with an increased surface stress resulting in a reduction in creep life.
- As expected from the review of the data, the best creep performance as evaluated by creep life is displayed by the polymer modified asphalt in all cases.

## **10.7 The compressive resilient modulus and the effective parameters**

1. The review of modulus of asphalt, its effective factors, available measurement techniques and relevant challenges are as follows:
  - The review showed that the modulus of asphalt using in Austroads mechanistic design can be either resilient modulus, flexural modulus, and/or dynamic modulus depending on the selected test procedures and design method. The various modulus are not interchangeable in design.
  - The modulus of asphalt largely relies on the aggregate structure, temperature sensitivity of material and the level of confinement. Other relevant effective factors on the modulus of asphalt are summarised in Table 2.6.
  - The available test methods to measure the modulus of asphalt are summarised in Table 9.1. Except dynamic modulus test (AASHTO TP62-03 2003), other types of tests cannot be performed in high temperature (more than 40°C) under high stress level.
  - Among three modulus measurement technique for asphalt mixes: axial, diametrical and triaxial test methods, the triaxial test is the best method to measure the modulus. The Dynamic modulus test (AASHTO TP62-03 2003) is one of them, however, some

researchers challenged the dynamic modulus test regarding the confinement system and loading situation (continuous haversine loading).

- Based on the above findings from the literature review, MCDC test was developed to assess the compressive modulus of asphalt capable to apply in mechanistic design procedure.
2. The compressive resilient modulus in different cycles were analysed for asphalt mixtures made of three types of bitumen in all three stages of MCDC test. The outcomes were as follows:
- The compressive resilient modulus for all selected samples was cycle dependent at the beginning of each stage (180 cycles).
  - Between 20,000 and 40,000 load cycles, which is a part of steady state for permanent strain results, the variation in compression resilient modulus is not significant. Therefore, the  $M_r$  in 20,000 cycles were calculated as a reference compressive resilient modulus in all samples
  - The better correlation was observed between air voids and compressive resilient modulus in early cycles (180) than late cycles (20,000)
  - The effect of load magnitude between 500kPa to 1000kPa was not significant in compressive resilient modulus in 20,000 cycles.

### **10.8 The MCDC + UWT test**

1. The combination of MCDC + UWT test was able to rank the asphalt manufactured with various binder types on the basis of its creep performance.
2. The combination of MCDC + UWT was also incorporated to measure the compressive resilient modulus of asphalts at elevated temperatures and can be used in flexible pavement design procedure.
3. The combination of MCDC + UWT tests with a mathematical model can provide the opportunity of estimation of creep life of heavy-traffic flexible pavement if the procedure can be validated with field data.

## 10.9 Limitations and Recommendations

Some of the limitations of this research are listed as follows:

1. The research only examined one aggregate grading of dense grade asphalt to focus on void and binder influence.
2. Temperature is an important parameter in ranking the creep sensitivity of asphalt mixes. During laboratory testing a constant temperature regime prevails. However in the field the asphalt temperature fluctuates according to the time of the day and prevailing environmental conditions.
3. The UWT technique was developed for samples with only one aggregate gradation and thickness.
4. MCDC test was validated by FEM modelling. More investigation is required to validate the test with real in-situ asphalt performance.

The recommendation are listed below for future research:

1. The development of the MCDC methodology is considered to greatly improve laboratory evaluation of asphalt creep potential. It is recommended that the methodology be further explored to investigate asphalt mixes with larger aggregate.
2. The influence of temperature fluctuation may be evaluated to drive a better understanding of creep performance. This could be studied by programming of UTS machine and improved data acquisition.
3. The UWT technique was able to provide better information for air void distribution and improved correlation with creep performance. Further research is required with regard to the effect of aggregate size and sample thickness on calibration.
4. Laboratory data was able to be extrapolated to predict creep potential, however, correlation between the power regression model developed and in-situ performance is essential.
5. Correlation of the MCDC with wheel tracker to extend the research tools available for evaluating creep.

## REFERENCES

- Adhikari, S, Shen, S & You, Z 2009, 'Evaluation of fatigue models of hot-mix asphalt through laboratory testing', *Transportation Research Record: Journal of the Transportation Research Board*, no. 2127, pp. 36-42.
- Ahari, AS, Forough, SA, Khodaii, A & Nejad, FM 2013, 'Modeling the primary and secondary regions of creep curves for SBS-modified asphalt mixtures under dry and wet conditions', *Journal of Materials in Civil Engineering*, vol. 26, no. 5, pp. 904-11.
- Ahmadinia, E 2017, 'Redesigning the Austroads creep procedure for the evaluation of permanent deformation of asphalt pavements in Australia', PhD thesis, University of Southern Queensland.
- Ahmadinia, E, Bullen, F & Ayers, R 2014, 'Creep mechanisms in asphaltic concrete', in *23rd australasian conference on the mechanics of structures and materials (ACMSM23)*, Southern Cross University (SCU), Australia.
- Ahmadinia, E, Bullen, F & Ayers, R 2017, 'Design of a laboratory test for investigating permanent deformation of asphalt', in *ICTHE 2017 : 19th International Conference on Transportation and Highway Engineering: Proceedings of the ICTHE 2017* : World Academy of Science, Engineering and Technology, Melbourne, Australia.
- Al-Qadi, I, Wang, H, Yoo, P & Dessouky, S 2008, 'Dynamic analysis and in-situ validation of perpetual pavement response to vehicular loading', *Transportation Research Record: Journal of the Transportation Research Board*, no. 2087, pp. 29-39.
- Ali, Y, Irfan, M, Ahmed, S & Ahmed, S 2017, 'Permanent deformation prediction of asphalt concrete mixtures—A synthesis to explore a rational approach', *Construction and Building Materials*, vol. 153, pp. 588-97.
- Arnold, G & Werkmeister, S 2010, *Pavement thickness design charts derived from a rut depth finite element model*. NZ Transport Agency research report no.427, pp. 84.
- Arnold, G, Werkmeister, S & Alabaster, D 2008, *Performance tests for road aggregates and alternative materials*. Land Transport New Zealand Research. Report 335. 102 pp.
- Austroads 2004, *Guide to Pavement Technology Part 2: Pavement Structural Design*. Austroads, Sydney, NSW.

Austrroads 2006, *Deformation resistance of asphalt mixture by wheel tracking test*, AGPT-T231. Austrroads, Sydney, NSW.

Austrroads 2007, *Determination of permanent deformation and resilient modulus characteristics of unbound granular materials under drained conditions*. AGPT-T053-07, Austrroads, Sydney, NSW.

Austrroads 2008a, *Guide to pavement technology part 4F: bituminous binders*. AGPT04F-08, Austrroads, Sydney, NSW.

Austrroads 2008b, *Testing Asphalt in Accordance with the Austrroads Mix Design Procedures*. AP-T100-08, Austrroads, Sydney, NSW.

Austrroads 2009a, *Guide to Pavement Technology Part 3: Pavement Surfacing*s. AGPT03-09, Austrroads, Sydney, NSW.

Austrroads 2009b, *Guide to asset management: part 5: Pavement Performance*. AGPT05-09, AUSTRROAD, Sydney NSW 2000 Australia.

Austrroads 2010, *Laboratory study on relationship between binder and asphalt rutting*. APT164/10, Austrroads, Sydney, NSW.

Austrroads 2012, *Guide to Pavement Technology Part 2: Pavement Structural Design*. AGPT02-12, Austrroads, Sydney, NSW.

Austrroads 2013, *Improved Design Procedures for Asphalt Pavements: Pavement Temperature and Load Frequency Estimation*. AP-T248-13 Austrroads, Sydney, NSW.

Austrroads 2014, *Guide to Pavement Technology Part 4B: Asphalt*. AGPT04B-14, Austrroads, Sydney, NSW.

Austrroads 2015, *Determination of Permanent Deformation Characteristics of Unbound Granular Materials by the Wheel-tracking Test*. AGPT-T054-15, Austrroads, Sydney, NSW.

Austrroads 2016, *Characterisation of Flexural Stiffness and Fatigue Performance of Bituminous Mixes*. AGPT-T274-16, Austrroads, Sydney, NSW.

Barksdale, RD 1972, 'Laboratory evaluation of rutting in base course materials', in *Presented at the Third International Conference on the Structural Design of Asphalt Pavements, Grosvenor House, Park Lane, London, England, Sept. 11-15, 1972*.

Beecroft, A & Petho, L 2015. 'P3\_Commissioning of Hamburg Wheel Tracking Device (HWDT) '. Project No: 007180. Final report. *National Asset Center of Excellence (NACOE)*.

Bonaquist, RF, Christensen, DW & Stump, W 2003, 'Simple performance tester for Superpave mix design: First-article development and evaluation', *Transportation Research Board*, vol. 513.

Brown, E, Cooley, L, Hanson, D, Lynn, C, Powell, B, Prowell, B & Watson, D 2002, 'NCAT test track design, construction and performance', *National Center for Asphalt Technology*, Auburn University.

Brown, ER & Cross, SA 1989, 'A study of in-place rutting of asphalt pavements', *National Center for Asphalt Technology*. vol. 58.

Brown, ER & Cross, SA 1992, 'A National Study of Rutting in Hot Mix (HMA) Pavements', *National Center for Asphalt Technology (No. NCAT 92-5)*.

Brown, S 1978, 'Material characteristics for analytical pavement design', *Developments in highway pavement engineering*, vol. 1, pp. 41-92.

Brown, S 1995, 'Practical test procedures for mechanical properties of bituminous materials', in *Proceedings of the Institution of Civil Engineers: Transport*. Vol. 111, no. 4, pp. 289-297.

Brown, S & Snaith, M 1974, 'The permanent deformation characteristics of a dense bitumen macadam subjected to repeated loading', in *Association of Asphalt Paving Technologists Proc.* Vol. 43, pp. 224-252

Brown, S, Cooper, K, Preston, J & Bell, C 1989, 'Development of a new procedure for bituminous mix design', in *Proceedings, 4th Eurobitume Symposium*. Madrid.

Brown, SF & Scholz, T 1998, 'Permanent deformation characteristics of porous asphalt determined in the confined repeated load axial test', *highways & transportation*, vol. 45, no. 12.

Brown, SF, Darter, M, Larson, G, Witczak, M & El-Basyouny, MM 2006, 'Independent Review of the " Mechanistic-Empirical Pavement Design Guide" and Software', *NCHRP research results digest*, no. 307.

BSI (1996) BS DD 226: *Method for determining resistance to permanent deformation of bituminous mixtures subject to unconfined dynamic loading*. BSI, London, UK.

Bullen, F & Preston, N 1992, 'Extending the use of the Nottingham asphalt tester', in *International Conference on Asphalt Pavements, 7th, 1992, Nottingham, United Kingdom*.

Castillo, D & Caro, S 2014, 'Probabilistic modeling of air void variability of asphalt mixtures in flexible pavements', *Construction and Building Materials*, vol. 61, pp. 138-46.

CEN (European Committee for Standardization) 2001, *Bituminous mixtures-test method for hot mix asphalt – Part 25: Dynamic creep test*, prEN 12697–25, CEN, Brussels, Belgium.

Cerni, G, Cardone, F, Virgili, A & Camilli, S 2012, 'Characterisation of permanent deformation behaviour of unbound granular materials under repeated triaxial loading', *Construction and Building Materials*, vol. 28, no. 1, pp. 79-87.

Choi, Y-T 2013, 'Development of a mechanistic prediction model and test protocol for the permanent deformation of asphalt concrete', PhD Thesis, North Carolina State University.

Coleri, E, Harvey, JT, Yang, K & Boone, JM 2012, 'A micromechanical approach to investigate asphalt concrete rutting mechanisms', *Construction and Building Materials*, vol. 30, pp. 36-49.

*Composition and Structure of Flexible Pavements*, 2017, (Online web page) <https://theconstructor.org/transportation/flexible-pavement-composition-and-structure/5499/>>.

*Creep (deformation)*, 2017, Wikipedia, [https://en.wikipedia.org/wiki/Creep\\_\(deformation\)](https://en.wikipedia.org/wiki/Creep_(deformation))>.

CROW, R 2010, *Standard Conditions of Contract for Works of Civil Engineering*, Technology Centre for Transport and Infrastructure.

De Beer, M, Fisher, C & Jooste, FJ 1997, 'Determination of pneumatic tyre/pavement interface contact stresses under moving loads and some effects on pavements with thin asphalt surfacing layers', in *Proceedings of the 8th international conference on asphalt pavements*, pp. 10-4.

De Carvalho, RLE 2012, 'Prediction of permanent deformation in asphalt concrete', PhD thesis. University of Maryland, College Park.

Di Benedetto, H, Partl, M, Francken, L & Saint André, CDLR 2001, 'Stiffness testing for bituminous mixtures', *Materials and Structures*, vol. 34, no. 2, pp. 66-70.

Dickinson, E 1981, 'Pavement temperature regimes in Australia: their effect on the performance of bituminous constructions and their relationship with average climate indicators'. *ARRB Group Limited*, no. 23.

Dołżycki, B & Judycki, J 2008, 'Behaviour of asphalt concrete in cyclic and static compression creep test with and without lateral confinement', *Road Materials and Pavement Design*, vol. 9, no. 2, pp. 207-25.

Dubois, V, De La Roche, C & Burban, O 2010, 'Influence of the compaction process on the air void homogeneity of asphalt mixtures samples', *Construction and Building Materials*, vol. 24, no. 6, pp. 885-97.

Eisenmann, J & Hilmer, A 1987, 'Influence of Wheel Load and Inflation Pressure on the Rutting Effect at Asphalt-Pavements-Experiments and Theoretical Investigations'. Sixth International Conference, Structural Design of Asphalt Pavements, Volume I, Proceedings, University of Michigan, July 13-17, 1987, Ann Arbor, Michigan', *Publication of: Michigan University, Ann Arbor*.

EN 2005, Bituminous mixtures. Test methods for hot mix asphalt. Cyclic compression test, BS EN 12697-25:2005, BSI.

Epps, J, Hand, A, Seeds, S, Scholz, T, Alavi, S, Ashmore, C, Monismith, C, Deacon, J, Harvey, J & Leahy, R 2002, *Recommended Performance-Related Specification for Hot-Mix Asphalt Construction: Results of the Westrack Project*, 0309066735.

Erkens, S 2002, 'Asphalt concrete response (ACRe): determination, modelling and prediction: Het gedrag van asfalt (ACRe): bepalen, modelleren en voorspellen', PhD thesis, Delft University of Technology.

Fernández-Gómez, WD, Vides-Berdugo, AC, Roncallo-Contreras, SP, Bautista-Rondón, F, Rondón-Quintana, HA & Reyes-Lizcano, FA 2016, 'Effects of environmental aging and ultra violet radiation on asphalt mixture dynamic modulus, permanent deformation and fatigue life', *Revista Facultad de Ingeniería Universidad de Antioquia*, no. 80, p. 89.

Francken, L 1977, 'Pavement Deformation Law of Bituminous Road Mixes in Repeated Triaxial Compression', in *Proc., 4th International Conference on the Structural Design of Asphalt Pavements*.

Francken, L & Clauwaert, C 1987, 'Characterization and structural assessment of bound materials for flexible road structures', in *Proceedings 6th International Conference on the Structural Design of Asphalt Pavements*, Ann Arbor, pp. 130-44.

Garba, R 2002, 'Permanent deformation properties of asphalt concrete mixtures', PhD thesis, Norwegian University of Science and Technology, Trondheim, Norway.

Garbacz, A & Garboczi, EJ 2003, *Ultrasonic evaluation methods applicable to polymer concrete composites*, US Department of Commerce, Technology Administration, National Institute of Standards and Technology, NISTIR 6975.

Gokhale, S, Choubane, B, Byron, T & Tia, M 2005, 'Rut initiation mechanisms in asphalt mixtures as generated under accelerated pavement testing', *Transportation research record: Journal of the transportation research board*, no. 1940, pp. 136-45.

Gribble, M & Patrick, J 2008, *Adaptation of the Austroads pavement design guide for New Zealand conditions*, research report 305, Land Transport New Zealand.

Gupta, A & Adhikari, S 2016, 'Review of Mechanistic-Empirical design approach for asphalt pavements', in *Functional Pavement Design: Proceedings of the 4th Chinese-European Workshop on Functional Pavement Design (4th CEW 2016, Delft, The Netherlands, 29 June-1 July 2016)*, CRC Press, p. 191.

Haddock, J, Hand, A & Fang, H 2002, *Contributions of pavement structural layers to rutting of hot mix asphalt pavements. NCHRP Report 468*, National Academy Press, Washington, DC.

Hafeez, I 2017, 'Investigating the creep response of asphalt mixtures under waveform loading', *Road Materials and Pavement Design*, pp. 1-18.

Harney, J & Popescu, L 2000, 'Rutting of Caltrans Asphalt Concrete and Asphalt-Rubber Hot Mix Under Different Wheels, Tire and Temperature-Accelerated Pavement Testing Evaluation', *Berkeley: Pavement Research Center, Institute of Transportation Studies, University of California*.

Harvey, J & Popescu, L 2000, 'Rutting of Caltrans Asphalt Concrete and Asphalt-Rubber Hot Mix Under Different Wheels, Tires and Temperatures-Accelerated Pavement Testing Evaluation', *University of California, Berkeley*.

Harvey, J, Monismith, C, Horonjeff, R, Bejarano, M, Tsai, B & Kannekanti, V 2004, 'Long-life AC pavements: A discussion of design and construction criteria based on California

experience', in *International Symposium on Design and Construction of Long Lasting Asphalt Pavements, 2004, Auburn, Alabama, USA*.

Hjort, M, Haraldsson, M & Jansen, JM 2008, *Road Wear from Heavy Vehicles: An Overview*, report number 08/2008, NVF Committee Vehicles and Transports, Nordiska vägtekniska förbundet.

Houel, A & Arnaud, L 2009, 'Damage characterization of asphalt in laboratory by ultrasonic wave propagation', *Non Destructive Testing in Civil Engineering, June 30th–July 3rd, Nantes, France*.

Hu, X, Zhou, F, Hu, S & Walubita, LF 2010, 'Proposed Loading Waveforms and Loading Time Equations for Mechanistic-Empirical Pavement Design and Analysis', *Journal of Transportation Engineering*, vol. 136, no. 6.

Huang, X & Zhang, Y 2010, 'A new creep test method for asphalt mixtures', *Road Materials and Pavement Design*, vol. 11, no. 4, pp. 969-91.

Huber, G & Heiman, G 1987, 'Effect of asphalt concrete parameters on rutting performance: a field investigation (with discussion)', in *Association of Asphalt Paving Technologists Proc.*

Hugo, F, Arraigada, M, Shuming, L, Zefeng, T & Kim, Y 2012, 'International case studies in support of successful applications of accelerated pavement testing in pavement engineering', in *Proceedings of the 4th international conference on accelerated pavement testing, Davis, CA, USA*, pp. 93-104.

Islam, MR & Tarefder, RA 2014, 'Determining thermal properties of asphalt concrete using field data and laboratory testing', *Construction and Building Materials*, vol. 67, pp. 297-306.

Javilla, B, Mo, L, Hao, F, An, S & Wu, S 2017, 'Systematic comparison of two-stage analytical rutting models of asphalt mixtures', *Construction and Building Materials*, vol. 153, pp. 716-27.

Jiani, W, Zhongjun, X, Yiqiu, T & Lei, Z 2013, 'Effect of Ultraviolet Aging on Asphalt Rheological Properties', *China Petroleum Processing & Petrochemical Technology*, vol. 15, no. 4, pp. 26-32.

Jouve, P, Martinez, J & Ragneau, E 1988, 'Modèle de calcul pour le dimensionnement des chaussées souples', *Bulletin de Liaison des Laboratoires des Ponts et Chaussées*, no. 156.

Kandhal, PS & Cooley, LA 2003, *Accelerated laboratory rutting tests: Evaluation of the asphalt pavement analyzer*, Transportation Research Board.

Khedr, SA 1986, 'Deformation mechanism in asphaltic concrete', *Journal of transportation engineering*, vol. 112, no. 1, pp. 29-45.

Koniditsiotis, C 1996, 'Accelerated Loading Facility (ALF)-does it actually do what it claims?', in *combined 18th ARRB transport research conference and Transit New Zealand land transport symposium, 2-6 September 1996, Christchurch, New Zealand part 3*.

Kumlai, S, Jitsangiam, P & Nikraz, H 2014, 'Comparison between resilient modulus and dynamic modulus of Western Australian hot mix asphalt based on flexible pavement design perspectives', in *26th ARRB Conference, Sydney, New South Wales, Australia*.

Lekarp, F, Isacsson, U & Dawson, A 2000, 'State of the art. I: Resilient response of unbound aggregates', *Journal of transportation engineering*, vol. 126, no. 1, pp. 66-75.

Levenberg, E, McDaniel, R & Nantung, T 2012, 'How low is too low? Assessing the risk of low air voids using accelerated pavement testing', *Advances in Pavement Design through Full-scale Accelerated Pavement Testing*, p. 249.

Ma, T, Zhang, D, Zhang, Y, Zhao, Y & Huang, X 2016, 'Effect of air voids on the high-temperature creep behavior of asphalt mixture based on three-dimensional discrete element modeling', *Materials & Design*, vol. 89, pp. 304-13.

Mamlouk, MS & Sarofim, RT 1988, 'Modulus of asphalt mixtures-an unresolved dilemma', *Transportation Research Record*, no. 1171, pp. 193-8.

Mansourkhaki, A & Sarkar, A 2015, 'Plastic deformation of asphalt mixture under waveform loading', in *Proceedings of the Institution of Civil Engineers-Transport*, Thomas Telford Ltd, pp. 200-11.

Masad, E, Muhunthan, B, Shashidhar, N & Harman, T 1999, 'Internal structure characterization of asphalt concrete using image analysis', *Journal of computing in civil engineering*, vol. 13, no. 2, pp. 88-95.

Masad, E, Jandhyala, V, Dasgupta, N, Somadevan, N & Shashidhar, N 2002, 'Characterization of air void distribution in asphalt mixes using X-ray computed tomography', *Journal of materials in civil engineering*, vol. 14, no. 2, pp. 122-9.

- Masada, T, Sargand, SM, Abdalla, B & Figueroa, JL 2004, *Material properties for implementation of mechanistic-empirical (ME) pavement design procedures*. NEN-EN 12697-25:2005, 'Bituminous mixtures. Test methods for hot mix asphalt -Part 25: Cyclic compression test'.
- Merbouh, Mh 2012, 'Effect of thermal cycling on the creep-recovery behaviour of road bitumen', *Energy Procedia*, vol. 18, pp. 1106-14.
- Merrill, D, Van Dommelen, A & Gaspar, L 2006, 'A review of practical experience throughout Europe on deterioration in fully-flexible and semi-rigid long-life pavements', *International Journal of Pavement Engineering*, vol. 7, no. 2, pp. 101-9.
- Moffatt, M, Jameson, G & Oliver, J 2012, 'Validating permanent deformation tests using accelerated pavement testing', in D Jones, et al. (eds), *Advances in Pavement Design through Full-scale Accelerated Pavement Testing.*, CRC Press. Taylor & Francis group., pp. 411-23.
- Mohd Hasan, MR, Hiller, JE & You, Z 2016, 'Effects of mean annual temperature and mean annual precipitation on the performance of flexible pavement using ME design', *International Journal of Pavement Engineering*, vol. 17, no. 7, pp. 647-58.
- Monismith, C, Epps, J & Finn, F 1985, 'Improved asphalt mix design', in *Proceedings, Association of Asphalt Paving Technologists Technical Sessions, San Antonio, Texas*, pp. 347-406.
- Monismith, C, Hicks, R, Finn, F, Sousa, J, Harvey, J, Weissman, S, Deacon, J, Coplantz, J & Paulsen, G 1994, *Permanent deformation response of asphalt aggregate mixes*. Rep. No. SHRP-A, 1994.
- Monismith, CL & McLean, DB 1972, 'Technology of Thick Lift Construction: Structural Design Considerations', AAPT.
- Monismith, CL, Ogawa, N & Freeme, C 1975, 'Permanent deformation characteristics of subgrade soils due to repeated loading', *Transportation Research Record*, no. 537.
- Montepara, A & Giuliani, F 2000, 'Performance testing and specifications for binder and mix. Comparison between ageing simulation tests of road bitumen', in *proceedings of the papers submitted for review at 2nd euraspalt and eurobitume congress, held 20-22 september 2000, barcelona, spain. book 1-session 1*.

Mounier, D, Di Benedetto, H & Sauzéat, C 2012, 'Determination of bituminous mixtures linear properties using ultrasonic wave propagation', *Construction and Building Materials*, vol. 36, pp. 638-47.

MRTS30 2016, *Transport and Main Roads Specifications MRTS30 Asphalt Pavements* Department of transport and main roads, State of Queensland.

Mulvaney, R & Worel, B 2002, 'MnROAD mainline rutting forensic investigation', *Commercially Unpublished Report to the Office of Materials and Road Research. Minnesota Department of Transportation*.

Muraya, PM 2007, 'Permanent deformation of asphalt mixes'. PhD thesis, TUDelf. [uuiid:2fb9695a-d0e8-46bf-94d1-6cdebd411712](https://doi.org/10.1001/2fb9695a-d0e8-46bf-94d1-6cdebd411712).

NCHRP (National Cooperative Highway Research Program) 2000, *Standard test method for simple performance test for permanent deformation based upon repeated load test of asphalt concrete mixtures, NCHRP 9-19*, TRB, National Research Council, Washington, DC, USA.

Newcomb, DE, Willis, R & Timm, DH 2010, *Perpetual asphalt pavements. A Synthesis*, , Asphalt Pavement Alliance IM-40., Lanham.

Norambuena-Contreras, J, Castro-Fresno, D, Vega-Zamanillo, A, Celaya, M & Lombillo-Vozmediano, I 2010, 'Dynamic modulus of asphalt mixture by ultrasonic direct test', *Ndt & E International*, vol. 43, no. 7, pp. 629-34.

Norouzi, A, Sabouri, M & Richard Kim, Y 2017, 'Fatigue life and endurance limit prediction of asphalt mixtures using energy-based failure criterion', *International Journal of Pavement Engineering*, vol. 18, no. 11, pp. 990-1003.

Nunn, M & Ferne, BW 2001, 'Design and assessment of long-life flexible pavements', *Transportation Research Circular*, vol. 503, no. 12, pp. 32-49.

Nunn, M, Brown, A & Guise, S 1998, 'Assessment of Simple Tests to Measure Deformation Resistance of Asphalt', *Transport Research Laboratory, Project Report PR/CE/92/98 March*.

Oliver, JWH, Alderson, AJ, Tredrea, PF & Karim, MR 1995, 'Results of the laboratory program associated with the ALF asphalt deformation trial', APRG report No. 12- ARR 272, Austroads Pavement Research Group, Australia

Ongel, A & Harvey, J 2004, 'Analysis of 30 years of pavement temperatures using the enhanced integrated climate model (EICM)', *Pavement Research Centre, University of California Davis*.

Öztürk, HI 2007, 'Parametric study on selected mathematical models for dynamic creep behavior of asphalt concrete', Master thesis, Middle East Technical University, Turkey.

Partl, MN, Bahia, HU, Canestrari, F, De la Roche, C, Di Benedetto, H, Piber, H & Sybilski, D 2012, *Advances in interlaboratory testing and evaluation of bituminous materials: state-of-the-art report of the RILEM technical committee 206-ATB*, vol. 9, Springer Science & Business Media.

Paute, J, Hornych, P & Benaben, J 1996, 'Repeated load triaxial testing of granular materials in the French Network of Laboratories des Ponts et Chaussées', in *flexible pavements. proceedings of the european symposium euroflex 1993 held in lisbon, portugal, 20-22 september 1993*.

*Pavement interactive*, 2012, <<http://www.pavementinteractive.org/rutting/>>.

Pell, P & Brown, S 1972, 'The characteristics of materials for the design of flexible pavement structures', in *Presented at the Third International Conference on the Structural Design of Asphalt Pavements, Grosvenor House, Park Lane, London, England, Sept. 11-15, 1972*.

Pérez, I & Gallego, J 2010, 'Rutting prediction of a granular material for base layers of low-traffic roads', *Construction and Building Materials*, vol. 24, no. 3, pp. 340-5.

Potter, DW & Youdale, GP 1998, *Review and Recommendation of Improvements to Australian Heavy Duty Pavement Design Practices.*, vol. Project Report 3 IET 1. , Australian Asphalt Pavement Association, .

Praticò, F & Moro, A 2012, 'Measurement of air void content in hot mix asphalts: Method and core diameter dependence', *Construction and Building Materials*, vol. 26, no. 1, pp. 344-9.

Preston, J 1991, 'The design of bituminous concrete mixes', University of Nottingham, UK.

Petersson, J. (2014) Deformation in the asphalt used on road surfaces [Online]. Nordic Road and Transport Research. Available: <http://nordicroads.com/about-nordic/> [Accessed].

Qi, X & Witczak, M 1998, 'Time-dependent permanent deformation models for asphaltic mixtures', *Transportation Research Record: Journal of the Transportation Research Board*, no. 1639, pp. 83-93.

Raad, L, Monismith, CL & Mitchell, JK 1977, *Fatigue behavior of cement-treated materials*. <http://onlinepubs.trb.org/Onlinepubs/trr/1977/641/641-002.pdf>.

Rahmani, E, Darabi, MK, Al-Rub, RKA, Kassem, E, Masad, EA & Little, DN 2013, 'Effect of confinement pressure on the nonlinear-viscoelastic response of asphalt concrete at high temperatures', *Construction and Building Materials*, vol. 47, pp. 779-88.

Ren, J & Sun, L 2017, 'Characterizing air void effect on fracture of asphalt concrete at low-temperature using discrete element method', *Engineering Fracture Mechanics*, vol. 170, pp. 23-43.

Reyes Ortiz, OJ & Camacho Tauta, JF 2008, 'Effect of ultraviolet radiation on an asphalt mixture s mechanical and dynamic properties', *Ingeniería e Investigación*, vol. 28, no. 3, pp. 22-7.

Ritter, J, Rabe, R & Wolf, A 2012, 'Accelerated pavement testing of two flexible road pavements to assess long-term structural performance', in *Proceedings of the 4th international conference on accelerated pavement testing, Davis, CA, USA*, pp. 225-36.

Ritter, JE, Jakus, K, Batakis, A & Bandyopadhyay, N 1980, 'Appraisal of biaxial strength testing', *Journal of Non-Crystalline Solids*, vol. 38, pp. 419-24.

Rolt, J 2001, 'long life pavements', *trl staff paper pa 3736/01. The World Bank Regional Seminar on Innovative Road Rehabilitation and Recycling Technologies, PA3736/01, Amman, Jordan*

Roy, N, Veeraragavan, A & Krishnan, JM 2013, 'Influence of air voids of hot mix asphalt on rutting within the framework of mechanistic-empirical pavement design', *Procedia-Social and Behavioral Sciences*, vol. 104, pp. 99-108.

Rushing, JF & Little, DN 2013, 'Static creep and repeated load as rutting performance tests for airport HMA mix design', *Journal of Materials in Civil Engineering*, vol. 26, no. 9, p. 04014055.

Santagata, E, Baglieri, O, Riviera, PP & Alam, M 2017, 'Correlating creep properties of bituminous binders with anti-rutting performance of corresponding mixtures', *International Journal of Pavement Research and Technology*, vol. 10, no. 1, pp. 38-44.

Shafabakhsh, G & Ani, OJ 2015, 'Experimental investigation of effect of Nano TiO<sub>2</sub>/SiO<sub>2</sub> modified bitumen on the rutting and fatigue performance of asphalt mixtures containing steel slag aggregates', *Construction and Building Materials*, vol. 98, pp. 692-702.

Sharp, K 1992, 'An evaluation of the Nottingham asphalt tester', in *Workshop on the Use of the MATTA for Laboratory Characterisation of Asphalt Mixes, 1992, Vermont South, Victoria, Australia*.

Sohm, J, Gabet, T, Horny, P, Piau, J-M & Di Benedetto, H 2012, 'Creep tests on bituminous mixtures and modelling', *Road Materials and Pavement Design*, vol. 13, no. 4, pp. 832-49.

Sousa, JB, Craus, J & Monismith, CL 1991, Summary report on permanent deformation in asphalt concrete, SHRP-A/IR-91-104, Strategic Highway Research Program, Washington D.C.

Sousa, JB, Deacon, JA & Monismith, CL 1991, 'Effect of laboratory compaction method on permanent deformation characteristics of asphalt-aggregate mixtures', *Journal of the Association of Asphalt Paving Technologists*, vol. 60.

Stephenson, G & Bullen, F 2000, 'A Review of the Design and Vacuum Creep Performance of Stone Mastic Asphalt', in *World of Asphalt Pavements, International Conference, 1st, 2000, Sydney, New South Wales, Australia*.

SA (Standards Australia) 1995, AS 2891.12.1: 'Method of sampling and testing asphalt 12.1, Determination of the permanent compressive strain characteristics of asphalt', Dynamic creep test. Standards Australia Sydney, NSW, Australia.

Stephenson, RW & Manke, PG 1972, 'Ultrasonic moduli of asphalt concrete', *Highway Research Record*, no. 404.

Steyn, WJ 2012, *Significant findings from full-scale accelerated pavement testing*, vol. 433, Transportation Research Board.

Su, K, Sun, L, Hachiya, Y & Maekawa, R 2008, 'Analysis of shear stress in asphalt pavements under actual measured tire-pavement contact pressure', *Proceedings of the 6th ICPT, Sapporo, Japan*, pp. 11-8.

Sullivan, BW 2015, 'Development of a long life design procedure for Australian asphalt pavements', PhD Thesis thesis, Curtin University, Curtin University.

Sun, L 2005, 'Structural behavior study for asphalt pavements', *China Communications, Beijing*, p. 7.

Tan, S, Low, B & Fwa, T 1994, 'Behavior of asphalt concrete mixtures in triaxial compression', *Journal of Testing and Evaluation*, vol. 22, no. 3, pp. 195-203.

Tashman, L, Masad, E, D'Angelo, J, Bukowski, J & Harman, T 2010, 'X-ray tomography to characterize air void distribution in superpave gyratory compacted specimens', *International Journal of Pavement Engineering*, vol. 3, no. 1, pp. 19-28.

Team, WF 1998, *Performance of Coarse-Graded Mixes at WesTrack—Premature Rutting. Final Report, FHWA, US Department of Transportation.*

Theyse, H 2000, 'The development of mechanistic-empirical permanent deformation design models for unbound pavement materials from laboratory and accelerated pavement test data', in *Proceedings of the fifth international symposium on unbound aggregates in roads*, pp. 285-93.

Tigdemir, M, Kalyoncuoglu, SF & Kalyoncuoglu, UY 2004, 'Application of ultrasonic method in asphalt concrete testing for fatigue life estimation', *NDT & E International*, vol. 37, no. 8, pp. 597-602.

Titi, HH, Elias, MB & Helwany, S 2006, *Determination of typical resilient modulus values for selected soils in Wisconsin*, ID 0092-03-11, Wisconsin Highway Research Program Project.

Tseng, K-H & Lytton, RL 1989, 'Prediction of permanent deformation in flexible pavement materials', in *Implication of aggregates in the design, construction, and performance of flexible pavements*, ASTM International.

Tsai, B-W, Coleri, E, Harvey, JT & Monismith, CL 2016, 'Evaluation of AASHTO T 324 Hamburg-Wheel Track Device test', *Construction and Building Materials*, vol. 114, pp. 248-60.

*Ultrasonic Pulse Velocity Test*, PT HESA LARAS CEMERLANG, Indonesia Engineering Consultant, <https://hesa.co.id/uji-mutu-dan-integritas-beton-dengan-ultrasonic-pulse-velocity-test/>.

Von Quintus, HL, Mallela, J & Jiang, J 2005, *Expected Service Life and Performance Characteristics of HMA Pavements in LTPP*, Final Report, Asphalt Pavement Alliance, Applied Research Associates. [http://www.asphaltroads.org/assets/control/content/files/IM024\\_LTPP\\_Report.pdf](http://www.asphaltroads.org/assets/control/content/files/IM024_LTPP_Report.pdf).

- Walubita, LF, Liu, W, Scullion, T & Leidy, J 2008, 'Modeling Perpetual Pavements Using the Flexible Pavement System (FPS) Software', in *Transportation Research Board 87th Annual Meeting*.
- Wang, J 2015, 'Characterization of Failure and Permanent Deformation Behaviour of Asphalt Concrete', PhD Thesis thesis, TUDelf.
- Werkmeister, S, Alabaster, D & Zealand, TN 2008, *Performance Tests for Road Aggregates and Alternative Materials*, Report 335, Land Transport New Zealand Research.
- Willis, R, Timm, D, West, R, Powell, B, Robbins, M, Taylor, A, Smit, A, Tran, N, Heitzman, M & Bianchini, A 2009, *Phase III NCAT test track findings*, NCAT report, 09-08 National Center for Asphalt Technology.
- Willis, R, Timm, D, West, R, Powell, B, Robbins, M, Taylor, A, Smit, A, Tran, N, Heitzman, M & Bianchini, A 2009, 'Phase III NCAT test track findings', *NCAT report*, pp. 09-8.
- Wilshire, B & Evans, R 1994, 'Acquisition and analysis of creep data', *The Journal of Strain Analysis for Engineering Design*, vol. 29, no. 3, pp. 159-65.
- Witczak, MW & Kaloush, K 2000, Specimen geometry and aggregate size effects in uniaxial compression and constant height shear tests. in *Proceedings of the Association of Asphalt Paving Technologists*. vol. 69, pp. 733-793, Asphalt Paving Technology 2000, Reno, NV, United States.
- Witczak, M, Schwartz, C & Von Quintus, H 2001, 'NCHRP Project 9-19: Superpave support and performance models management', *Interim Report, Federal Highway Administration, National Cooperative Highway Research Program*.
- Witczak, M, Mamlouk, M, Souliman, M & Zeiada, W 2013, *Laboratory validation of an endurance limit for asphalt pavements*, NCHRP 762, National Cooperative Highway Research Program.
- Witczak, M, Kaloush, K, Pellinen, T, El-Basyouny, M & Von Quintus, H 2002, *Simple performance test for Superpave mix design*, NCHRP 465, National Cooperative Highway Research Program.
- Wolff, H 1992, 'The elasto-plastic behaviour of granular pavement layers in South Africa', University of Pretoria, South Africa.
- Wu, J & Airey, G 2009, 'The influence of aggregate interaction and aging procedure on bitumen aging', *Journal of Testing and Evaluation*, vol. 37, no. 5, pp. 402-9.

Xie, S & ZHENG, C 2003, 'effects of the tire-pavement contact pressure on asphalt pavement', in *Proceedings of the Eastern Asia Society for Transportation Studies*.

Yang, X, You, Z, Hiller, J & Watkins, D 2016, 'Updating and augmenting weather data for pavement mechanistic-empirical design using ASOS/AWOS database in Michigan', *International Journal of Pavement Engineering*, pp. 1-9.

Yang, X, You, Z, Hiller, J & Watkins, D 2017, 'Sensitivity of flexible pavement design to Michigan's climatic inputs using pavement ME design', *International Journal of Pavement Engineering*, vol. 18, no. 7, pp. 622-32.

Zargar, M, Ahmadiania, E, Bullen, F & Ayers, R 2017, 'Investigating the effect of asphalt mixture structure on permanent deformation of laboratory asphalt samples using Ultrasonic Wave Transmission (UWT) technique', *12th International Conference of Eastern Asia Society For Transportation Studies "Safe, Green and Integrated Transport"*, Eastern Asia Society for Transportation Studies, Ho Chi Minh City, Vietnam.

Zargar, M, Banerjee, S, Bullen, F & Ayers, R 2017, 'An Investigation into the Use of Ultrasonic Wave Transmission Techniques to Evaluate Air Voids in Asphalt', in *global civil engineering conference (gcec2017): proceedings of the global civil engineering conference (gcec2017) kuala lumpur, malaysia*.

Zhang, J, Pei, J & Zhang, Z 2011, 'Development and validation of viscoelastic-damage model for three-phase permanent deformation of dense asphalt mixture', *Journal of Materials in Civil Engineering*, vol. 24, no. 7, pp. 842-50.

Zhang, J, Pei, J & Zhang, Z 2012, 'Development and Validation of Viscoelastic-Damage Model for Three-Phase Permanent Deformation of Dense Asphalt Mixture', *Journal of Materials in Civil Engineering*, vol. 24, no. 7.

Zhang, J, Fan, Z, Fang, K, Pei, J & Xu, L 2016, 'Development and validation of nonlinear viscoelastic damage (NLVED) model for three-stage permanent deformation of asphalt concrete', *Construction and Building Materials*, vol. 102, pp. 384-92.

Zhou, F & Scullion, T 2002, 'Vesys5 rutting model calibrations with local accelerated pavement test data and associated implementation', *Texas Transportation Institute*, vol. 88.

Zhou, F, Fernando, E & Scullion, T 2010, *Development, calibration, and validation of performance prediction models for the Texas ME flexible pavement design system*, Texas Transportation Institute, Texas A & M University System.

## APPENDIX A

### *Literature review related tables*

Table 1: A comparison of empirical test methods for evaluation permanent deformation of asphalt mixtures (Sousa et al. 1991; Gibb 1996; Brown et al. 2001; Witzcak, 2002; Zhou et al. 2008; Partl et al., 2012; Ahmadinia et al., 2017)

		Sample shape and dimension	Advantages	Disadvantages	Confinement situation
Empirical tests	Marshal test	Cylindrical, 4 inch diameter × 2.5 inch height or 6 inch diameter × 3.75 inch height	<ul style="list-style-type: none"> <li>* Easy to implement</li> <li>* Equipment generally available in labs</li> <li>* Standardized for mix design - short test time</li> </ul>	<ul style="list-style-type: none"> <li>* Not able to correctly predict and rank asphalt mixture for rutting</li> </ul>	Unconfined
	Hveem test	Cylindrical, 4 inch diameter × 2.5 inch height	<ul style="list-style-type: none"> <li>* Short test time</li> <li>* Triaxial load applied</li> </ul>	<ul style="list-style-type: none"> <li>* Special compacter is needed for test (California kneading compacter)</li> <li>* Not able to correctly predict and rank asphalt mixture for rutting</li> </ul>	Semi-confined
	Gyratory testing machine	Loose sample	<ul style="list-style-type: none"> <li>* Simulate the action of rollers during construction</li> <li>* Criteria available</li> <li>* Parameters are generated during compaction</li> </ul>	<ul style="list-style-type: none"> <li>Equipment not widely available - not able to correctly predict and rank asphalt mixture for rutting</li> </ul>	Unconfined

Table 2: A comparison of fundamental test methods for evaluation permanent deformation of asphalt mixtures (Sousa et al. 1991; Gibb 1996; Brown et al. 2001; Witzcak, 2002; Zhou et al. 2008; Partl et al., 2012; Ahmadinia et al., 2017)

		Sample shape and dimension	Advantages	Disadvantages	Confinement situation
Fundamental tests	Uniaxial creep	Cylindrical, 4 inch diameter × 8 inch height	<ul style="list-style-type: none"> <li>* Wide spread, well known</li> <li>* Easy to implement</li> <li>* Test equipment generally available in labs</li> <li>* More technical information</li> </ul>	<ul style="list-style-type: none"> <li>* Ability to predict permanent deformation is questionable</li> <li>* Restricted test temperature and load levels do not simulate field situations</li> <li>* Does not simulate field dynamic phenomena</li> </ul>	Unconfined
	Uniaxial repeated Load		<ul style="list-style-type: none"> <li>* Better expresses traffic conditions</li> </ul>	<ul style="list-style-type: none"> <li>* Equipment is more complex</li> <li>* Restricted test temperature and load levels does not simulate field situations</li> </ul>	Unconfined

Fundamental tests	Uniaxial dynamic modulus		<ul style="list-style-type: none"> <li>* Capability of determining the damping as a function of frequency for different temperatures</li> <li>* Non-destructive tests</li> </ul>	<ul style="list-style-type: none"> <li>* Equipment is more complex</li> <li>* Difficult to obtain 2:1 ratio specimens in lab</li> </ul>	Unconfined
	Triaxial creep		<ul style="list-style-type: none"> <li>* Relatively simple test and equipment</li> <li>* Test temperature and load levels better simulate field conditions than unconfined</li> <li>* Potentially inexpensive</li> </ul>	<ul style="list-style-type: none"> <li>* Requires a triaxial chamber</li> <li>* Confinement increases complexity of the test</li> </ul>	Confined
	Triaxial repeated load		<ul style="list-style-type: none"> <li>* Test temperature and load levels better simulate field conditions than unconfined</li> <li>* Better expresses traffic conditions</li> <li>* Can accommodate varied specimen sizes</li> <li>* Criteria available</li> </ul>	<ul style="list-style-type: none"> <li>* Equipment is more complex and expensive</li> <li>* Requires a triaxial chamber</li> </ul>	Confined
	Triaxial dynamic modulus		<ul style="list-style-type: none"> <li>* Ability to determine the damping as a function of frequency for different temperatures</li> <li>* Non-destructive tests</li> <li>* Provides necessary input for structural analysis</li> </ul>	<ul style="list-style-type: none"> <li>* At high temperature, it is a complex test system (small deformation measurement sensitivity is needed at high temperature)</li> <li>* Some possible minor problems due to stud, LVDT arrangement.</li> <li>* Equipment is more complex and expensive</li> <li>* Requires a triaxial chamber</li> </ul>	Confined
	Diametral creep	Cylindrical, 4 inch diameter × 2.5 inch height	<ul style="list-style-type: none"> <li>* Easy to implement</li> <li>Equipment is relatively simple and generally available in most labs</li> <li>* Specimen is easy to fabricate</li> </ul>	<ul style="list-style-type: none"> <li>* State of stress is non-uniform and strongly dependent on the shape of the specimen</li> <li>* Maybe inappropriate for estimating permanent deformation</li> <li>* High temperature (load) changes in the specimen shape affect the state of stress and the test measurement significantly</li> <li>* Found to overestimate creep</li> <li>* For the dynamic test, the equipment is complex</li> </ul>	Unconfined
	Diametral repeated load		<ul style="list-style-type: none"> <li>* Easy to implement</li> <li>* Specimen is easy to fabricate</li> </ul>		Unconfined
	Diametral dynamic modulus		<ul style="list-style-type: none"> <li>* Specimen is easy to fabricate</li> <li>* Non-destructive test</li> </ul>		Unconfined
	ST frequency sweep test – shear dynamic	Cylindrical, 6 inch diameter × 2 inch height	<ul style="list-style-type: none"> <li>* The applied shear strain simulates the effect of road traffic</li> <li>* AASHTO standardized procedure available</li> </ul>	<ul style="list-style-type: none"> <li>* Equipment is extremely expensive and rarely available</li> <li>* Test is complex and difficult to</li> </ul>	Confined

Fundamental tests			* Master curve could be drawn from different temperatures and frequencies * Non-destructive test	run, usually needs special training	
	SST repeated shear at constant height		* The applied shear strains simulate the effect of road traffic * AASHTO procedure available	* Equipment is extremely expensive and rarely available * Test is complex and difficult to run, usually need special training * More than three replicate are needed	Confined
	Triaxial shear strength test		* Short test time	* Much less used * Confined specimen requirements add complexity	Confined
	Hollow cylindrical	1 inch wall thickness 18 inch high 9 inch external diameter	* Almost all states of stress can be duplicated. * Capability of determining the damping as a function of frequency for different temperatures for shear as well as axial	* Sample preparation is tedious. * Expensive equipment * Cores cannot be obtained from the pavement.	Confined

Table 3: A comparison of Simulative test methods for evaluation permanent deformation of asphalt mixtures (Sousa et al. 1991; Gibb 1996; Brown et al. 2001; Witzcak, 2002; Zhou et al. 2008; Partl et al., 2012; Ahmadinia et al., 2017)

		Sample shape and dimension	Advantages	Disadvantages	Confinement situation
Simulative tests	Asphalt pavement analyser	Cylindrical 6 inch x 3.5 or 4.5 inch or Beam	* Simulates field traffic and temperature conditions * Simple to perform * 3-6 samples can be tested at the same time * Most widely used LWT in the US * Guidelines (criteria) are available	* Relatively expensive except new table top version	Semi-confined
	Hamburg wheel-tracking device	Beam 10.2in.x 12.6in. x 1.6in.	* Widely used in Germany * Capable of evaluating moisture-induced damage * Two samples tested at same time	* Less potential to be accepted widely in the world	Semi-confined
	French rutting tester	Beam, 7.1in.x 19.7 in.x 0.8 to 3.9in.	* Successfully used in France * Two HMA slabs can be tested at one time	* Not widely available	Semi-confined

Simulative tests	The small scale UK Wheel tracking tester	Cylindrical 200 mm diameter or a slab of dimensions	* Simulates field traffic and temperature conditions * Simple to perform	* Not widely available	Semi-confined
	The prototype small-scale UK Wheel tracking tester	305 x 280 x 100 mm.	* 3 samples can be tested at the same time	* Not widely available	Semi-confined
	Superfos construction rut tester	Cylindrical 150 mm diameter 75 mm height or Beam (5 in x12 in x3 in)	* Simulates field traffic and temperature conditions * Simple to perform * 3 samples can be tested at the same time	* Not widely available	Semi-confined
	Georgia load wheel tester	Cylindrical 150 mm diameter 75 mm height		* Not widely available	Semi-confined
	Purdue university Wheel tracking device	Slab 290mm x 310mm x desired height	* Simulates field traffic and temperature conditions * Simple to perform * 3 samples can be tested at the same time	* Not widely available	Semi-confined
	Model mobile loading simulator	Real pavement is a sample for this test	* Real multilayer pavement can be tested * Real asphalt on the road can be tested	* Not widely available * Relatively expensive except new table top version	Semi-confined in the lab and full-confined in the field
	Transportek wheel tracking test	Slab, 400mm x 100mm	* Simulates field traffic and temperature conditions * Simple to perform	* Not widely available * Relatively expensive except new table top version	Semi-confined
	Accelerated testing facility	Real pavement is a sample for this test	* Real multilayer pavement can be tested * Real asphalt on the road can be tested	* Not widely available * Relatively expensive except new table top version	Semi-confined in the lab and full-confined in the field

Table 4: Models to predict the creep deformation in unbound and bound materials (Choi 2013; Javilla et al., 2017)

No.	Model	Model parameters	References
1	$\varepsilon_p = a + b \text{Log} N$	a,b = regression coefficient	Barksdale (1972)
2	$\text{Log } \varepsilon_p = a + b \text{Log} N + c(\text{Log} N)^2 + D(\text{log} N)^3$	a,b,c,d = regression coefficient	Monismith and Mclean (1972)
3	$\text{Log } \varepsilon_p = a + b \text{Log} N$	a,b = regression coefficient	Brown, snaith 1974
4	$\varepsilon_p = aN^b$	a,b = regression coefficient	Monismith et al., 1975
5	$\varepsilon_p = \delta(T_{load})N^a\sigma^{n-1}[\sigma_z - 0.5 * (\sigma_x + \sigma_y)]$	a,b,T, $\delta(T)$ , $\sigma$	Monismith et al., 1977
6	$\varepsilon_p = (q/a)^b N$	a,b,q = regression coefficient	Brown and Bell (1977)
7	$\varepsilon_p = aN^b + C(e^{dN} - 1)$	a,b,c,d = regression coefficient	Franken (1977)
8	$\varepsilon_p/N = A_a N^{-m}$	$A_a, m$	Khedr (Ohio state university) (1986)
9	$\varepsilon_p = a + b(N^{0.5})$	a,b = regression coefficient	Einsenmann and Hilmer (1987)
10	$\varepsilon_p = aN^b + c(\exp(dN) - 1)$	a,b,c,d = regression coefficient	Franken and Clauwaeatn (1987)
11	$\varepsilon_p = \frac{a\sqrt{N}}{\sqrt{N} + b}$	a,b = regression coefficient	Paute et al., 1988
12	$\varepsilon_p = aN^b + c$	a,b,c = regression coefficient	Paute et al., 1988
13	$\varepsilon_p = \varepsilon_0 \exp(-(\rho/N)^b)$	$\varepsilon_0, \rho, b$ = regression coefficients	Tseng and Lytton (1989)
14	$\varepsilon_p = (aN + b)(1 - \exp(-cN))$	a,b,c = regression coefficients	Wolf (1992)
15	$\varepsilon_p = \theta_1(1 - e^{\theta_2 N}) + \theta_3(e^{-\theta_4 N} - 1)$	$\varepsilon_p, \theta_1, \theta_3, \theta_2, \theta_4$	Wilshire and Evans (1994)
16	$\varepsilon_p = a(1 - N/100)^{-b}$	a,b = regression coefficients	Paute et al., 1996
17	$\varepsilon_p = aN + b(1 - \exp(cN))$	a,b,c = regression coefficient	Theyse (2000)
18	$\varepsilon_p = aN + \frac{bN}{[1 + (\frac{bN}{c})^d]^{1/d}}$	a,b,c,d = regression coefficient	Theyse (2000)
19	$\frac{\varepsilon_p}{\varepsilon_r} = 10^{aT} b N^c$	$\varepsilon_r, N, T, a, b, c$	MEPDG (2002)
20	$\varepsilon_p = aN^b + (cN + d)(1 - \exp(-EN))$	a,b,c,d = regression coefficient	Perez and Galego (2010)
21	$\varepsilon_p = a + bN - c(\exp(-dN))$	a,b,c,d: material regression parameters	Cerni et al., 2012
23	$\varepsilon_p = a \text{Ln} N + B$	a,b = regression coefficient	Ahari et al., 2013
24	$\varepsilon_p = aN + B(N^{0.5})$	a,b = regression coefficient	Ahari et al., 2013
25	$\varepsilon_p = a + b(N^c + \exp(dN))$	a,b,c,d = regression coefficient	Ahari et al., 2013
26	$\varepsilon_p = \frac{a + bN}{(c + N)^\alpha}$	A, C = regression coefficient regarding primary region B, $\alpha$ = regression coefficient regarding secondary region	Choi (2013), Subramanian (2013)

\* $\varepsilon_p$  = Creep deformation, N = Number of load cycle, a,b,c = Regression coefficient  $T_{load}$  = Load time,  $\delta(T)$  = Temperature function,  $\sigma$  = equivalent stress defined as a function of principal stress,  $A_a$  = Material property, function of resilient modulus and applied stress, m = Material parameter,  $\theta_1, \theta_3$  = Primary and tertiary strain,  $\theta_2, \theta_4$  = rate parameters quantifying the curvature of the primary and tertiary stages, T = temperature,  $\varepsilon_r$  = Resilient modulus,  $\alpha$

## APPENDIX B

### *Comparison of air voids of the whole sample with air voids at the centre of sample*

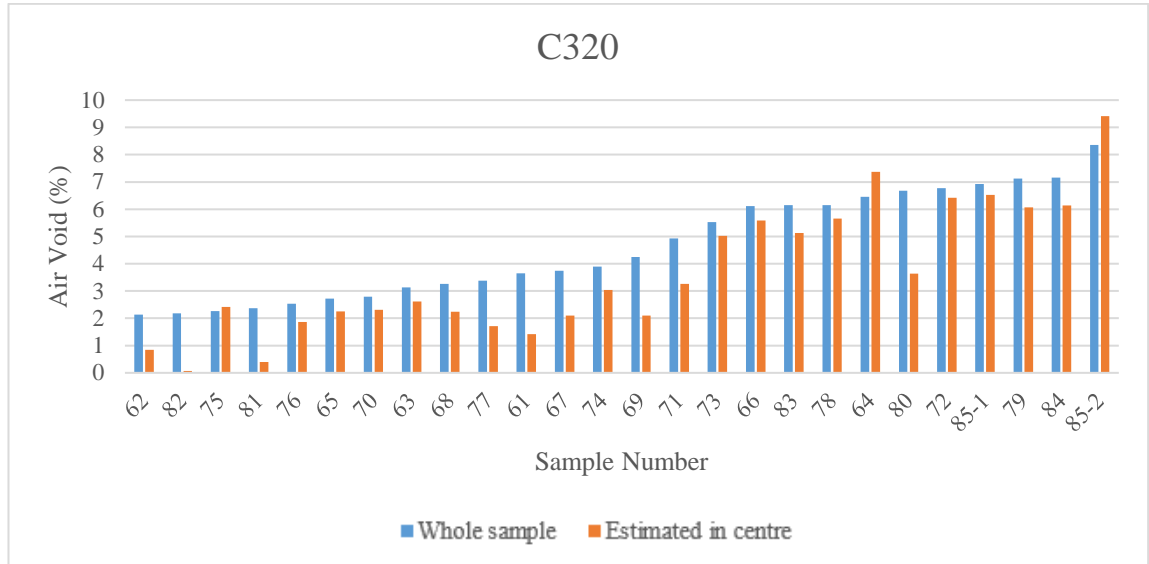


Figure 1: Conventional asphalt: Air voids of the whole sample vs. estimated air voids at the centre of sample

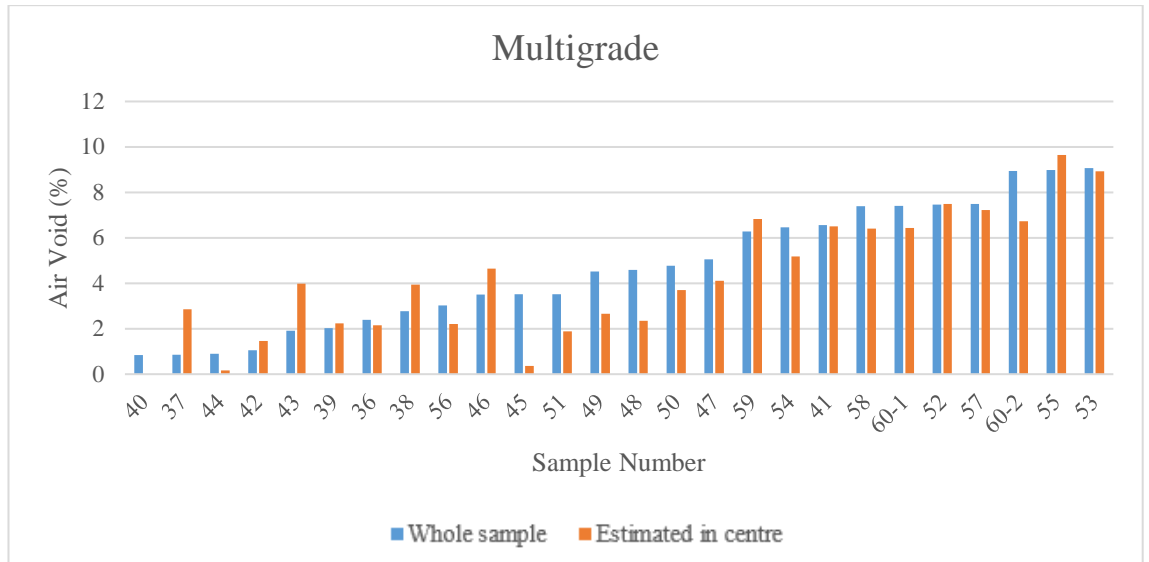


Figure 2: Multigrade asphalt: Air voids of the whole sample vs. estimated air voids at the centre of sample

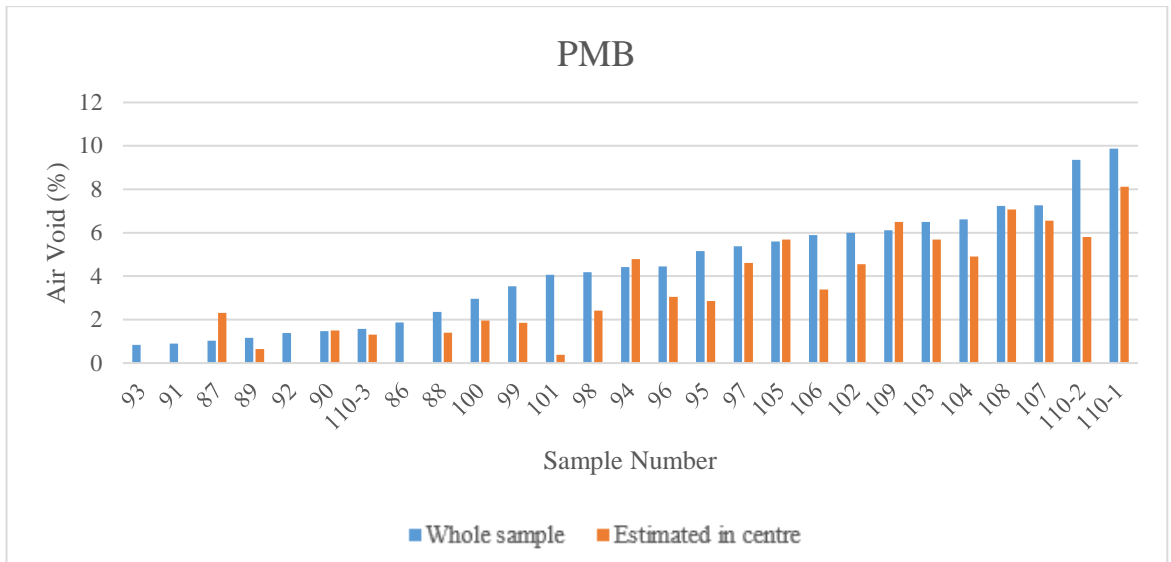


Figure 3: Polymer modified asphalt: Air voids of the whole sample vs. estimated air voids at the centre of sample

## Appendix C

*FEM modelling outputs for various laboratory and in-situ conditions.*

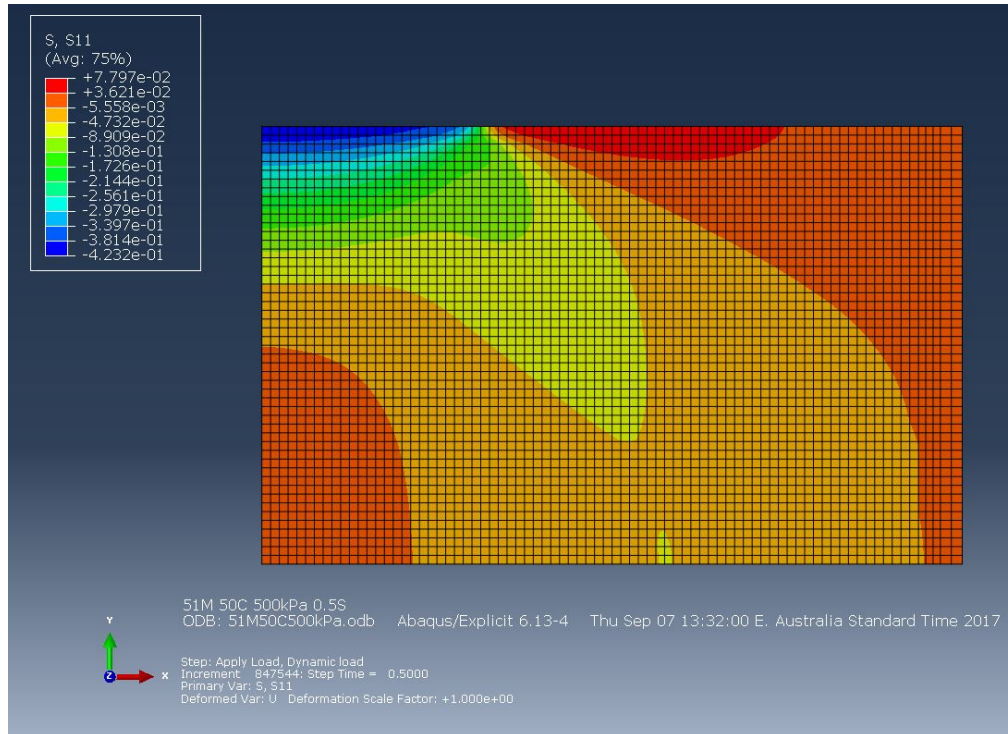


Figure 1: 51M, 500kPa,  $S_{11}$ , Confined laboratory sample

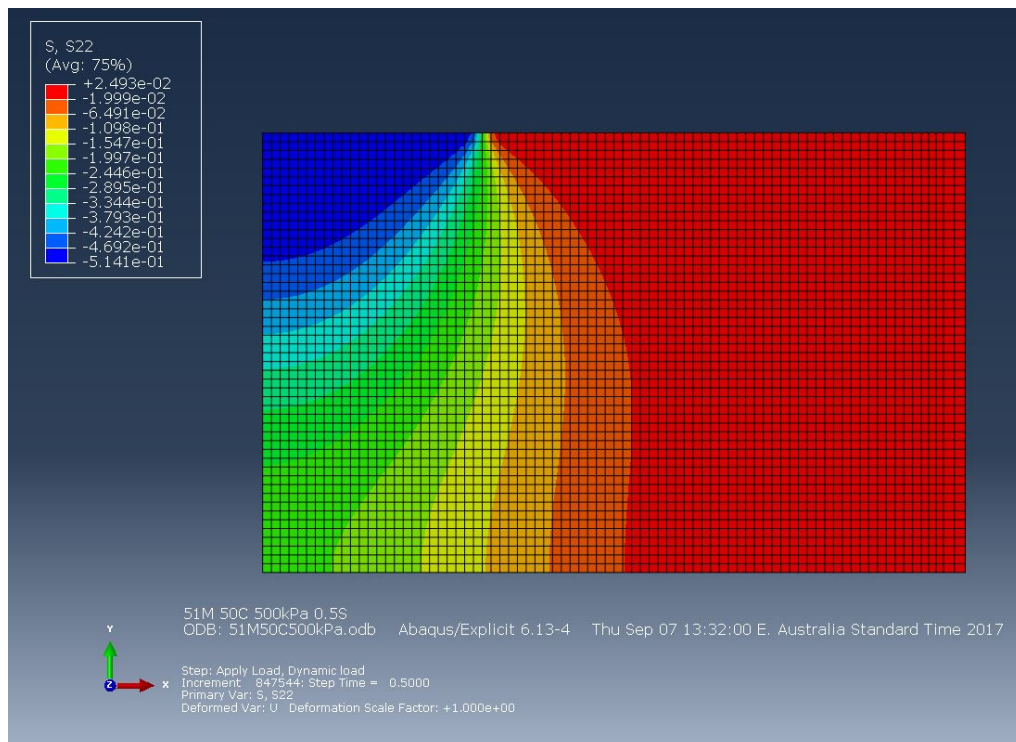


Figure 2: 51M, 500kPa,  $S_{22}$ , Confined laboratory sample

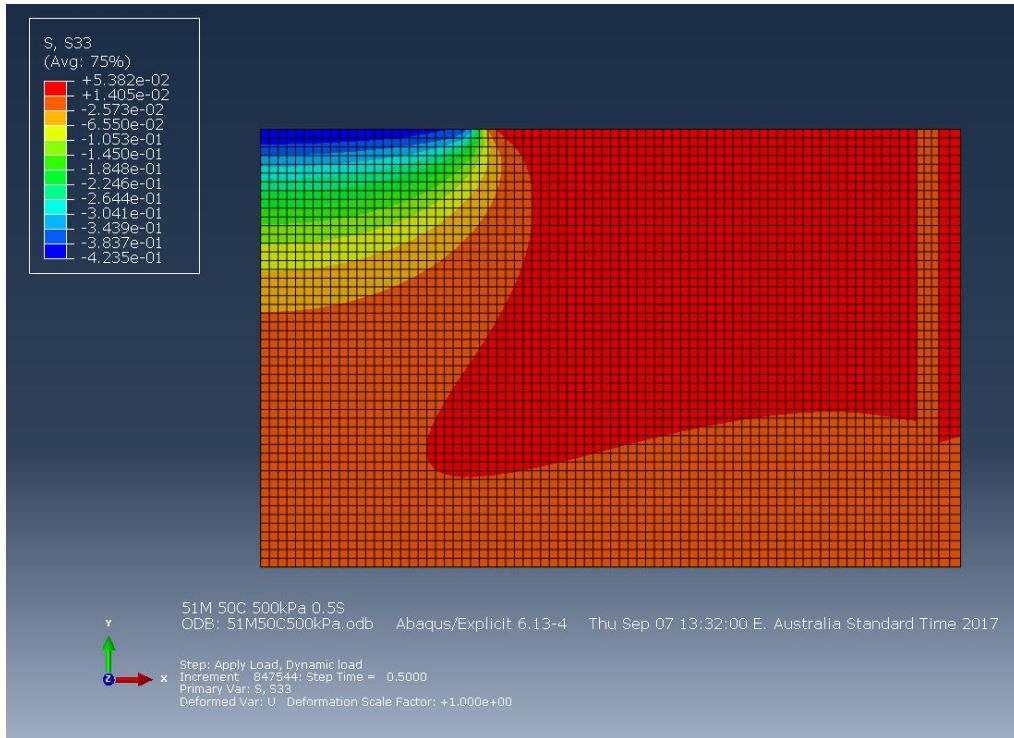


Figure 3: 51M, 500kPa, S33, Confined laboratory sample

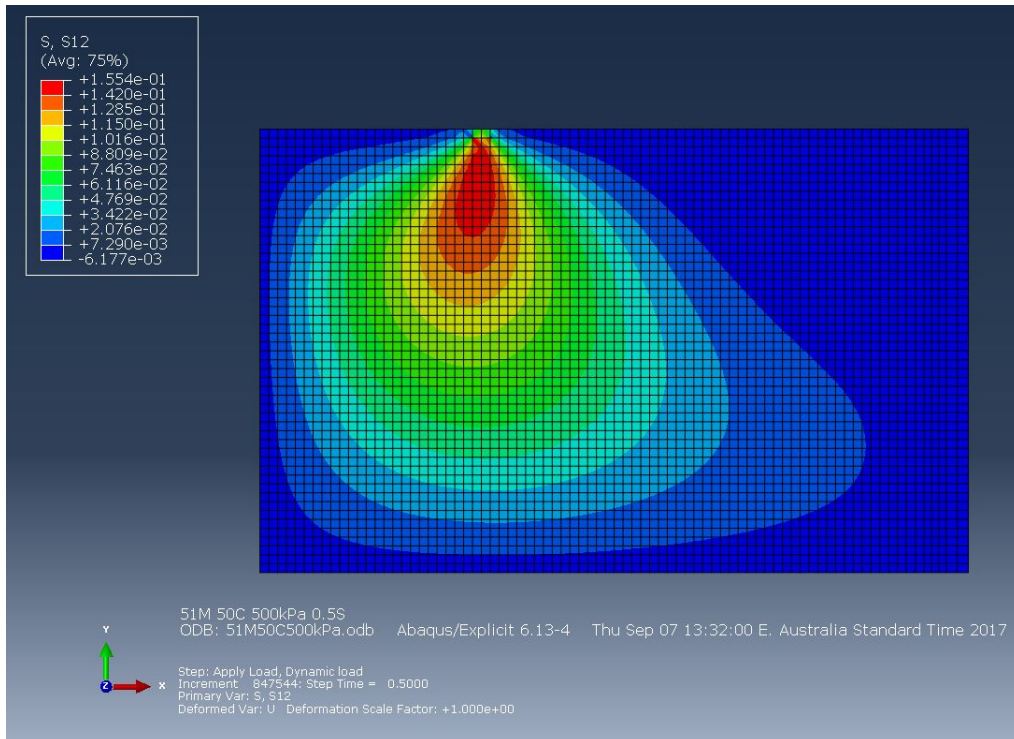


Figure 4: 51M, 500kPa, S12, Confined laboratory sample

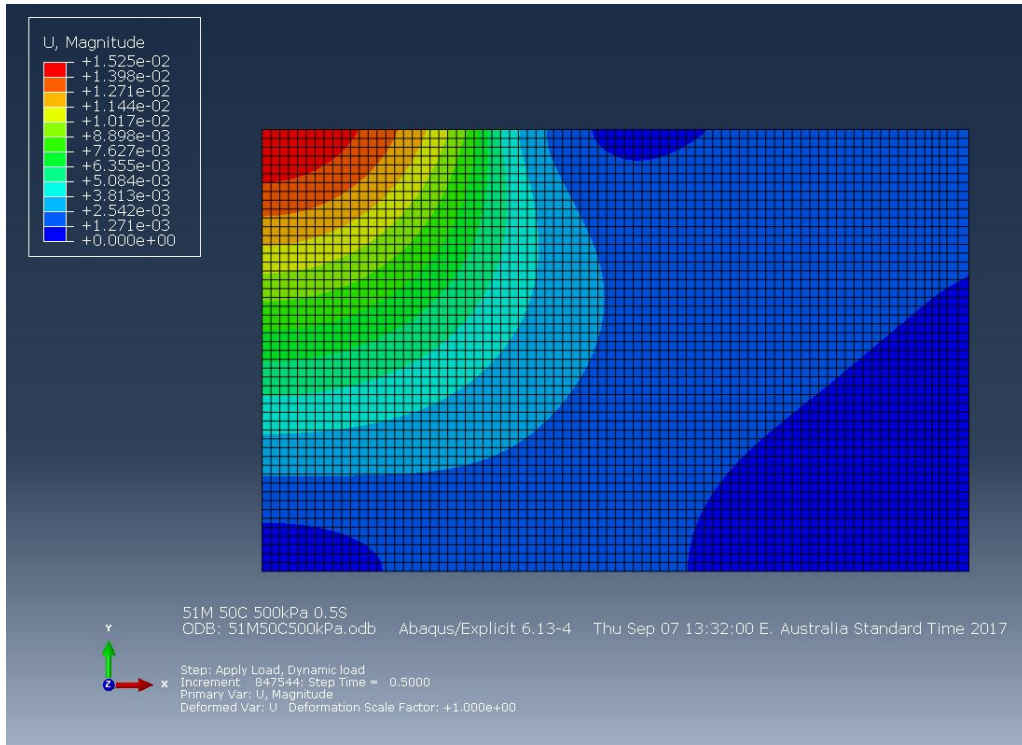


Figure 5: 51M, 500kPa, U Magnitude, Confined laboratory sample

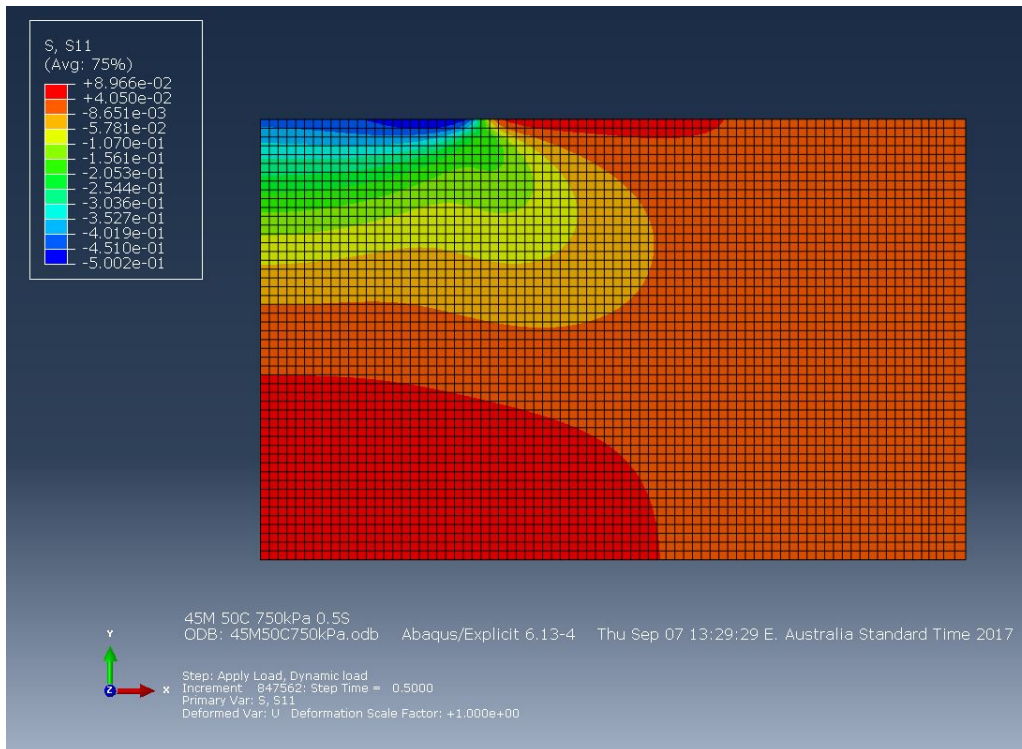


Figure 6: 45M, 750kPa, S11, Confined laboratory sample

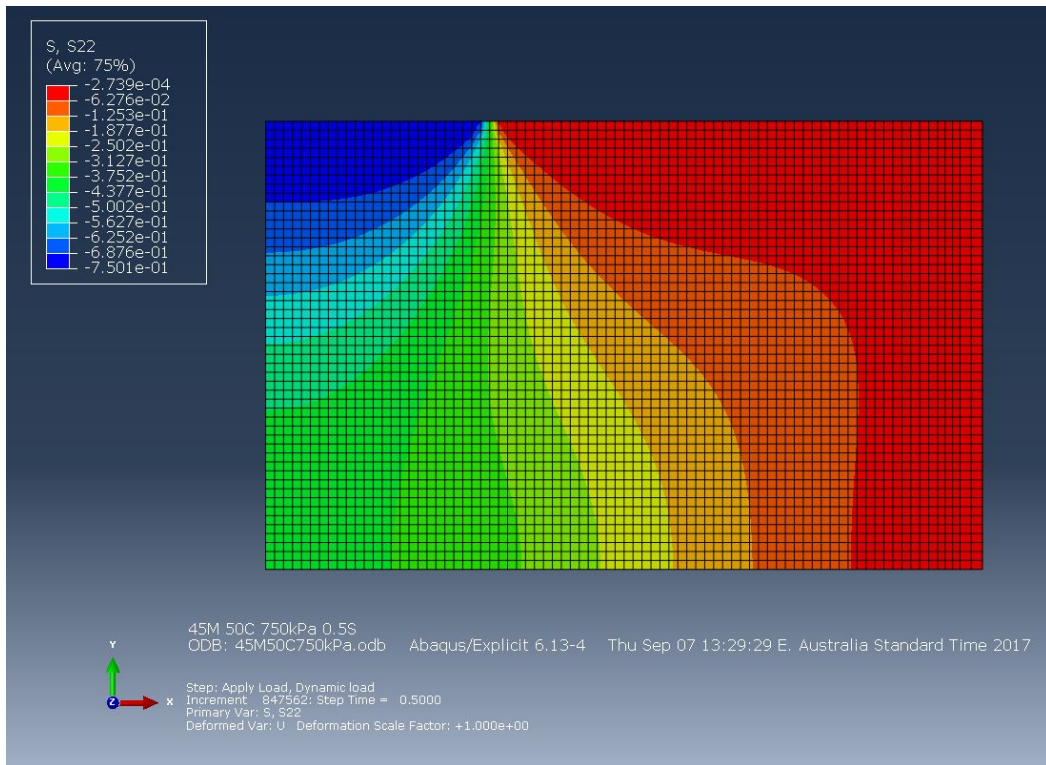


Figure 7: 45M, 750kPa, S22, Confined laboratory sample

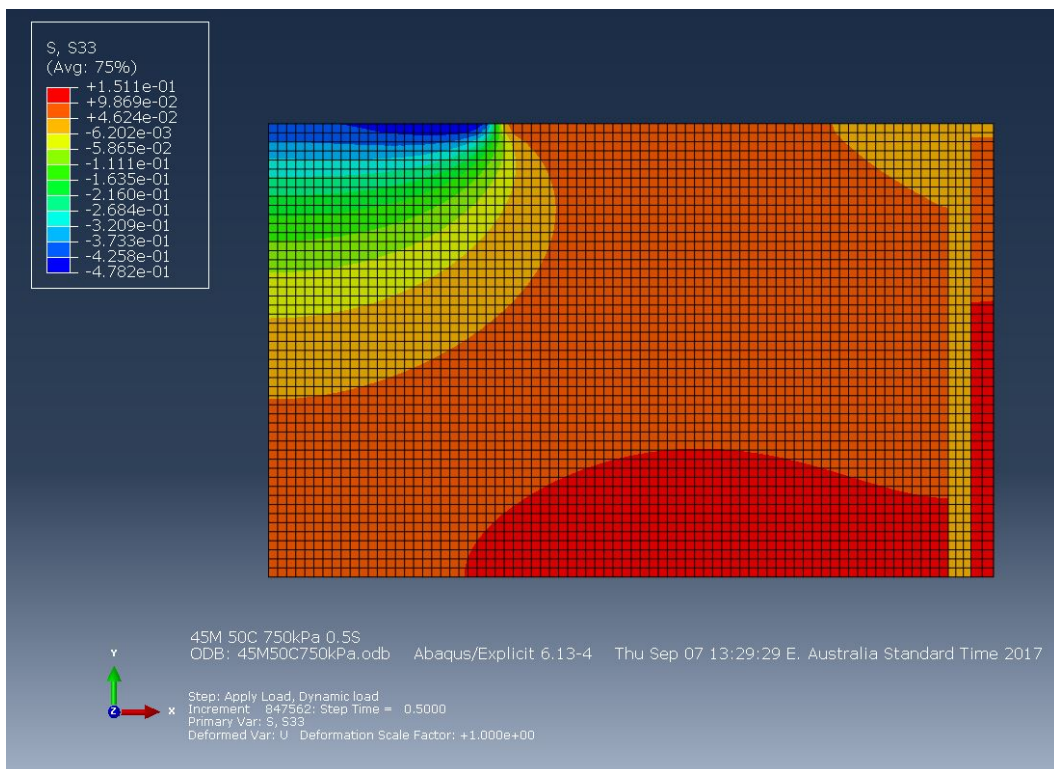


Figure 8: 45M, 750kPa, S33, Confined laboratory sample

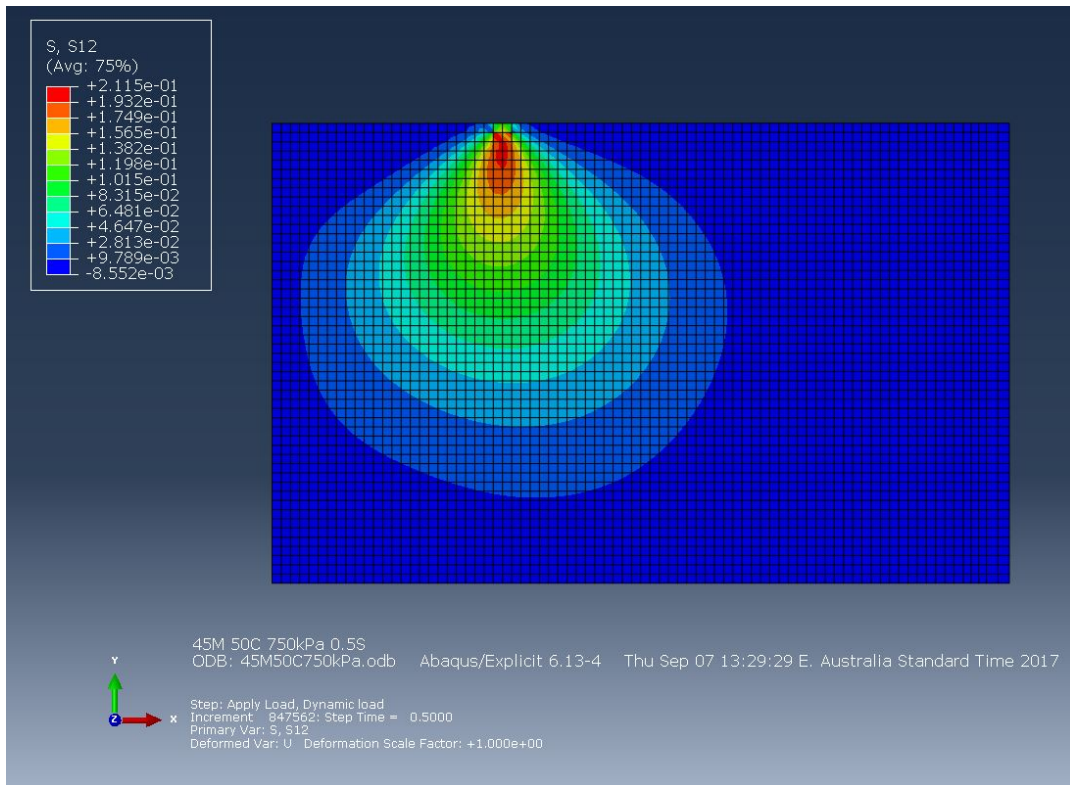


Figure 9: 45M, 750kPa, S12, Confined laboratory sample

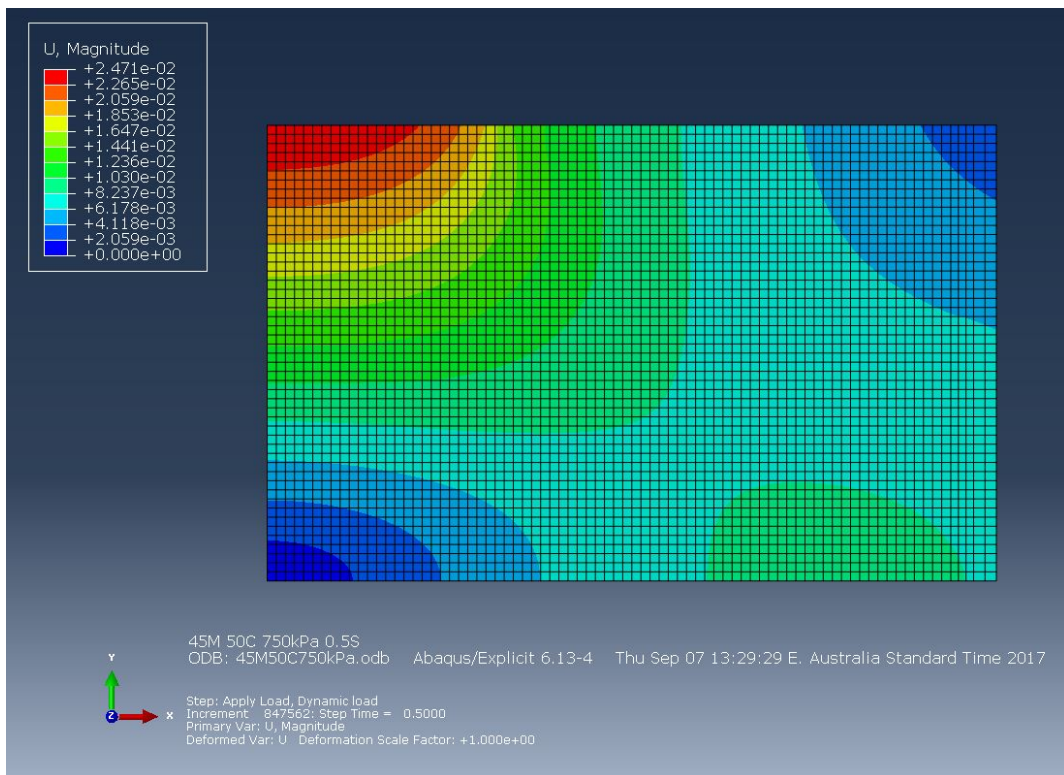


Figure 10: 45M, 750kPa, U Magnitude, Confined laboratory sample

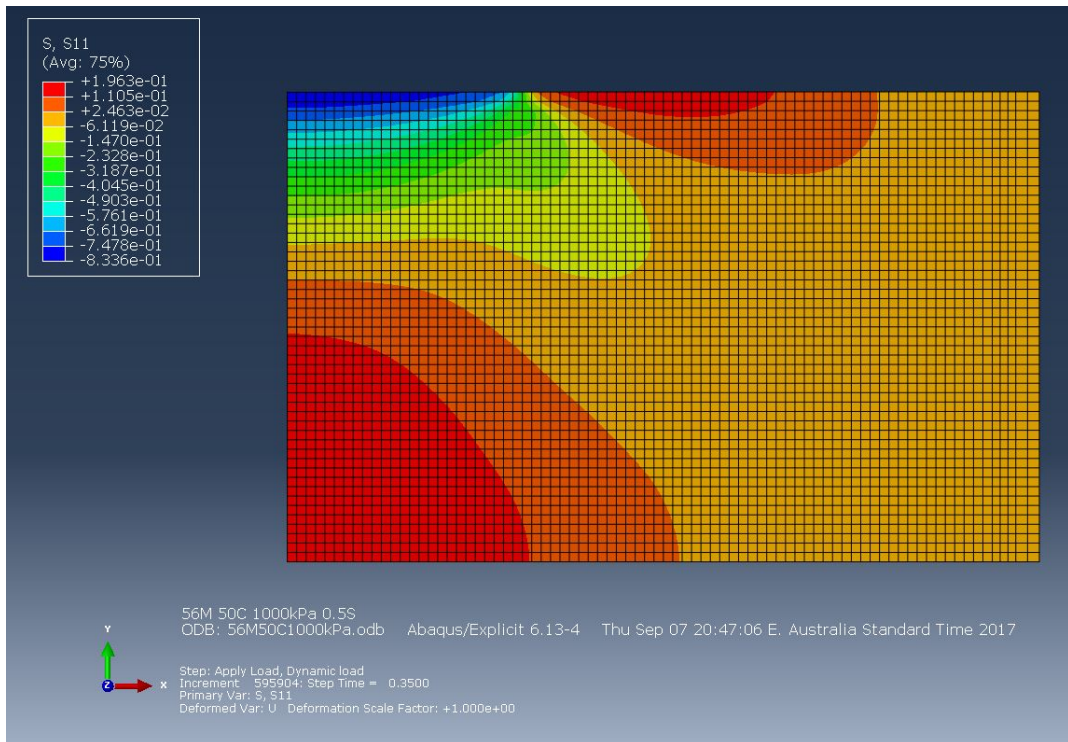


Figure 11: 56M, 1000kPa, S11, Confined laboratory sample

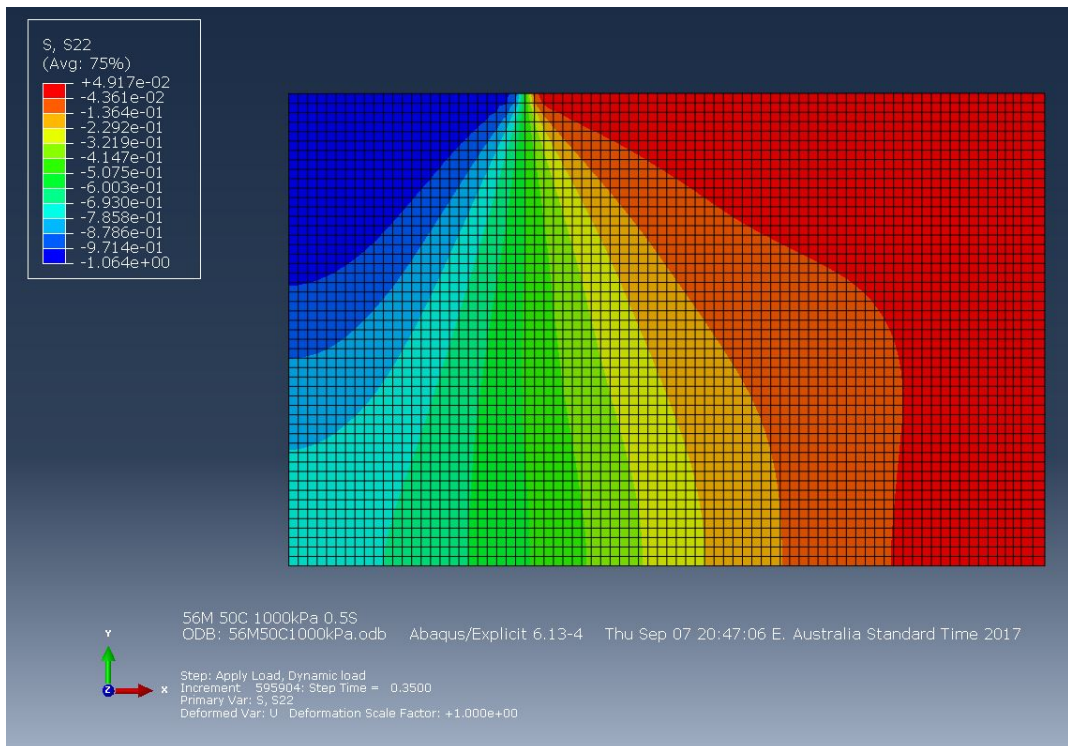


Figure 12: 56M, 1000kPa, S22, Confined laboratory sample

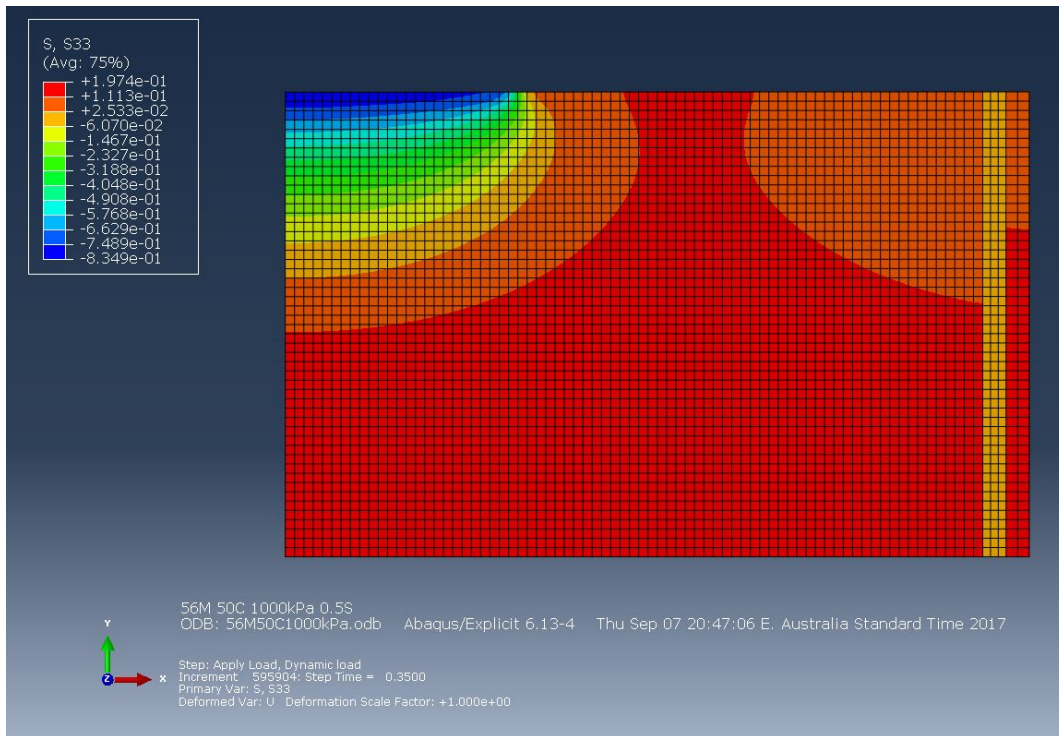


Figure 13: 56M, 1000kPa, S33, Confined laboratory sample

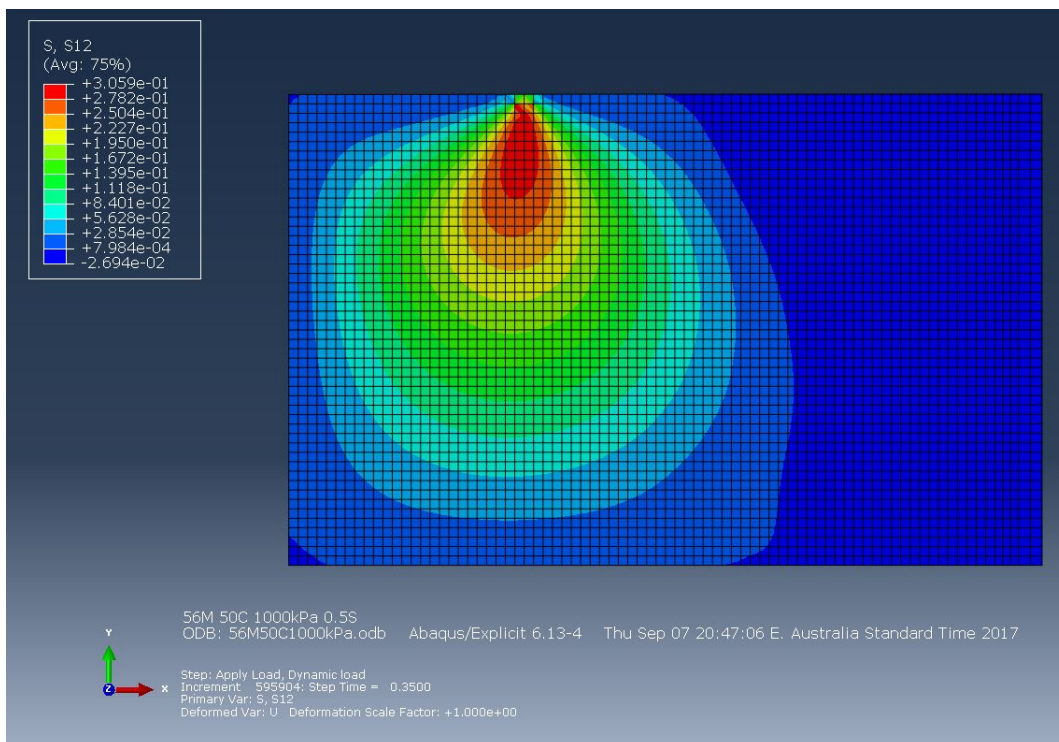


Figure 14: 56M, 1000kPa, S12, Confined laboratory sample

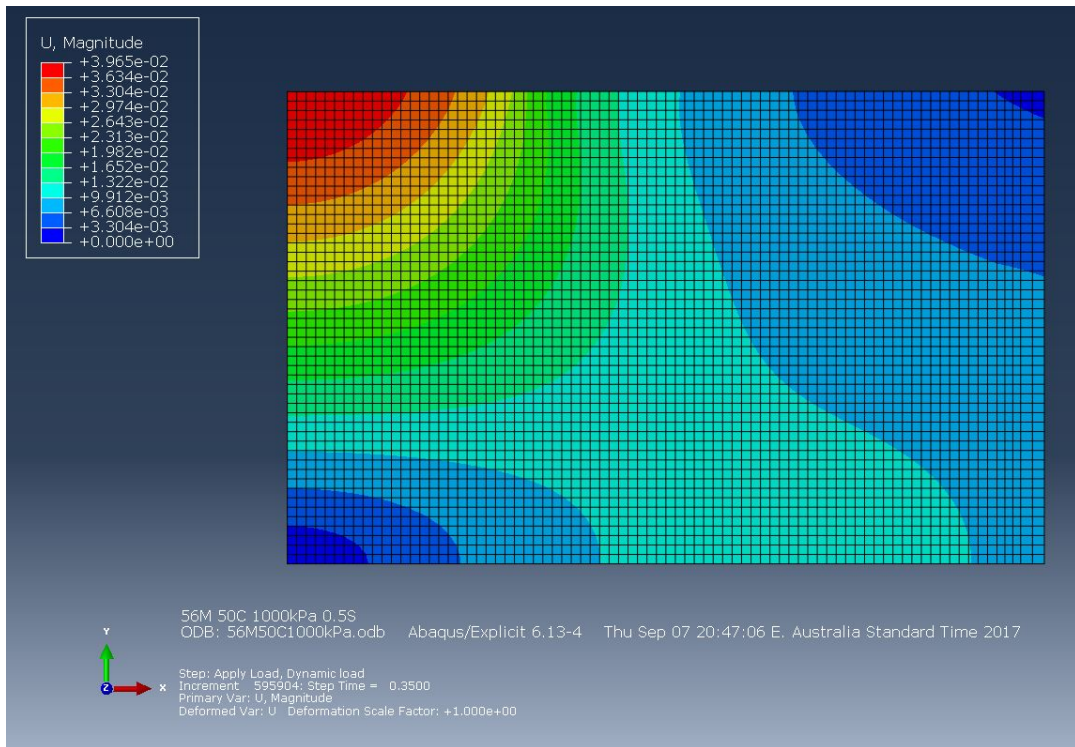


Figure 15: 56M, 1000kPa, U Magnitude, Confined laboratory sample

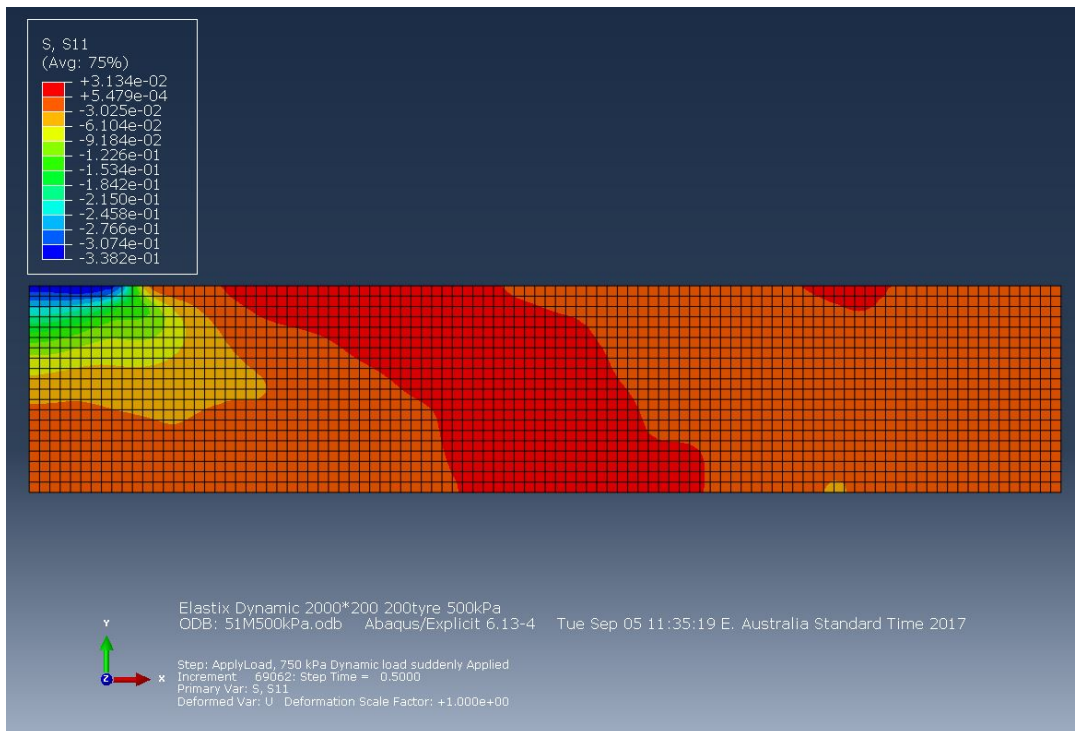


Figure 16: 51M, 500kPa, S11, asphalt layer

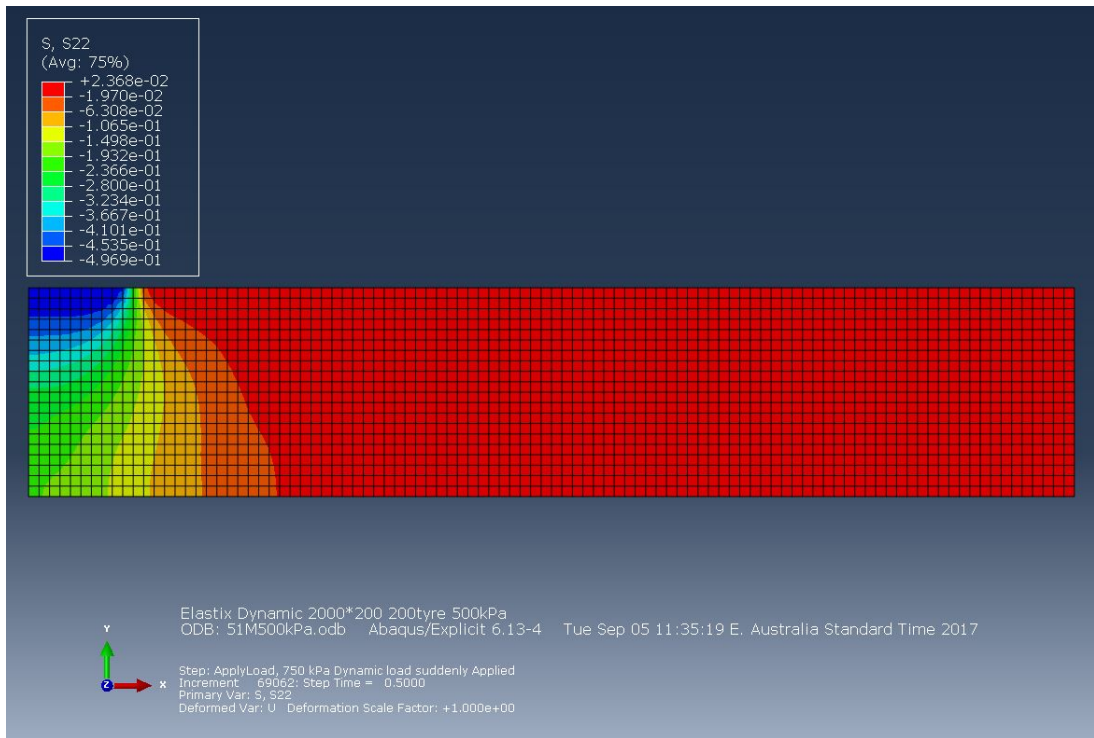


Figure 17: 51M, 500kPa, S22, asphalt layer

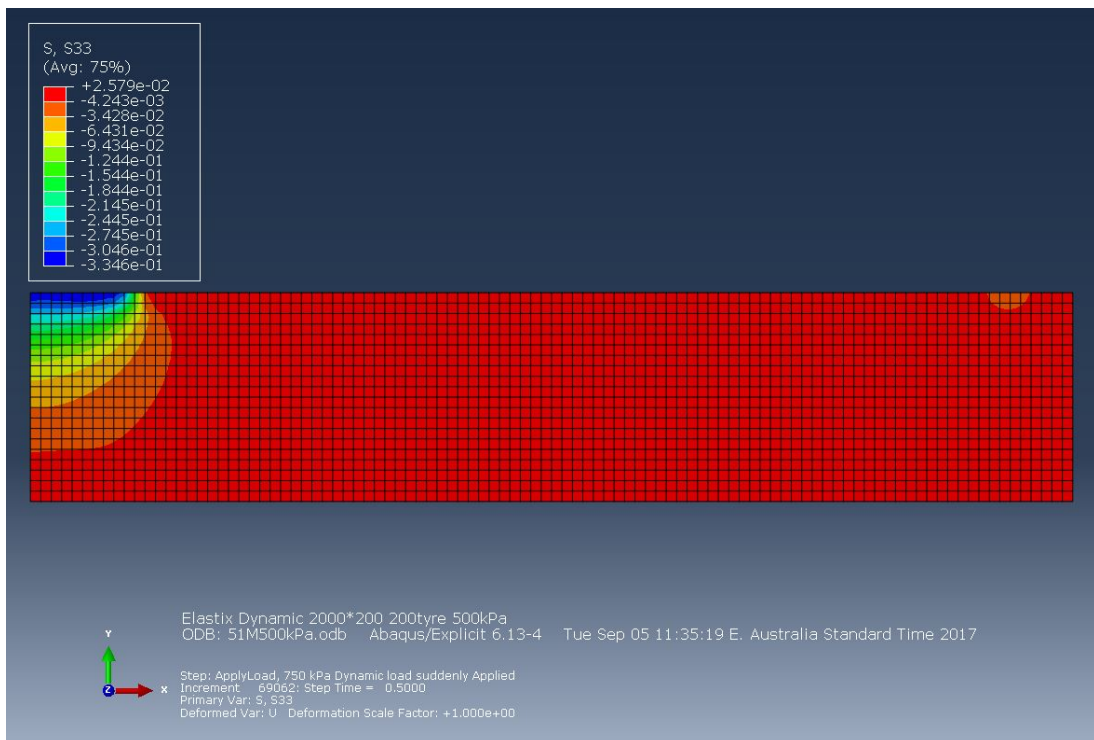


Figure 18: 51M, 500kPa, S33, asphalt layer

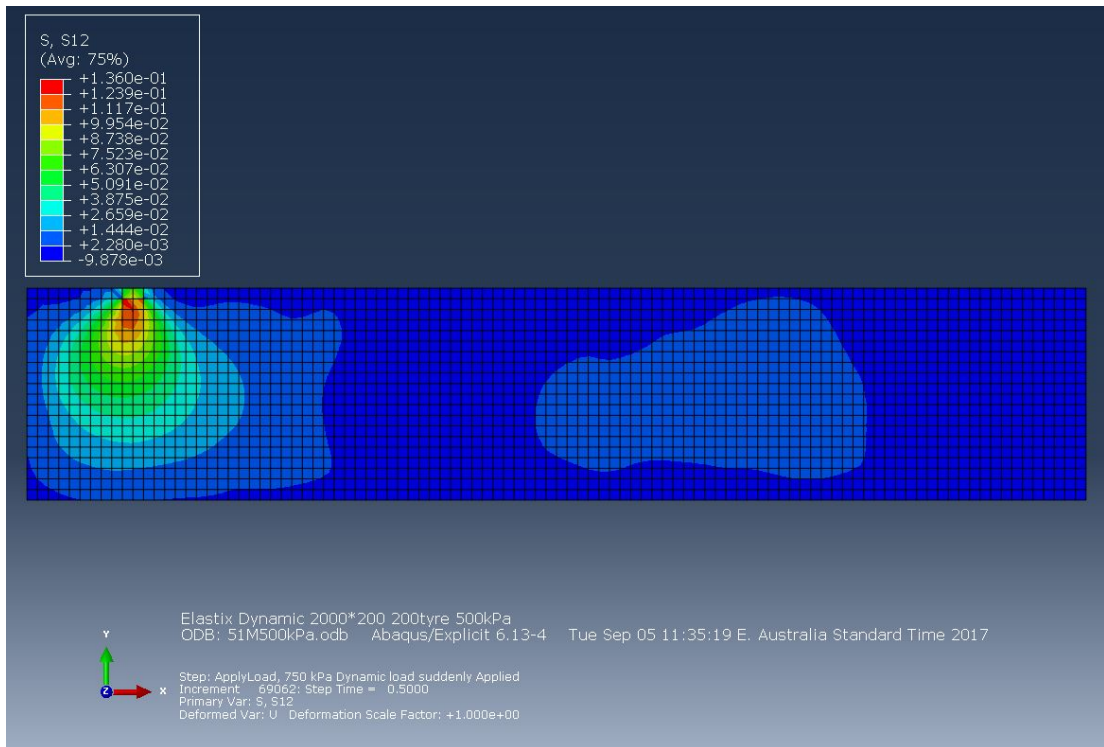


Figure 19: 51M, 500kPa, S12, asphalt layer

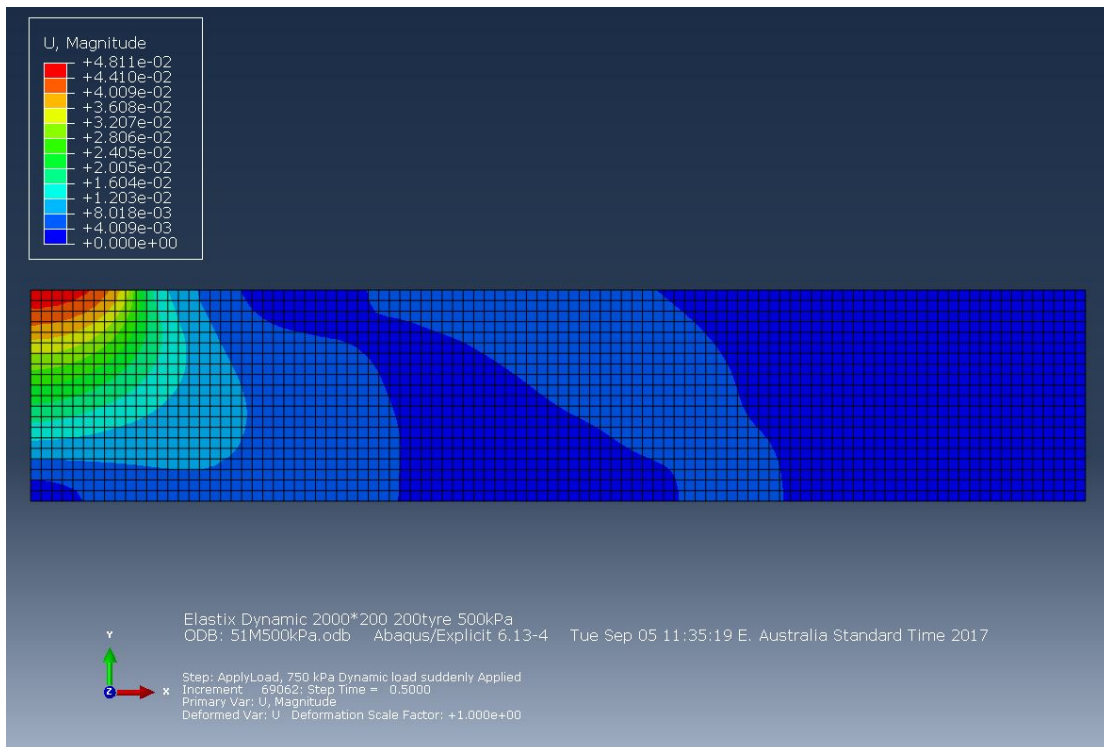


Figure 20: 51M, 500kPa, U Magnitude, asphalt layer

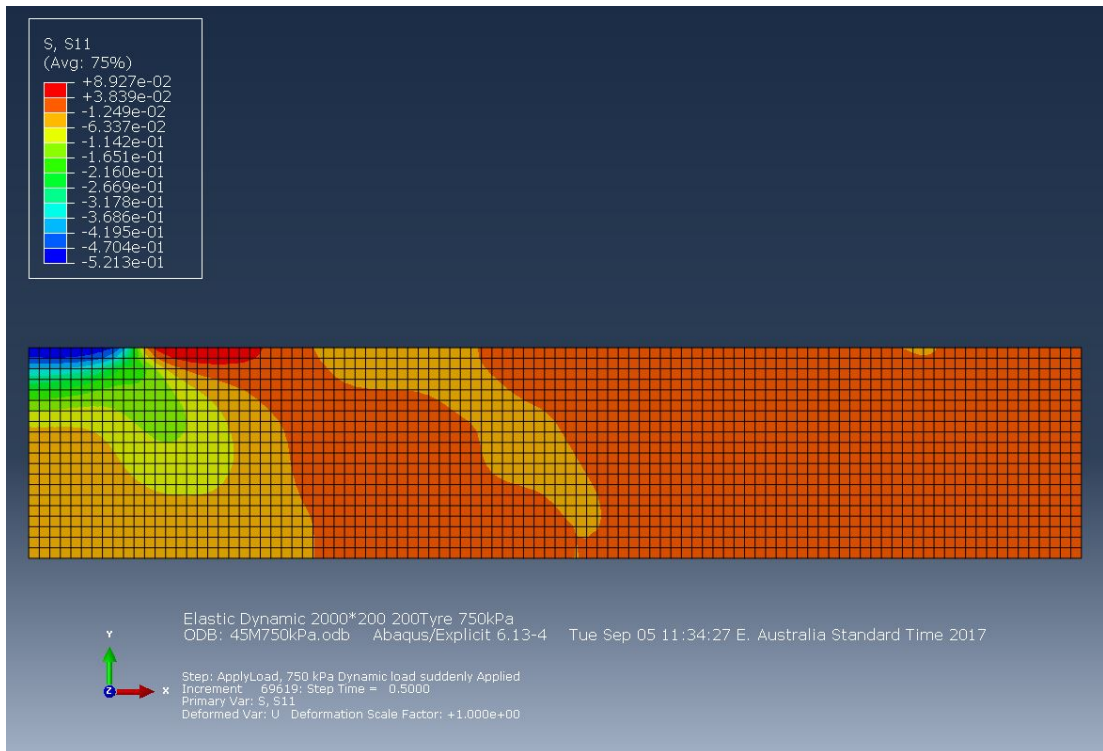


Figure 21: 45M, 750kPa, S11, asphalt layer

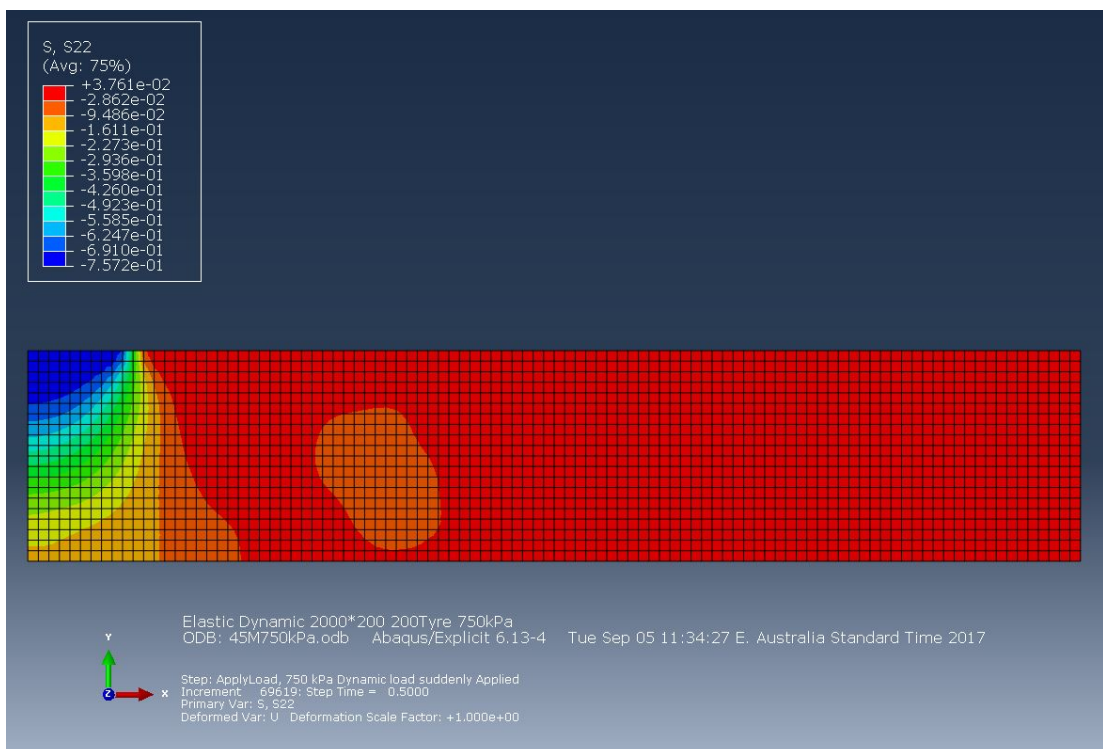


Figure 22: 45M, 750kPa, S22, asphalt layer

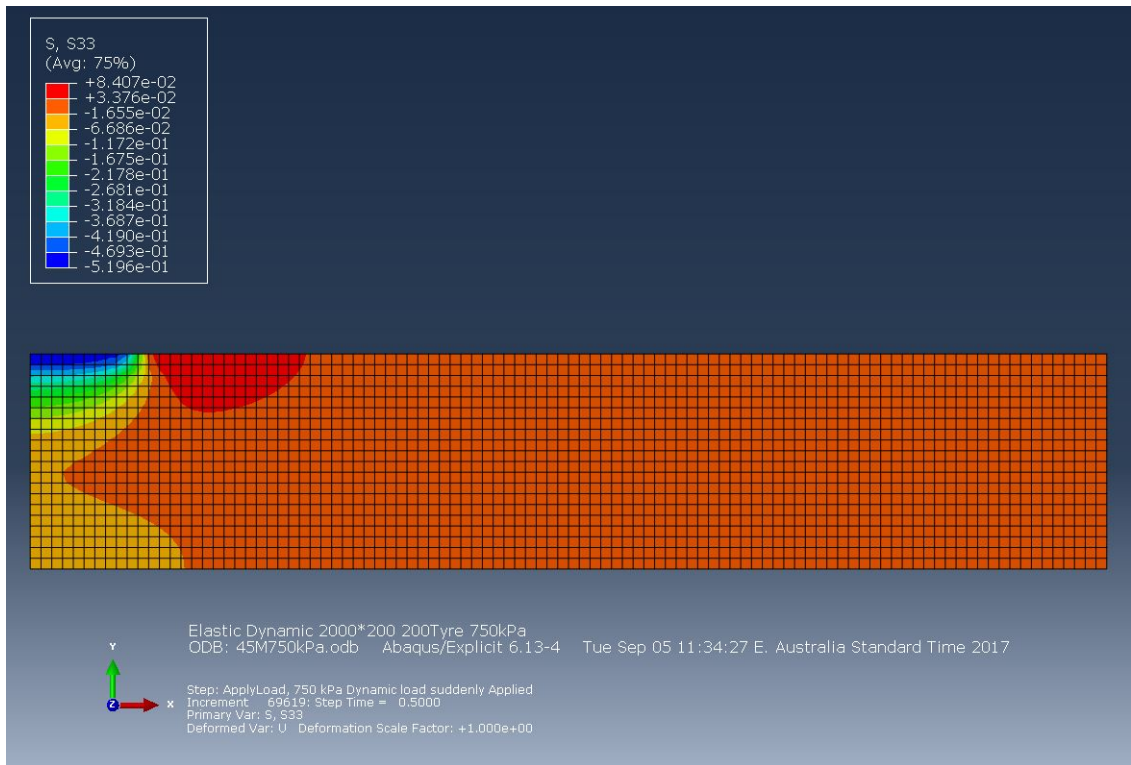


Figure 23: 45M, 750kPa, S33, asphalt layer

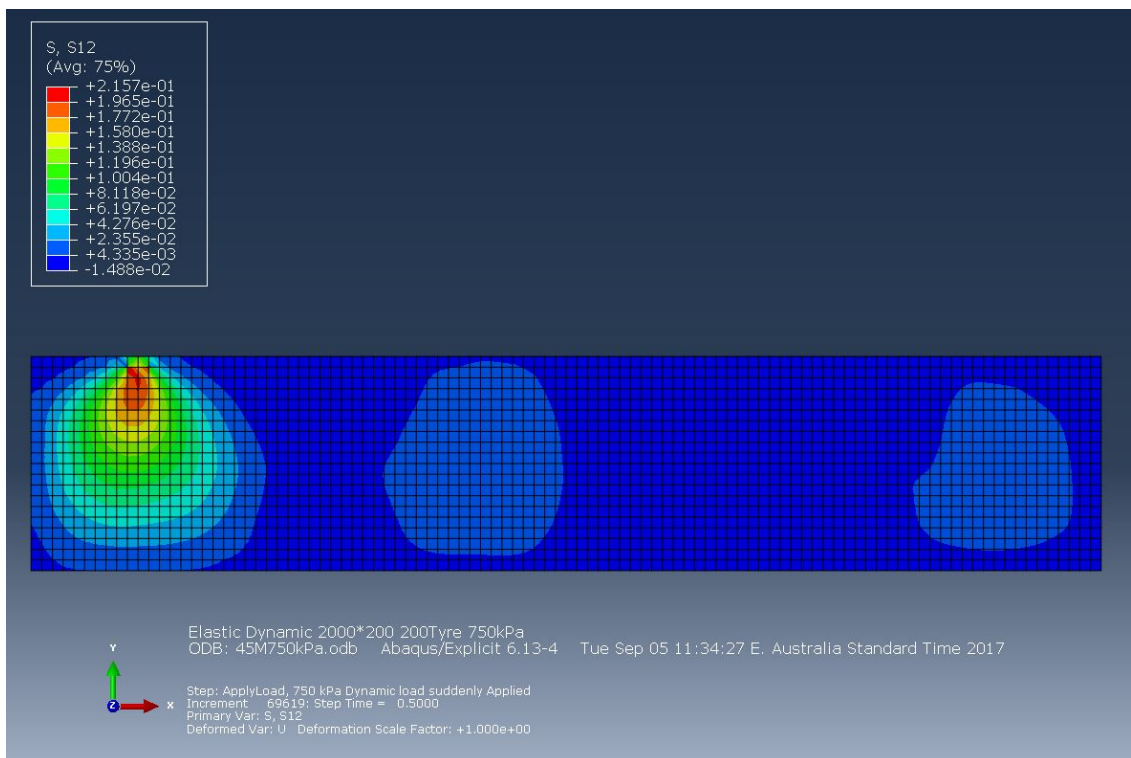


Figure 24: 45M, 750kPa, S12, asphalt layer

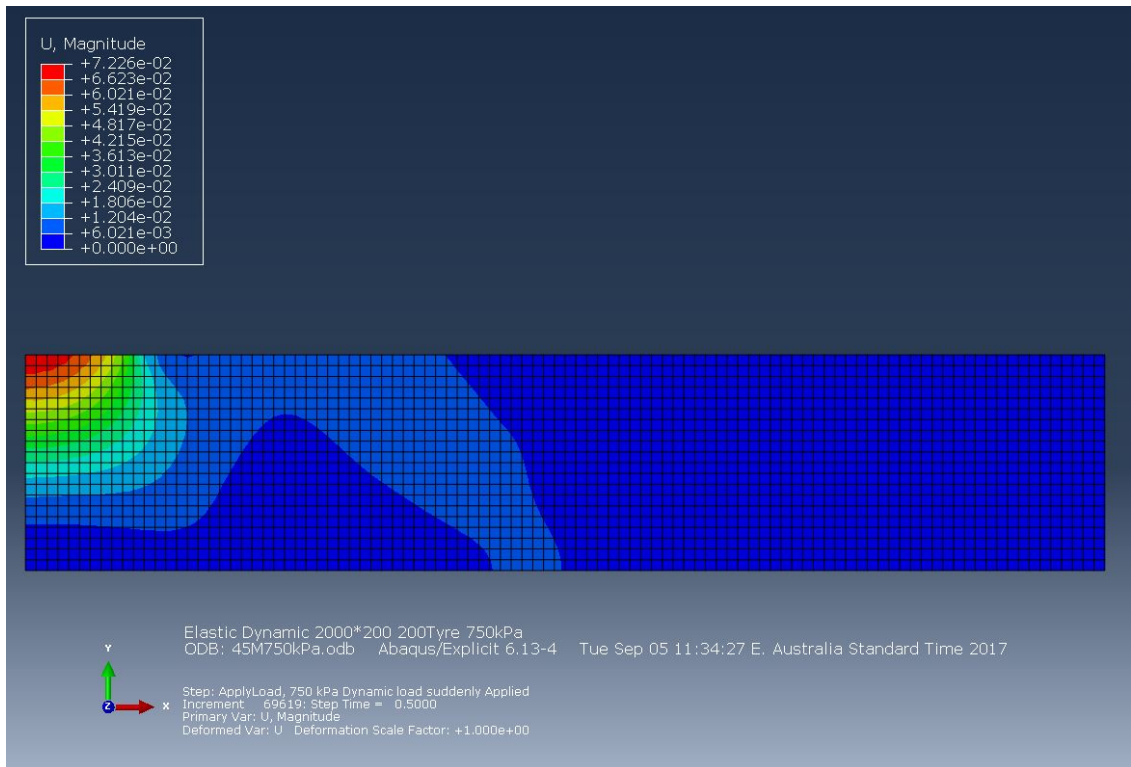


Figure 25: 45M, 750kPa, U Magnitude, asphalt layer

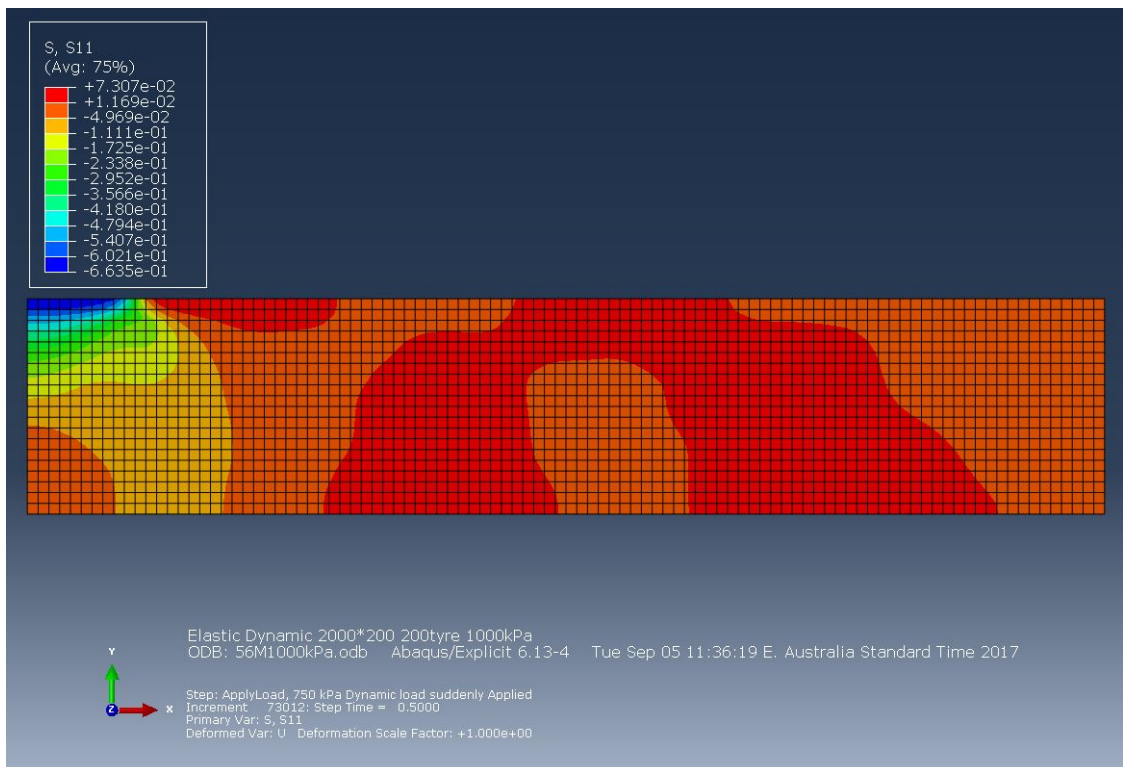


Figure 26: 56M, 1000kPa, S11, asphalt layer

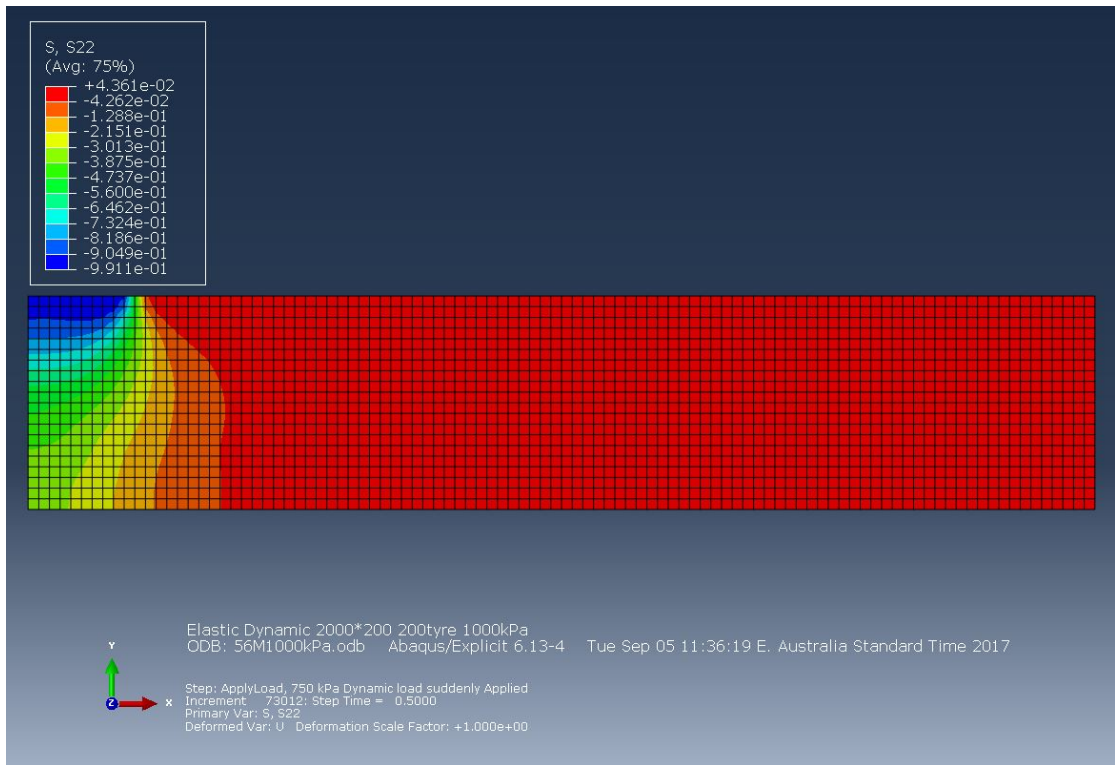


Figure 27: 56M, 1000kPa, S22, asphalt layer

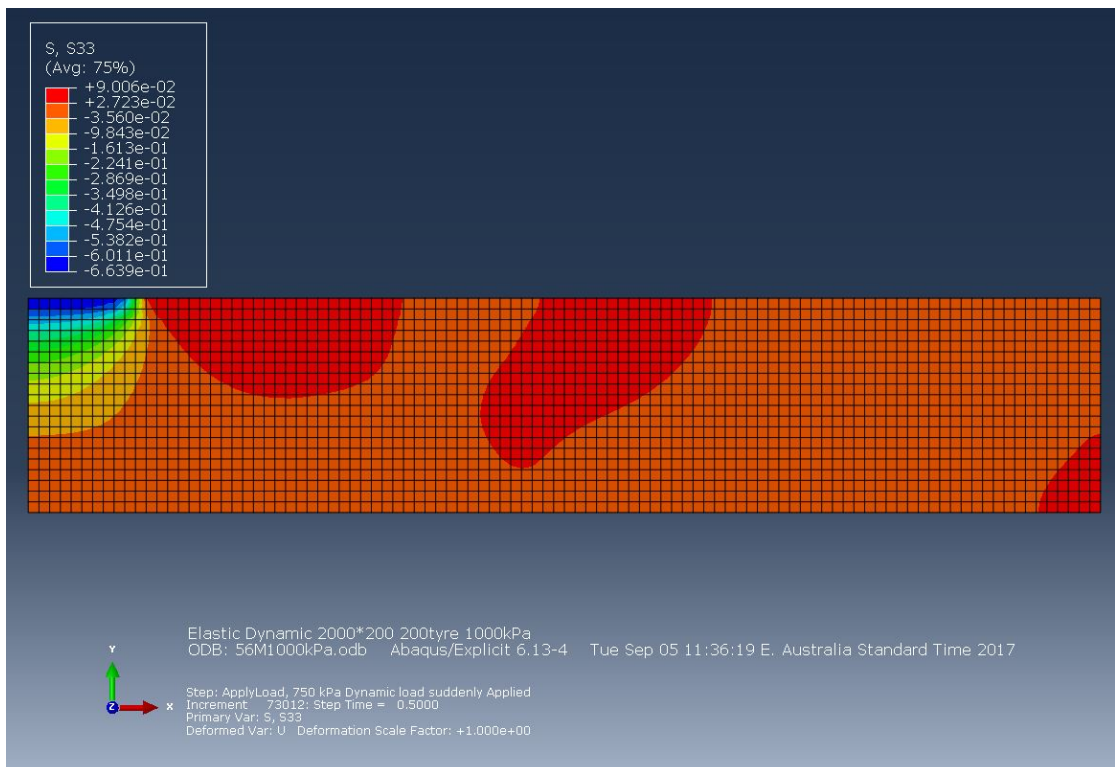


Figure 28: 56M, 1000kPa, S33, asphalt layer

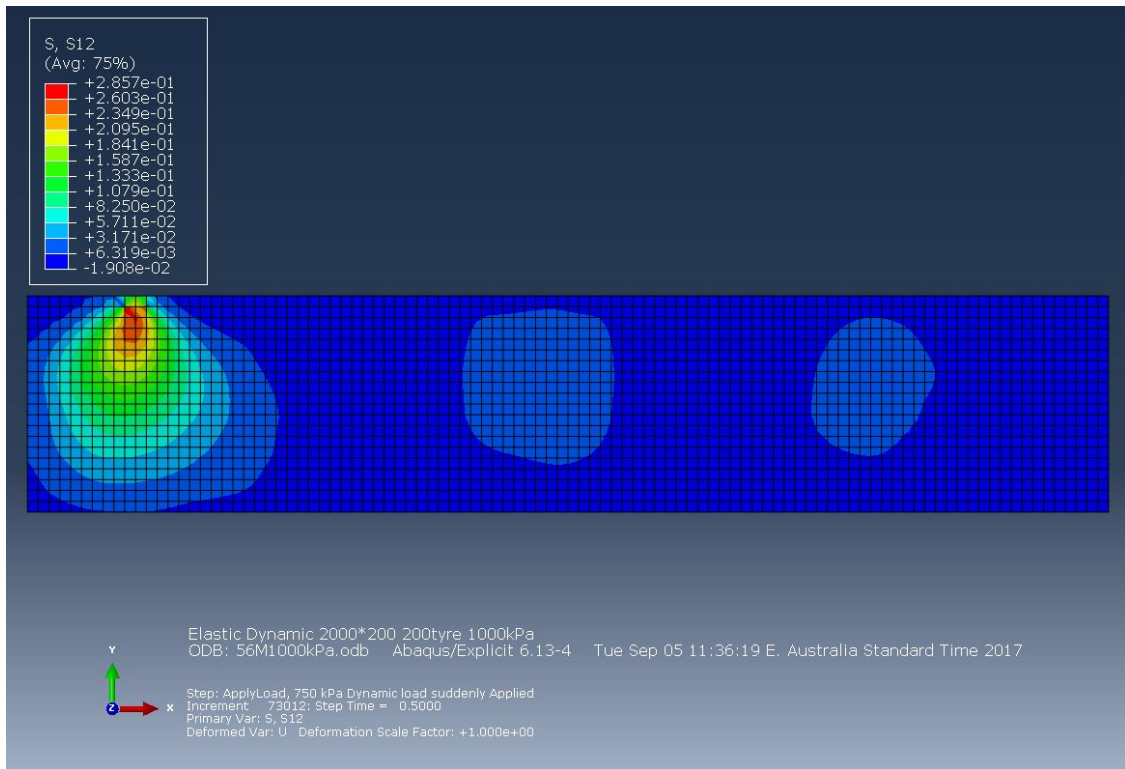


Figure 29: 56M, 1000kPa, S12, asphalt layer

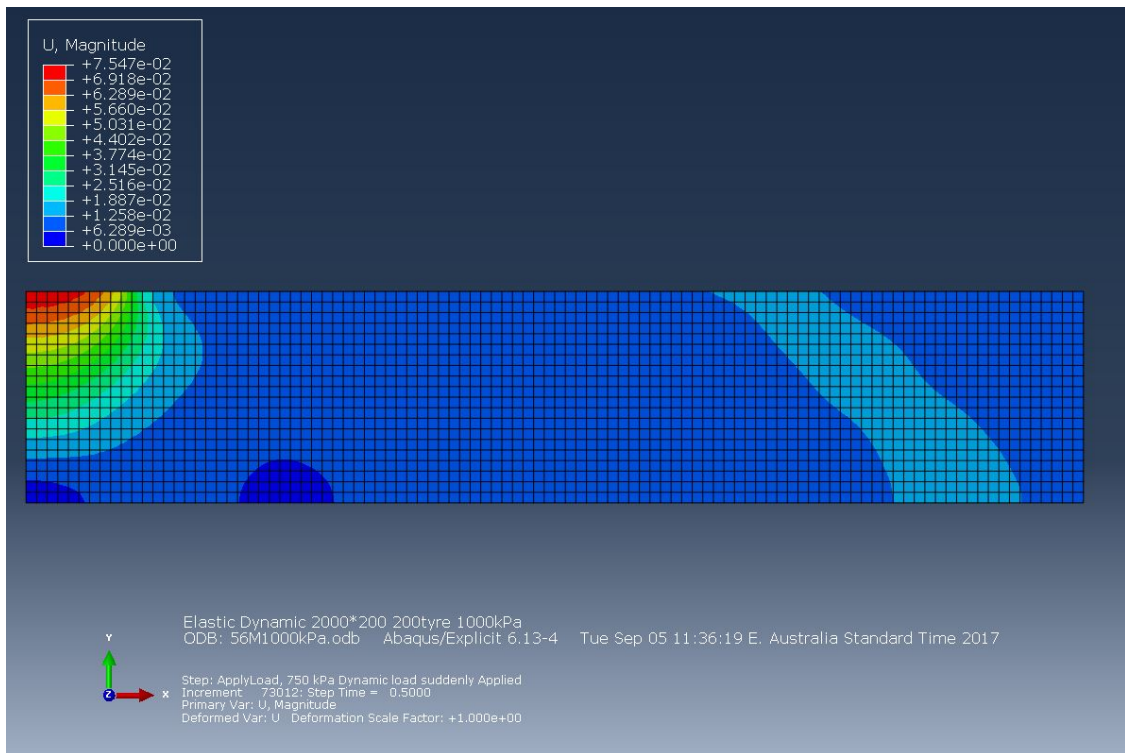


Figure 30: 56M, 1000kPa, U Magnitude, asphalt layer

## APPENDIX D

### Raw MCDC test related data

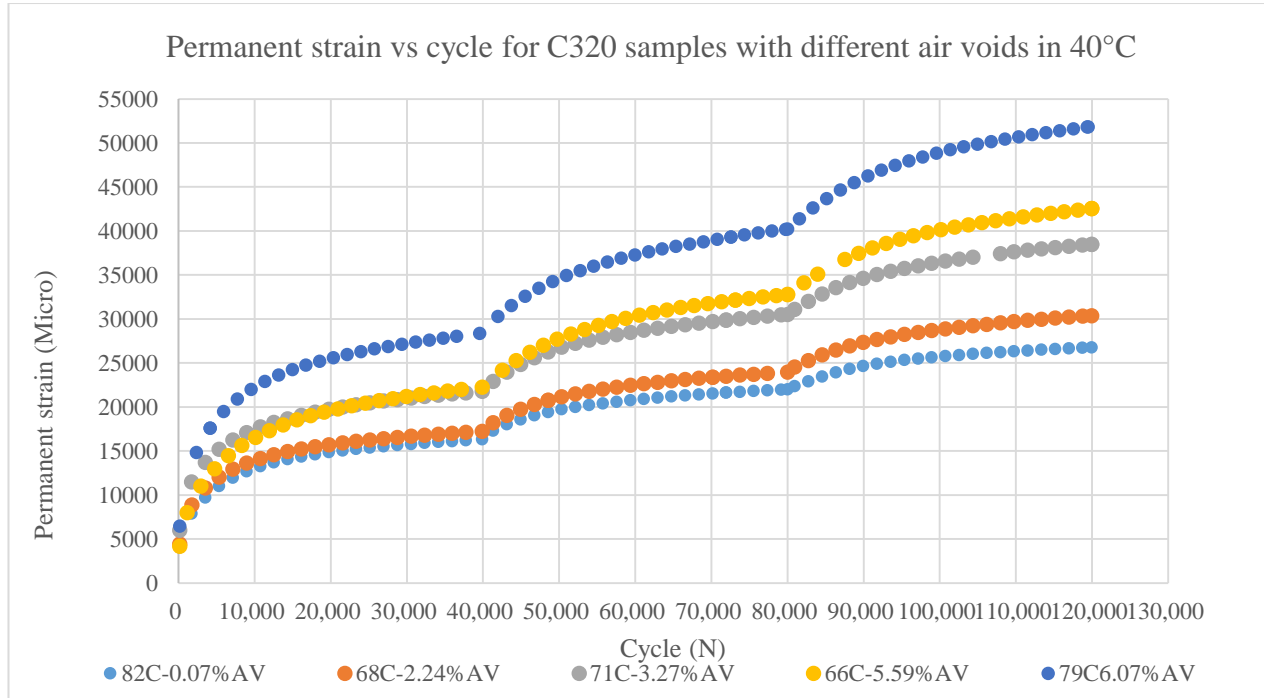


Figure 1: MCDC test results for conventional samples in 40°C

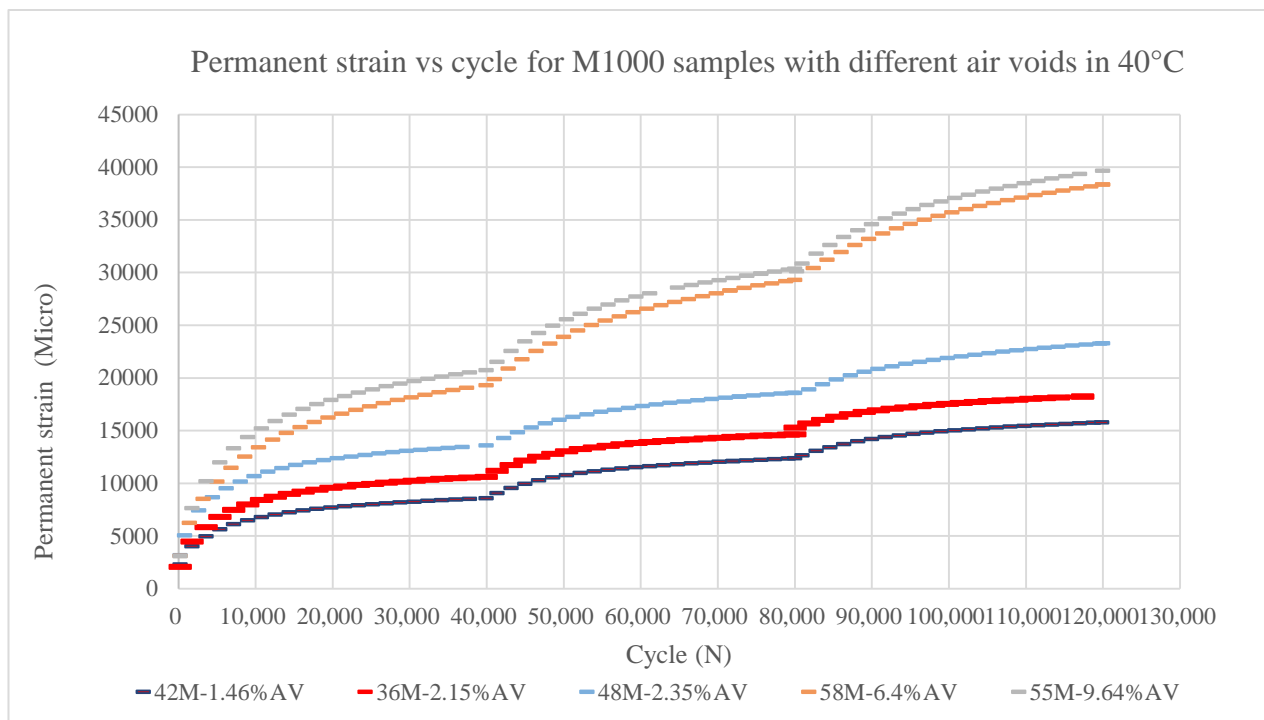


Figure 2: MCDC test results for Multigrade samples in 40°C

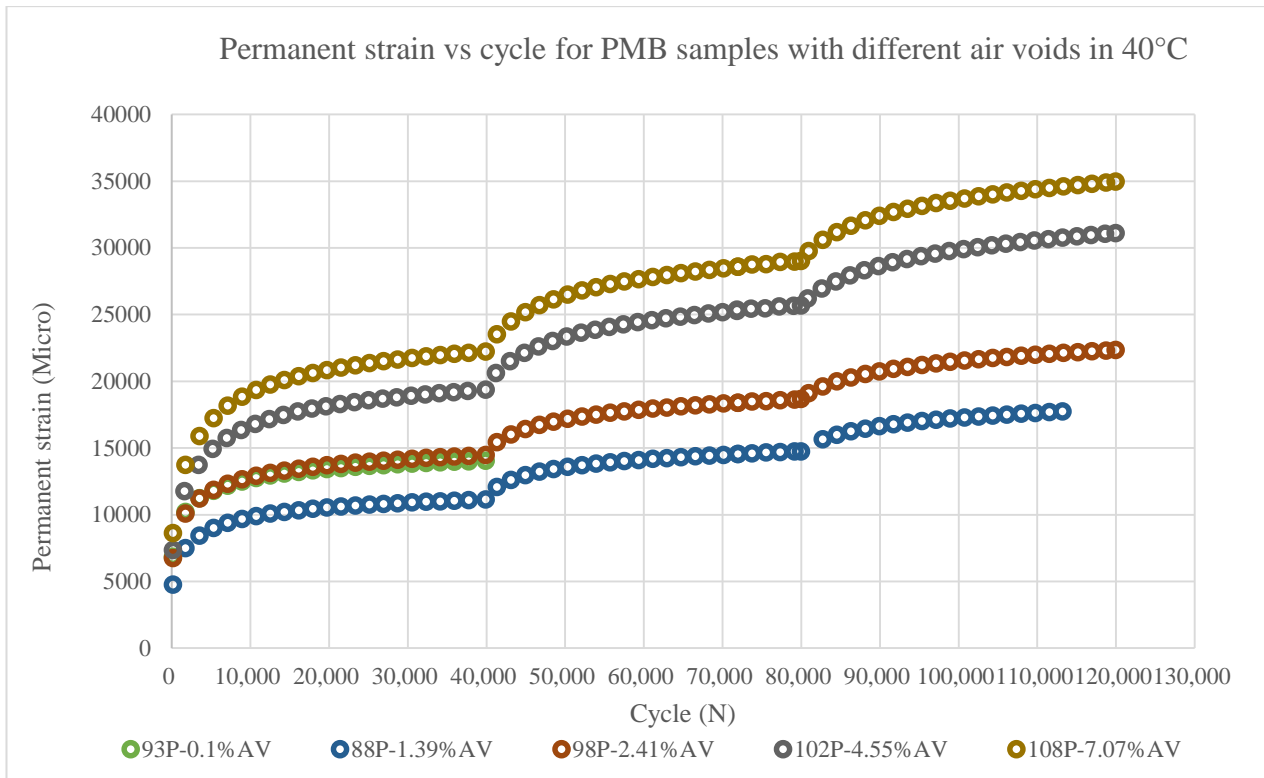


Figure 3: MCDC test results for PMB samples in 40°C

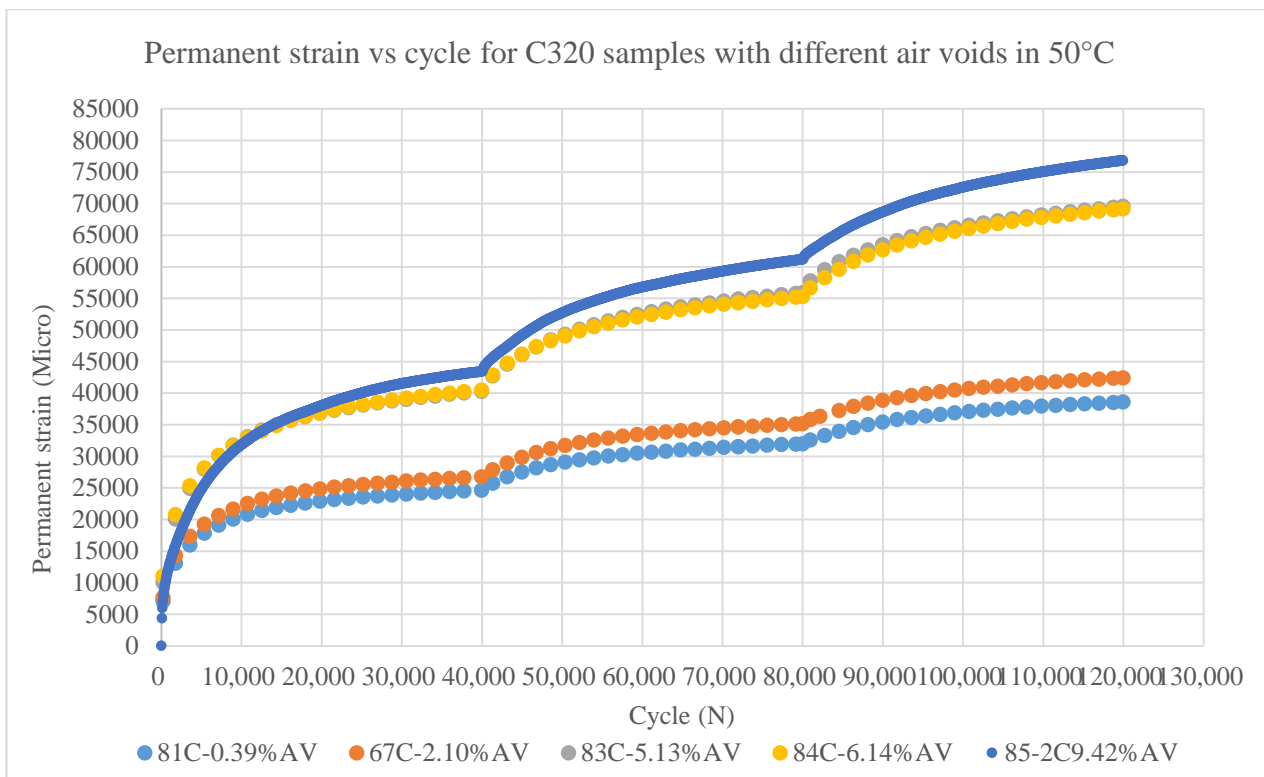


Figure 4: MCDC test results for conventional samples in 50°C

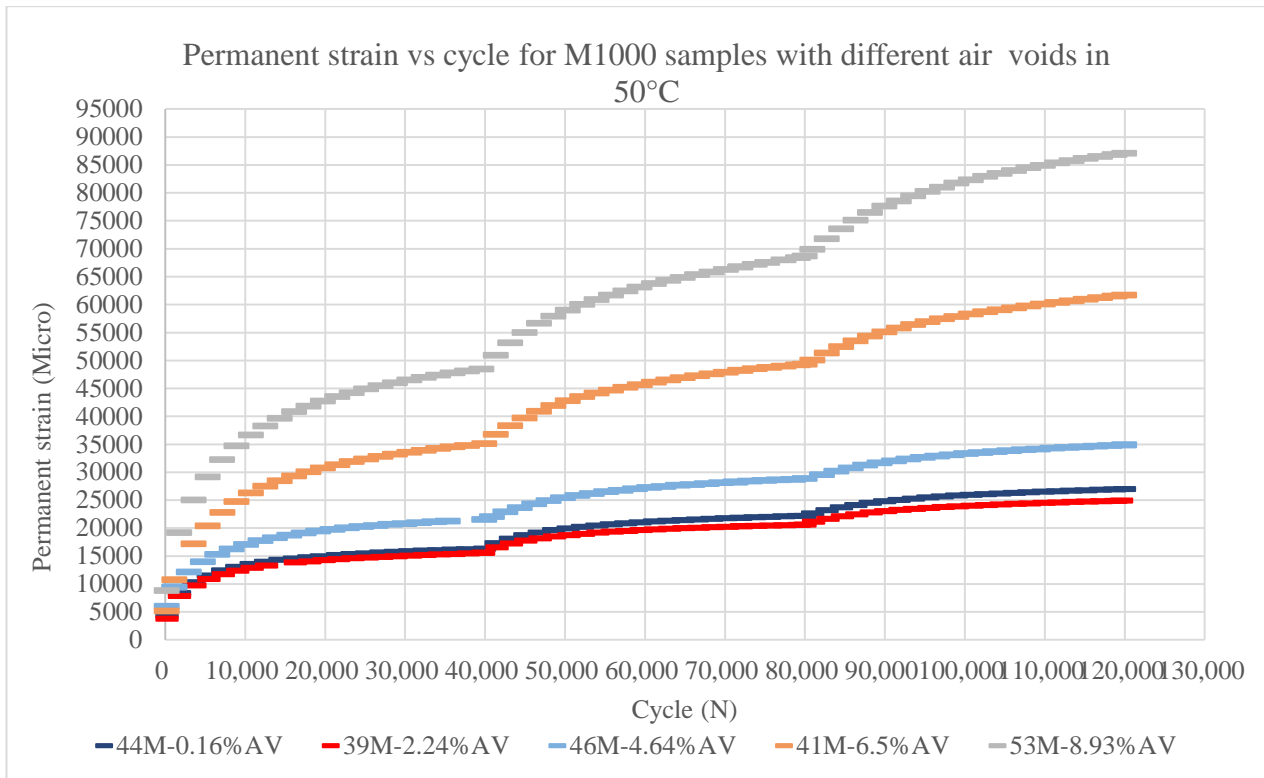


Figure 5: MCDC test results for Multigrade samples in 50°C

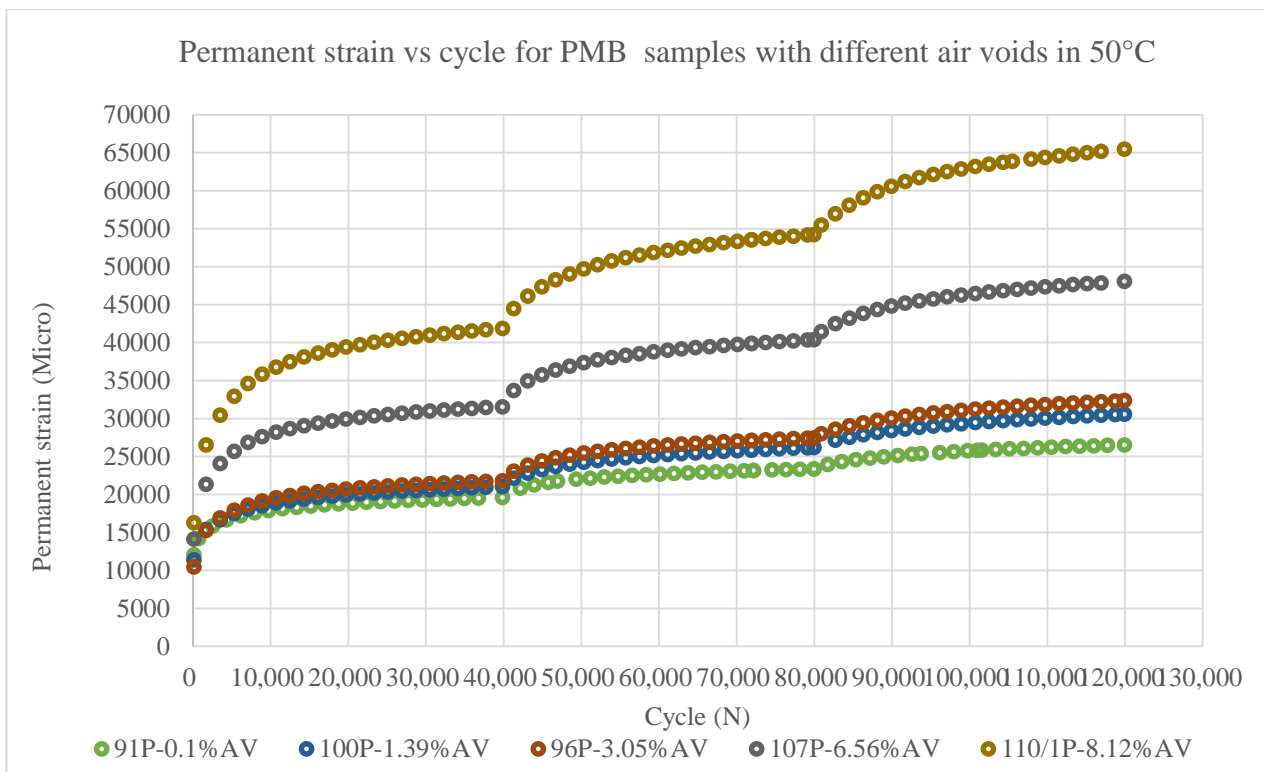


Figure 6: MCDC test results for PMB samples in 50°C

## APPENDIX E

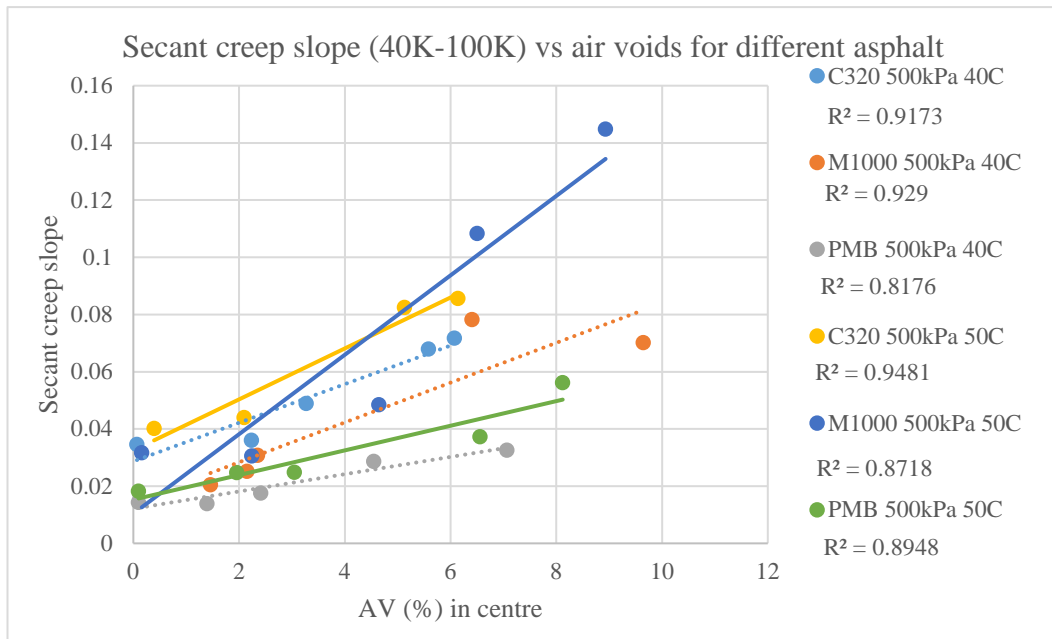


Figure 1: Secant creep slope of three types asphalt with different air voids under 500kPa

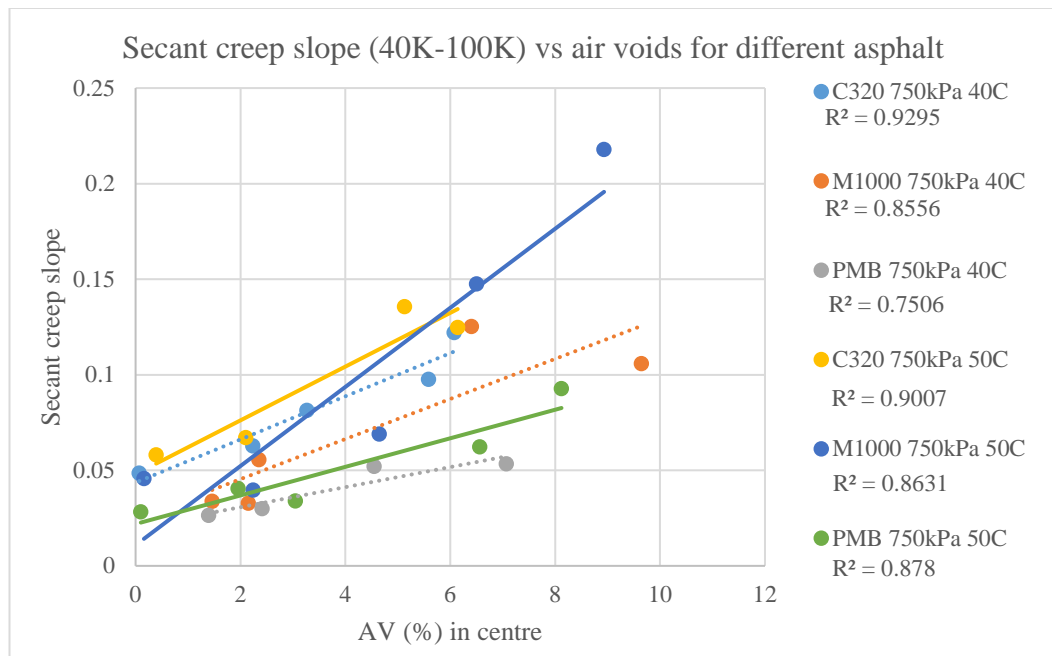


Figure 2: Secant creep slope of three types asphalt with different air voids under 750kPa

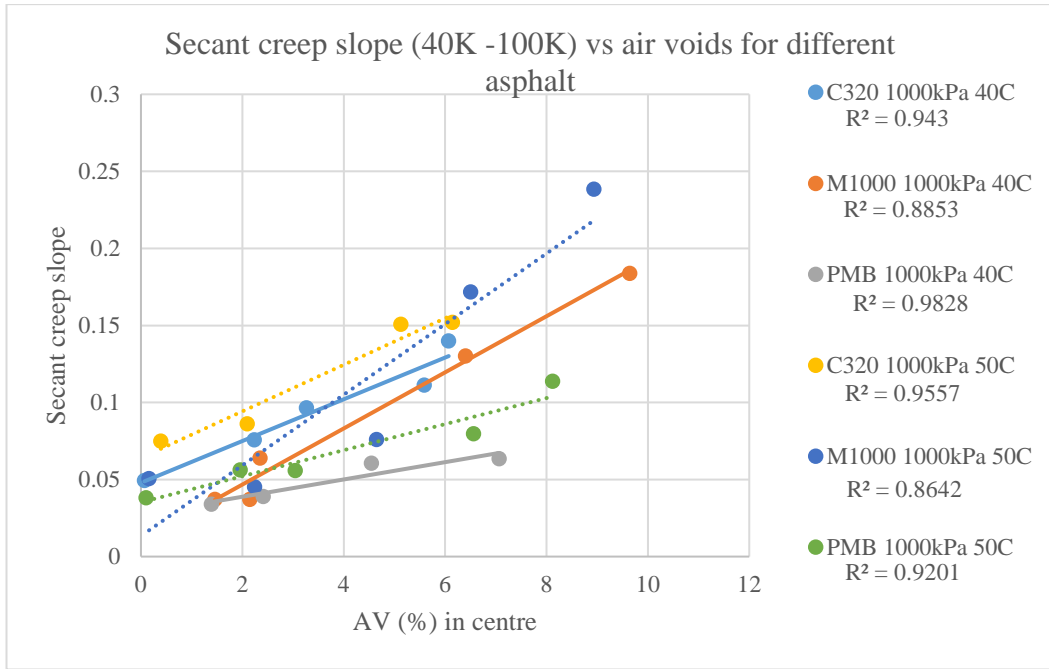


Figure 3: Secant creep slope of three types asphalt with different air voids under 1000kPa

## APPENDIX F

Table 1: Test results related to the asphalt mix manufactured by C320

Stress (kPa)	T (°C)	Sample number	Ultrasonic velocity (m/s)	AV (%) in the whole sample	AV (%) in centre	MR (180 cycles)	MR (20K cycles)	MR (40K cycles)	creep slope (100k to 500K cycles)	Permanent Strain (20K cycles)
500	40	82	4784	2.18	0.07	4959	2241	2150	0.0107	15061
		68	4655	3.27	2.24	3868	2514	2406	0.0110	15914
		71	4594	4.93	3.27	3040	1804	1778	0.0152	20006
		66	4456	6.12	5.59	3800	2388	2419	0.0222	19783
		79	4427	7.12	6.07	2853	1798	1795	0.0227	25612
	50	81	4768	2.37	0.39	2367	1272	1093	0.0119	23129
		67	4663	3.74	2.10	1960	972	947	0.0129	25099
		83	4483	6.15	5.13	1348	907	865	0.0252	37273
		84	4423	7.15	6.14	1707	980	900	0.0263	37364
		85-2	4228	8.36	9.42	-	-	-	-	-
750	40	82	4784	2.18	0.07	-	2109	2261	0.0200	20902
		68	4655	3.27	2.24	-	2420	2113	0.0265	22637
		71	4594	4.93	3.27	-	1685	1635	0.0350	28721
		66	4456	6.12	5.59	-	2438	2185	0.0437	30737
		79	4427	7.12	6.07	-	1777	1699	0.0544	37626
	50	81	4768	2.37	0.39	-	1303	1174	0.0237	30657
		67	4663	3.74	2.10	-	934	970	0.0273	33653
		83	4483	6.15	5.13	-	947	958	0.0565	52882
		84	4423	7.15	6.14	-	944	960	0.0526	52428
		85-2	4228	8.36	9.42	-	-	-	-	-
1000	40	82	4784	2.18	0.07	-	2155	2228	0.0265	25771
		68	4655	3.27	2.24	-	2331	2264	0.0427	28886
		71	4594	4.93	3.27	-	1606	1560	0.0542	36568
		66	4456	6.12	5.59	-	2439	2367	0.0628	40704
		79	4427	7.12	6.07	-	1747	1719	0.0787	49221
	50	81	4768	2.37	0.39	-	1253	1234	0.0405	37082
		67	4663	3.74	2.10	-	970	1018	0.0467	40709
		83	4483	6.15	5.13	-	952	917	0.0821	66553
		84	4423	7.15	6.14	-	927	1058	0.0849	66054
		85-2	4228	8.36	9.42	-	-	-	-	-

Table 2: Test results related to the asphalt mix manufactured by M1000

Stress (kPa)	T (°C)	Sample number	Ultrasonic velocity (m/s)	AV (%) in the whole sample	AV (%) in centre	MR (180 cycles)	MR (20K cycles)	MR (40K cycles)	creep slope (100k to 500K cycles)	Permanent Strain (20K cycles)
500	40	42	4544	1.05	1.46	3617	3685	3649	0.0065	7939
		36	4507	2.40	2.15	3264	2555	2497	0.0079	9827
		48	4497	4.58	2.35	3369	2805	2698	0.0096	12555
		58	4283	7.39	6.40	2749	2264	2197	0.0276	16981
		55	4113	8.99	9.64	2651	2212	2206	0.0237	18626
	50	44	4612	0.90	0.16	2638	1541	1460	0.0096	15145
		39	4503	2.03	2.24	2674	1561	1569	0.0094	14399
		46	4376	3.51	4.64	2140	1316	1341	0.0148	19724
		41	4278	6.56	6.50	1846	1172	1116	0.0355	31334
		53	4150	9.06	8.93	1440	880	816	0.0471	43484
750	40	42	4544	1.05	1.46	-	3389	3294	0.0146	11634
		36	4507	2.40	2.15	-	2595	2527	0.0135	13911
		48	4497	4.58	2.35	-	2701	2595	0.0238	17343
		58	4283	7.39	6.40	-	2333	2093	0.0619	26589
		55	4113	8.99	9.64	-	2208	2145	0.0492	28034
	50	44	4612	0.90	0.16	-	1471	1461	0.0183	21154
		39	4503	2.03	2.24	-	1467	1544	0.0159	19710
		46	4376	3.51	4.64	-	1426	1335	0.0292	27217
		41	4278	6.56	6.50	-	1167	1115	0.0644	46102
		53	4150	9.06	8.93	-	830	791	0.0994	63737
1000	40	42	4544	1.05	1.46	-	3320	3276	0.0208	15040
		36	4507	2.40	2.15	-	2557	2466	0.0194	17629
		48	4497	4.58	2.35	-	2493	2342	0.0372	22055
		58	4283	7.39	6.40	-	2205	2058	0.0803	35708
		55	4113	8.99	9.64	-	1980	1908	0.1765	37084
	50	44	4612	0.90	0.16	-	1561	1588	0.0274	25923
		39	4503	2.03	2.24	-	1588	1516	0.0239	23999
		46	4376	3.51	4.64	-	1440	1432	0.0412	33284
		41	4278	6.56	6.50	-	1123	1158	0.099	58277
		53	4150	9.06	8.93	-	735	908	0.1364	82334

Table 3: Test results related to the asphalt mix manufactured by PMB

Stress (kPa)	T (°C)	Sample number	Ultrasonic velocity (m/s)	AV (%) in the whole sample	AV (%) in centre	MR (180K cycles)	MR (20K cycles)	MR (40K cycles)	creep slope (100k to 500K cycles)	Permanent Strain (20K cycles)
500	40	93	4527	0.84	0.10	1359	1019	991	0.0041	13491
		88	4467	2.36	1.39	1877	1235	1241	0.0041	10598
		98	4419	4.19	2.41	1334	1030	1064	0.0051	13790
		102	4319	6.00	4.55	1243	977	1027	0.0084	18279
		108	4202	7.23	7.07	1257	1006	999	0.0094	21019
	50	91	4527	0.89	0.10	962	905	845	0.0052	18797
		100	4441	2.96	1.96	729	630	654	0.0072	20011
		96	4390	4.45	3.05	920	843	938	0.0071	20807
		107	4225	7.27	6.56	750	749	727	0.0106	30098
		110-1	4152	9.87	8.12	736	616	655	0.0164	39678
750	40	93	4527	0.84	0.10	-	-	-	-	-
		88	4467	2.36	1.39	-	1477	1451	0.0103	14166
		98	4419	4.19	2.41	-	1140	1116	0.0125	17933
		102	4319	6.00	4.55	-	1051	1067	0.0205	24562
		108	4202	7.23	7.07	-	1090	1101	0.0218	27811
	50	91	4527	0.89	0.10	-	903	921	0.0108	22636
		100	4441	2.96	1.96	-	681	669	0.0162	25191
		96	4390	4.45	3.05	-	893	916	0.016	26459
		107	4225	7.27	6.56	-	760	763	0.0242	38922
		110-1	4152	9.87	8.12	-	662	663	0.036	52116
1000	40	93	4527	0.84	0.10	-	-	-	-	-
		88	4467	2.36	1.39	-	1418	1449	0.0175	17274
		98	4419	4.19	2.41	-	1171	1175	0.0207	21545
		102	4319	6.00	4.55	-	1055	1071	0.032	29897
		108	4202	7.23	7.07	-	1116	1140	0.0333	33693
	50	91	4527	0.89	0.10	-	905	930	0.0193	25750
		100	4441	2.96	1.96	-	721	698	0.0297	29401
		96	4390	4.45	3.05	-	974	955	0.0296	31175
		107	4225	7.27	6.56	-	741	765	0.0425	46412
		110-1	4152	9.87	8.12	-	733	700	0.0605	63137